THE GEOLOGY AND GEOCHEMISTRY OF THE BRIDGETOWN FORMATION OF THE MALMESBURY GROUP, WESTERN CAPE PROVINCE

by

Nina Slabber

June 1995

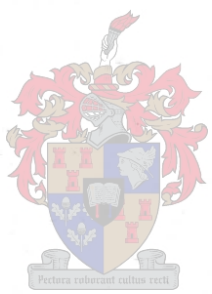

Supervisor: Dr. R. Scheepers

Thesis presented in partial fulfillment of the requirements for the degree of Master of Science at the University of Stellenbosch.

DECLARATION:

I the undersigned hereby declare that the work contained in this thesis is my own original work and has not previously in its entirety or in part been submitted at any university for a degree.

SIGNATURE DATE

ABSTRACT

A number of small greenstone bodies of the Bridgetown Formation are exposed as elongated lenses and dykes within metasediments of the Malmesbury Group in the Western Cape Province, South Africa. The Malmesbury Group is part of the Neoproterozoic to Cambrian (Namibian) Saldania Subprovince which is the southern continuation of a Pan-African mobile belt system.

A detailed geological and geochemical study was conducted on the largest outcrop of the Bridgetown Formation, situated 20km east of the town Moorreesburg.

The Bridgetown Formation consists of a meta-volcano-sedimentary sequence that experienced polyphase deformation and metamorphism up to the lower greenschist facies. Tectonically, the Bridgetown Formation is included in the Boland tectonic domain, east of the Piketberg-Wellington fault zone that is suggested to run 5km west of Heuningberg and subparallel to the Berg River. This agrees with Rabie's (1974) original subdivision of the tectonic domains.

The Bridgetown Formation consists of: i) A basal unit of poorly differentiated alkaline metabasalt with a within-plate tectonomagmatic fingerprint. ii) An intermediate unit of poorly differentiated tholeiitic metabasalt, intruded by a younger tholeiitic metabasite with a low degree of differentiation. Both members of the intermediate unit have ocean-floor basalt (P-type MORB) and island arc basalt fingerprints. iii) An upper unit of poorly differentiated as well as more evolved alkaline metabasalts, interlayered with metatuff with an alkaline basaltic composition, metasedimentary rocks with a marine origin, and graphitic schists and muscovite-quartz schists, both with a continental crust provenance. iv) An overlying metasedimentary sequence including dolomite, massive and oolitic chert, jasper and jaspilite.

The Bridgetown Formation probably also comprises a lower metamorphosed ultramafic unit, indicated by the association of Ni- and Cr-rich talc bodies, Ni-and Cr-rich banded chert, chlorite schist and small dolomite-talc-chlorite bodies at Spitskop, situated directly northwest of the main greenstone body.

The sequence of eruptive stages and the geochemistry of the metavolcanics resemble Hawaiian volcanism, indicated by an initial deep water stage of alkaline magmatism, followed by main tholeiitic edifice and post-caldera alkaline magmatism.

Post-caldera alkaline magmatism occurred contemporaneously with deposition of sediments and chemical precipitates (carbonates and cherts).

The Bridgetown metavolcanics have no magmatic association with either the Bloubergstrand volcanics or mafic and intermediate plutonic rocks in the Malmesbury Group. However, some physical and geochemical similarities exist between the Bridgetown Formation and the age related Grootderm Formation of the Marmora Terrane (Gariep Supergroup) which is considered to represent ophiolitic material. The Bridgetown Formation probably represents segments of oceanic crust, including seamounts of oceanic islands, which were tectonically emplaced in an accretionary prism zone during subduction of oceanic crust underneath the Kalahari Craton, 600 to 700 Ma ago. This resulted in the present spatial configuration of various small greenstone bodies in the Malmesbury Group.

To date no exploitable mineral deposits have been found in the Bridgetown Formation. However, Au and As anomalies in stream sediment and soil samples, taken in the Spitskop area, require further attention. It is suggested that the gold and arsenic is hosted in brittle deformed clear to milky quartz veins which developed at zones of competency contrasts in all the lithologies in the Spitskop area.

SAMEVATTING

'n Aantal klein groenskisliggame van die Bridgetown Formasie is blootgestel as verlengde lense en gange binne metasedimente van die Malmesbury Groep in die Wes-Kaap Provinsie, Suid-Afrika. Die Malmesbury Groep is deel van die Neoproterozoïese tot Kambriese (Namibiese) Saldania Subprovinsie wat die suidelike voortsetting is van 'n Pan-Afrikaanse mobiele gordel sisteem.

'n Gedetaileerde geologiese en geochemiese studie is gedoen op die grootste dagsoom van die Bridgetown Formasie, geleë 20km oos van die dorp Moorreesburg.

Die Bridgetown Formasie bestaan uit 'n metavulkanies-sedimentêre opeenvolging wat polifase vervorming en metamorfisme tot en met die laer groenskis fasies ondergaan het. Die Bridgetown Formasie word hier in die Boland tektoniese domein ingedeel deur die Piketberg-Wellington verskuiwingsone 5km wes van Heuningberg, subparallel aan die Bergrivier, te plaas. Dit stem ooreen met Rabie (1974) se oorspronklike verdeling van die tektoniese domeine.

Die Bridgetown Formasie bestaan uit: i) 'n Basale eenheid wat hoofsaaklik bestaan uit min gedifferensieerde alkali-metabasalte met binneplaat tektonomagmatiese eienskappe. ii) 'n Intermediêre eenheid wat bestaan uit min gedifferensieerde tholeiitiese metabasalt en 'n jonger intrusiewe tholeiitiese metabasiet wat 'n lae graad van differensiasie ondergaan het. Beide intermediêre eenhede het oseaanvloer-basalt (P-tipe MORB) en eilandboog basaltiese eienskappe. iii) 'n Boonste eenheid wat bestaan uit min gedifferensieerde asook meer gedifferensieerde alkali-metabasalte, tussengelaagd met metatuf met 'n alkali-basaltiese samestelling; metasedimentêre gesteentes met 'n mariene oorsprong, en grafitiese skiste en kwarts-muskoviet skiste, beide met 'n kontinentale kors oorsprong. iv) 'n Oorliggende metasedimentêre opeenvolging wat dolomiet, massiewe en oolitiese chert, jaspis en jaspiliet insluit.

Die Bridgetown Formasie sluit moontlik ook 'n onderliggende gemetamorfiseerde ultramafiese eenheid in; aangedui deur die assosiasie van Ni- en Cr-ryke talkliggame, Ni- en Cr-ryke gebande chert, chlorietskis en klein dolomiet-talk-chloriet liggame by Spitskop, geleë direk noordwes van die hoof groensteenliggaam.

Die opeenvolging van magmatisme en die geochemie van die metavulkaniese gesteentes stem ooreen met Hawaiiese vulkanisme, naamlik 'n diepwater stadium,

gekarakteriseer deur alkaliese magmatisme, gevolg deur 'n hoof tholeiitiese opbouing en post-kaldera alkaliese magmatisme. Die post-kaldera alkaliese magmatisme het gelyktydig plaasgevind met afsetting van sedimente en chemiese presipitate (karbonate en cherte).

Die Bridgetown metavulkaniese gesteentes het geen magmatiese assosiasie met óf die Bloubergstrand vulkaniese gesteentes óf mafiese en intermediêre plutoniese gesteentes in die Malmesbury Groep nie. Fisiese en geochemiese ooreenkomste bestaan egter tussen die Bridgetown Formasie en die Grootderm Formasie van die Marmora Terrein (Gariep Supergroep) wat beskou word as ofiolitiese materiaal. Die Bridgetown Formasie verteenwoordig moontlik segmente van oseaankors, insluitende oseaan-eilande, wat tektonies in 'n mélange sone ingeplaas is tydens subduksie van oseaankors onder die Kalahari Kraton in (600 tot 700 Mj gelede). Dit verklaar die huidige ruimtelike verspreiding van verskeie klein groensteenliggame in die Malmesbury Groep.

Tot en met hede is geen ontginbare mineraalafsettings in die Bridgetown Formasie ontdek nie. Au en As anomalië in stroomsediment- en grondmonsters, geneem in die Spitskop area, behoort egter verdere aandag te geniet. Daar is voorgestel dat die goud en arseen voorkom in brosvervormde helder tot melkerige kwartsare wat ontwikkel het in swak sones in al die litologië in die Spitskop area.

CONTENTS

LIST OF FIGURES IN TEXT

Fig. 4.3 The average composition of basaltic-andesitic rocks (ruled area); mean value of tholeiites indicated (square). Plagioclase commonly between An 65 and An 40 (Winkler, 1976).

Fig. 4.4 The chemical composition of unit 5 plotted on ACF and A'FK diagrams. Fields of various magmatic and sedimentary rocks as given by Nockolds (1954) and Ronov and Klebnikova (1957).

Fig. 5.1 Discriminant analysis on major and trace elements of greenstone units of the Bridgetown Formation.

Fig. 5.2 Plot of total alkalis versus silica for greenstone units of the Bridgetown Formation which indicates the nomenclature of normal (i.e. non-potassic) volcanic rocks (Cox et al., 1979).

Fig. 5.3 Zr/TiO_2 - Ce diagram (Winchester and Floyd, 1977) showing the delimited fields for common volcanic rocks.

Fig. 5.4 Alkalis-silica plot of greenstone units of the Bridgetown Formation. The solid curve is the line chosen by Irvine and Barager (1971) for making a general distinction between alkaline and subalkaline compositions.

Fig. 5.5 Ol'-Ne'-Q' projections (Irvine and Barager, 1971) of greenstone units of the Bridgetown Formation. Plots are in % cation equivalents based on the cation norm.

Fig. 5.6 Magmatic discrimination diagrams of Winchester and Floyd (1977) using immobile elements. (A) SiO_2 versus Zr/TiO_2. (B) SiO_2 versus Nb/Y. (C) Zr/TiO_2 versus Nb/Y. (D) Ga/Sc versus Nb/Y.

Fig. 5.7 AFM diagram of greenstone units of the Bridgetown Formation. The solid curve serves to separate tholeiitic and calc-alkaline compositions.

Fig. 5.8 An-Ab'-Or projections of greenstone units for distinguishing K-poor, "common" and K-rich variants (Irvine and Barager, 1971). Plots are in % cation equivalents.

Fig. 5.9 Variation of Al_2O_3 with FeO/(FeO + MgO) weight percent ratio in the greenstone units. Note that total Fe is calculated as FeO.

Fig. 5.10 Wt percent TiO_2 versus wt percent MgO for greenstone units of the Bridgetown Formation.

Fig. 5.11 SiO_2 versus MgO (wt%) for greenstone units of the Bridgetown Formation. Division between low-Mg and high-Mg basalts are based on those of Redman and Keays (1985).

Fig. 5.12 Tectonomagmatic discrimination diagram using Ti, Zr and Y (Pearce and Cann, 1973).

Fig. 5.13 Application of the Nb-Zr-Y diagram (Meschede, 1986) to discriminate between magmas from different tectonic environments.

Fig. 5.14 MnO*10 - TiO_2 - P_2O_5*10 discriminant diagram for basalts and basaltic andesites of oceanic regions (Mullen, 1983).

Fig. 5.15 Incompatible element abundances, normalized to primitive mantle values, in greenstone units of the Bridgetown Formation, and ocean island basalt (OIB), N-type MORB and E-type MORB. Average compositions of selected mafic magmas and normalizing factors are from Sun and McDonough (1989).

Fig. 5.16 Harker variation diagrams of K_2O, Na_2O, Ba, Rb, Sr and CaO for the greenstone units.

LIST OF TABLES IN TEXT

Table 6.4 Oxygen isotope composition of quartz veins and banded chert at Spitskop.

LIST OF PLATES IN TEXT

Plate 3.12 Unit 2. The lower half of the photomicrograph represents dark lamellae consisting of chlorite, actinolite, titanite and magnetite which envelope porphyroblasts of albite and calcite. The upper half of the photomicrograph represents light lamellae which are made up of calcite and quartz. A few large brown titanite granules with ilmenite rims occur in the light areas. Plane light.

Plate 3.13 Highly laminated light khaki chlorite-calcite-quartz-actinolite schist (unit 1).

Plate 3.14 Poorly laminated light khaki chlorite-calcite-quartz-actinolite schist (unit 1).

Plate 3.15 Unit 1. Poorly laminated dark green zone, consisting of chlorite, actinolite, magnetite; minor titanite, quartz, calcite and albite; and accessory muscovite and epidote. Plane light.

Plate 3.16 Dark olive green augen chlorite-actinolite-magnetite-calcite schist (unit 3).

Plate 3.17 Unit 3. An anhedral porphyroblast of epidote enveloped by the schistose chlorite-actinolite-magnetite mineral fabric to give an 'augen' texture. Plane light.

Plate 3.18 Olive green epidote-actinolite-titanite-chlorite schist (unit 11).

Plate 3.19 Unit 11. The light zone in the middle of the photomicrograph consists of granular epidote, actinolite, quartz, chlorite and albite. The darker zones contain additional titanite, magnetite and ilmenite. Plane light.

Plate 3.20 Light grey green quartz-orthoclase-biotite-muscovite fels (unit 5).

Plate 3.21 Unit 5. A coarse-grained fels which is made up of randomly orientated biotite, quartz, muscovite and orthoclase with minor chlorite, calcite, actinolite and magnetite. Plane light.

Plate 3.22 Intrusive olive green augite-actinolite metabasite (unit 10).

Plate 3.23 Unit 10. Actinolite fibres, an alteration product of augite, occur at the interface between the augite and its pressure shadow. Deformed actinolite fibres are indicators of shearing. Crossed polars.

Plate 3.24 Lensoid inclusions in greenstones on the farm Kamina. They consist of augite phenocrysts in a microcrystalline groundmass of augite, albite, titanite and minor chlorite, actinolite, magnetite and epidote. Plane light.

Plate 3.25 Graphitic schist from borehole AE2.

Plate 3.26 Oolitic dolomite from borehole CE1.

Plate 3.27 Oolitic chert on the farm Palestina.

Plate 3.28 Oolitic chert on the farm Palestina consisting of a microcrystalline quartz rim surrounding an inner zone of macrocrystalline quartz. Crossed polars.

Plate 3.29 Banded chert at Spitskop. Small irregular cracks in the chert are filled with spinel and micas. The red-brown spinel grains are Al- and Mg-rich chromite grains with a dark magnetite rim. Plane light.

Plate 3.30 Chlorite schist at Spitskop. Rounded porphyroclasts of albite in a groundmass of chlorite, magnetite and fine-grained quartz and albite. The albite porphyroclasts are partly altered to saussurite and contain small alkali feldspar inclusions. Crossed polars.

ABBREVIATIONS FOR MINERALS

ab : albite
ac : actinolite
au : augite
af : alkali feldspar
bt : biotite
cc : calcite
cl : chlorite
do : dolomite
ep : epidote
he : hematite
il : ilmenite
la : labradorite
mn : magnetite
mus : muscovite
or : orthoclase
py : pyrite
q : quartz
sp : spinel
ti : titanite

1. INTRODUCTION

A number of greenstone bodies are exposed as small elongated lenses and dykes within metasediments of the Malmesbury Group (Fig. 2.4) in the Western Cape Province (Fig. 2.1).

This study is mainly concerned with the largest greenstone body outcropping along the Berg River, 20 kilometres east of the town Moorreesburg. The greenstones, accompanied by small mafic dykes, dolomite, chert and minor graphitic schists and muscovite-quartz schists constitute the Bridgetown Formation.

To date the greenstones and associated rock types of the Bridgetown Formation have not been studied in any detail. The aim of this study is to:

i) determine the tectono-stratigraphic relationship between the Bridgetown Formation and other formations of the Malmesbury Group;

ii) determine the tectono-stratigraphic and genetic relationships between the greenstones, mafic dykes, dolomite, chert, graphitic schists and muscovite-quartz schists of the Bridgetown Formation;

iii) characterize physical, mineralogical and geochemical heterogeneities within the main greenstone body;

iv) compare the Bridgetown Formation with other Pan-African metavolcano-sedimentary sequences; and to

v) evaluate the economic potential of the area between the farms Spitskop and Winkelhaaksvlei.

Extensive mapping of the area was done on a scale of 1:10 000, aiding the compilation of a 1:15 000 scale map presented as Sheet A. Each lithological component of the Bridgetown Formation was sampled for petrographical and geochemical studies, using outcrop samples as well as relatively fresh borehole core of twelve boreholes, drilled into the greenstones by the Department of Environmental Affairs in 1983; and made available by the Geological Survey.

The area around Spitskop (Fig. 2.4), situated directly northwest of the main greenstone body, was also included in this study. Inclusion of the Spitskop area was motivated by the presence of a few small greenschist outcrops. Soil and stream sediment sampling in the Spitskop area revealed gold and arsenic anomalies which also warranted further investigation.

2. REGIONAL GEOLOGY

2.1. MALMESBURY GROUP

Polyphase deformed metasediments and metavolcanics of the Malmesbury Group are exposed in the Western Cape Province as inliers within the Palaeozoic Cape Supergroup. The Kango, Kaaimans and Gamtoos Groups in the Western Cape Province and Eastern Cape Province (Fig. 2.1) have been correlated with the Malmesbury Group. These Groups have structural and stratigraphic similarities, are of pre-Cape age and form part of the Saldania Subprovince (Hartnady, 1969) which is the southern continuation of a Pan-African mobile belt system. This belt system includes the Gariep Subprovince in the Northern Cape and the Damara Province in Namibia and is probably related to the Dom Feliciano Belt in Brazil (Fernandes et al., 1992; Fig. 2.2).

The Malmesbury Group constitutes a poorly understood sequence; the reason being poor exposure of the meta-volcano-sediments which are very susceptible to weathering and mechanical break-down. Although the Malmesbury Group has continuously been subjected to low intensity exploration, few prospects warranted follow-up drilling, thus contributing little to unravel the lithostratigraphy and structure. Hartnady et al. (1974) divided the Malmesbury Group into three terranes separated by two large northwest-striking fault zones (Fig. 2.3). These two zones of pre-Cape faulting and shearing are named the Saldanha-Franschhoek zone and the Piketberg-Wellington zone. The lithostratigraphy of the Malmesbury Group is summarized in Table 2.1 (Sheet 3318 Cape Town, 1990; Theron, 1990). It is not always clear whether boundaries between strongly contrasting lithological successions are stratigraphic or tectonic (Hartnady et al., 1974). Correlation across the two major fault zones has not been possible; therefore the stratigraphic relationship between the Tygerberg, Boland and Swartland terranes is still unknown. The Klipheuwel Group overlies parts of the Tygerberg and Boland terranes unconformably, mainly along the Tygerberg-Swartland and Swartland-Boland terrane boundaries. It was apparently deposited in fault-related basins as a result of

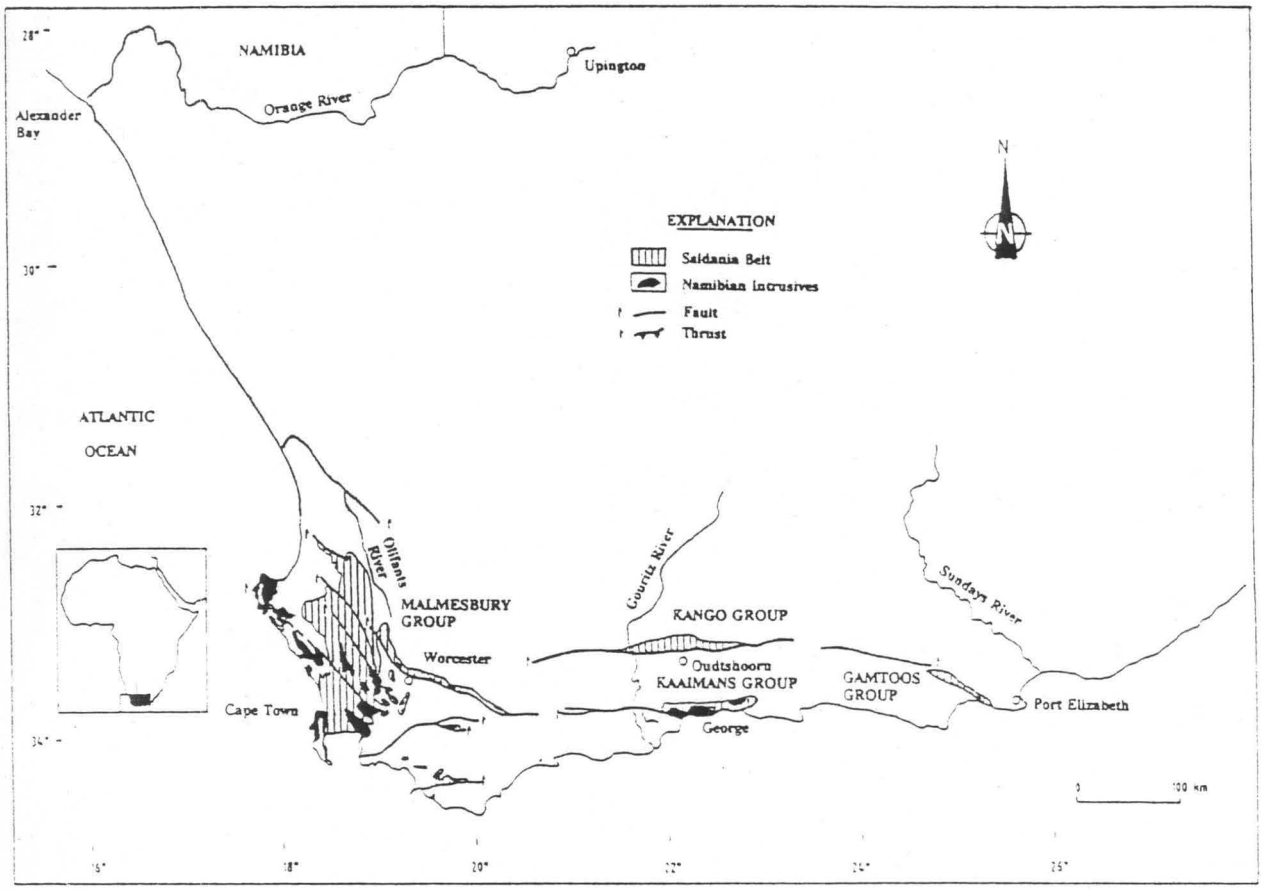

Figure 2.1. Geographic distribution of the Malmesbury Group and related Groups in the Saldania Subprovince (Gresse and Scheepers, 1993).

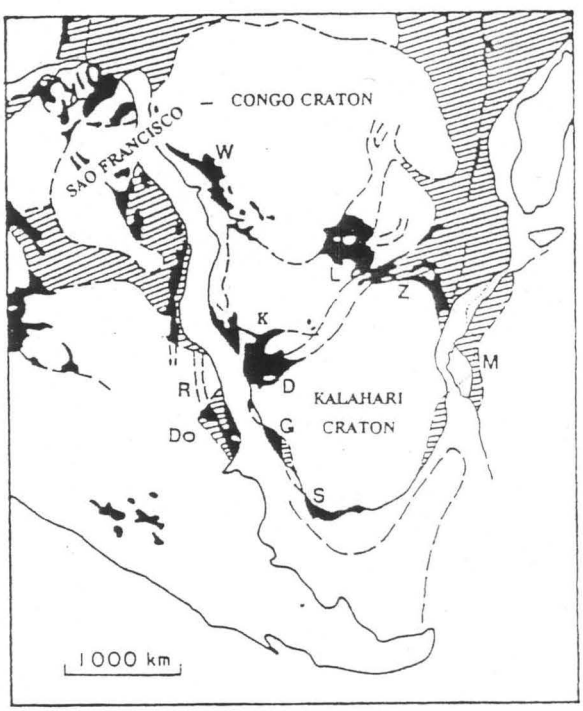

Figure 2.2. The Saldania Belt in the framework of Pan-African orogenic belts in western Africa, eastern South America and East Antarctica (after Porada, 1979; Groenewald et al., 1991 and Frimmel et al., 1992). D-Damara Belt, Do-Dom Feliciano Belt, G-Gariep Belt, K-Kaoko Belt, L-Lufilian Arc, M-Maudheim Belt, R-Ribeiro Belt, S-Saldania Belt, W-West Congolian Belt, Z-Zambezi Belt.

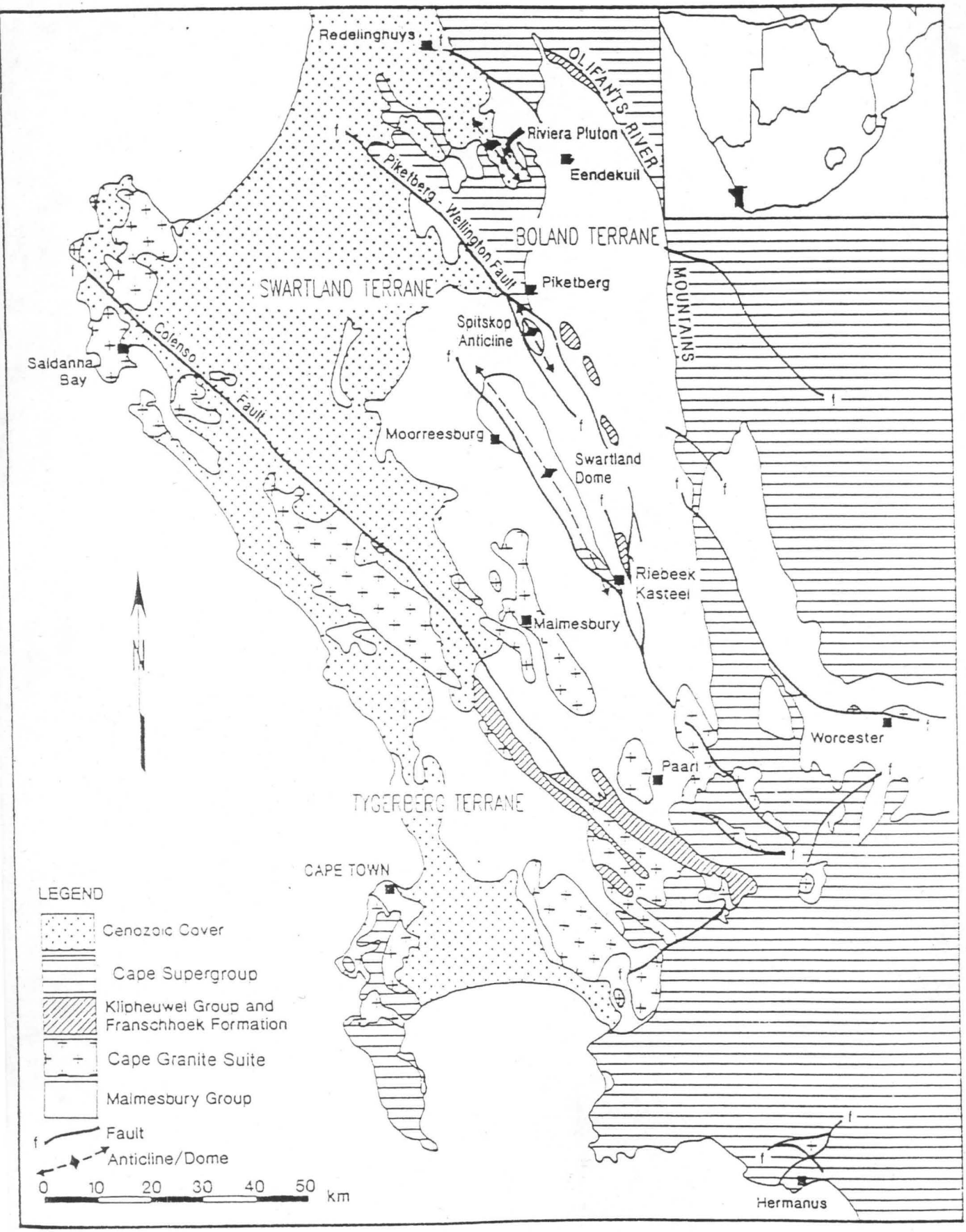

Figure 2.3. Distribution of the fault-bounded tectono-stratigraphic domains of the Malmesbury Group (Gresse and Scheepers, 1993; modified by Rozendaal and Scheepers, 1994).

Table 2.1 Lithostratigraphy of the Malmesbury Group (Sheet 3318 Cape Town, 1990).

Group	MALMESBURY		
Terrane	**Tygerberg**	**Swartland**	**Boland**
Formation	**Tygerberg (Nt):** Graywacke, phyllite and quartzitic sandstone; interbedded lava and tuff.	**Franschhoek (Nf):** Grey, feldspathic conglomerate, grit and sandstone with minor shale. **Moorreesburg (Nm):** Graywacke and phyllite with beds and lenses of quartz schist, limestone and grit; quartz-sericite schist with occational limestone lenses. **Bridgetown (Nbr):** Greenstone with dolomite and chert lenses. **Klipplaat (Nk):** Quartz schist with phyllite beds and minor limestone and chlorite-schist lenses. **Berg River (Nb):** Schist and fine-grained graywacke with beds and lenses of quartz schist and limestone.	**Porterville (Npo):** Phyllite shale, schist and graywacke with dark-grey limestone, sporadic quartzitic sandstone beds and conglomerate beds. **Piketberg (Np):** Grit and graywacke.

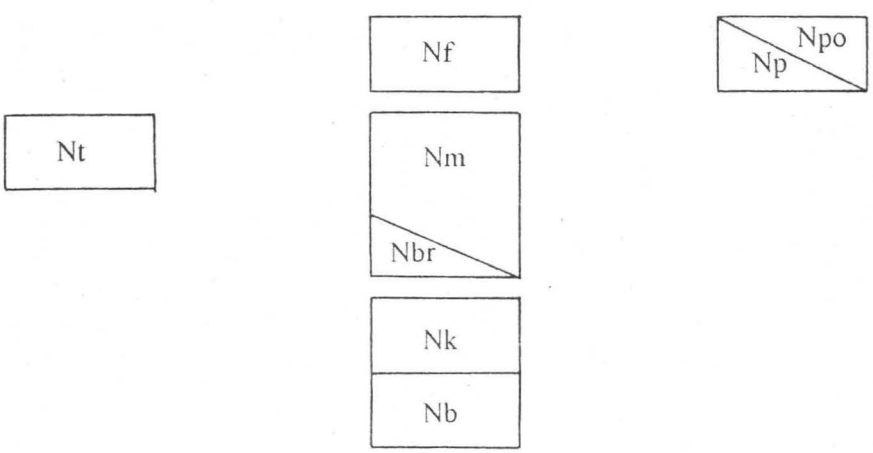

late reactivation or normal faulting along these zones, before the deposition of the Ordovician Table Mountain Group (Gresse and Scheepers, 1993).

The variety and distribution of lithological units in the Malmesbury Group indicate a complex depositional history. Hartnady et al. (1974) suggested that the metasediments are of marine origin and that both continental shelf and continental slope environments were involved. The Tygerberg and Moorreesburg Formations both include graywackes and phyllites which indicate a possible turbidite origin. These may form part of a geosynclinal succession at the margin of an oceanic trench or basin. With the exception of the Moorreesburg Formation which includes graywackes, the Swartland terrane shows an assemblage of quartz-mica schists, quartz and mica schists, carbonate lenses and fine-grained quartzites which may indicate a shelf-sea depositional environment. A near shore environment was suggested for the Boland terrane, based on the presence of coarse-grained quartzites, quartz schists and psammites with conglomerates and phyllite bands (Hartnady et al., 1974; Von Veh, 1983; Haughton, 1933; Visser et al., 1981; Dunlevy, 1992). The above interpretation of the depositional environments for the three terranes is complicated by the following: 1) The stratigraphic positions of the Franschhoek, Kaaimansgat and Bridgetown Formations are still unknown; 2) graywackes and phyllites which might suggest a turbidite sequence, are also present in the Boland terrane; and 3) the Boland terrane includes a volcanic unit which is not typical of a near shore environment.

The Malmesbury Group was deformed and metamorphosed to low grades during the late Precambrian Saldanian orogenic episode (Hartnady, 1969). Major differences in style and history of deformation exist between the three tectono-stratigraphic terranes (Hartnady et al., 1974). The Swartland terrane appears to be tectonically more complex than the two terranes which flank it, with at least two or three phases of deformation and cleavage formation (Hartnady, 1974). The Boland terrane was always regarded as structurally more simple with one phase of near-upright, near isoclinal folds and one prominent near-vertical cleavage which strikes NNW. The

Tygerberg terrane displays mainly one phase of tight, upright isoclinal folding with axial planes striking NW.

The Malmesbury Group was intruded by approximately 25 high-level granitoid plutons during a late to post-orogenic stage (Gresse and Scheepers, 1993). The Cape Granite Suite appears to be composed of an older set of intrusions (600-580 Ma) with some S-type characteristics. They are mainly found in the south-western Tygerberg terrane. A younger episode of granitoids followed (± 560-500 Ma) which can broadly be described as having I- to A-type characteristics. A period of anorogenic A-type magmatism with a maximum age of 516 ± 15 Ma (Schoch et al., 1975) ended the granitoid plutonism. This sequence of events may indicate a multiple collision history for the Saldania Belt consisting of early (± 600 Ma) collision magmatism followed by a younger event of arc magmatism from about 560 Ma and ending with anorogenic granite intrusions above a dormant subduction zone some time after 516 Ma (Gresse and Scheepers, 1993). During intrusion of the A-type granitoids extensional faulting, vertical and lateral displacement occurred, which resulted in the spatial configuration of the various terranes at the present erosional levels (Rozendaal and Scheepers, 1994). The oldest reliable age for the Cape Granite Suite (585 ± 20 Ma; recalculated after Schoch et al., 1975) is regarded as the minimum age for the Malmesbury Group. The maximum age of the Malmesbury Group is represented by the supposed basement (Namaqua Province, ±950 Ma; Burger et al., 1973).

2.2. GREENSTONES IN THE MALMESBURY GROUP

Rabie (1974a) was the first to ascribe the term 'greenstones' to greenish, mafic rocks in the Malmesbury Group. Fig. 2.4. shows the localities of all the greenstone outcrops in the Malmesbury metasediments.

In Rabie's geological map of the Moorreesburg-Wellington area (1974a, mapped in 1948), he listed the greenstones under 'intrusive rocks' in the legend and also distinguished between Boland and Swartland intraformational greenstones. Rabie

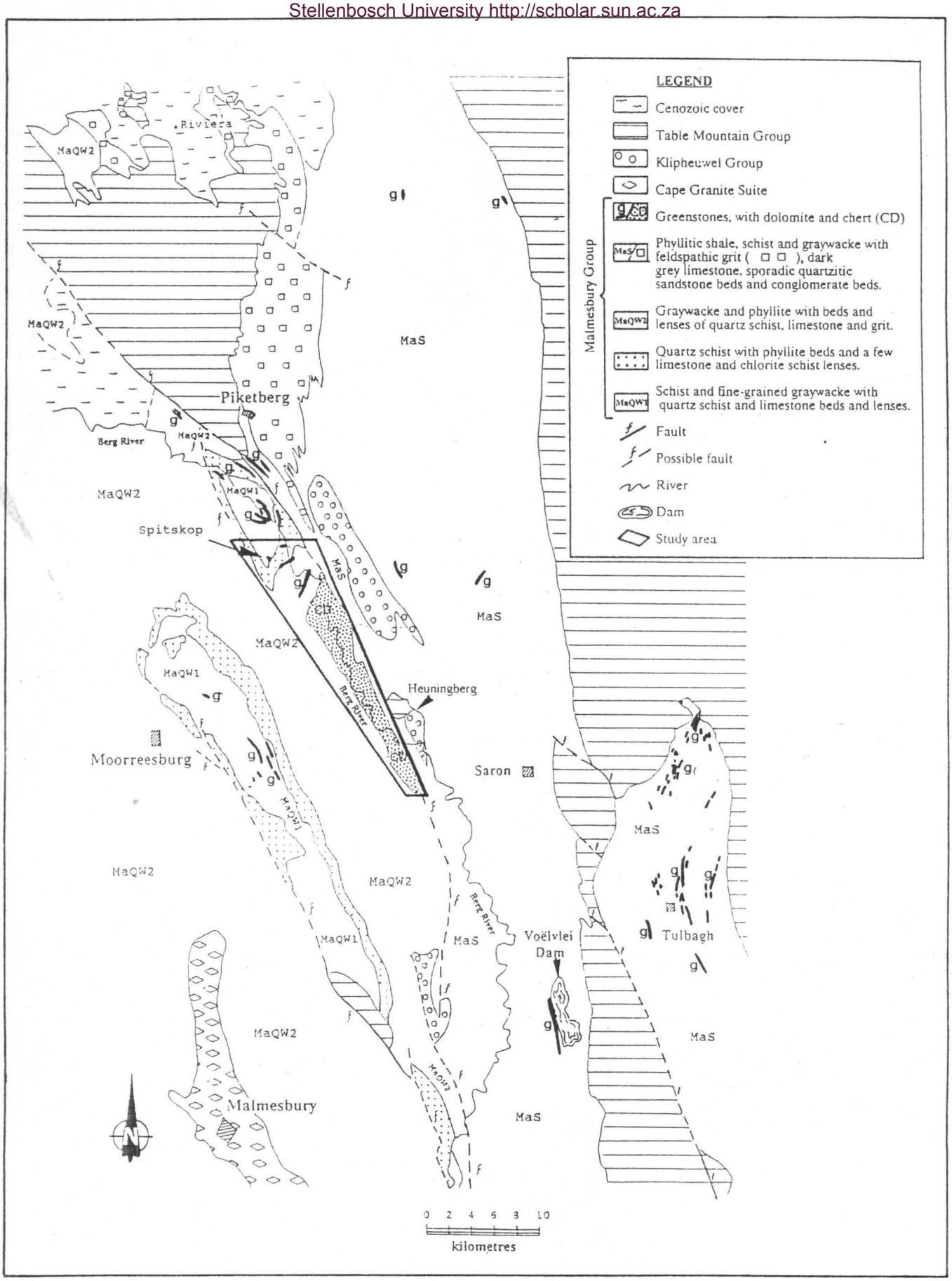

Figure 2.4. Distribution of greenstones in the Malmesbury Group. The study area is outlined.

placed the Piketberg-Wellington fault zone, which serves as the Swartland-Boland terrane boundary, 5km west of Heuningberg subparallel to the course of the Berg River. Thus, according to Rabie, the greenstones which outcrop along the Berg River as well as greenstones near Voëlvlei Dam, belong to the Boland terrane. Rabie depicted these greenstones as intrusive sheets and lavas with minor tuffs or volcanic ashes and small intrusive dykes. The greenstones along the Berg River (later referred to as the Bridgetown Formation by Hartnady et al., 1974), are associated with chert and dolomite. According to Rabie a small dolomite outcrop is also in contact with the greenstones near Voëlvlei Dam. Detailed diamond drilling aimed at outlining the perimeters of the Riviera W-Mo deposit north of Piketberg (Fig. 2.4), intersected a metamorphosed volcano-sedimentary sequence similar to the Bridgetown Formation and the Voëlvlei metavolcanics (Rozendaal et al., 1994). They support Rabie's (1974b) original subdivision of the terranes, because it accommodates the above correlation by including the Bridgetown, Voëlvlei and Riviera greenstones in the Boland terrane. Rozendaal et al. (1994) depicted these greenstones as probably upthrusted and infolded tectonic fragments of a larger metavolcanic unit lower down in the succession.

Rabie (1974a) mapped a few small greenstone outcrops in the Swartland terrane, 8km east of the town Moorreesburg (Fig. 2.4), which he described as intraformational greenstone sills. They are concentrated along the crest of a broad antiform trending in a north-north-westerly direction. These bodies have been sheared and deformed, but have not been converted into schists and are therefore probably younger than the Berg River greenstones (De Villiers, 1969). Thin layers of calcareous quartzite with limestone pockets also occur along the crest of the antiform and it is believed that this calcareous zone is the lowest in the succession (De Villiers, 1969).

Various greenstone dykes are present in the Tulbagh area (Fig. 2.4). They occur as swarms in the Malmesbury metasediments and are cross-cut by younger dolerite dykes. The greenstone dykes are subparallel, cutting discordantly across the NW-SE trending fold and cleavage fabric of this area; thus appearing to be post- or late

tectonic (Hartnady and Hälbich, 1985). They are also of pre-Cape age as they are truncated by the basal Table Mountain Group unconformity on the slopes of the Winterhoek mountains. To date very little work has been done on the dykes. Jacobs (1974) did major and trace element analyses as well as microscopic work on eight highly altered samples from various dykes. From his work it is clear that major chemical and mineralogical differences exist between the greenstone dykes.

An attempt was made to distinguish between the different types of greenstones in the Malmesbury Group, by designating the term Bridgetown type greenstones to the fine-grained variety and Kleinvlei type to the coarse-grained variety (Sheets 3318B Malmesbury and 3319A Ceres, 1975; Visser et al., 1981). It is suggested that these authors made an over simplified classification of the greenstones without taking mineralogical and geochemical differences into account. Most of the greenstone outcrops have never been studied in detail. Little is known about their tectono-stratigraphic setting, mineralogy, geochemistry and age.

3. GEOLOGY OF THE AREA BETWEEN SPITSKOP AND WINKELHAAKSVLEI

The study area includes the Bridgetown Formation which outcrops along the Berg River as well as the area around Spitskop, situated directly northwest of the main greenstone body. Inclusion of the Spitskop area in the study area was motivated by the following: a) a few greenschist outcrops are present in this area and b) stream sediment and soil sampling in the Spitskop area revealed gold anomalies which warranted further investigation. Detailed mapping was done between the farms Spitskop and Winkelhaaksvlei (Sheet A, in pocket).

3.1. TECTONO-STRATIGRAPHY

A lithostratigraphic subdivision of the Malmesbury Group between the farms Spitskop and Winkelhaaksvlei is given in Table 3.1. It was compiled by combining structural data of the area with a few contact relationships in outcrops and borehole sections. Relationships between lithologies are further illustrated in cross-sections A-A' and B-B' (Figs. 3.1 and 3.2) through the Bridgetown Formation and the Spitskop area alternatively.

As a result of generally poor exposure, intense deformation and metamorphism, it is not always clear whether boundaries between strongly contrasting lithologies are stratigraphic or tectonic. For these reasons the lithostratigraphy in Table 3.1 is represented as non-facing.

The geology of the area will be discussed under three headings: a) Bridgetown Formation, b) phyllites in contact with the Bridgetown Formation and c) Spitskop area. This is done because the tectono-stratigraphic relationship between the Bridgetown Formation and surrounding formations (Moorreesburg and Porterville Formations) is not yet known. The geology of the Spitskop area is discussed separately, because continuity in the lithostratigraphy is disrupted by numerous faults.

Table 3.1 Lithostratigraphy of the Malmesbury Group between the farms Spitskop and Winkelhaaksvlei.

A. Area along the main greenstone body.

Terrane	Formation		Lithology (non-facing)
Boland?	Porterville?		Graywacke with feldspathic grit and conglomerate
			Quartz schist (quartzite)
		ph	Phyllite
	Bridgetown		Chert (oolitic, massive and jasper-rich)
			Dolomite with small greenstone bodies (> >)
			Muscovite-quartz schist
		5	Light grey green quartz-orthoclase-biotite-muscovite fels (unit 5) with graphitic schist lenses (• •)
		11	Olive green epidote-actinolite-titanite-chlorite schist (unit 11)
		4 3	Dark olive green augen chlorite-actinolite-magnetite-calcite schist (unit 3)
		1	Laminated light khaki chlorite-calcite-quartz-actinolite schist (unit 1) with graphitic schist lenses (• •) *
		2	Laminated dark grey chlorite-albite-magnetite-calcite schist (unit 2)
			Highly sheared, finely laminated olive green chlorite-magnetite-actinolite schist (unit 4) with dolomite lenses
		9	Laminated olive green epidote-actinolite-chlorite schist (unit 9)
		10	Intrusive olive green augite-actinolite metabasite (unit 10)
		7	Porphyroblastic albite-epidote-magnetite-chlorite-actinolite fels (unit 7)
		6 8	Light olive green chlorite-albite-titanite schist bands (unit 8)
			Laminated olive green chlorite-actinolite-magnetite schist (unit 6)
Boland?	Porterville?	ph	Phyllite
			Limestone lens
			Grit (marker)
		ph	Phyllite
			Greenschist
			Graywacke
			Greenschist
			Quartz-feldspar-sericite schist
(Continuity disrupted by faults)			B. Spitskop area
Boland?	Porterville?		Banded chert
			Chlorite schist with small talc bodies
			Serpentinite?
			Quartz-feldspar-sericite schist
			Limestone lens
			Chlorite schist
			Chlorite schist
			Quartz schist (quartzite)

* Unit 1 is probably equivalent to a banded phyllite, interlayered with chert and graphitic schist lenses (Indicated as (Δ) on Sheet A).

Figure 3.1. Section A-A' (Sheet A) through the Bridgetown Formation.

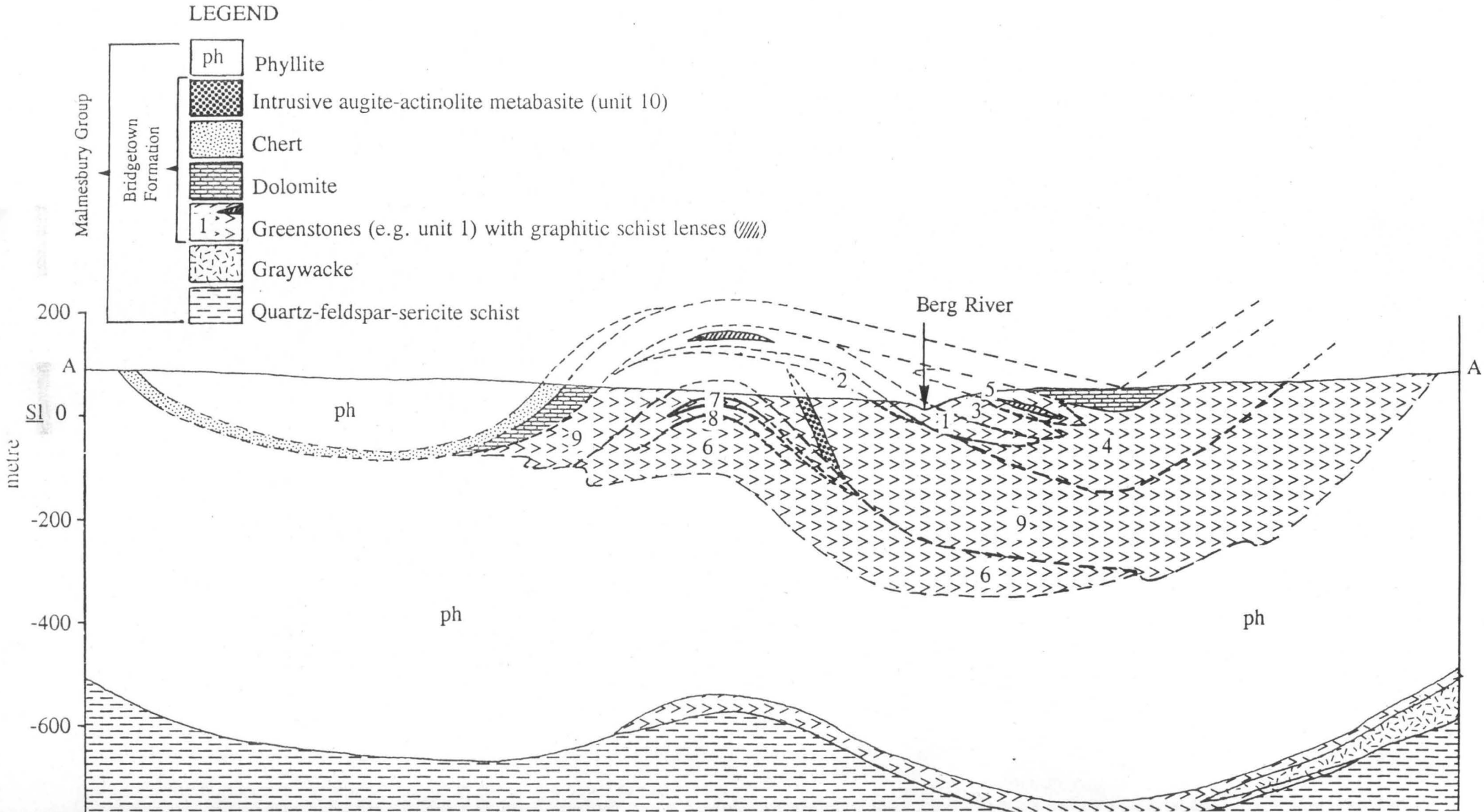

Figure 3.2. Section B-B' (Sheet A) through the Spitskop antiform.

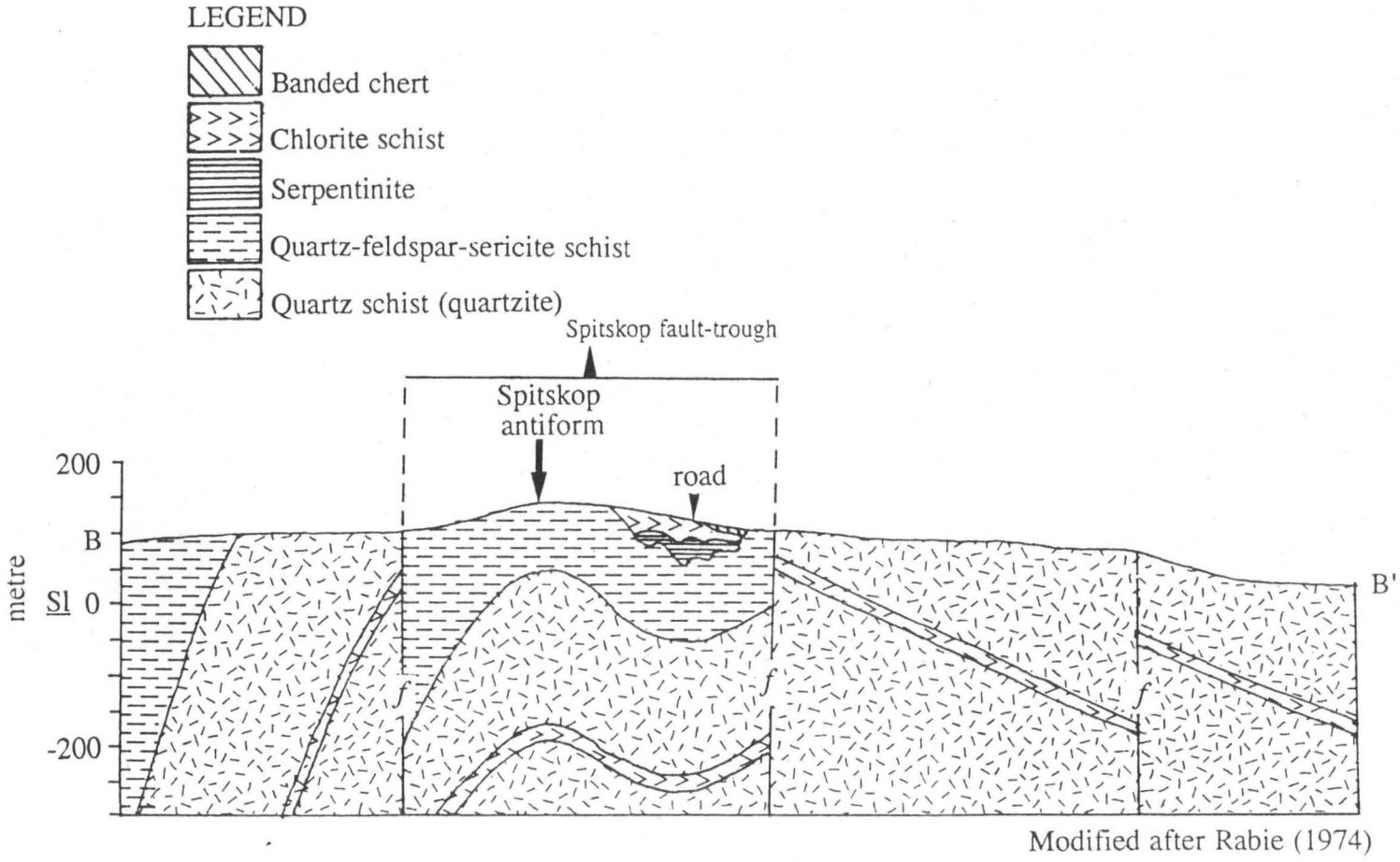

Modified after Rabie (1974)

3.2. BRIDGETOWN FORMATION

The Bridgetown Formation is a NNW trending lensoid outcrop, about 15km long and three kilometres wide at the most. It consists of a sequence of greenstones, intruded by a mafic dyke; chert and dolomite with minor graphitic schist and shale. The transition between the Bridgetown Formation and adjoining formations (Moorreesburg and Porterville Formations), which consists mainly of phyllites, is gradational.

The Bridgetown Formation was first mapped in 1948 by Rabie; unfortunately the D.Sc. thesis which should have accompanied the map was never completed. De Villiers (1969) wrote a short descriptive paragraph on the Bridgetown Formation in an abstract of "The Geology of the Country between Riebeek-Kasteel and Moorreesburg". An honours project by Jacobs (1974) was called "Orientation survey of the lavas at Bloubergstrand, the greenstones of the Bridgetown Complex and some dyke rocks". The project included a petrographical and geochemical study on ten greenstone samples of the Bridgetown Formation. The project did not include any field work and sample positions are poorly indicated, therefore the geochemical results are of limited value. The South African Geological Survey published a geological map of the Koringberg-Hermon area (1975) which included the simplified geology of the Bridgetown Formation. The map was accompanied by a short description of the Bridgetown Formation by Visser et al. (1981) and De Villiers (1979). Recent mapping of the Bridgetown Formation (Sheet A) agrees with the "Geological Map of the Moorreesburg-Wellington Area" by Rabie (1974a, mapped in 1948) in many aspects.

The core of twelve boreholes, drilled into the Bridgetown Formation by the Department of Environmental Affairs (1983), were made available by the Geological Survey in 1993. The drilling project was part of an engineering-geology feasibility investigation of three alternative sites for the proposed Vogelstruisdrift dam (Van der Merwe, 1983). The boreholes were drilled along three sections. For convenience, they will be referred to as Sites A, B and C. The location of the three sections and

the geology of the area are indicated in Fig. 3.3. Site topography and geology along each section are illustrated in Figs. 3.4, 3.5 and 3.6. The relatively fresh borehole core revealed different greenstone units within the main greenstone body, interlayered with lenses of graphitic schist and dolomite (the different greenstone units are discussed under section 3.2.1.). This contributed significantly towards unravelling the stratigraphy of the Bridgetown Formation.

3.2.1. GREENSTONES

The body of greenstone which outcrops along the Berg River is the main constituent of the Bridgetown Formation. It weathers relatively easily, its position thus probably determined the course of the Berg River in this area (De Villiers, 1969). Outcrops are restricted to the banks of the Berg River and are sometimes exposed in small streams. The main greenstone body is fairly continuous between the farms Vryheid and Winkelhaaksvlei and covers an area of approximately 20km by 1.8km. A few smaller outcrops occur directly northwest of the main greenstone body and will be discussed under the "Spitskop area" (section 3.4.4).

The main greenstone body is lithologically complex, consisting of different greenstone units interlayered with metasedimentary units, and cross-cut by a younger intrusive dyke.

The greenstones have been subjected to low-grade regional metamorphism, namely the lower greenschist facies. Most of the original minerals have been altered to secondary minerals such as chlorite, quartz, albite, calcite, actinolite, epidote, titanite, muscovite, magnetite and ilmenite. The greenstones have experienced more than one deformation event. A dominant penetrative foliation with a general NNW-SSE strike and near-vertical dip is probably coeval with peak regional metamorphism. The greenstone-metasediment contacts are intensely deformed; layers of greenstone alternating with layers of phyllite and graphitic schist.

Ten different greenstone units and a younger intrusive dyke were identified in borehole core and in outcrops. These units will be discussed in vertical order of

Figure 3.3. Locations of boreholes drilled along three sections: Sites A, B and C.

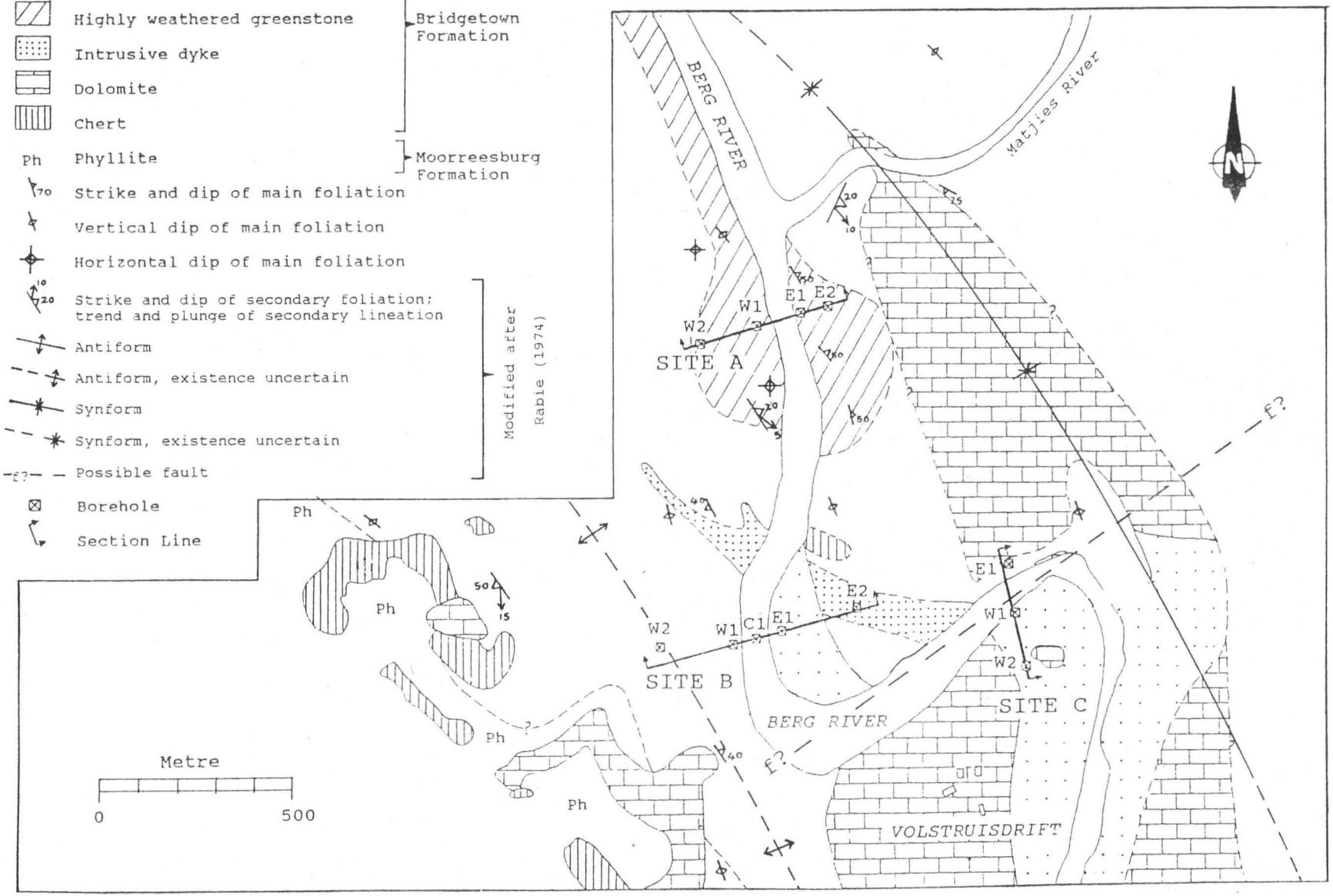

Figure 3.4. Geological cross-section of Site A.

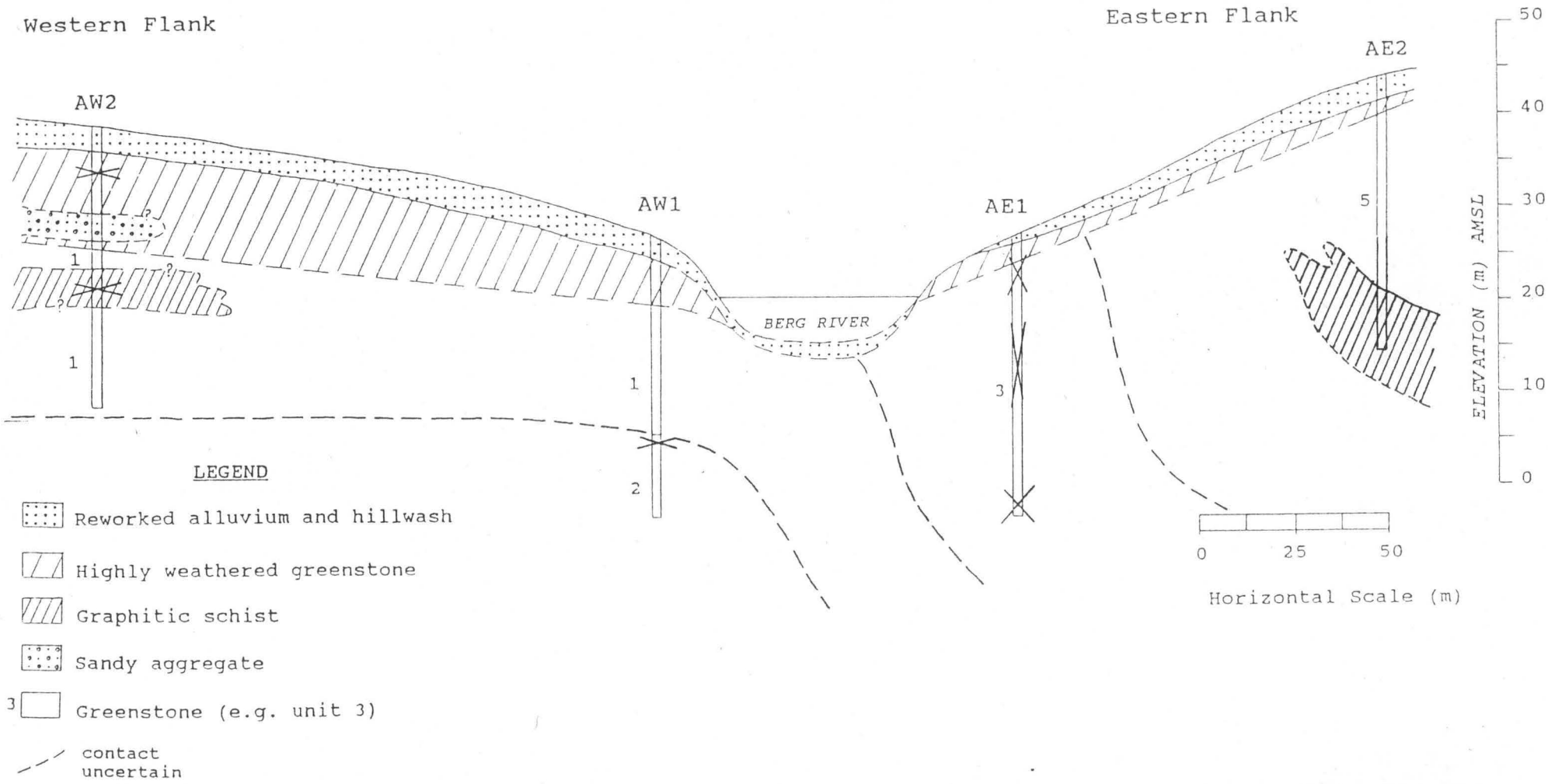

Figure 3.5. Geological cross-section of Site B.

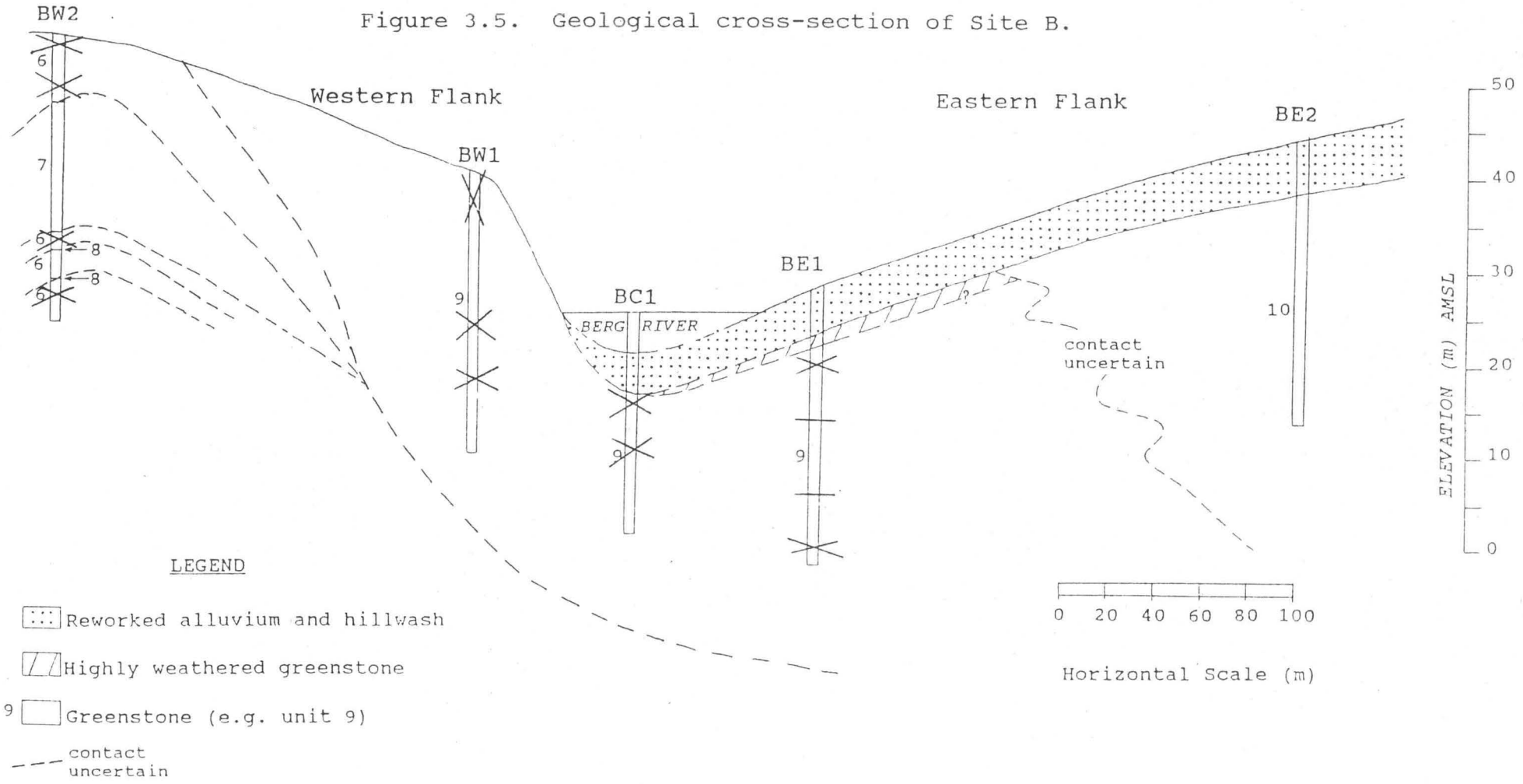

Figure 3.6. Geological cross-section of Site C.

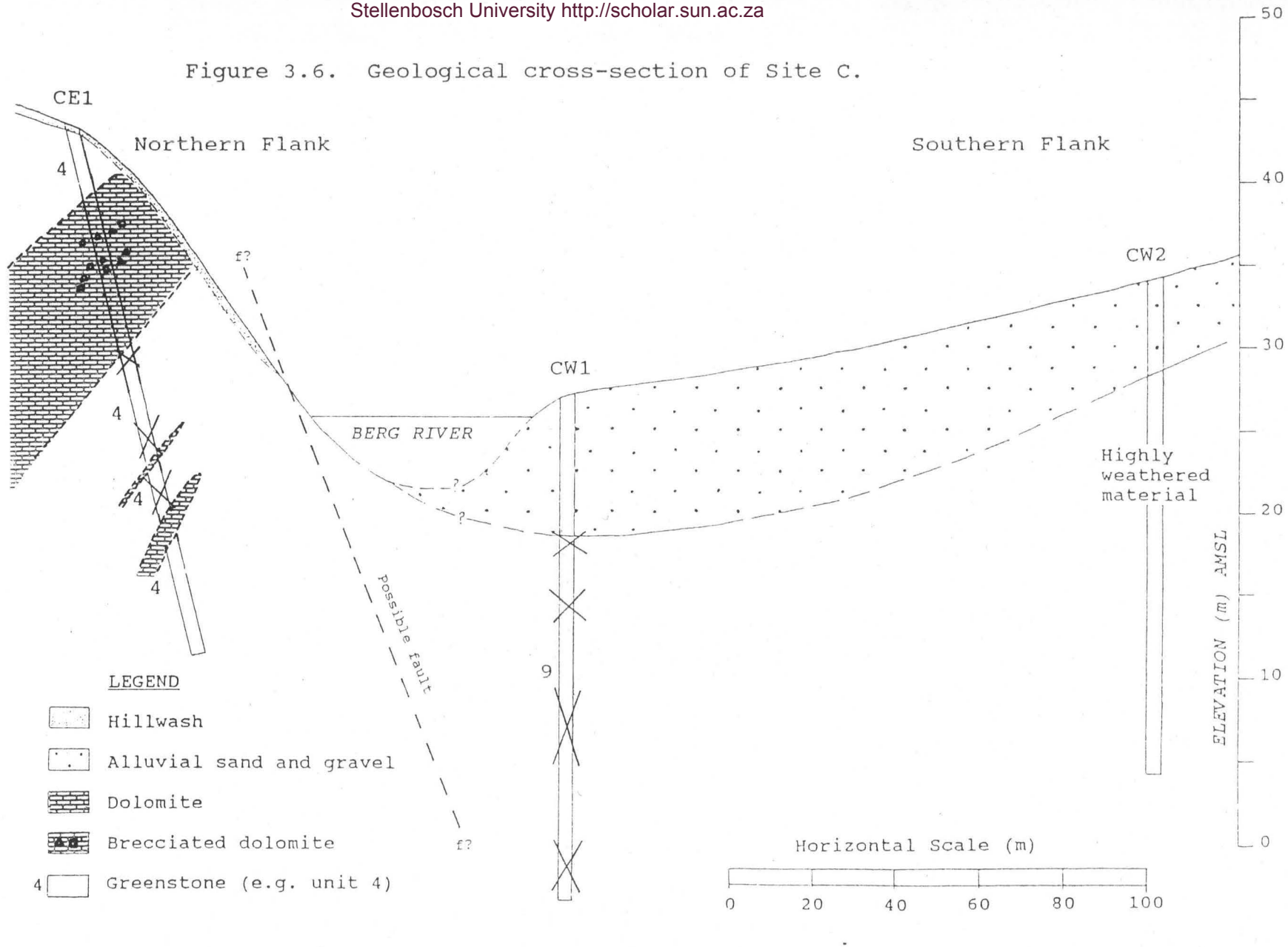

occurrence. A descriptive summary of the different greenstone units and the younger intrusive dyke is also given in Table 3.2.

i) Laminated olive green chlorite-actinolite-magnetite schist (unit 6):

Unit 6 was intersected to a depth of 30m in borehole BW2 which was drilled into the crest of a broad antiform (Figs. 3.3 and 3.5). In borehole BW2 unit 6 is interlayered with units 7 and 8.

Unit 6 is a fine- to medium-grained, dark grey green schist, laminated parallel to the foliation (Plate 3.1).

The unit consists mainly of the following minerals (in decreasing abundance): chlorite, rodded and needle-like actinolite, stringers of magnetite and hematite, calcite, albite (Ab_{94-98}), granular titanite, quartz, epidote and accessory muscovite. These minerals have been segregated into alternating dark green, black, light green and white lamellae as well as white and pink speckles and lenses. The black lamellae have a very high opaque mineral content and the green lamellae consist mainly of chlorite, actinolite and titanite in varying proportions. The light lamellae, speckles and lenses are made up mainly of calcite with minor quartz. Some calcite-rich lamellae and lenses often contain porphyroblasts of anhedral to euhedral epidote (Plate 3.2).

The lamellae are slightly contorted and their distribution and width vary considerably. The opaque-rich lamellae are usually intensely deformed and contain plenty irregular fine- to coarse grained calcite and quartz inclusions. The following microstructures indicate a history of deformation: a) undulose extinction in quartz, b) deformation twins in calcite, c) fragmented crystals, d) subgrain development in quartz-rich lenses and e) ribbon quartz.

A 5m wide zone in unit 6 contains dark grey to purple lenses that are less than 1.5cm wide, contain black magnetite and white calcite-quartz speckles, and are elongated parallel to the foliation.

Table 3.2. A descriptive summary of the different greenstone units and the younger intrusive dyke.

Name	cl-ac-mn schist	cl-ab-ti schist	ab-ep-mn-cl-ac fels	ep-ac-cl schist	cl-mn-ac schist	cl-ab-mn-cc schist	cl-cc-q-ac schist	cl-ac-mn-cc schist	ep-ac-ti-cl schist	q-or-bt-mus fels	intrusive au-ac metabasite
Unit	6	8	7	9	4	2	1	3	11	5	10
Location	Bh BW2	Bh BW2	Bh BW2	Bh BW1, BC1, BE1 & CW1	Bh CE1	Bh AW1	Bh AW1 & AW2	Bh AE1	Drie Heuwels	Bh AE2	Bh BE2
Colour	dark grey green	light olive green	dark green (maroon tint)	olive green	olive to grey green	dark grey	light khaki	dark grey green	olive green	light grey green to light brown	olive green
Texture	-fine to medium grained -laminated parallel to the foliation	-fine grained -homogeneous	-medium grained -homogeneous	-fine grained -alternating highly and poorly laminated zones	-fine grained -laminated parallel to the foliation	-fine grained -laminated parallel to the foliation	-fine grained -alternating highly and poorly laminated zones	-fine grained -laminated parallel to the foliation	-medium grained -homogeneous	-coarse grained -homogeneous	-medium to coarse grained -homogeneous
Structure	foliated	foliated	-relatively massive -have experienced brittle deformation	-foliated -foliation is highly contorted in places	-foliated -foliation is intensely deformed and sheared	foliated	highly schistose	foliated	relatively massive, poorly foliated	massive	relatively massive, poorly foliated
Mineralogy ** major, * minor and - accessory minerals	ab* ac** ep* cc* cl** ti* q* mn** he* mus -	ab* cl** ti* q* mn* af*	ab** ac** ep** cc - cl** ti* q* mn** he*	ab* ac** ep** cc* cl** ti* q* mn* mus -	ab* ac** ep* cc* cl** ti* q* mn**	ab** ac* ep - cc** cl** ti* q* mn** il*	ab* ac* ep - cc** cl** ti - q* mn* il - mus -	ab* ac** ep* cc** cl** ti* q* mn** il -	ab* ac** ep** cc - cl* ti* q* mn* il*	 ac - cc - cl* q** mn* mus* or** bt**	la - ac** ep - cc - cl* ti - q - mn* il - au**
Micro textures (minerals in decreasing abundance)	-alternating black, green and white lamellae and lenses -black lamellae: mainly mn -green lamellae: cl, ac, ti, mus -light lamellae and lenses: cc and minor q	crypto-crystalline ab, q, af and slightly larger ti and mn are surrounded by cl	randomly oriented porphyroblasts of ab and ep in a groundmass of mn, cl, ac, ti and q	-alternating dark and light lamellae and lenses -dark lamellae: ep, ac, cl, mn and ti -light lamellae and lenses: cc and minor q	-alternating dark and light lamellae and lenses -dark lamellae: cl, ac, mn, ti -light lamellae and lenses: cc, ab and minor q and ep -shear zones: porphyroclasts of cc, q and ab in an ultra-fine cc matrix	-alternating dark and light lamellae and lenses -dark lamellae: cl, ac, mn and il which envelope porphyroblasts of ab, cc, ep and ti -light lamellae and lenses: -mainly cc and q -a few large ti granules with ilmenite rims occur in some lenses	-alternating dark green, light grey, and cream to white lamellae (graded bedding?) -dark green zones: cl, ac, mn, ti, q, cc, ab, mus, ep -light grey lamellae: q -white to cream lamellae: cc	-alternating dark and light lamellae and lenses -dark lamellae: cl, ac, mn, ab, cc, q, ti and il which envelope ep augen -light lamellae and lenses: mainly cc with minor q and ep	-light lenses occur in an olive green foliated groundmass -groundmass: ep, ac, mn, ti, cl, il, q, ab -light lenses: ep, q, ac, cl, ab	-minerals are randomly oriented -bt occurs as laths -q occurs as polygonal aggregates -or is anhedral with numerous inclusions of cl, ac, cc and mn	-phenocrysts of augite are enveloped by a foliated groundmass of ac, cl, mn and accessory ep, il, ti, cc and q -augite contains big labradorite crystals (ophitic texture) -ac fibres and cl occur at the augite grain boundaries
Superimposed veins	plenty irregular q-cc stringers and speckles	a few small q-cc veins	-plenty irregular q-cc inclusions -contain pink cc veins (up to 20cm wide) and green epidote bands (up to 30cm wide)	-plenty q-cc veins in highly laminated zones -some veins contain pink cc	-plenty -irregular white and pink cc stringers occur along shear faces	-plenty -three ages of q-cc veins	-plenty -three ages of q-cc veins	-few -two ages of q-cc veins - cc is white and pink	a few q-cc veins	a few small q-cc veins	a few q-cc and plagioclase veins
Mineralization	no visible mineralization	no visible mineralization	no visible mineralization	no visible mineralization	pyrite mineralization is restricted to the greenstone-dolomite contacts	well-mineralized with pyrite	well-mineralized with pyrite	euhedral disseminated pyrite occurs in a 1m wide altered zone	a few disseminated pyrrhotite grains	pyrite mineralization is restricted to the greenstone-graphitic schist contact	a few disseminated pyrite grains

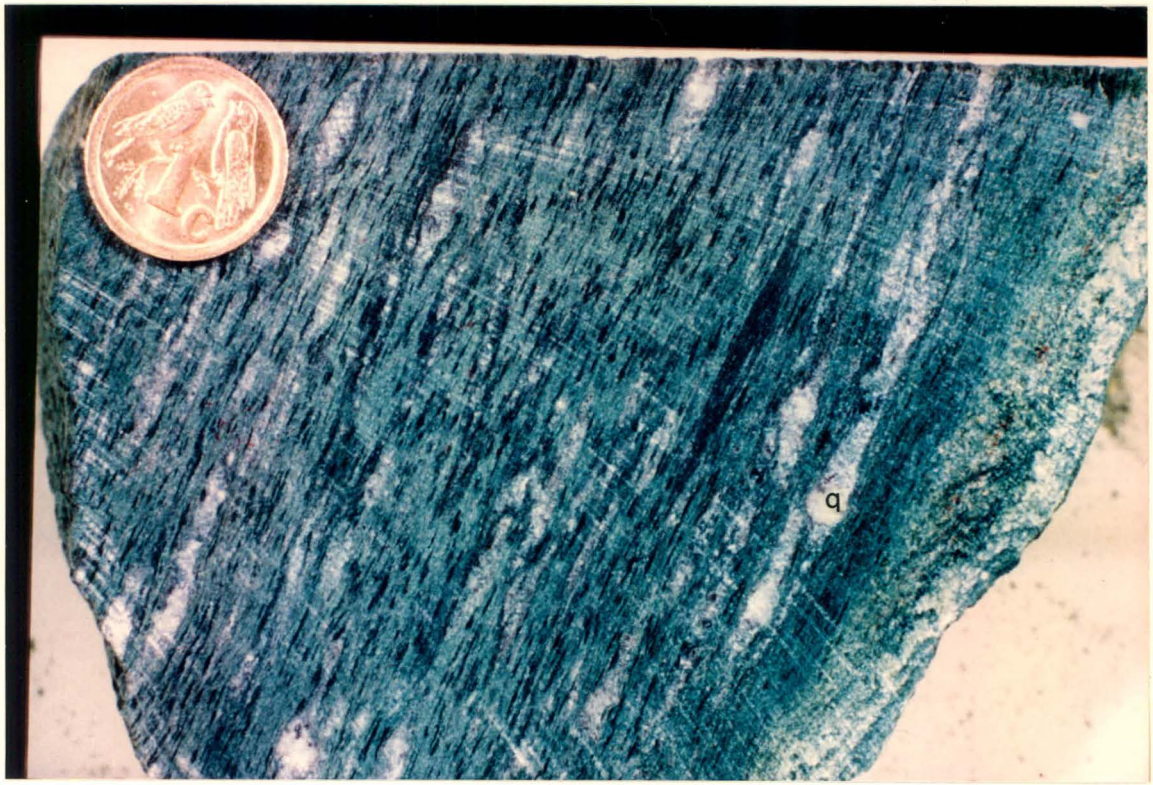

Plate 3.1 Laminated olive green chlorite-actinolite-magnetite schist (unit 6).

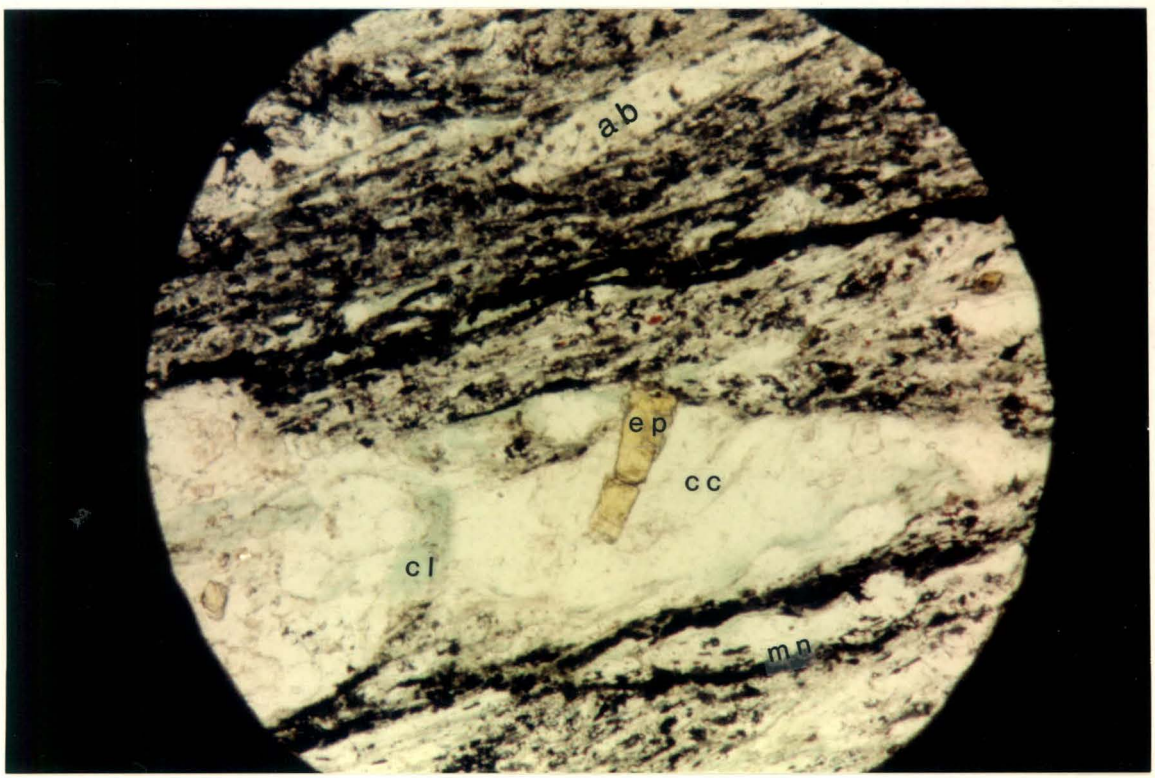

Plate 3.2 Unit 6. A calcite-rich lens containing anhedral to euhedral porphyroblasts of epidote. Plane light.

ii) Light olive green chlorite-albite-titanite schist bands (unit 8):

Unit 8 occurs as two small zones, less than 20cm wide, within unit 6 (borehole BW2, Fig. 3.5). These two zones are light olive green, fine grained, foliated and relatively homogeneous except for a few small (less than 3mm wide) quartz-calcite lamellae and lenses parallel to the foliation (Plate 3.3).

Unit 8 consists of titanite, magnetite, chlorite and cryptocrystalline albite, minor quartz and accessory alkali feldspar (Plate 3.4). The titanite granules are anhedral and have a foggy appearance. The light lamellae and lenses consist of fine- to coarse-grained calcite and accessory quartz. These lenses have suffered some degree of deformation as indicated by deformation twins in the calcite and undulose extinction in the quartz.

A 5cm dark grey green (magnetite-rich) zone occurs at the contact between unit 8 and 6 (Plate 3.3).

iii) Porphyroblastic albite-epidote-magnetite-chlorite-actinolite fels (unit 7):

Unit 7 occurs as a highly altered 14 metre wide zone within unit 6 (borehole BW2, Fig. 3.5). It is medium grained, poorly foliated and dark green with a maroon tint. Irregular secondary light green epidote bands, quartz-calcite stringers and speckles, and pink calcite veins (up to 20 cm wide) occur along joints and shear faces (Plate 3.5). Large pink calcite veins and lenses are not restricted to unit 7 and have been found in a highly foliated greenstone outcrop on the farm Vogelstruisdrift.

The epidote bands are up to 30cm wide and are associated with zones of brittle deformation where brecciated hostrock is enclosed in a light green mass of epidote.

The more homogeneous zones consist of porphyroblasts of albite (Ab_{99}) and epidote in a groundmass of chlorite, actinolite, magnetite, hematite, and minor titanite and quartz (Plate 3.6). The albite occurs as randomly orientated subhedral laths, usually enveloped by magnetite. The epidote grains vary from fine to coarse grained and anhedral to euhedral. They are often surrounded by a reaction rim of chlorite and magnetite. Actinolite occurs as very small randomly orientated rodded

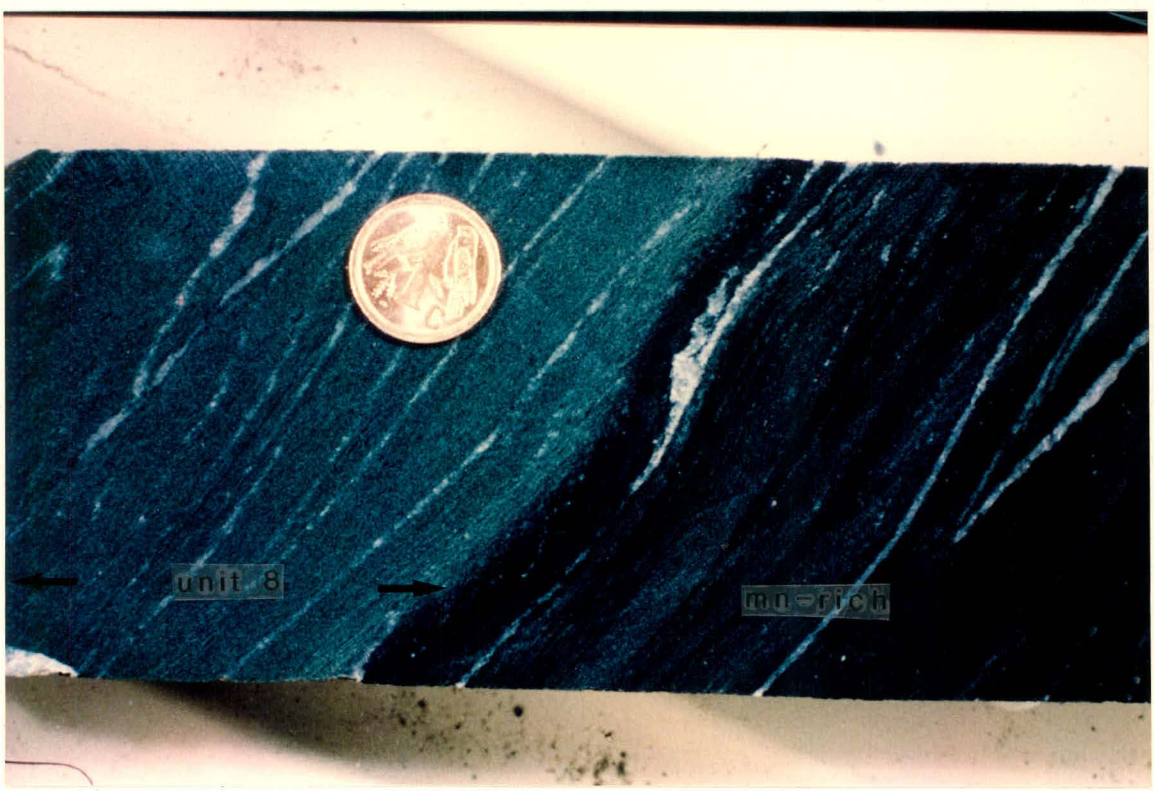

Plate 3.3 Light olive green chlorite-albite-titanite schist bands (unit 8).

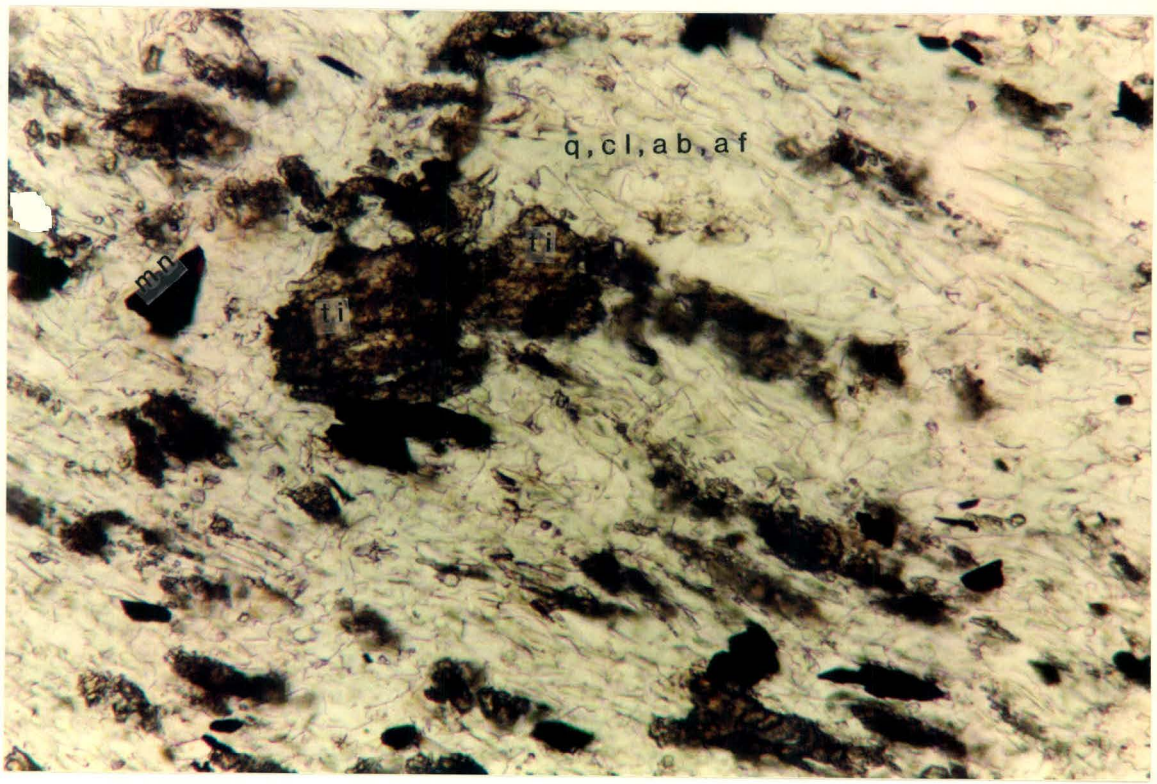

Plate 3.4 Unit 8. A fine-grained foliated rock which consists of titanite, magnetite, chlorite and microcrystalline quartz, albite and accessory alkali feldspar. Plane light.

Plate 3.5 Porphyroblastic albite-epidote-magnetite-chlorite-actinolite fels (unit 7).

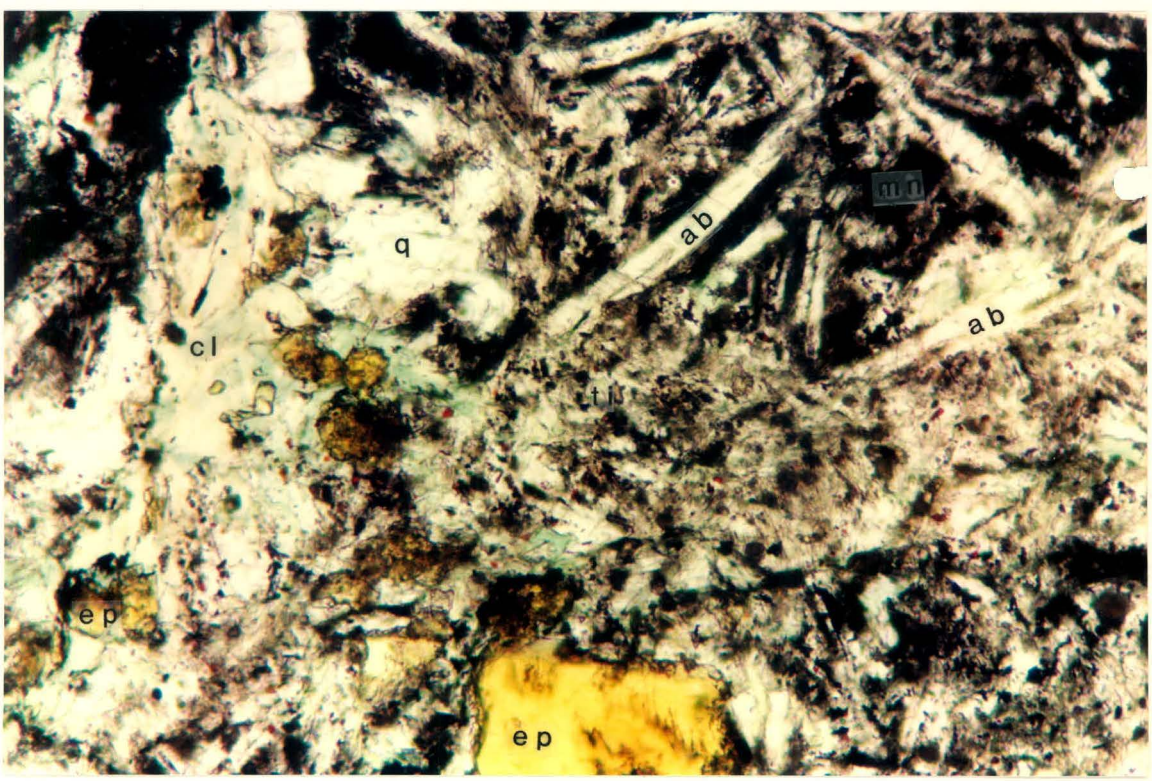

Plate 3.6 Unit 7. Porphyroblasts of albite and epidote in a groundmass of chlorite, titanite, actinolite, magnetite, hematite and quartz. Plane light.

and needle-like crystals. The maroon tint in unit 7 is due to the presence of finely dispersed hematite grains. The quartz is anhedral and displays undulose extinction.

Unit 7 was probably subjected to metasomatism, after regional metamorphism, as indicated by its coarse-grained nature, randomly orientated minerals, and secondary epidote and calcite bands along joints and shear zones.

iv) Laminated olive green epidote-actinolite-chlorite schist (unit 9):

Unit 9 was intersected in boreholes BW1, BCI, BE1 and CW1 (Figs. 3.3, 3.5 and 3.6). From these boreholes it is concluded that unit 9 has a minimum stratigraphic thickness of 30 metres.

Unit 9 is a fine-grained olive green rock which consists of alternating highly and poorly laminated zones (Plate 3.7). The poorly laminated zones are olive green, poorly foliated and relatively homogeneous. The highly laminated zones are laminated with light green, black, dark green and white lamellae and lenses parallel to the foliation. The lamellae are highly contorted in places and the width and distribution of individual lamellae vary considerably in this zone.

The poorly laminated zones consist mainly of the following minerals in decreasing abundance: granular epidote, rodded and needle-like actinolite, chlorite, stringers of anhedral magnetite; minor titanite, quartz, calcite, muscovite and albite (Plate 3.8). In the highly laminated zones these minerals have been segregated into alternating dark and light lamellae. The darker the lamellae, the higher the opaque mineral content. White lamellae and lenses consist mainly of fine-grained anhedral calcite and minor quartz. Unit 9 has a very high epidote content which occurs as fine- to coarse-grained anhedral granules and euhedral crystals. The anhedral epidote granules sometimes contain inclusions of titanite and ilmenite. The epidote has a foggy appearance due to the presence of leucoxene which is an alteration product of ilmenite.

A few highly altered zones in unit 9 are mineralogically similar to unit 7, consisting of randomly orientated porphyroblasts of albite and epidote, enveloped by magnetite and actinolite with minor hematite, titanite, chlorite and quartz.

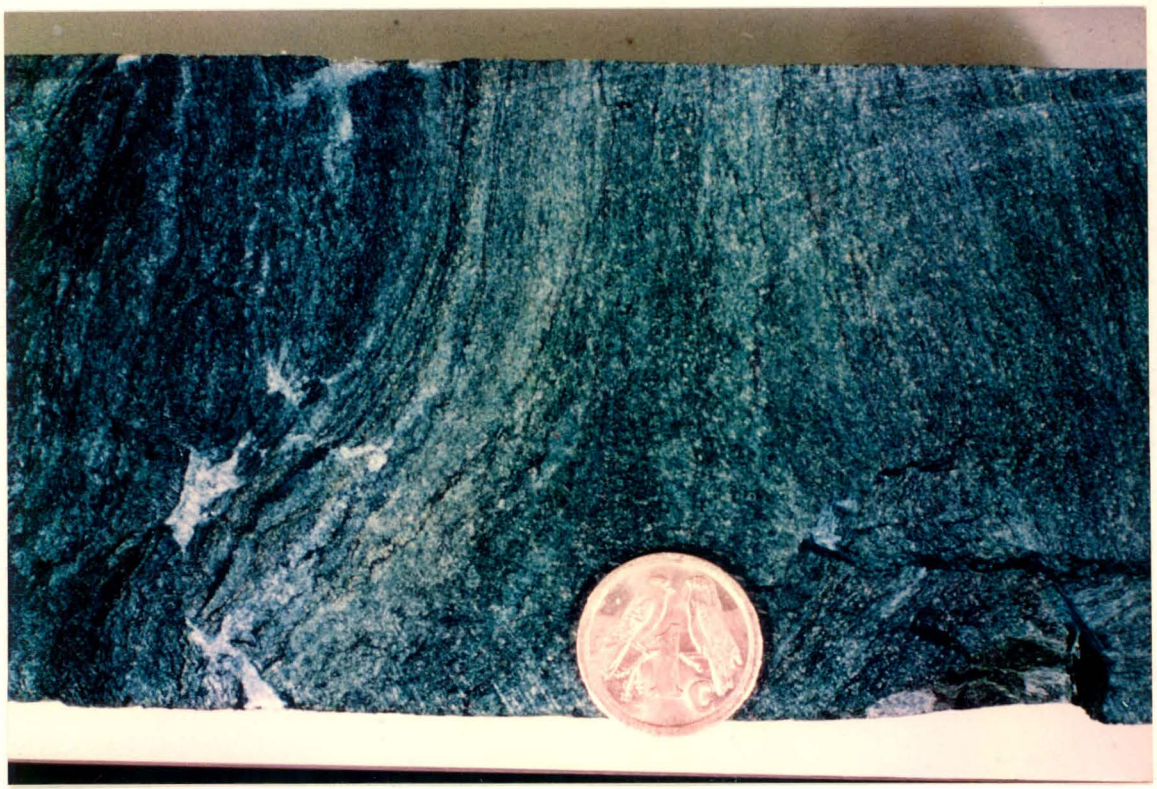

Plate 3.7 Laminated olive green epidote-actinolite-chlorite schist (unit 9).

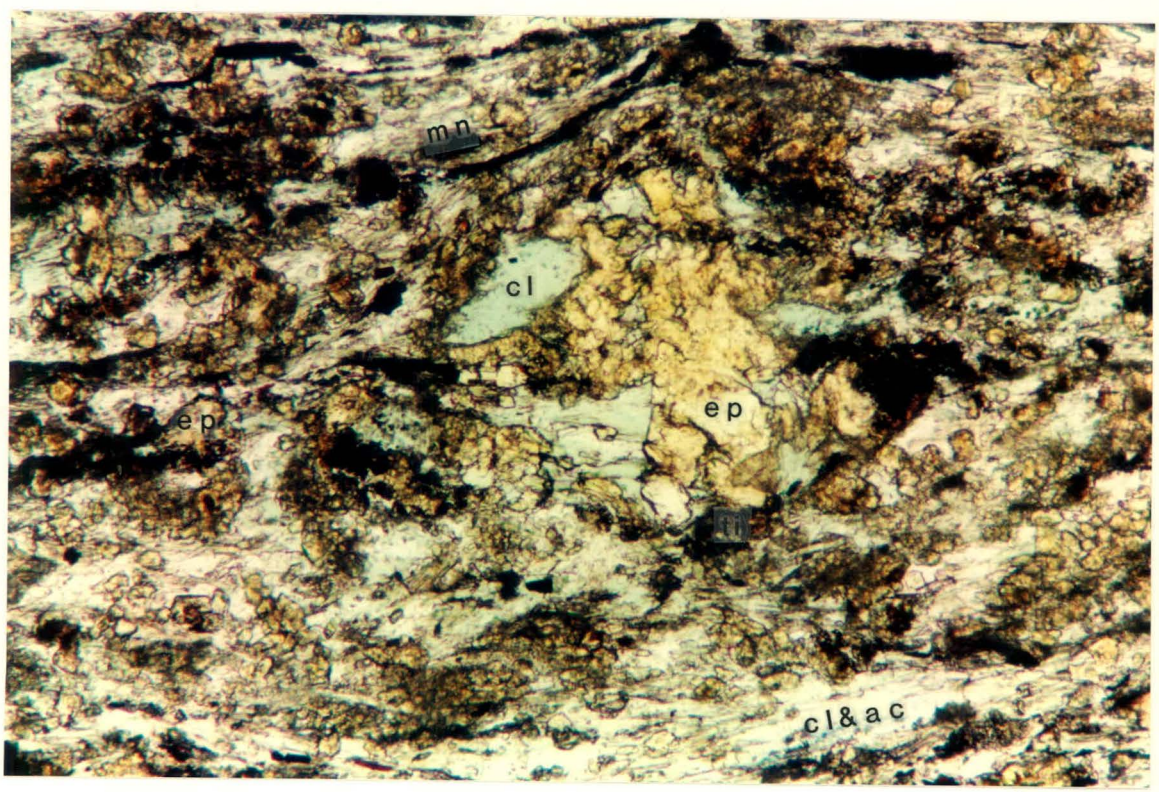

Plate 3.8 Unit 9. A fine-grained laminated rock which consists of granular epidote, actinolite, chlorite, magnetite and minor titanite, quartz, calcite, muscovite and albite.

Jaspilite lenses, less than 20cm wide, are present in outcrops of unit 9 in the vicinity of borehole collar BW1.

v) Highly sheared, finely laminated olive green chlorite-magnetite-actinolite schist (unit 4):

Unit 4 was intersected in borehole CE1 up to a depth of 45 metres (Figs. 3.3 and 3.6). In borehole CE1 the greenstone is in contact with a few dolomite lenses, of which one is 13m wide and the others less than 1m wide.

Unit 4 is olive to grey green, fine grained, highly foliated and finely laminated with dark olive green and light lamellae and lenses. The dark lamellae are made up mainly of chlorite, small rodded and needle-like actinolite, fine-grained cubic magnetite and minor titanite. The light lamellae and lenses consist of anhedral calcite, albite, minor quartz and accessory epidote.

The lamellae have been subjected to more than one episode of folding and shearing (Plate 3.9). Overall the greenstone has suffered intense deformation which is probably related to local faulting. Irregular white and pink calcite stringers occur along shear faces. These inclusions have also been subjected to later shearing events. The shear zones are irregular and mylonitic, consisting of porphyroclasts of calcite, quartz and albite in an ultra fine-grained matrix of calcite (Plate 3.10). Other indicators of shearing in unit 4 is the presence of S-C fabrics and mica-fish structures on microscopic scale. The S-C fabric involves the intersection of two cleavages S and C. The C surfaces are parallel to the shear zone margin whilst the S-surface are oblique to this (Barker, 1989). This give rise to a texture which is commonly described as fish-scale. Mica-fish are lozenge-shaped structures which involves the deformation of pre-existing porphyroblasts which are deformed by a combination of brittle and crystal-plastic processes (Barker, 1989).

The greenstone-dolomite contacts are irregular but sharp and the greenstone is laminated parallel to the contacts. Greenstone adjacent to the contacts is highly altered. It is light olive green with numerous yellow-brown lamellae which include fine-grained pyrite. The contacts are probably tectonic and the small dolomite lenses appear to have been injected into the greenstone during plastic deformation.

Plate 3.9 Highly sheared, finely laminated olive green chlorite-magnetite-actinolite schist (unit 4).

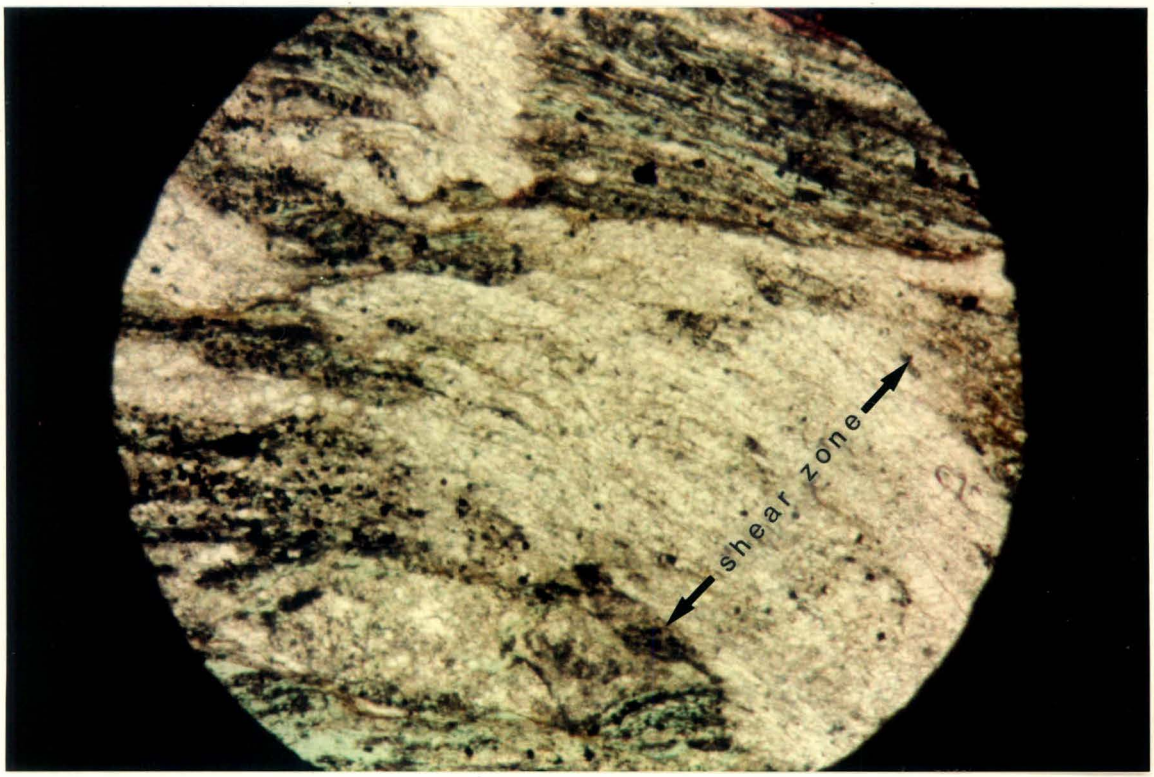

Plate 3.10 Unit 4. A well-developed continuous cleavage is intensely deformed by shearing. Plane light.

vi) Laminated dark grey chlorite-albite-magnetite-calcite schist (unit 2):

Unit 2 is in contact with unit 1 in borehole AW1 (Figs. 3.3 and 3.4) at a depth of 21 metres. It is fine grained and dark grey with light grey to white lamellae and lenses (width <1cm) parallel to the foliation (Plate 3.11). The distribution and concentration of the light lamellae and lenses vary throughout unit 2.

The dark grey zones consist of stringers of chlorite, small rodded and needle-like actinolite, anhedral magnetite and accessory ilmenite. These stringers envelope aligned porphyroblasts of anhedral albite (Ab_{96-99}), calcite and accessory epidote and titanite. The light lamellae and lenses consist mainly of calcite and quartz with accessory albite, titanite, ore minerals, chlorite and actinolite. The calcite and quartz are anhedral, fine to coarse grained and show signs of deformation such as deformation twins in calcite and undulose extinction in quartz. A few relatively large subhedral titanite granules with ilmenite rims occur in the light areas (Plate 3.12).

Unit 2 is mineralized with pyrite which occurs as disseminated anhedral grains (maximum diameter of 5mm) and stringers parallel to the foliation. The pyrite mineralization is not associated with superimposed calcite veins.

A few shear zones, 10 to 30cm wide, are present in unit 2. These zones have a light khaki colour due to alteration, and lamellae are highly contorted and brecciated. One of these shear zones occurs on the contact between units 1 and 2.

vii) Laminated light khaki chlorite-calcite-quartz-actinolite schist (unit 1):

Greenstone unit 1 was intersected in boreholes AW1 and AW2 (Figs. 3.3 and 3.4). It has been subjected to severe weathering to depths of up to 15 metres. Relatively fresh greenstone is fine grained, light khaki, stained brown and laminated parallel to the foliation with dark green, light grey, cream and white lamellae. Some zones are highly laminated (Plate 3.13) and others are only slightly laminated (Plate 3.14).

The dark green zones are mainly composed of chlorite, small rodded and needle-like actinolite, anhedral magnetite; minor titanite, quartz, calcite and albite; and

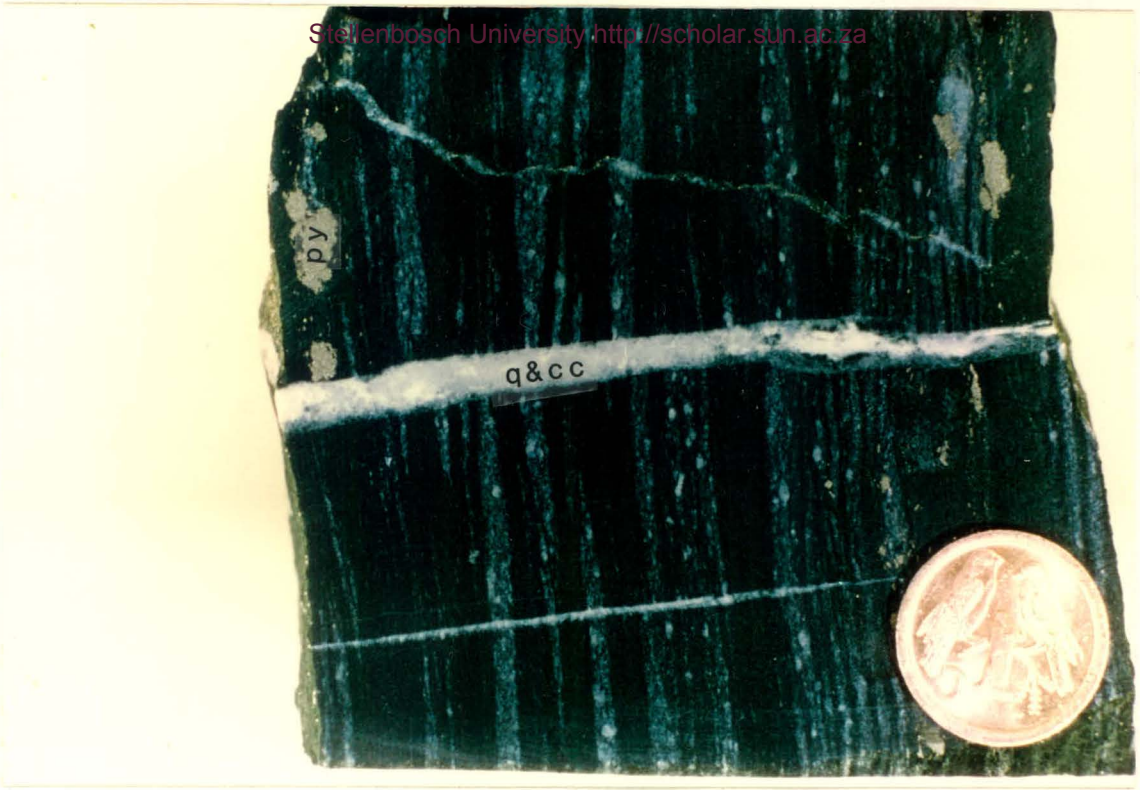

Plate 3.11 Laminated dark grey chlorite-albite-magnetite-calcite schist (unit 2).

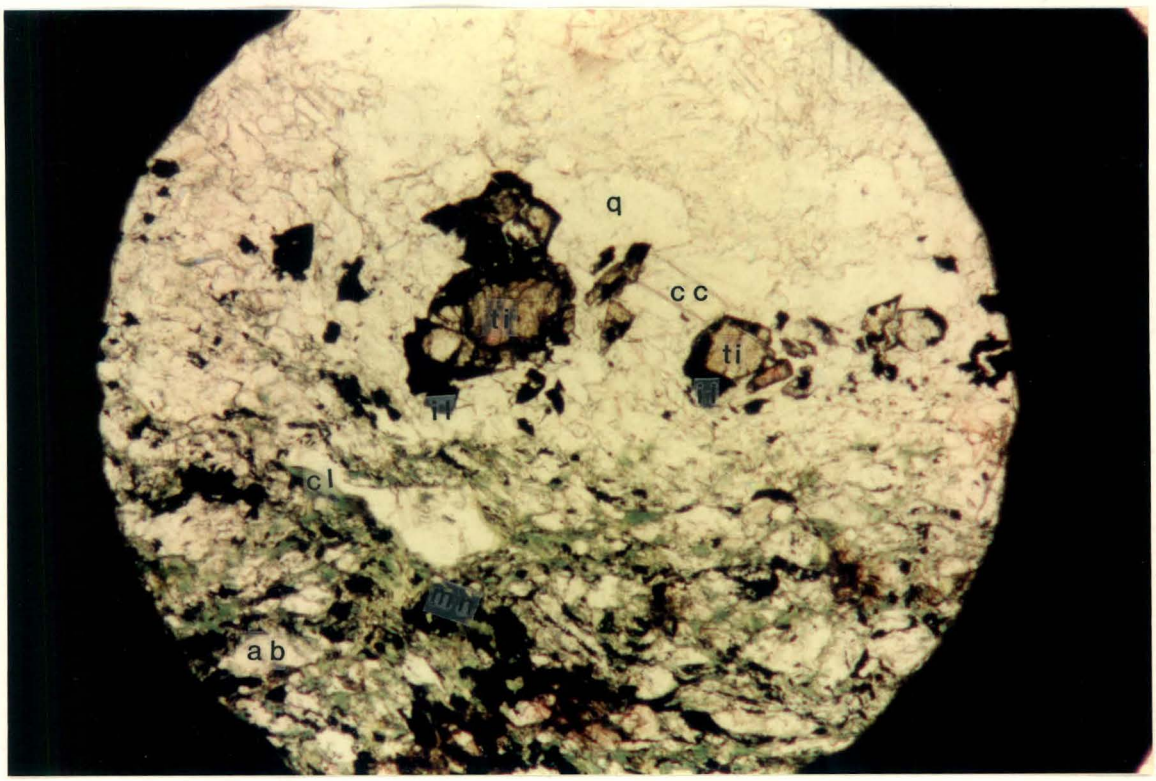

Plate 3.12 Unit 2. The lower half of the photomicrograph represents dark lamellae consisting of chlorite, actinolite, titanite and magnetite which envelope porphyroblasts of albite and calcite. The upper half of the photomicrograph represents light lamellae which are made up of calcite and quartz. A few large brown titanite granules with ilmenite rims occur in the light areas. Plane light.

Plate 3.13 Highly laminated light khaki chlorite-calcite-quartz-actinolite schist (unit 1).

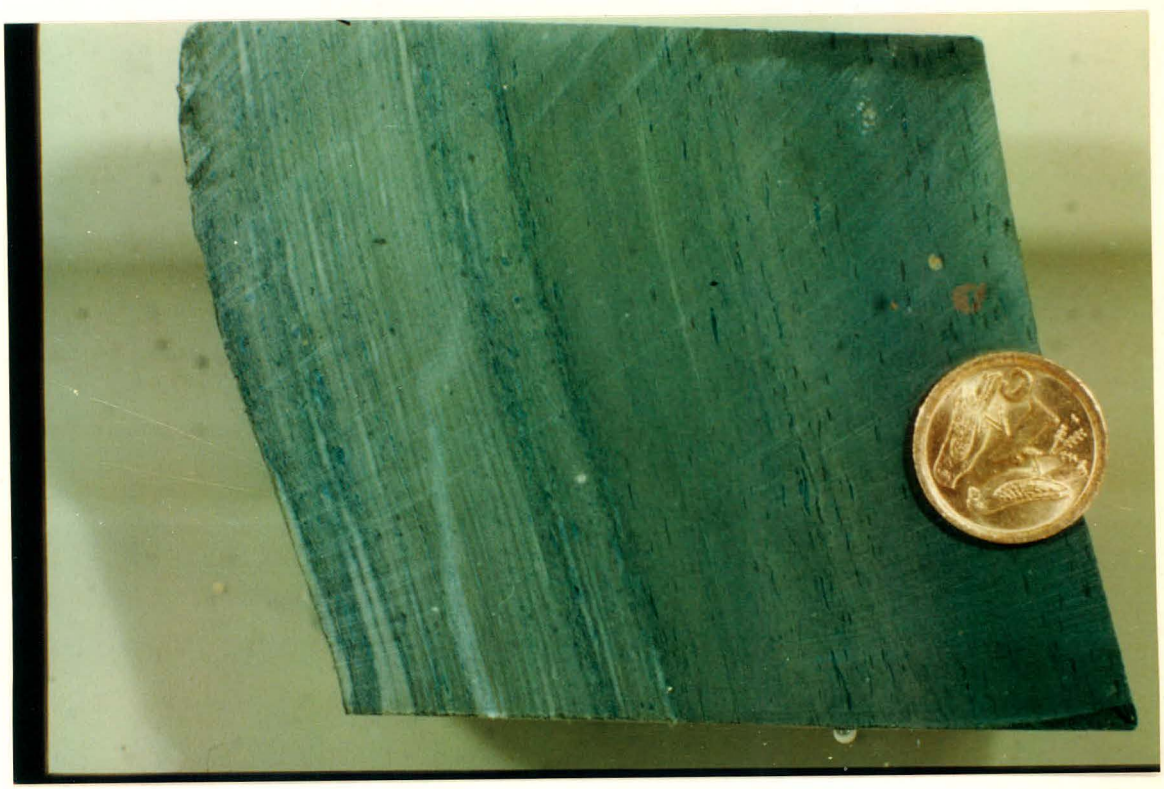

Plate 3.14 Poorly laminated light khaki chlorite-calcite-quartz-actinolite schist (unit 1).

accessory muscovite and epidote (Plate 3.15). The light grey lamellae consist mainly of quartz and the white to cream lamellae of calcite.

The highly laminated zones contain more quartz- and calcite-rich lamellae than the poorly laminated zones. In the highly laminated regions the lamellae appear to grade from dark green chlorite-rich lamellae into cream coloured calcite-rich lamellae, to grey quartz-rich lamellae. These laminated textures (graded bedding?) are often associated with waterlain tuffs (Heiken and Wohletz, 1985) as well as downwind air-fall deposits of surtseyan volcanic activity where water floods into the top of an open vent (Cas and Wright, 1987).

Some highly laminated zones have been subjected to shearing causing brecciation and severe contortion of the lamellae.

Pyrite mineralization occurs through the whole of unit 1, but is especially concentrated in calcite-rich lamellae, on joint faces, in shear zones and along vein margins.

A graphitic schist lens occurs within unit 1. The contacts are sharp and the greenstone on the contacts are highly to moderately weathered, containing abundant pyrite.

Unit 1 shows some correlation with a few outcrops on the farms Gousblomkraal, Vogelstruisdrift, Rooihoogte and Vrugbaar (Sheet A) which consist of alternating layers of banded phyllite with chert and graphitic schist lenses. Rabie (1974a) mapped some of these outcrops as tuffs or volcanic ashes.

viii) Dark olive green augen chlorite-actinolite-magnetite-calcite schist (unit 3):

Unit 3 was intersected in borehole AE1 (Figs. 3.3 and 3.4). A great part of the borehole was drilled subparallel to the foliation and lamination, thus revealing little variation in the greenstone.

The greenstone is dark grey green, fine grained and laminated parallel to the foliation with white lamellae, lenses and speckles (Plate 3.16). The density of the lamellae vary throughout the unit.

The dark grey green zones consist of the following minerals in decreasing abundance: chlorite, rodded and needle-like actinolite, anhedral stringers of

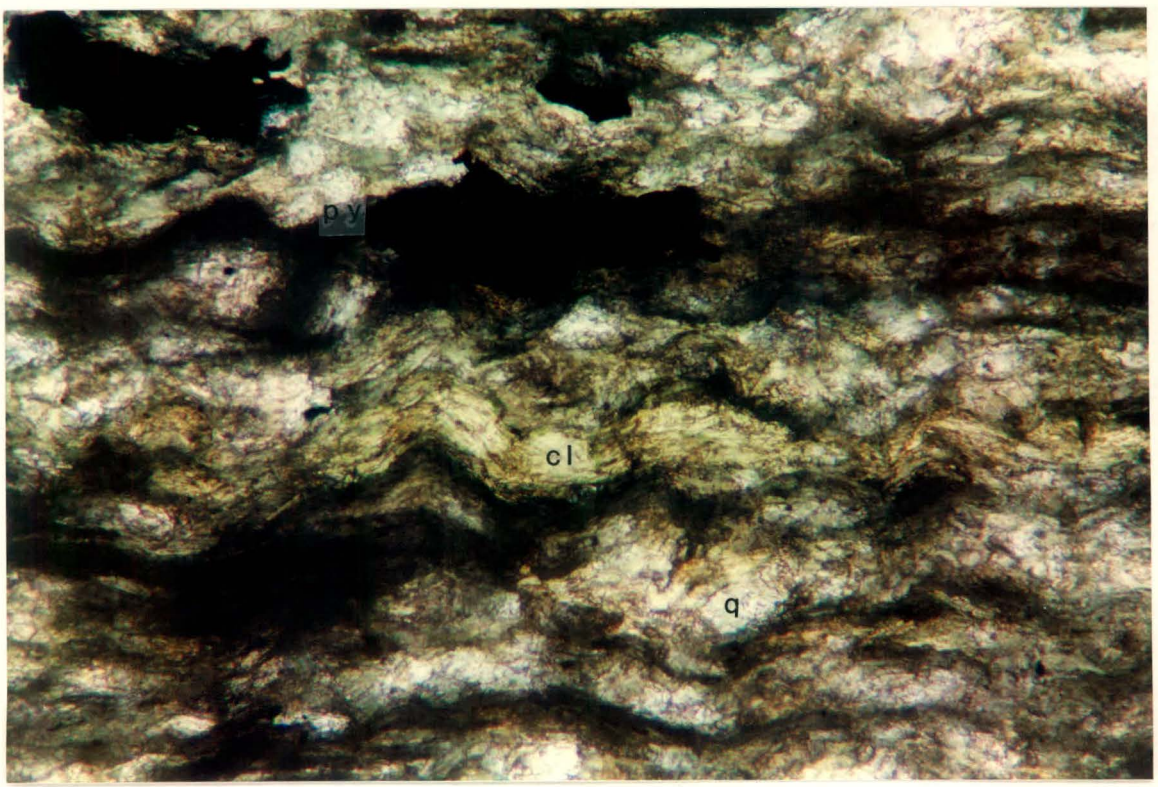

Plate 3.15 Unit 1. Poorly laminated dark green zone, consisting of chlorite, actinolite, magnetite; minor titanite, quartz, calcite and albite; and accessory muscovite and epidote. Plane light.

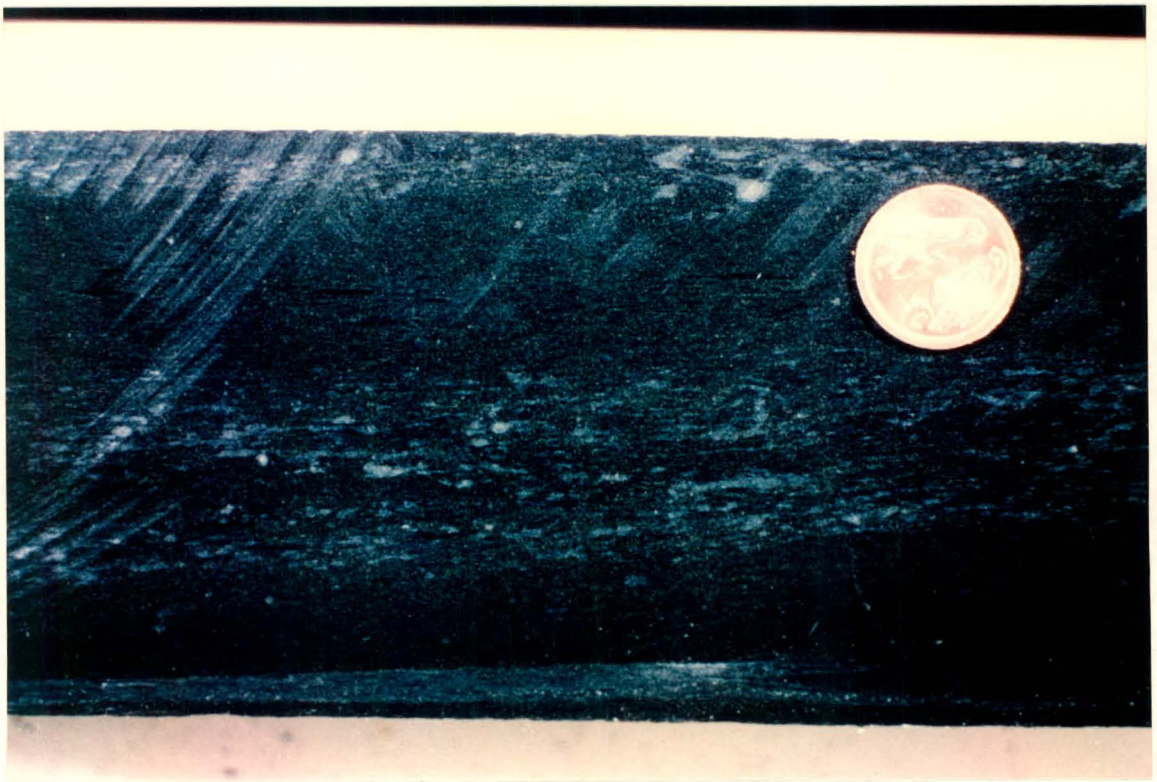

Plate 3.16 Dark olive green augen chlorite-actinolite-magnetite-calcite schist (unit 3).

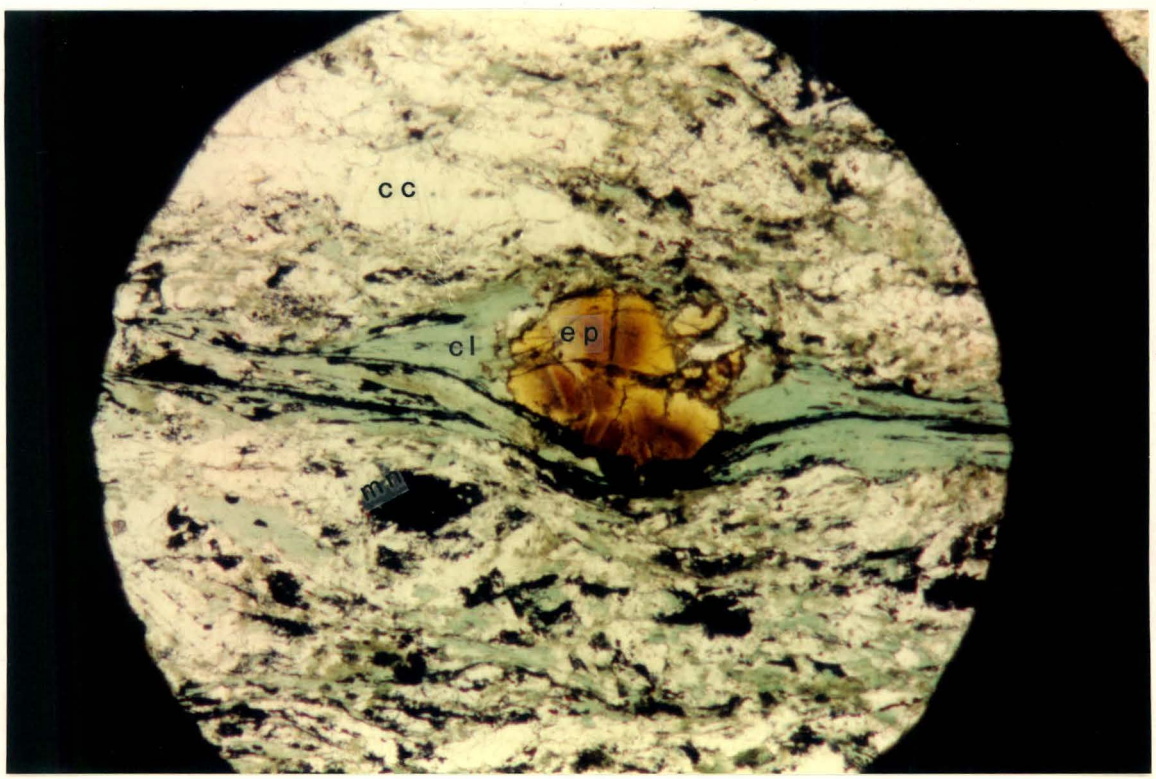

Plate 3.17 Unit 3. An anhedral porphyroblast of epidote enveloped by the schistose chlorite-actinolite-magnetite mineral fabric to give an 'augen' texture. Plane light.

magnetite, albite (Ab_{97-99}), calcite, quartz, small granules of titanite and accessory ilmenite. A few relatively large anhedral porphyroblasts of epidote are enveloped by the schistose chlorite-actinolite-magnetite mineral fabric to give a "augen" texture (Plate 3.17). In some samples these "augen" also include calcite, albite, quartz and accessory actinolite and magnetite. The light lamellae and lenses consist mainly of calcite with minor quartz and epidote.

A few highly altered zones also include light green epidote bands. Some of the altered zones have been subjected to intense deformation as can be deduced from isoclinal folded lamellae and the development of crenulation cleavage with gradational boundaries.

Pyrite mineralization is restricted to a 1m wide altered zone with thin khaki lamellae. Euhedral pyrite is disseminated throughout the zone and appears to be younger than the foliation.

ix) Olive green epidote-actinolite-titanite-chlorite schist (unit 11):

Unit 11 outcrops at the farm Drie Heuwels where it is overlain by dolomite (Sheet A, samples NSF/2.5-2.8). In hand specimen it is olive-green, medium grained and massive with only a poor foliation and no visible lamellae (Plate 3.18).

Although poorly foliated in hand specimen, a well-developed continuous cleavage is recognizable in thin section. Light lenses occur in an olive green foliated groundmass. The lenses contain anhedral granular epidote, quartz, small rodded and needle-like actinolite, chlorite and albite (in decreasing abundance, Plate 3.19). Some epidote grains contain small titanite inclusions. The darker foliated groundmass contain additional granular titanite and opaque stringers which consist of ilmenite and magnetite.

Unit 11 contains a few disseminated euhedral pyrrhotite grains.

Unit 11 might be correlated with a poorly foliated greenstone outcrop on the other side of the Berg River on the farm Heuningberg.

Plate 3.18 Olive green epidote-actinolite-titanite-chlorite schist (unit 11).

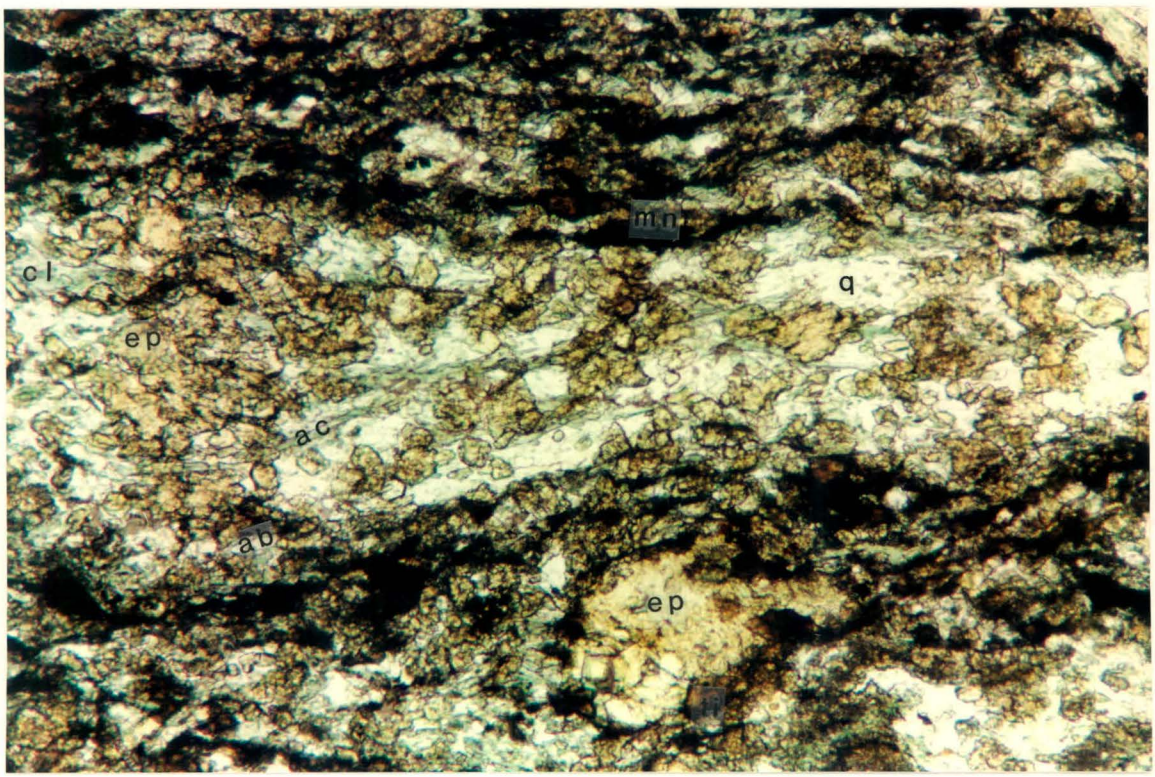

Plate 3.19 Unit 11. The light zone in the middle of the photomicrograph consists of granular epidote, actinolite, quartz, chlorite and albite. The darker zones contain additional titanite, magnetite and ilmenite. Plane light.

x) Light grey green quartz-orthoclase-biotite-muscovite fels (unit 5):

Unit 5 was intersected in borehole AE2 (Figs. 3.3 and 3.4). The greenstone is highly to moderately weathered, coarse grained, relatively massive with little evidence of foliation and lamination. It is light grey-green to light brown with a porphyroblastic texture (Plate 3.20). White micas are abundant in the highly weathered zones.

It consists mainly of quartz, orthoclase (Or_{93-97}), biotite, muscovite and minor chlorite, calcite, actinolite and magnetite (Plate 3.21). Biotite occurs as randomly orientated tabular laths with inclusions of magnetite. Although the biotite laths show no alignment, they were subjected to some degree of strain which led to kinking of some biotite crystals. The quartz occurs as polygonal aggregates and stabby laths which is probably the product of metamorphic recrystallization. The orthoclase is anhedral and appears turbid due to numerous inclusions of chlorite, small rodded and needle-like actinolite, calcite and magnetite.

Unit 5 is in contact with graphitic schist in borehole AE2 (Fig. 3.4). The contact is gradational consisting of alternating light grey poorly foliated greenstone bands and dark grey graphitic schist bands. Stringers of fine-grained pyrite occur in the greenstone at the contact.

xi) Intrusive olive green augite-actinolite metabasite (unit 10):

On the farms Toorkrans and Vogelstruisdrift (Sheet A) an intrusive metabasite, unit 10, is exposed as a dyke within the greenschists. Borehole BE2 was drilled into the metabasite up to a depth of 30 metres (Figs. 3.3 and 3.5). The medium- to coarse-grained metabasite is probably intrusive into unit 9 which was intersected in adjacent boreholes BE1, BC1 and BW1 (Figs. 3.3 and 3.5).

The metabasite is olive green, poorly foliated but well-jointed (Plate 3.22). From a depth of 23 metres it is moderately foliated, medium to fine grained with a few grey to olive green bands (width <1cm) parallel to the foliation. The metabasite has a rounded weathering surface and weathers positively relative to the highly foliated greenstones. The body's intrusive nature is indicated by its cross-cutting

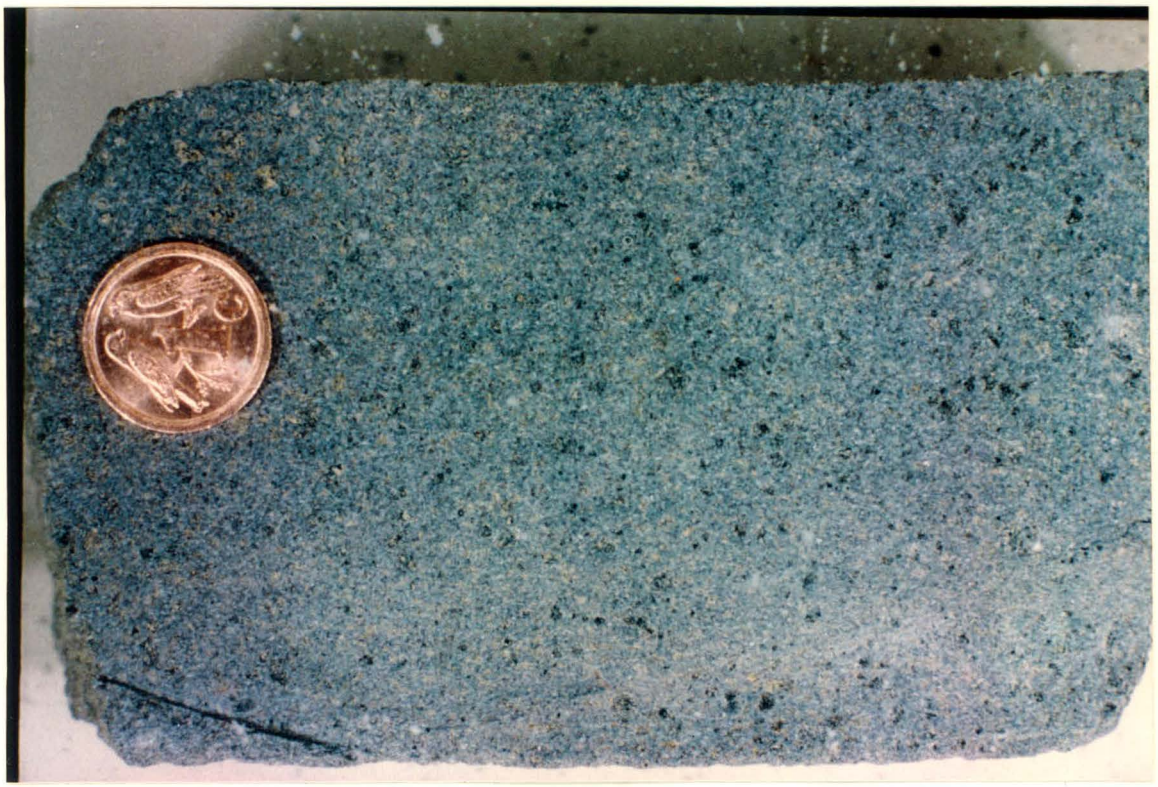

Plate 3.20 Light grey green quartz-orthoclase-biotite-muscovite fels (unit 5).

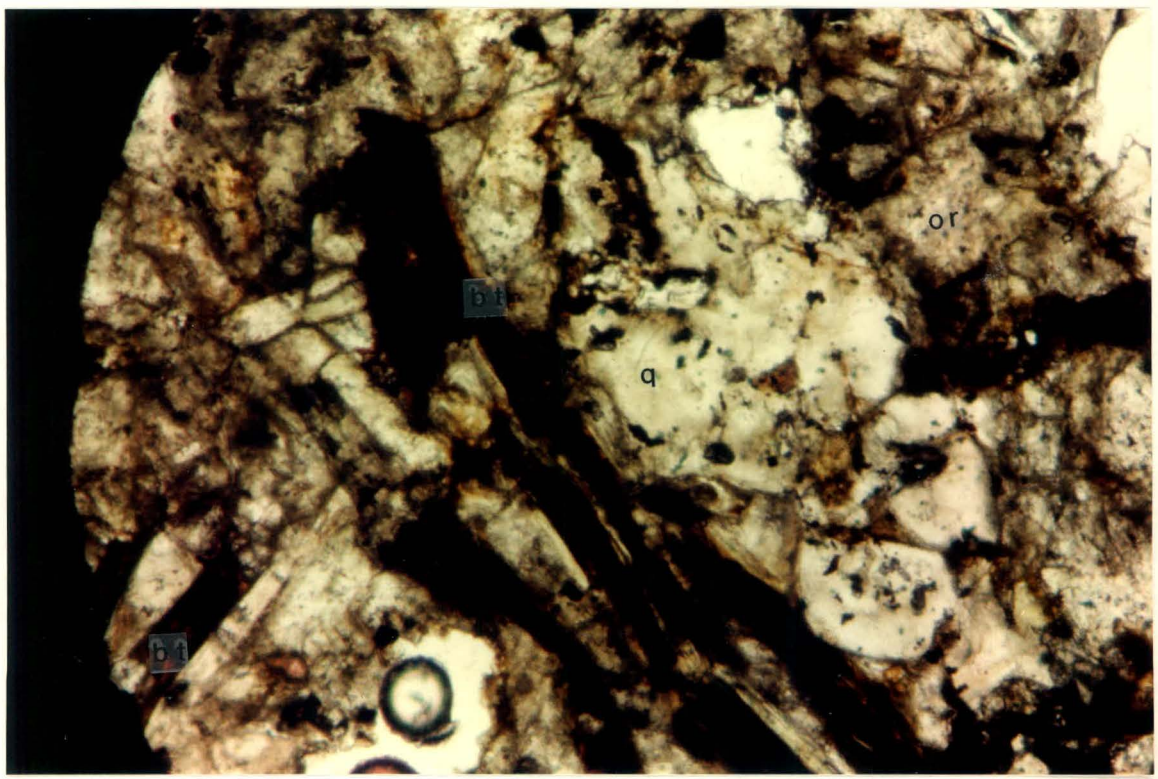

Plate 3.21 Unit 5. A coarse-grained fels which is made up of randomly orientated biotite, quartz, muscovite and orthoclase with minor chlorite, calcite, actinolite and magnetite. Plane light.

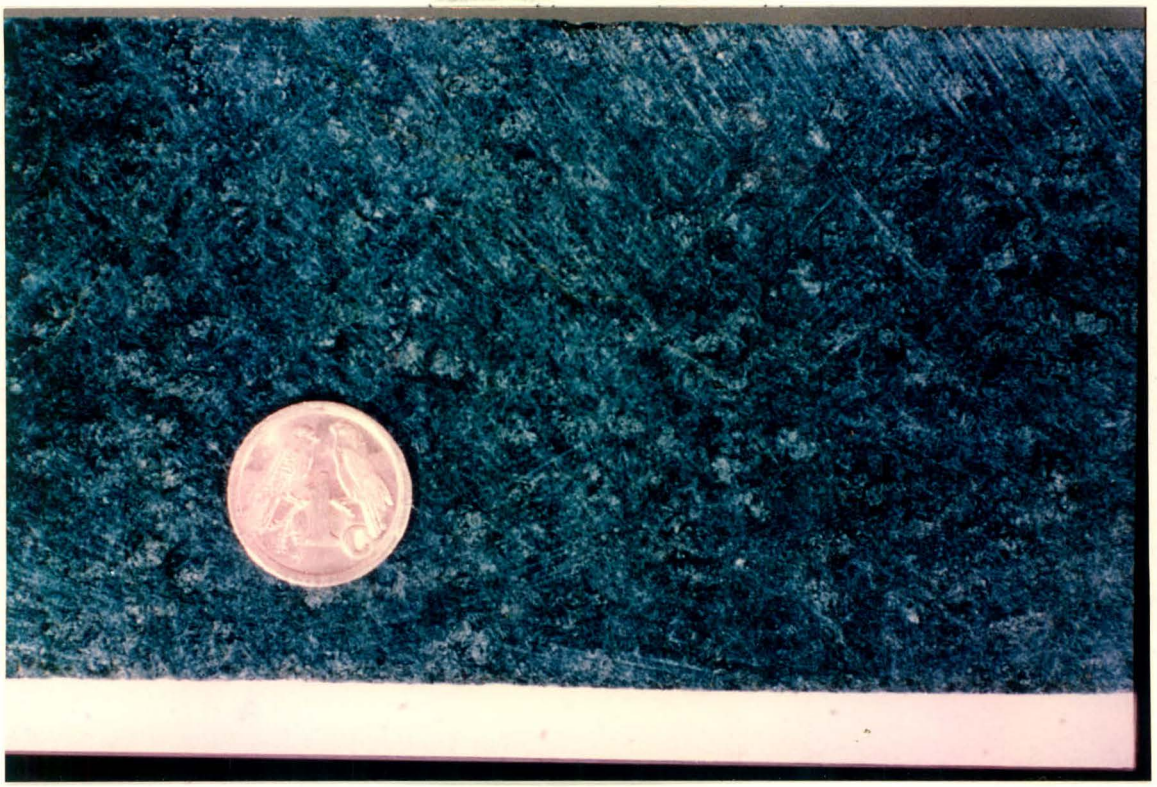

Plate 3.22 Intrusive olive green augite-actinolite metabasite (unit 10).

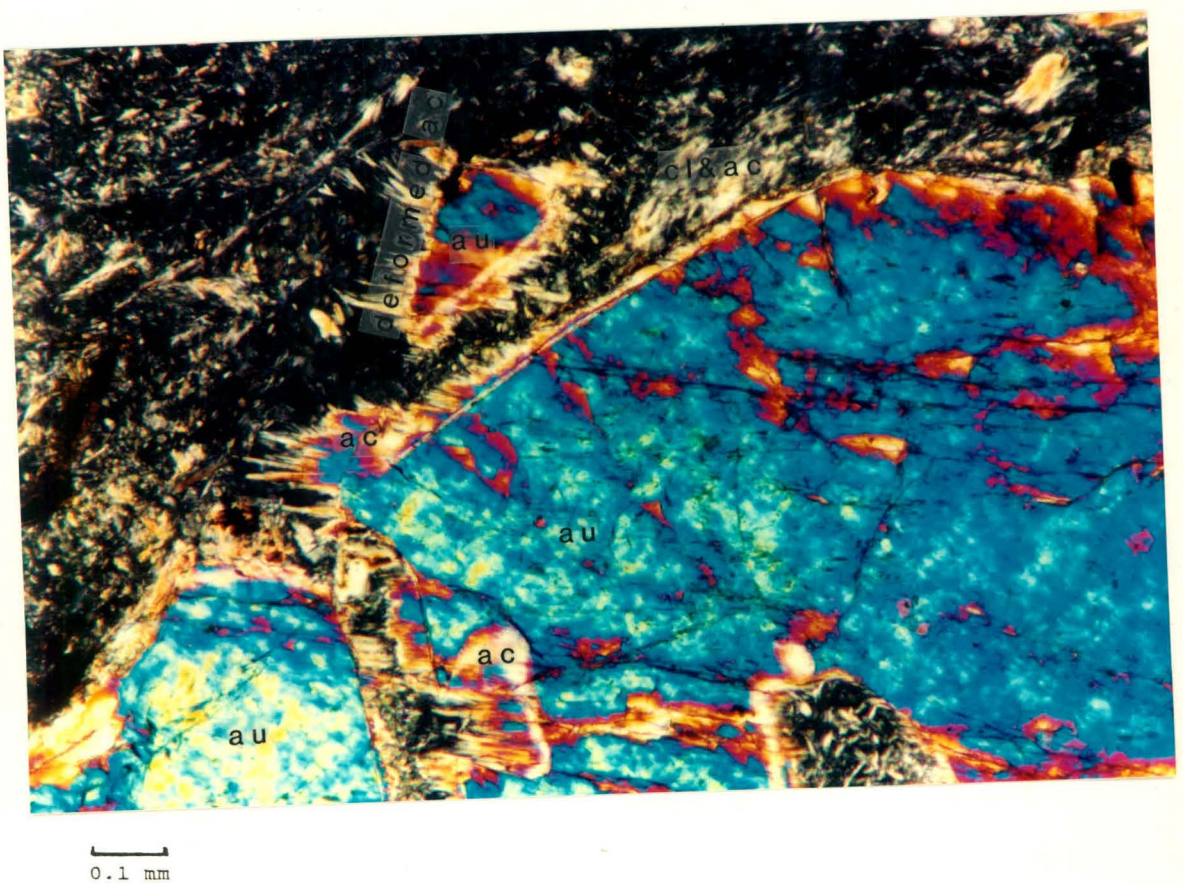

Plate 3.23 Unit 10. Actinolite fibres, an alteration product of augite, occur at the interface between the augite and its pressure shadow. Deformed actinolite fibres are indicators of shearing. Crossed polars.

relationship relative to the main foliation of the greenschist. Greenschist at the contact contains numerous epidote-quartz lenses and nodules.

Mineralogically it consists of phenocrysts of clinopyroxene which were chemically classified as augite according to the enstatite-ferrosilite-wollastonite ternary diagram of Morimoto (1989, Fig. 5, Appendix). The augite grains are enveloped by a highly foliated matrix of actinolite and chlorite; minor magnetite, ilmenite, titanite; and accessory epidote, calcite and quartz. The augite is in various stages of alteration. A great deal of the original augite grains now consist of secondary minerals. The alteration products, in decreasing order of abundance, include a) rodded actinolite crystals, b) chlorite which is probably an alteration product of actinolite, c) small inclusions of ilmenite which is partially altered to leucoxene, and d) a few rather big labradorite crystal. The labradorite crystals occur as inclusions in the augite which gives it an ophitic texture. Actinolite occurs mostly at the interface between the augite and its pressure shadow.

The asymmetry of the pressure shadows, deformed actinolite fibres (Plate 3.23) and fragmented augite crystals are definite indicators of shearing. In less deformed samples the augite phenocrysts are bigger and the percentage groundmass is less. The original rock type probably consisted primarily of coarse-grained augite, thus classifying as a clinopyroxenite. The alteration products (actinolite, chlorite and minor ilmenite, leucoxene and labradorite) currently make up most of the groundmass which is the product of successive events of shearing.

xii) Lensoid inclusions in greenstones:

At the farm Kamina (Sheet A), greenstone (unit unknown) is foliated around small lensoid inclusions. The inclusions have a light purple colour, are very hard with an average diameter of 1.5cm. Microscopy revealed that they consist mainly of augite phenocrysts in a microcrystalline groundmass of augite, albite, titanite and minor chlorite, actinolite, magnetite and epidote (Plate 3.24). The augite phenocrysts are subhedral to euhedral and comprise 10 to 15% of the rock. Hourglass twins and sector zoning are common in the augite grains (phenocrysts and groundmass). Some augite grains are partially altered to chlorite and a few grains contain

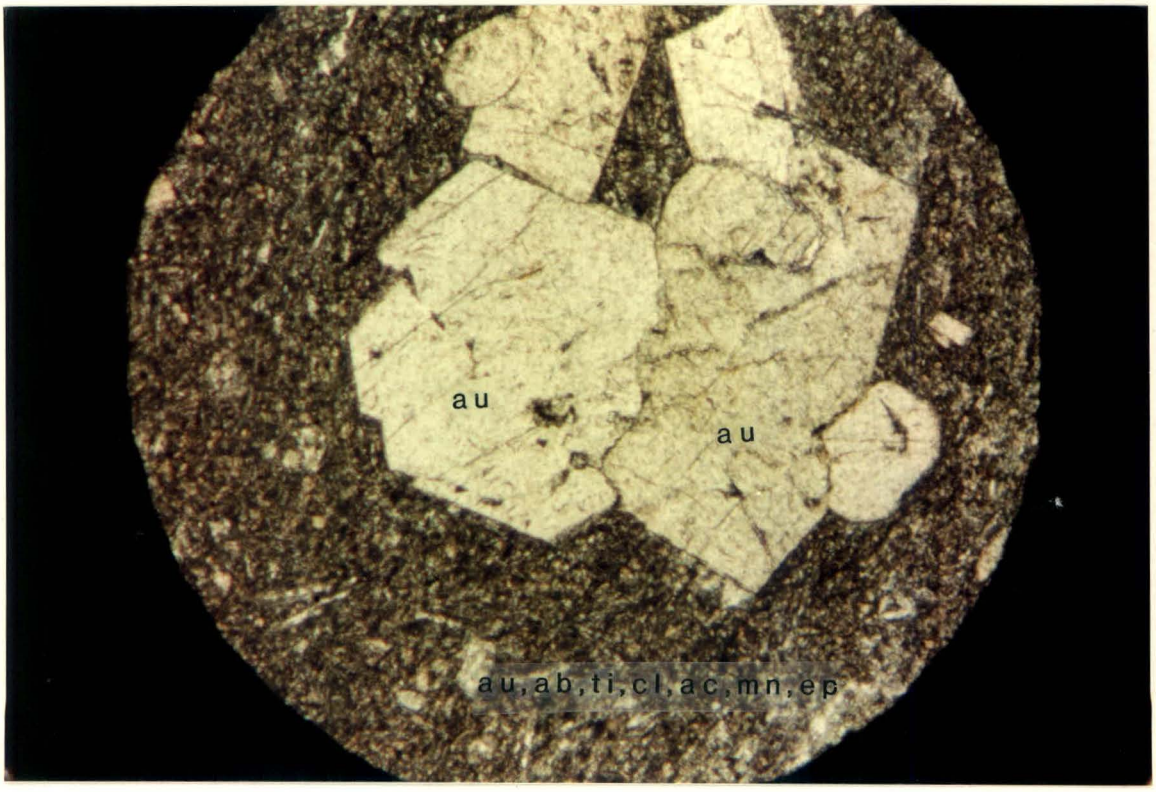

Plate 3.24 Lensoid inclusions in greenstones on the farm Kamina. They consist of augite phenocrysts in a microcrystalline groundmass of augite, albite, titanite and minor chlorite, actinolite, magnetite and epidote. Plane light.

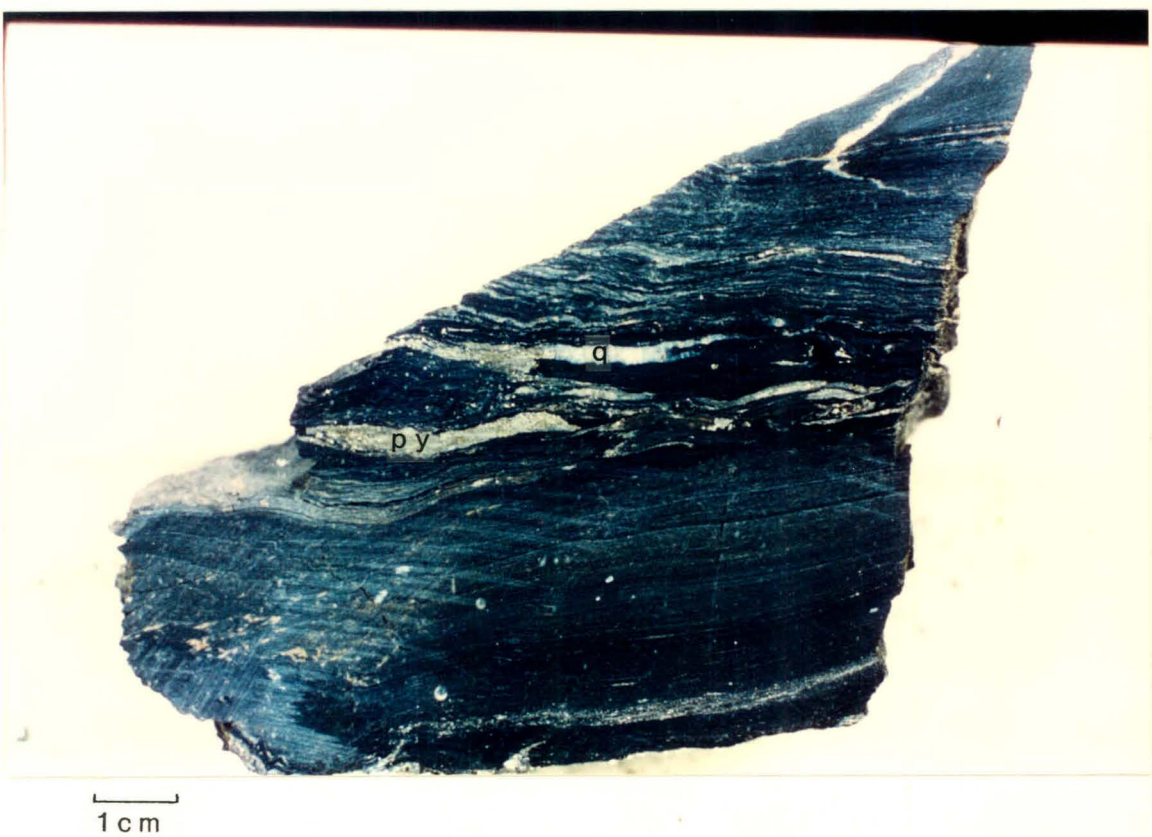

Plate 3.25 Graphitic schist from borehole AE2.

inclusions of epidote. From the mineralogy of these lensoid inclusions it is concluded that they are not amygdales, but rather represent unfoliated remnants of a boudinage structure. The lensoid inclusions probably represent remnants of a more competent metabasite, surrounded by incompetent metatuff or metabasalt.

Nine of the ten greenstone units identified were encountered in boreholes drilled along three section between the farms Vogelstruisdrift and Toorkrans. This area includes only a small portion of the main greenstone body. This indicates that the main greenstone body is highly heterogeneous and therefore additional greenstone units, other than the ten encountered, can be expected.

3.2.2. GRAPHITIC SCHISTS

Graphitic schists occur as lenses within the greenstones and at greenstone-metasediment contacts where they alternate with layers of phyllite, greenstone and carbonate lenses.

Graphitic schist lenses were encountered in greenstone unit 1 (waterlain tuffs?) and unit 5, in boreholes AW2 and AE2 alternatively (Figs. 3.3 and 3.4). In borehole AW2 the graphitic schist lens is four metres thick and was intersected at a depth of 15 metres. The contact between greenstone unit 1 and the graphitic schist is sharp. In borehole AE2 graphitic schist was intersected at a depth of 23,2 metres, from where it continued up to the end of the borehole at a depth of 30 metres. The contact between greenstone unit 5 and the graphitic schist is gradational; bands of greenstone alternating with bands of graphitic schist.

The graphitic schists are highly foliated, fine grained, and laminated parallel to the foliation with alternating light grey, dark grey and black lamellae (Plate 3.25). A few quartz lenses and lamellae, less than 1cm wide occur parallel to the foliation. The graphitic schists are well-mineralized with pyrite which is mostly concentrated in the quartz-rich lenses and lamellae, along joint faces and as disseminated euhedral grains.

The two graphitic schist lenses are petrographically very similar. The light grey lamellae consist of quartz, muscovite, chlorite and small rodded and needle-like

actinolite which might indicate a greenstone component. The darker the lamellae the higher the graphite and pyrite content. Further away from the contacts the greenstone component becomes less and the graphitic schist becomes darker coloured.

Both graphitic schist lenses are intensely deformed. The lamellae and foliation have been subjected to more than one folding episode which resulted in asymmetrical folds with a smaller set of asymmetrical folds superimposed on their limbs. Various types of crenulation cleavages were recognized in thin section. They include crenulation cleavage with gradational boundaries, zonal cleavage with discrete boundaries and fracture-bounded discrete cleavage. Gradational crenulation cleavage is often re-crenulated and truncated by zonal or discrete cleavage, indicating a complex polyphase deformation history. Cleavage zones contain less quartz and a higher proportion of mica. Quartz lenses have been subjected to progressive ductile and brittle deformation as indicated by undulose extinction, sub-grain development, fragmented crystals and ribbon quartz.

On the farms Gousblomkraal, Vogelstruisdrift, Rooihoogte and Vrugbaar (Sheet A) graphitic schists are interlayered with phyllite, greenstone and carbonate lenses. Jasper-rich lenses are often present in these zones. The graphitic schists occur as thin bands, a few centimetres wide, as well as thick lenses of a few metres wide. Rabie (1974a) mapped these outcrops as tuffs or volcanic ashes. In these outcrops the graphitic schists are highly weathered, soft, dark grey and fine grained with no visible mineralization.

3.2.3. MUSCOVITE-QUARTZ SCHIST

On the farm Tweevlei dolomite overlies a dark coloured muscovite-quartz schist. The schist is fine-grained, homogeneous, highly foliated and dark grey with a purple tint. No banding or quartz lenses are visible in the outcrops.

The schist consists of ± 60% muscovite which envelopes microcrystalline quartz lenses and magnetite and hematite grains. Minor chlorite is also present. Red discoloration is related to oxidized magnetite forming hematite.

Two deformation phases are recognizable in the schists: a) one during which the schists were foliated and b) a later episode during which the foliation was folded into open folds (wave-length is 6m). The dolomite-schist contact dips approximately 60 to 70 degrees in an easterly direction. The contact is defined by a thin olive green chloritic zone, 1 to 20cm wide. The dolomite appears somewhat weathered and friable at the contact and it encloses small fragments of chlorite.

3.2.4. DOLOMITE

On its western side the main greenstone body is for most of its length in contact with dolomite (Sheet A). The width of the dolomite varies from a few metres across to approximately 800m wide at the farm Vogelstruisdrift. The dolomite is currently being mined at Bridgetown (Sheet A), mostly for agricultural use. Recently, dolomite was encountered up to depths of 70 metres in boreholes drilled by PPC at the farm Vogelstruisdrift (M. Taylor. pers. comm., 1994). In these boreholes banding, dipping steeply in an easterly direction, was encountered in the dolomite. Structurally the boreholes were drilled into the western limb of a broad synform (Sheet A).

Generally the dolomite is light grey to cream, fine grained, massive and fairly pure. Small veins and inclusions of chert are present in the dolomite. The chert inclusions are often white and/or grey but laminated maroon/dark grey chert is also present. Some of the clear chert inclusions are probably chalcedony. Milky and clear quartz veinlets occur along joints in the dolomite. Disseminated pyrite and pyrrhotite are often found in highly jointed dolomite.

In thin section, dolomite from the Bridgetown quarry is made up of fine- to medium-grained anhedral dolomite which appears foggy in places. The dolomite crystals show no preferred orientation and no primary sedimentary structures were observed. This is probably due to recrystallization of the dolomite during low-grade regional metamorphism. Most crystals display deformation twins which formed in response to some degree of stress. The dolomite is cross-cut by numerous fine irregular fractures which are filled with hematite, magnetite and euhedral macrocrystalline dolomite and microcrystalline quartz growing perpendicular to the walls of the fractures.

In borehole CE1 (Fig. 3.6) dolomite lenses occur within greenstone unit 4. The largest lens (13m wide) contains small spherical inclusions consisting of medium- to coarse-grained anhedral dolomite (Plate 3.26). The inclusions have an average diameter of 0.3mm and are mostly spheroidal, but a few ellipsoidal inclusions are also present. The dolomite crystals in the inclusions show no preferred orientation. The dolomite surrounding the inclusions is microcrystalline and anhedral with a foggy greyish appearance. These inclusions probably represent ghost inclusions which were preserved during dolomitization of oolithic limestone.

At the farm Bridgetown irregular zones which consist of a pink dolomite matrix with fragments of different rock types, occur in the dolomite body. These zones are interpreted as karsts which were filled by slumping of overlying material.

Dolomite outcrops with a laminated appearance occur on the farm Matjiesrivier, on the northern bank of the Matjies River. The dolomite is poorly foliated and consists of alternating dark grey/maroon and light grey/pink lamellae with a few small chert inclusions.

On the farms Tweevlei and Bridgetown (Sheet A) greenstone occurs as small sill- or dyke-like bodies in the dolomite sequence. One of these greenstone bodies outcrop next to the Bridgetown dolomite quarry. It is approximately 5m wide, 60m long and weathers negatively relative to the surrounding dolomite. The greenstone is fine grained, olive-green and highly foliated parallel to the greenstone-dolomite contact. The boundary between the greenstone and the dolomite is not clear-cut and some degree of mixing of the two rock types has taken place. A similar dyke-like greenstone body in dolomite at Tweevlei, encloses small jasper-rich chert lenses.

3.2.5. CHERT

Associated with greenstones and dolomite are bodies of chert, mostly found where phyllites border the greenstones. The chert bodies are elongated parallel to the pelite-greenstone contact with a maximum width of 60 metres. Most of the chert outcrops occur along the western border of the main greenstone body where they are associated with dolomite, whereas along the eastern greenstone contact only a

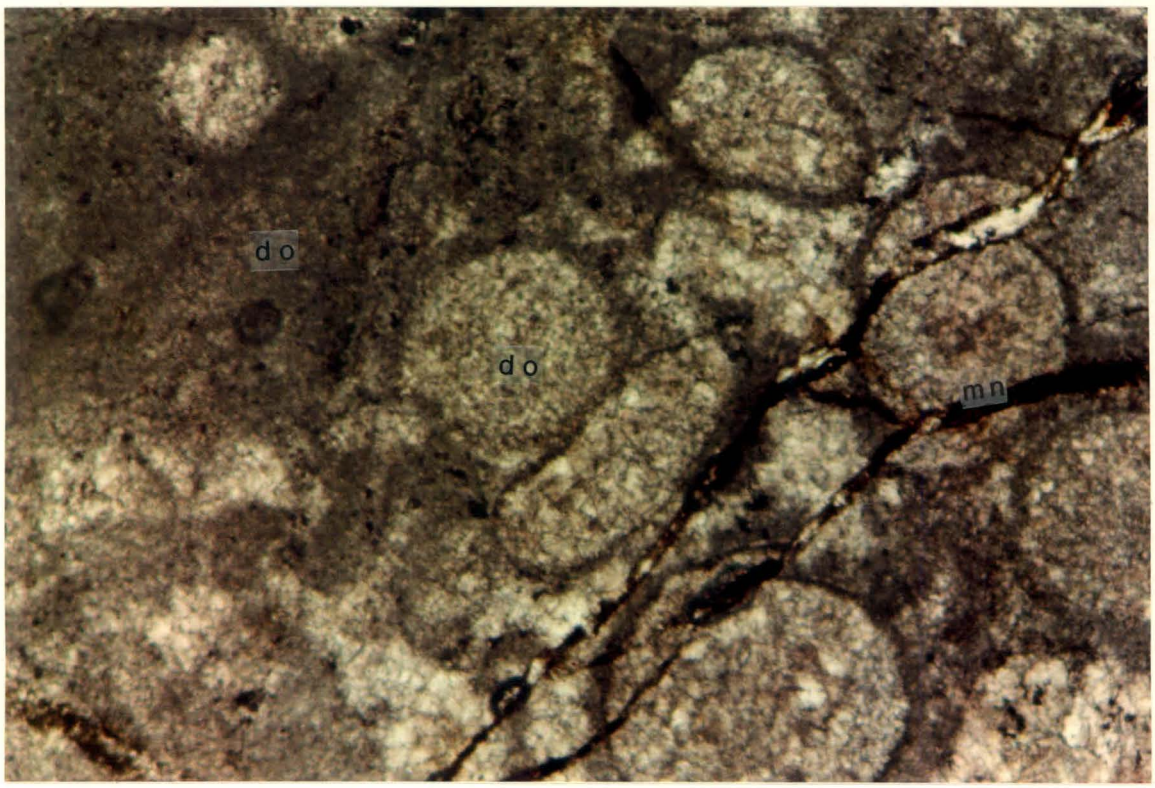

Plate 3.26 Oolitic dolomite from borehole CE1.

few chert outcrops were mapped. Small chert bodies in the greenstone are associated with dolomite.

The cherts vary considerably in colour, texture and degree of deformation. The following types of chert occur in the Bridgetown Formation:

i) White, grey and translucent massive chert.

Most of the chert outcrops fall in this category. These cherts often appear black to dark red-brown as the result of the presence of a crust composed of manganese and iron oxides. Some of the outcrops have a light brown to cream colour and can easily be mistaken for silcrete.

The following two massive chert samples were studied in thin section:

a) Grey massive chert (location: De Pont, Sheet A, Sample NSF/3.2)

The chert is a relatively pure rock consisting of microcrystalline, anhedral quartz and accessory hematite. The quartz is equigranular, shows no preferred orientation and displays undulose extinction. A few fractures are filled with recrystallized macrocrystalline anhedral quartz.

b) White to cream massive chert (location: Tweevlei, Sheet A, Sample NSF/3.6)

The chert consists mainly of microcrystalline anhedral quartz which has a foggy appearance due to the presence of numerous very small inclusions. The rock also contains coarse-grained recrystallized quartz which is anhedral and displays undulose extinction and sub-grain development. Disseminated anhedral hematite grains occur as an accessory mineral.

ii) Oolitic chert.

Oolitic chert was found on the farms Vogelstruisdrift and Palestina (Sheet A; Samples NSF/7 and NSF/3.4).

At Vogelstruisdrift the oolitic chert is associated with massive chert, jaspilite, dolomite and greenstones which have been described as tuffs (Rabie, 1974a), alternating with phyllites, carbonate lenses and graphitic schists. In hand specimen the chert contains flattened white to cream 'ooids' (diameter <3mm) surrounded by a translucent chert matrix. In thin section the 'ooids' consist of cryptocrystalline anhedral quartz with dark grey amorphous inclusions concentrated at the rim. The

'ooids' vary considerably in shape; from spherical to lenticular. The matrix consists of microcrystalline quartz which surrounds an innermost zone of macrocrystalline quartz.

The oolitic chert on Palestina occurs within a massive white to cream lenticular chert body located in phyllite. The oolitic chert consists of white to grey flattened spheres (diameter: 1 to 3mm) in a massive light brown matrix (Plate 3.27). In thin section the spheres consist of cryptocrystalline anhedral quartz. Some include coarser-grained microcrystalline concentric rings of anhedral quartz which often surround an inner zone of macrocrystalline quartz (Plate 3.28). Some oolites are composed entirely of macrocrystalline quartz. The macrocrystalline quartz displays undulose extinction and sub-grain development probably in response to strain experienced during deformation. The matrix is composed of cryptocrystalline quartz and an amorphous material which is too fine grained for optical identification.

Zonal structures in the oolitic spheres on Palestina resemble structures found in oolitic carbonates entirely replaced by silica (Hesse, 1989). The zonation results from inward progression of the replacement and reflects decreasing silicon activity and/or decreasing permeability as the ooid rim gets sealed off by silicification.

iii) Jasper and jaspilites

Jasper and jaspilite occur in cherts on the farms Vogelstruisdrift, Vrugbaar and Kleindrif (Sheet A). Jaspilites also occur as lenses within the greenstones. Jaspilite lenses are found in greenstone unit 9, banded greenstone with graphitic schist and carbonate lenses (tuffs?) and in greenstones which occur as small dyke-like bodies in the dolomites at Tweevlei.

Jasper on the farm De Pont (Sheet A, Sample NSF/3.1) was studied in thin section. In outcrop it is a massive red rock in contact with massive grey chert. Although relatively massive in hand specimen, discrete structural grain is defined by orientated fine- to coarse-grained quartz grains in thin section. The quartz has a cloudy appearance due to the presence of numerous very small hematite inclusions. The rock also includes coarse-grained anhedral to subhedral hematite and accessory calcite. The following microstructures in the quartz typify progressive ductile shearing, recovery and recrystallization: a) undulose extinction, b) serrated

Plate 3.27 Oolitic chert on the farm Palestina.

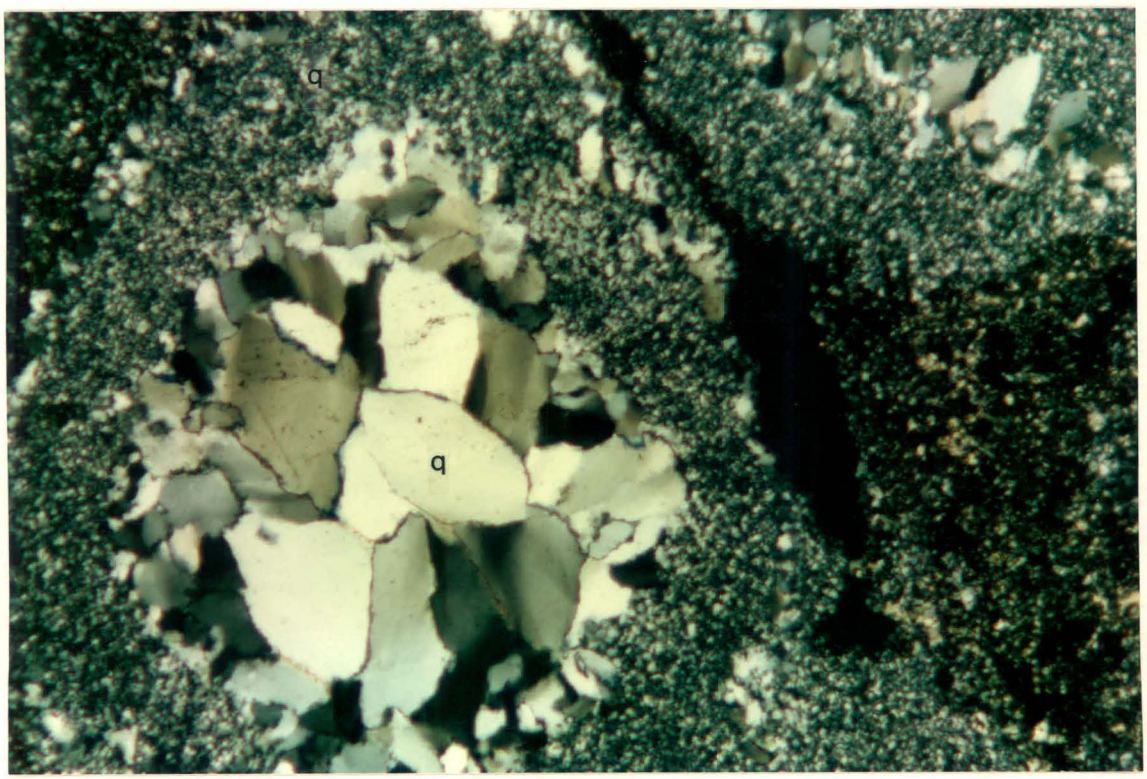

0.13 mm

Plate 3.28 Oolitic chert on the farm Palestina consisting of a microcrystalline quartz rim surrounding an inner zone of macrocrystalline quartz. Crossed polars.

grain boundaries, c) sub-grain development and d) elongated grains with a ribbon quartz texture.

3.2.6. SUPERIMPOSED VEINS

The Bridgetown Formation is cut by various ages of superimposed veins.

Veins cross-cutting the greenstones consist mainly of quartz and/or calcite. The width of the veins seldom exceeds 3 centimetres. The largest veins usually enclose irregular pieces of the greenstone, and involve some brecciation. Veins are usually associated with small shear zones and joints, and some veins formed by means of the crack-seal mechanism. This involves multistage crack opening and vein infill in response to fluctuations in fluid pressure (Barker, 1989). Characteristically such veins contain thin inclusion bands parallel to the vein walls which represents detached screens of the wall rock. Generally the superimposed veins are not associated with any mineralization, except for unit 1 where pyrite is concentrated along quartz-calcite vein margins. The different vein types and their abundance in the greenstone units are summarized in Table 3.2.

Other rock types of the Bridgetown Formation do not contain any calcite veins and are cross-cut by monomineralic quartz veins of different ages. It is thus concluded that calcite, in veins cross-cutting the greenstones, was derived primarily from the greenstones. This is further illustrated by the fact that veins cross-cutting graphitic schist lenses, which are interlayered with the greenstones, do not contain any calcite.

In the dolomites a few milky and clear quartz veins occur mostly along joints. Plenty irregular milky and clear quartz veins are present in most of the chert outcrops. Milky quartz veins, up to 20cm wide, cut through massive cherts at the farm Gousblomkraal. Cherts often contain boxwork textures where quartz veins intersect each other. The muscovite-quartz schist on the farm Tweevlei do not contain any quartz veins in the outcrop.

Quartz and calcite veins of all ages have been subjected to some degree of strain as displayed by microstructures such as undulose extinction, deformation twinning,

serration and sub-grain development. Most of the veins cross-cut the dominant penetrative foliation and are therefore either late tectonic or post-tectonic.

3.3. PHYLLITES IN CONTACT WITH THE BRIDGETOWN FORMATION

The main greenstone body is bordered mainly by phyllites. According to Rabie (1974a) Tweevlei clayslates and phyllites occur along the western and northern boundary of the greenstone body and Porterville clayslates mostly along its eastern boundary. Rabie included both the Tweevlei and Porterville units in the Boland terrane.

According to the geological map of the Koringberg-Hermon area (Sheets 3318B-Malmesbury and 3319A-Ceres, 1975), phyllites of the Moorreesburg Formation occur west of the greenstone body and phyllites of the Porterville Formation east of the body. The Moorreesburg Formation was incorporated in the Swartland terrane and the Porterville Formation in the Boland terrane by placing the Piketberg-Wellington fault zone at the eastern greenstone-metasediment contact.

No abrupt transition was found between phyllites of the Swartland terrane and phyllites of the Boland terrane. Phyllites along the greenstone contacts are intensely deformed, layers of greenstone at some localities alternating with layers of phyllite (De Villiers, 1979). At the western greenstone boundary phyllites are mostly in contact with dolomite and chert.

According to de Villiers (1969) the phyllites have been subjected to low-grade metamorphism, namely the lower greenschist facies. The metamorphism appears to be approximately contemporaneous with the main tectonic phase. The phyllites have suffered polyphase deformation. A well-defined foliation with a general NW-SE strike is present in all the metasediments.

Quartz-rich and quartz-poor schists are also found interlayered with the phyllites. The schists and phyllites are yellow brown, grey and light khaki coloured and often stained red to purple along joints. Most of the outcrops are friable, soft and clayey due to severe weathering.

A few thin limestone outcrops (up to 50 metres wide) occur in the phyllites on the farms Matjiesrivier and Noukloof (Sheet A). The limestone is fine grained, dark

coloured to nearly black, fairly pure and shows signs of intense folding. Rabie (1974a) also mapped a grit marker interlayered with the phyllites.

On the farm Voorwaarts the phyllites grade into a quartz schist which Rabie (1974a) mapped as the Vogelvlei quartzite. Similar rock types, the Spitskop quartz schists (mapped by Rabie, 1974a), flank the Spitskop antiform.

Milky quartz veins and lenses are abundant in the phyllites. Some occur parallel to the main foliation and others occur mostly along joints. The veins have an average width of 1cm, but massive quartz zones of up to 2 metre wide (on the farm Gousblomkraal) are also present. Usually associated with the quartz veins are red-brown to black iron- and manganese-enriched zones, parallel to the foliation and along joints. Iron and manganese were probably displaced during the silicification process. On the farms Dasdrif and Drieheuwels, these zones are up to 30cm wide. The phyllites and schists are often capped with ferricrete and silcrete, especially along the eastern greenstone-metasediment contact.

3.4. SPITSKOP AREA

The area around Spitskop includes part of a domal feature, the Spitskop antiform, as mapped by Rabie (1974b). Rabie included the Spitskop antiform in the Boland terrane. Visser et al. (1973, 1981) correlated stratigraphic units in this structure with similar ones in the Swartland dome, a broad antiform, trending north-north-west between Moorreesburg and Riebeek Kasteel, in the Swartland terrane. Visser et al. (1973, 1981) consequently included the Spitskop antiforms in the Swartland terrane by moving the Swartland-Boland terrane boundary to a position east of the Spitskop antiform.

The area around Spitskop is stratigraphically and tectonically complex, having a wide variety of lithological units, the stratigraphic relationships of which are obscured by faulting. The lithologies include quartz schists, quartz-feldspar-sericite schists, banded chert and greenschists. Their tectono-stratigraphic relationships are illustrated in Table 3.1 and Section B-B' (Fig. 3.2).

3.4.1. QUARTZ SCHIST

Quartz schist in the Spitskop area (mapped by Rabie, 1974a) is light grey to cream coloured and varies from fairly massive to highly foliated (Sheet A). It consists of a dense mosaic of quartz grains with accessory albite, chlorite, sericite and calcite (De Villiers, 1969). The massive quartz schists have the appearance of a quartzite. The foliated quartz schists contain red-brown speckles of oxidized material and the highly foliated quartzites have a banded appearance consisting of alternating dark and light grey recrystallized quartz lamellae. The foliation in the quartz schist probably developed during thrusting or later shearing.

Similar rock types occur higher up in the succession (e.g. quartz schist on the farm Kamina).

3.4.2. QUARTZ-FELDSPAR-SERICITE SCHIST

Highly weathered light yellow brown to grey green quartz-feldspar schists which grade into light grey quartz-sericite schists, outcrop in the region of Spitskop and the Misverstand dam (Sheet A). The schists are in contact with quartz schists, phyllites and graywackes but their stratigraphic relationships are nowhere clearly exposed.

The schists are medium grained, highly foliated with milky quartz lenses (up to 10cm wide) parallel to the main foliation. The schists are laminated in places with alternating quartz- and mica-rich lamellae, parallel to the main foliation, which is probably the result of mineral segregation during metamorphism. De Villiers (1969) distinguished between quartz-rich and quartz-poor schists, representing altered graywacke and shale respectively. The former consists of quartz, feldspar, chlorite, sericite and calcite with accessory ore minerals, apatite, tourmaline, zircon and epidote. The quartz-poor schists consist of chlorite and sericite with small variable amounts of quartz and feldspar.

The schists have been subjected to at least three phases of deformation. A dominant, penetrative foliation with NW-SE strike has been subjected to more than one folding episode, regionally and locally.

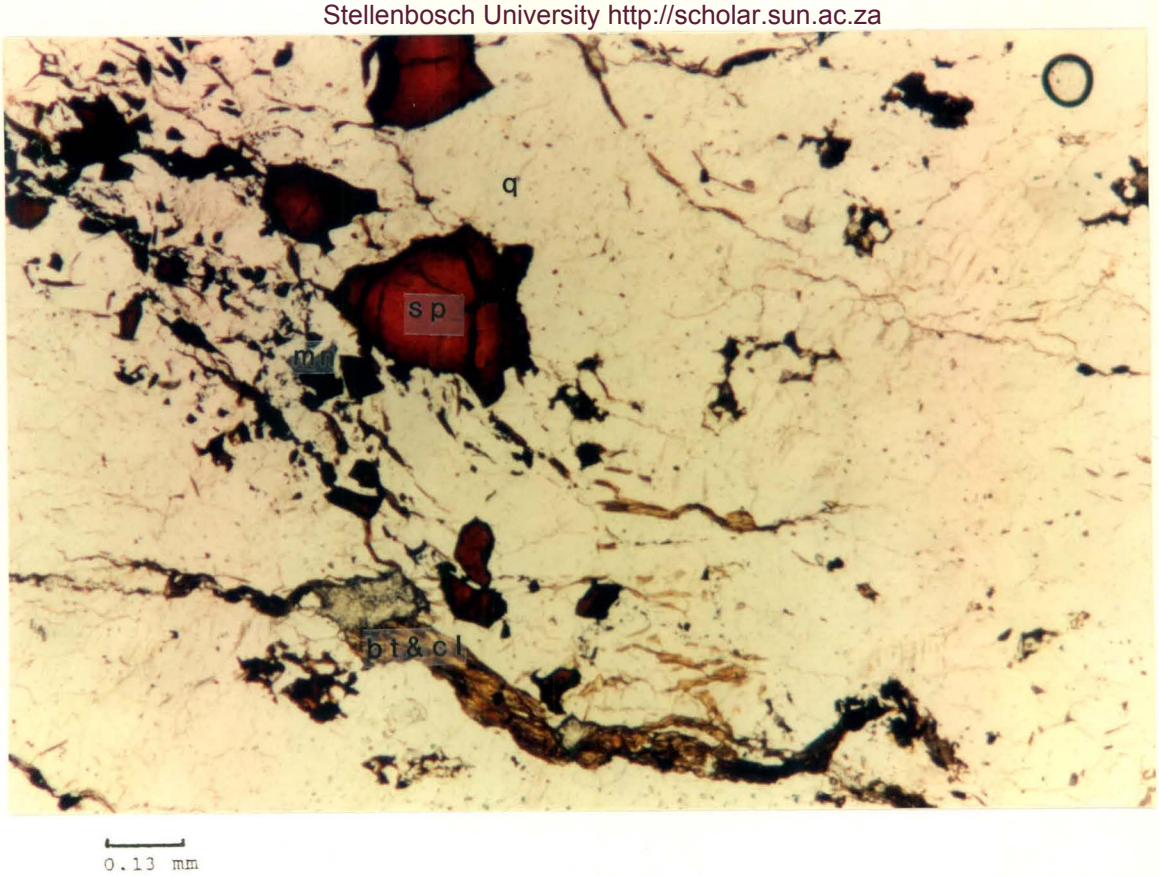

Plate 3.29 Banded chert at Spitskop. Small irregular cracks in the chert are filled with spinel and micas. The red-brown spinel grains are Al- and Mg-rich chromite grains with a dark magnetite rim. Plane light.

Plate 3.30 Chlorite schist at Spitskop. Rounded porphyroclasts of albite in a groundmass of chlorite, magnetite and fine-grained quartz and albite. The albite porphyroclasts are partly altered to saussurite and contain small alkali feldspar inclusions. Crossed polars.

A few carbonate bodies outcrop in the quartz-feldspar-sericite schists. A small limestone body (150m by 50m) occurs on the farm Misverstand (Sheet A). It is light-coloured, medium grained, homogeneous and poorly foliated, appearing dark grey in the outcrops as the result of the presence of a crust composed of manganese and iron oxides. Another carbonate body (250m by 150m) outcrops north of Spitskop in the quartz-feldspar-sericite schists. The outcrop surface is rough and the rock appears mottled due to the presence of irregular inclusions of chlorite, quartz, oxidized material and micas.

3.4.3. BANDED CHERT

At Spitskop a banded chert overlies quartz-feldspar-sericite schist and greenschist exposed in a road-cutting through the south-eastern flank of Spitskop. The contact between the quartz-feldspar-sericite schist and the chert is gradational; the schist becoming more siliceous near the contact.

The chert is highly resistant to weathering and is probably responsible for the relict high topography at Spitskop. Similar rocks were also found northeast of Spitskop adjacent to the Berg River (Sheet A).

The chert consists of alternating light grey and dark grey quartz bands (width <1cm) which are separated by yellow brown to red-brown iron-rich faces. Micas and euhedral fine-grained pyrite and magnetite are concentrated along some of these faces. At some localities the chert is yellow brown and massive with poorly developed agate-like features.

In thin section the banded chert is made up of fine- to medium-grained anhedral quartz which shows little orientation. The quartz displays undulose extinction, serration of boundaries and sub-grain development which developed in response to strain.

Small irregular discontinuous fractures cut through the quartz fabric. They are filled with a brown-green mica and spinel grains (Plate 3.29). The spinel grains are subhedral to euhedral and consist of a red-brown core which is surrounded by a black opaque rim. Microprobe analyses were done on a few spinel grains (Table 14, Appendix). Analyses were done on the red-brown core (analyses 4, 5 and 6) and

the dark red to black rim (analyses 7 to 11). The core has a high Al_2O_3 (26%), Cr_2O_3 (44 to 45%), FeOt (14 to 17%) and MgO (13 to 15%) content, which classifies it as an Al- and Mg-rich chromite. The darker rim has a much lower MgO content (0,67 to 2,36%) and a higher total FeO content (32 to 34%). The Cr_2O_3 content is only slightly lower and the Al_2O_3 content is similar, thus classifying as a Al-rich chromite. A few fragmented opaque grains which represent the outer part of the dark rim (analyses 1, 2 and 3) have the composition of magnetite with minor SiO_2, MgO and Al_2O_3. This probably indicates increasing replacement of Mg by Fe^{+2} and Cr by Fe^{+3} towards the edge of the spinel grain.

Nine analyses were done on the brown green mica (Table 15, Appendix). Little consistency was found between the different analyses. Generally the micas have a low K_2O (0.22 to 2.18%) content and a relatively high Cr_2O_3 (1.43 to 4.66%) content. Their compositions do not agree with that of typical micas and seem to represent mixtures of biotite and chlorite.

The occurrence of the spinel grains and micas along fractures in the banded chert might indicate that their crystallization is related to a hydrothermal event.

3.4.4. GREENSCHISTS

A few small greenschist bodies outcrop in the Spitskop area. They occur mainly as intraformational bodies, but are also found in the quartz schists. Most of the small outcrops are highly weathered, some only recognizable by olive green fragments scattered through the wheatfields and by dark red-brown soil, in places covered with a secondary carbonate crust.

Two small, highly altered greenschist bodies occur in the quartz schist. Both are bordered by massive quartz veins which probably represent fault zones in the quartz schist.

A 50m wide greenschist zone occurs along the eastern and south-eastern quartz schist/quartz-feldspar-sericite schist contact. It is fine grained, grey to olive-green and highly foliated. The boundary between the quartz schist and the greenschist is transitional. Both are transected by numerous quartz veins.

Fresh greenstone (about 500m wide) outcrops on the farm Misverstand along the quartz-feldspar-sericite schist/phyllite contact (Sheet A). It is dark grey, fine grained, highly foliated and laminated with alternating dark grey and light grey lamellae parallel to the foliation. The quartz-feldspar-sericite schist is phyllitic at the greenstone contact, containing numerous quartz veins and zones enriched in iron (up to 1m wide). Directly north of this greenstone body, on the farm Klipplaat, small outcrops of a highly weathered carbonate rock containing fragments of greenschist may represent highly weathered greenstone (Sheet A).

At Spitskop a 150m by 150m outcrop of chlorite schist was exposed in a road-cutting through the south-eastern flank of Spitskop (Sheet A). The chlorite schist occurs within the quartz-feldspar-sericite schists and both rock types are overlain by a banded chert. The chlorite schist is also bordered by a possible fault zone which is outlined by a massive quartz vein at the quartz schist contact.

The chlorite schist is olive-green, fine grained, highly foliated and folded and cut by milky quartz veins. In thin section it has a mylonitic appearance, consisting of microcrystalline anhedral quartz, albite and stringers of chlorite which envelope porphyroclasts of albite. The albite porphyroclasts are rounded and some are fragmented (Plate 3.30). They are partly altered to saussurite and contain small euhedral alkali feldspar inclusions. A few red-brown to black anhedral hematite grains are mostly associated with the chlorite stringers.

Associated with the chlorite schist are small irregular Ni- and Cr-rich massive talc bodies, containing specks of oxidized material, and a small dolomite-talc-chlorite outcrop (10m by 60m) which occurs along joints within the banded chert. A carbonate rock, probably representing altered greenstone (discussed under section 3.4.2.), outcrops in the quartz-feldspar-sericite schists, directly north of Spitskop (Sheet A).

The association of Ni- and Cr-rich talc-rock and chlorite schist at Spitskop may indicate the presence of ultramafic rocks. Talc or rocks rich in talc, accompanied by minerals such as tremolite, anthophyllite, chlorite, magnesite, dolomite, magnetite and quartz, often form when ultramafic rocks are exposed to SiO_2-saturated, frequently CO_2-bearing, aqueous pore fluids during metamorphism (Evans and

Guggenheim, 1988). Nickel-rich varieties can occur in the sapprolite zone of laterites developed on serpentinized ultramafic rocks (Maynard, 1983), as well as in a nickel-rich ore deposit by reaction at the contact between quartzite and ultramafic rocks (De Waal, 1970). Although no ultramafic rocks outcrop at Spitskop, the possibility exists that it might underlie the banded chert and that the Ni-rich talc is a reaction product of the banded chert and a metamorphosed ultramafic body.

3.4.5. SUPERIMPOSED VEINS

The area around Spitskop is characterized by massive quartz bodies and veins, up to 60 metre wide (on the farm Vondelong, Sheet A) outcropping as conspicuous ridges in the quartz schist and at the quartz schist boundaries. Many of these quartz bodies occur along shear and fault zones and joint systems. The quartz is milky to grey and fairly pure. On the farm Geeldam East (Sheet A) some of the massive quartz bodies have a light pink colour.

Quartz veins, usually intensely folded, are plentiful in the quartz-feldspar-sericite schists. They occur mostly parallel to the foliation and along joint and shear faces. Small iron- and manganese-enriched zones are associated with the quartz veins. The iron and manganese were probably displaced during the silicification process. At some localities a thin crust of precipitated iron and manganese oxides are found on the weathering surfaces of the schists.

A few massive milky to grey quartz outcrops, up to a few metres wide, occur in the quartz-feldspar-sericite schists. Several massive quartz bodies outcrop on the northern flank of Spitskop, adjacent to the banded chert contact. These bodies have been subjected to more than one episode of brittle deformation and are mineralized with pyrite, galena and sphalerite. Boxwork textures are plentiful near the surface where pyrite has been removed during weathering.

Quartz veins of various ages are present in the greenschists, occurring parallel to the foliation as well as along joints and small shear zones. Quartz veins in the

chlorite schist at Spitskop are up to 10cm wide, and some have boxwork textures filled with limonite, indicating the replacement of pyrite.

At least four different ages of milky and clear quartz veins are present in the banded chert at Spitskop. The veins have an average width of 1cm, but some are up to 10cm wide. The chert has a boxwork texture, especially where numerous quartz veins intersect each other. The banded chert and some quartz veins have been subjected to more than one episode of brittle deformation. Massive milky to grey quartz outcrops (up to 2m wide) also occur in the banded chert. The quartz is generally fairly pure and massive, but some of the outcrops are highly sheared, and boxwork textures were found in a few outcrops.

3.5. STRUCTURAL GEOLOGY

The structural geology of the area between Spitskop and Winkelhaaksvlei was described in considerable detail by Rabie (1974b). He compiled structural and geological maps of the Moorreesburg-Wellington area. The main structural features on Sheet A represent a combination of structural data from Rabie (1974b) and recent field work.

The position of the Piketberg-Wellington fault zone is still unresolved. According to Hartnady et al. (1974b) the Piketberg-Wellington fault zone marks the Swartland-Boland terrane boundary. Rabie (1974b) located the Piketberg-Wellington fault zone 5km west of Heuningberg, running subparallel to the course of the Berg River and swerving in a westerly direction at the farm Bridgetown, consequently including the Bridgetown Formation and the Spitskop antiform in the Boland terrane. Hartnady et al. (1974) suggested that the Piketberg-Wellington fault zone runs along the eastern boundary of the main greenstone body, thus including the Bridgetown Formation and the Spitskop antiform in the Swartland terrane.

The original subdivision of the terranes by Rabie (1974b) appears more feasible than the present subdivision, and is supported by the following:

a) Little evidence was found for the existence of a fault at the eastern greenstone boundary, except for zones (15 to 20 metre wide) of superficially silicified schist on the farms Heuningberg and Vryheid.

b) The phyllites west of the present 'fault zone' is similar to the phyllites east of the 'fault zone', and no abrupt contact was found between them.

c) The greenstones of the Bridgetown Formation exhibit one prominent cleavage which strikes NNW and is almost everywhere near-vertical, which is characteristic of the structural style of the Boland terrane.

d) Rabie's subdivision includes the Bridgetown Formation, the Voëlvlei metavolcanics and the Riviera metavolcanics which are lithologically very similar, in a single terrane.

It is therefore more feasible to include the whole area between Spitskop and Winkelhaaksvlei (Sheet A) in the Boland terrane. Consequently, phyllites of the Moorreesburg Formation along the western boundary of the Bridgetown Formation now become part of the Porterville Formation.

The metasediments and metavolcanics between Spitskop and Winkelhaaksvlei have suffered polyphase deformation. A well-defined foliation with a general NNW-SSE strike is present in the metasediments and metavolcanics. The foliation was regionally folded into antiformal structures and locally into small near-upright tight folds. This agrees with the structural style of the Boland terrane which was always regarded as structurally more simple than the Swartland terrane, with one phase of near-upright, near isoclinal folds and one prominent cleavage which strikes NNW and is almost everywhere near-vertical (Hartnady et al., 1974). One of the antiformal structures, the Spitskop antiform, was mapped by Rabie (1974b) as a broad antiform trending NNW between Spitskop and Rooihoogte (8km west of Voëlvlei Dam). The antiform axis runs through the south-eastern flank of Spitskop and continues subparallel to the western boundary of the Bridgetown Formation to Sandberg in the south (Sheet A). On Sheet A the position of the antiform between the farms Geeldam and Bridgetown was slightly modified by moving it 1,8km to the east so as to coincide with a broad antiform between the farms Gousblomkraal and Bridgetown. A northwest trending synform axis running through the crest of Spitskop (Rabie,

1974b) is correlated with a NNW-SSE trending synform between Matjiesrivier and Kamina (Sheet A). A well developed lineation in the schists and phyllites is approximately parallel to the axis of the synforms and antiforms, plunging 2 to 25° in a south-easterly direction between the farms Spitskop and Kamina. The synforms and antiforms are mostly southward plunging between the farms Spitskop and Kamina, and northward plunging in the area of the farm Dasdrif.

Faulting in the Bridgetown Formation is obscured by poor exposure of the metavolcanics which are very susceptible to weathering. A fault zone, cutting through the bend in the Berg River and running parallel to a near-vertical cliff at the farm Toorkrans, was mapped by Rabie (1974b). Although this fault zone is poorly exposed, shearing is prominent in core of borehole CE1 which was drilled into unit 4 next to the fault zone. Dolomite lenses which alternate with greenstone unit 4 in borehole CE1, also contain brecciated zones (60cm to 1,5m wide) which consist of a dark grey carbonate matrix with angular fragments of cream coloured dolomite. It is concluded that the contact between units 4 and 9 (Fig. 3.6) is fault related in this area. Borehole core also revealed small shear zones (10 to 30cm wide) within greenstone units 1 and 2, and brittle deformation within unit 7.

On the farm Bridgetown a vertical face of dolomite reveals consecutive episodes of shearing and faulting. The shearing event is represented by a highly foliated zone (up to 50cm wide) in the massive dolomite. The foliated material consists of alternating fine-grained yellow brown, red-brown, dark grey and grey green bands which pass gradually into an adjacent zone of brittle deformation. The foliated zone generally dips 20 to 30 degrees in a northerly direction. It represents either a slip-zone along ductile intrusive material or a thrust fault along which the dolomite underwent brittle deformation and metasomatic transformation. A younger fault zone, dipping 50° in a northerly direction, displaced the highly foliated zone by 30cm. Dolomite suffered brittle deformation without foliation along the younger fault zone. The dolomite is highly jointed with a near-vertical set of joints which cuts through the shear zones.

Between the farms Dasdrif and Winkelhaaksvlei zones of brecciated chert occur in the massive chert bodies (Sheet A). These zones are up to 50 metres wide and

consist of fragments of dark grey, white, maroon and translucent angular chert fragments in a fine-grained yellow brown siliceous matrix. According to Goodwin (1962) brecciated chert horizons are common in cherts associated with greenstones. They are thought to have formed soon after deposition by wave action or slumping, and are probably not related to faulting.

In the Spitskop area faulting is visibly more distinct, being defined by conspicuous ridges of massive quartz in the quartz schists and at the quartz schist boundaries. Rabie (1974b) mapped two major fault zones which borders the Spitskop fault-trough (Fig. 3.2). Contacts between the quartz-feldspar-sericite schists and the quartz schists at Spitskop are therefore fault related and not stratigraphic.

4. METAMORPHIC PETROLOGY OF THE BRIDGETOWN FORMATION

The rocks in the area between Spitskop and Winkelhaaksvlei have experienced low-grade regional metamorphism up to the lower greenschist facies, according to De Villiers (1969). The metamorphism appears to be approximately contemporaneous with the main tectonic phase. Although outcrops of plutonic rocks are absent in this area, the possible presence of unexposed plutons of the Cape Granite Suite and related contact metamorphism should not be ruled out. In this section the metamorphic petrology of the greenstones and associated rock types of the Bridgetown Formation are discussed.

4.1. GREENSTONES

A detailed mineralogical study of the greenstone units focussed on mineral composition and metamorphic grade. The greenstone units (excluding unit 5) consist of the following metamorphic minerals: albite (An_{0-2}), actinolite, epidote, calcite, chlorite, titanite, magnetite, ilmenite and muscovite. Some quartz is always present. Many combinations of these minerals occur depending on the nature of the original rock, the degree of deformation of the rock and the degree of alteration. Unit 10, the younger intrusive dyke, is the only unit which contains relict igneous minerals (e.g. augite). In the other units none of the original minerals or textures were preserved, except for banding within some units which might indicate graded bedding.

The mineral parageneses of the greenstone units (excluding units 5 and 8 which do not contain epidote) are represented on an ACF diagram (Fig. 4.1). It should be noted that mineral compositions of individual units were not plotted in Fig. 4.1 due to insufficient FeO and Fe_2O_3 data for the chlorites. Plots of the different minerals in Fig. 4.1 represent average mineral compositions for mafic greenschists (Winkler, 1976). However, the average chemical compositions of the different greenstone units (excluding unit 5) were plotted on the ACF diagram to indicate that the rock compositions fall in the chlorite-epidote-actinolite equilibrium triangle.

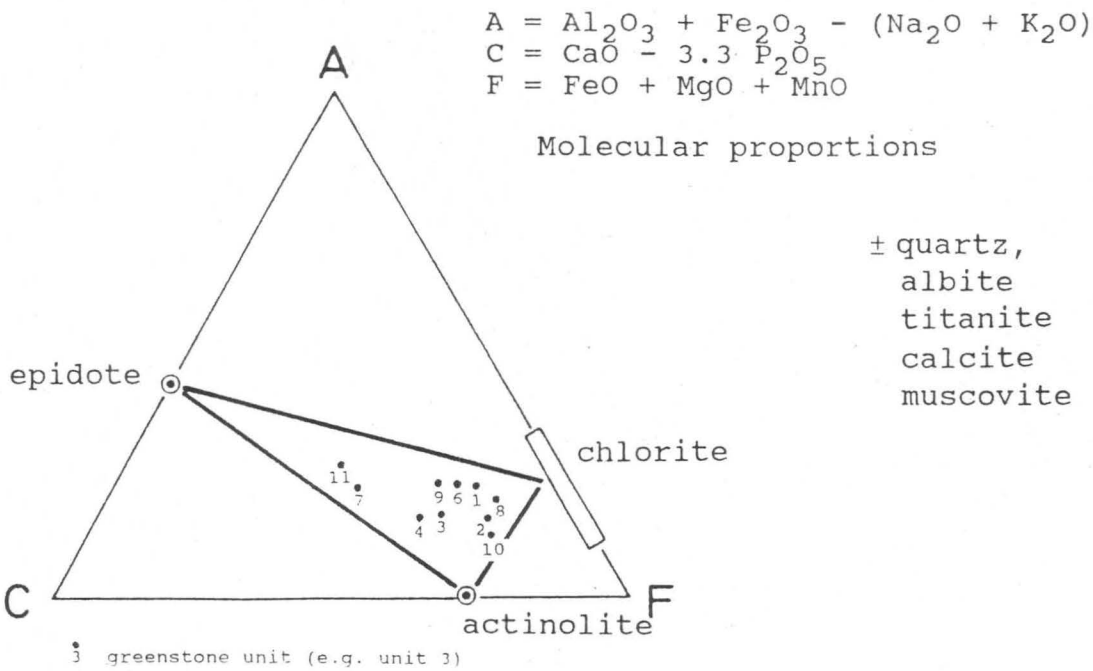

Figure 4.1. ACF diagram showing mineral parageneses in the greenstone units (excluding units 5 and 8). The average chemical compositions of the different greenstone units (excluding unit 5) fall in the chlorite-epidote-actinolite equilibrium triangle.

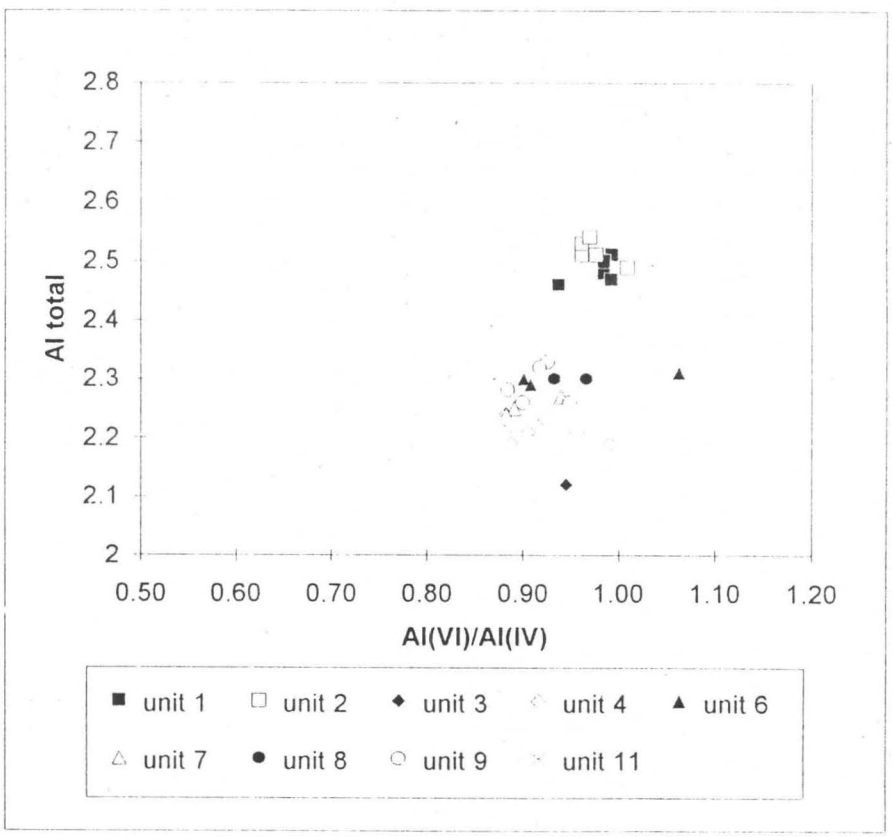

Figure 4.2 Plot of Al_{total} versus Al_{vi}/Al_{iv} (Turpin, 1984) for chlorites of the different greenstone units.

Microprobe analyses revealed compositional variations for chlorites between units (Table 8, appendix). The main difference between chlorites from different units is their FeO_t content. Unit 8 has the lowest FeO_t content of 10%; units 3, 4, 6, 7 and 9 have FeO_t values between 11 and 17%, and units 1, 2 and 11 have FeO_t values between 23 and 30%. Compositional variations between chlorites from different units are further illustrated in a plot of Al_{total} versus Al_{vi}/Al_{iv} (Fig. 4.2). Chlorite of units 1 and 2 has a much higher Al_{total} content than chlorite from other units. Because of the variety of chemical substitutions that are possible in the chlorite structure, structural classification schemes are recommended by most authors in stead of chemical classification schemes. Because XRD analyses were not performed on the chlorites, a chemical classification scheme, recommended by Hey (1954), was adopted. According to Hey (1954) the chlorites classify as oxidized chlorites (Fe_2O_{3t} >4%). With Si contents between 2.71 and 2.91 (calculated on the basis of 14 oxygen), they plot at the boundary between thuringite and chamosite.

The presence of actinolite rather than hornblende indicates that the greenstone units are in the greenschist facies and not the epidote-amphibolite facies. The absence of biotite in the greenstone units (excluding unit 5) indicates mineral assemblages typical of the lower greenschist facies. Secondary minerals such as calcite, quartz and epidote cross-cutting foliation indicate post-metamorphic alteration.

When reviewing the metamorphism of mafic rocks, it is interesting to start with the magmatic parageneses of basaltic-andesitic rocks and to observe the metamorphic changes that take place during low-grade metamorphism. The main constituents of basalts and andesites are plagioclase (from about An 70 to 40) and clinopyroxene, commonly augite, and additional hypersthene and/or olivine (Winkler, 1976). Figure 4.3 gives the average composition of the most common basalt type; the ruled area indicates the common range of basalts and andesites (Winkler, 1976). The dotted line indicates the field occupied by the Bridgetown greenstones (excluding unit 5). Other than SiO_2, the main components are CaO, Na_2O and Al_2O_3 from plagioclase; CaO, MgO, FeO and some Al_2O_3 from augite; and MgO and FeO from olivine and/or hypersthene (Winkler, 1976). After low-grade metamorphism, Na_2O is a major component only in albite and MgO and FeO may be united to form (Mg,Fe)O.

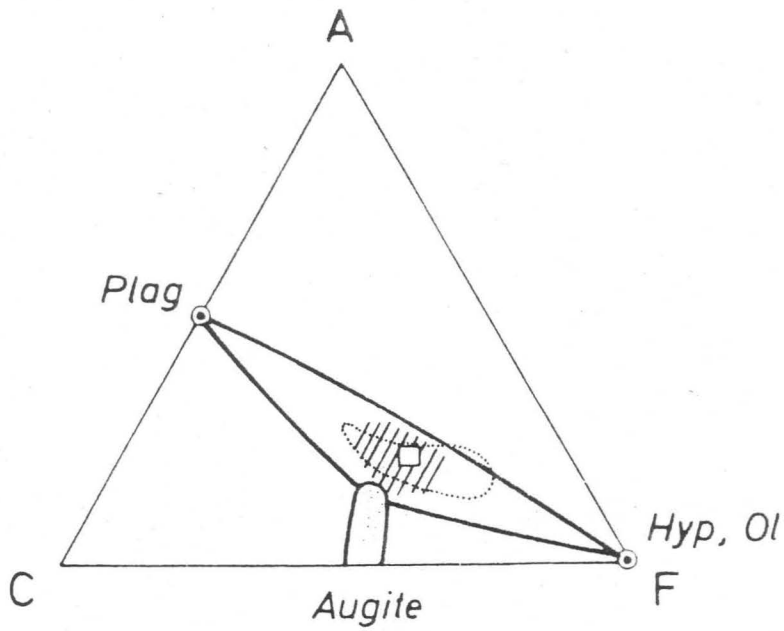

Figure 4.3. The average composition of basaltic-andesitic rocks (ruled area); mean value of tholeiites indicated (square). Plagioclase commonly between An 65 and An 40 (Winkler, 1967). The dotted line indicates the field occupied by the Bridgetown greenstones (excluding unit 5).

During low-grade metamorphism up to the greenschist facies augite and hornblende becomes unstable and decomposes to actinolite, chlorite and epidote.

Mineralogically, unit 5 differs considerably from the other greenstone units. It consists mainly of (in decreasing abundance): quartz, orthoclase, randomly orientated biotite with minor muscovite, chlorite, calcite and magnetite. This mineral assemblage is more typical of a metamorphic rock formed from a pelitic rock rather than a mafic volcanic rock. The chemical composition of unit 5 was plotted on ACF and A'KF diagrams to establish if the rock was primarily magmatic or sedimentary (Fig. 4.4). According to Nockolds (1954) and Ronov and Khlebnikova (1957), different rock types occupy specific fields in the ACF and A'KF diagrams. In the ACF diagram unit 5 does not plot in any specific field, but in the A'KF diagram it plots near the basaltic rock composition. It is therefore deduced that the F-parameters of unit 5 is too high to classify it as a metasediment. The high quartz content indicates that unit 5 either represents a metamorphosed intermediate volcanic rock, or a mafic volcanic rock, contaminated by a sedimentary component.

The temperatures of prograde metamorphism can be bracketed by the following:
a) The presence of chlorite and actinolite indicates alteration at temperatures between 350 and 450°C (Liou et al., 1974).
b) The presence of titanite also limits hydrothermal metamorphism to temperatures below 600°C at $P_{(fluid)} < 3$ kbar and QMF buffer (Elthon, 1982).

4.2. GRAPHITIC SCHISTS

The mineral paragenesis chlorite + muscovite + actinolite indicates that the graphitic schists experienced greenschist facies metamorphism.

Organic matter is highly sensitive to metamorphic conditions. The presence of graphite is indicative of low-grade metamorphism (Frey, 1987). True graphite is formed at 450°C and pressures of 2 to 6 kbar (Landis, 1971). Taylor (1971) quotes temperatures of about 300°C for graphite formation in rocks which underwent shear.

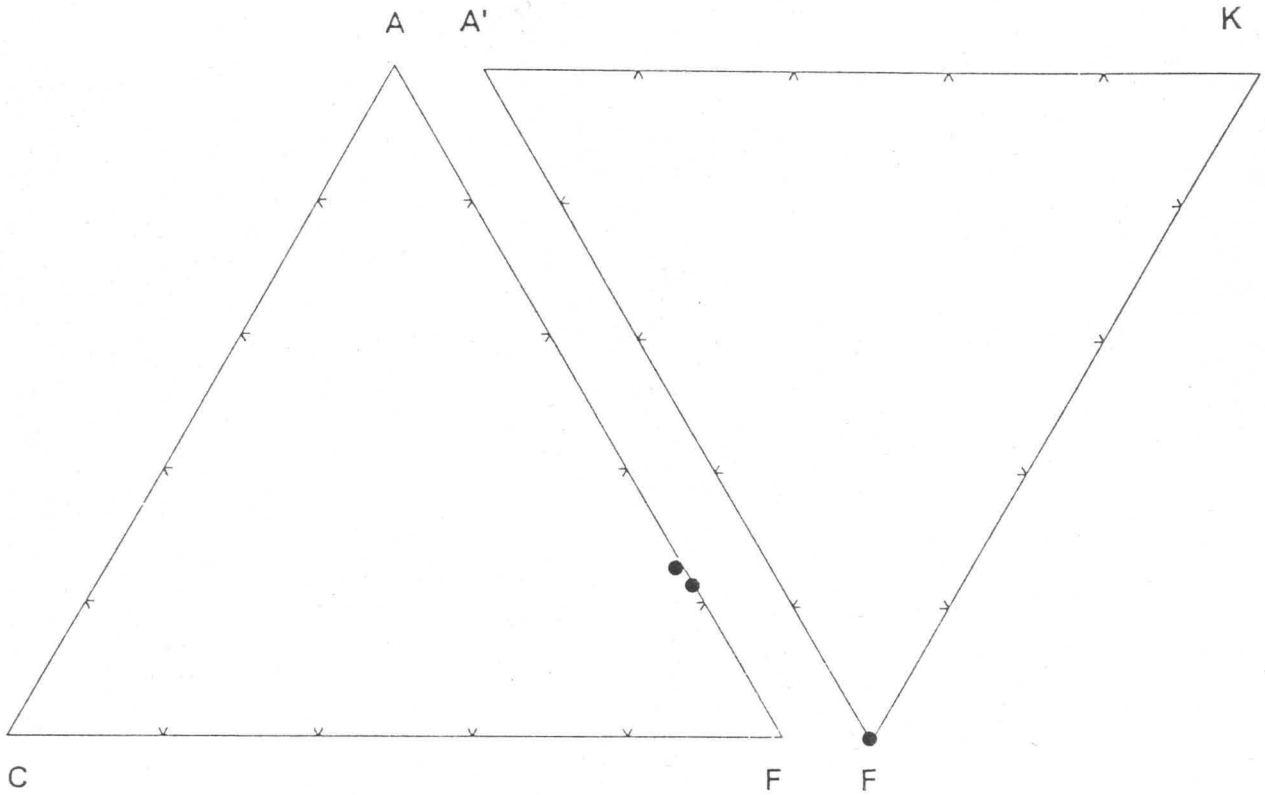

$A = Al_2O_3 + Fe_2O_3 - (Na_2O + K_2O)$
$C = CaO - 3.3\ P_2O_5$
$F = FeO + MgO + MnO$

$A' = Al_2O_3 + Fe_2O_3 - (Na_2O + K_2O + CaO)$
$K = K_2O$
$F = FeO + MgO + MnO$

Molecular proportions

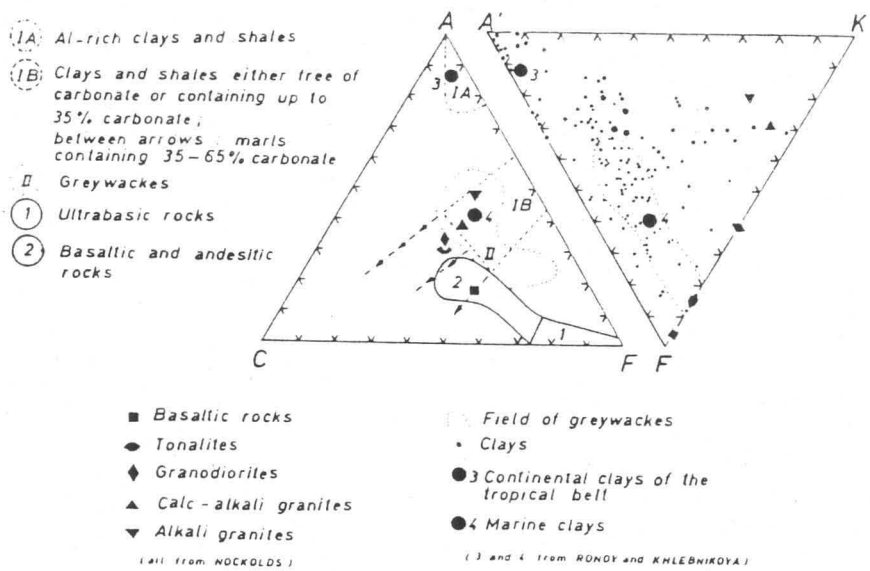

Figure 4.4. The chemical composition of unit 5 plotted on ACF and A'FK diagrams. Fields of various magmatic and sedimentary rocks as given by Nockolds (1954) and Ronov and Khlebnikova (1957).

The graphitic schist lenses, interlayered with the greenstones, probably represent shales which contained organic carbon; which were converted to graphitic schists during polyphase deformation and prograde metamorphism up to the lower greenschist facies.

4.3. DOLOMITE

During low-grade metamorphism the first reaction in a rock consisting of dolomite and quartz (with or without calcite) and containing interstitial water will lead to the formation of talc and calcite, according to the equation:

$$3\ CaMg(CO_3)_2 + 4\ SiO_2 + 1\ H_2O = 1\ Mg_3[(OH)_2/Si_4O_{10}] + CaCO_3 + 3\ CO_2$$

(Winkler, 1976)

XRD analysis of a dolomite sample from the Bridgetown dolomite quarry, revealed the presence of a small amount of talc. The reaction to form talc occurs from 400°C to 490°C where XCO_2 = 0.35 to 0.9 and Pf = 1Kb (XCO_2 = mole fraction of CO_2, Pf = total fluid pressure; Winkler, 1976). Increasing Pf increases the temperature of the formation of talc. The absence of minerals such as tremolite and diopside indicates that dolomite of the Bridgetown Formation did not exceed the greenschist facies grade. The latter corresponds to the low-grade regional metamorphic event which also effected the surrounding Malmesbury beds.

4.4. CONCLUSION

The Bridgetown Formation (greenstones and associated rock types) has experienced metamorphism up to lower greenschist facies, which corresponds to the metamorphic grade of the surrounding metasediments. It is deduced that the Bridgetown Formation and the surrounding Malmesbury beds have been subjected to the same regional metamorphic event, probably contemporaneous with the main deformation event during which a well-defined, near-vertical foliation with a general

NNW-SSE strike developed. This proves that the greenstones are not later intrusions.

5. GEOCHEMISTRY OF THE BRIDGETOWN FORMATION

As previously stated (section 4.1) the original mineralogy of greenstones of the Bridgetown Formation is obscured by metamorphic recrystallization, therefore investigation of their pre-metamorphic characteristics has to be based on their chemical composition. As a first step the geochemical dataset was statistically analyzed to test the validity of the mapping and petrographic classification of the different greenstone units. The subsequent magmatic and tectonomagmatic classification of each unit was done by employing various major and trace element diagrams. Relatively immobile elements were employed to exclude the effect of metamorphism and alteration on the primary distribution of major and trace elements in the greenstones.

Major and trace element geochemistry of dolomite, chert, graphitic schist and muscovite-quartz schist were also investigated to determine their association with the greenstones.

5.1. GREENSTONES

Eighty-seven fresh greenstone samples, mostly from borehole core, were analyzed for major and trace elements by XRF in powdered whole rock samples (Tables 2 and 3, Appendix). Sample positions in borehole core are given in Figs. 1, 2 and 3 (Appendix). Average major and trace element chemistry for each greenstone unit are listed in Table 5.1. Most of the greenstone units are represented by more than two samples, except for units 2, 5 and 8 which are represented by only two samples. These units are either small or highly weathered. Samples were generally taken some distance from superimposed veins to remove the influence of quartz and calcite veins on the geochemistry of the greenstones.

5.1.1. DISCRIMINANT ANALYSIS

Discriminant analysis is a multivariant statistical method to determine how well a specific sample identifies with a predetermined group. The purpose of this exercise

Table 5.1. Average whole rock major and trace element chemistry of the different greenstone units.

Unit	1			2	3			4			5	6			7			8	9			10			11		
n	8			2	7			13			2	4			3			2	27			13			4		
	x	s	se	x	x	s	se	x	s	se	x	x	s	se	x	s	se	x	x	s	se	x	s	se	x	s	se
SiO_2	49.67	7.47	5.28	43.17	42.45	3.47	2.62	37.64	4.85	2.69	51.06	45.01	3.22	3.22	48.93	1.36	1.57	46.54	43.13	3.21	1.23	42.13	1.35	0.75	43.93	0.36	0.36
TiO_2	2.42	0.62	0.44	4.82	2.03	0.26	0.19	2.62	0.54	0.30	1.23	1.77	0.15	0.15	1.19	0.07	0.08	1.78	1.30	0.14	0.05	0.79	0.11	0.06	3.56	0.06	0.06
Al_2O_3	14.71	0.93	0.66	14.21	12.73	1.38	1.04	11.70	2.11	1.17	14.63	14.54	0.61	0.61	14.77	0.84	0.97	14.96	14.63	1.04	0.40	11.20	0.99	0.55	14.51	0.37	0.37
Fe_2O_3	2.07	0.67	0.48	2.83	6.33	1.20	0.90	5.74	1.62	0.90	1.18	7.63	1.53	1.53	9.08	0.28	0.32	4.08	6.81	2.50	0.96	2.73	0.85	0.47	5.60	0.29	0.29
FeO	8.19	1.31	0.93	10.35	5.91	1.44	1.08	6.25	1.34	0.74	9.42	3.70	0.71	0.71	2.41	0.83	0.96	4.49	4.86	2.19	0.84	8.47	0.65	0.36	6.65	0.41	0.41
MnO	0.08	0.04	0.03	0.20	0.14	0.03	0.02	0.17	0.04	0.02	0.31	0.10	0.03	0.03	0.11	0.01	0.01	0.18	0.13	0.02	0.01	0.16	0.00	0.00	0.17	0.01	0.01
MgO	6.00	1.86	1.32	4.15	9.20	2.67	2.01	9.46	0.82	0.45	11.26	9.63	0.66	0.66	4.91	1.79	2.07	12.65	11.15	2.96	1.14	18.43	2.27	1.26	4.62	0.31	0.31
CaO	4.22	2.90	2.05	6.31	7.80	3.80	2.86	10.82	5.68	3.14	0.66	5.59	1.80	1.80	7.09	3.01	3.48	4.43	7.93	2.29	0.88	7.92	0.60	0.33	11.96	0.36	0.36
Na_2O	2.50	0.86	0.61	5.64	3.01	0.88	0.67	2.13	1.45	0.80	0.05	3.92	1.77	1.77	7.31	0.32	0.37	3.85	1.85	1.50	0.58	0.81	0.73	0.40	1.25	0.65	0.65
K_2O	1.60	0.89	0.63	0.31	1.52	0.47	0.35	0.61	0.79	0.44	1.81	1.00	0.68	0.68	0.16	0.06	0.07	0.34	0.79	0.51	0.20	0.36	0.32	0.18	0.44	0.12	0.12
P_2O_5	0.40	0.13	0.09	2.03	0.27	0.04	0.03	0.50	0.11	0.06	0.46	0.22	0.05	0.05	0.13	0.02	0.03	0.20	0.13	0.02	0.01	0.07	0.01	0.01	0.51	0.01	0.01
H_2O-	0.29	0.16	0.12	0.28	0.37	0.42	0.32	0.39	0.17	0.10	0.48	0.25	0.01	0.01	0.24	0.06	0.06	0.21	0.24	0.06	0.02	0.58	0.38	0.21	0.28	0.08	0.08
H_2O+	6.27	2.17	1.53	4.54	7.47	2.16	1.63	10.94	4.04	2.24	6.63	6.59	1.91	1.91	4.68	1.43	1.66	5.95	5.97	2.30	0.88	5.26	0.64	0.35	3.35	0.56	0.56
TOTAL	99.38	0.36	0.25	100.03	99.98	0.36	0.27	99.78	0.63	0.35	100.25	100.43	0.44	0.44	101.35	0.36	0.42	100.20	99.80	0.75	0.29	100.03	0.83	0.46	97.65	0.37	0.37
Mo	0.81	0.56	0.40	2.06	0.84	0.57	0.43	0.46	0.49	0.27	0.29	0.67	0.46	0.46	0.10	0.07	0.08	0.88	0.52	0.49	0.19	0.45	0.46	0.26	1.36	0.22	0.22
Nb	37.33	7.80	5.51	37.27	23.20	3.98	3.00	55.61	12.20	6.76	12.95	20.36	3.12	3.12	9.89	0.60	0.69	19.56	11.54	1.67	0.64	6.11	0.84	0.46	42.50	0.57	0.57
Zr	239.33	22.65	16.01	232.03	128.43	16.84	12.71	190.46	42.02	23.28	237.69	108.50	8.12	8.12	72.32	4.41	5.10	111.90	79.46	8.87	3.41	47.27	6.25	3.46	269.90	1.33	1.33
Y	32.52	4.29	3.03	51.19	20.41	3.88	2.93	26.13	3.26	1.80	24.18	21.71	2.41	2.41	20.87	1.80	2.08	23.11	20.09	2.08	0.80	13.05	2.24	1.24	34.17	0.72	0.72
Sr	131.33	66.02	46.66	303.80	149.92	59.86	45.18	209.42	119.13	66.00	50.06	44.01	8.05	8.05	94.71	19.05	22.03	59.40	212.04	123.40	47.46	170.02	76.25	42.25	780.33	68.41	68.41
U	0.94	0.67	0.47	0.89	1.46	0.50	0.38	1.74	0.70	0.39	6.77	1.56	0.05	0.05	1.57	0.04	0.04	1.13	1.47	0.41	0.16	1.52	0.77	0.43	1.00	0.00	0.00
Rb	39.62	22.68	16.03	10.07	51.26	12.00	9.06	22.15	17.55	9.72	71.61	19.73	14.49	14.49	4.90	1.20	1.39	5.56	23.37	14.30	5.50	16.66	11.62	6.44	9.74	3.14	3.14
Th	8.10	2.84	2.01	4.08	1.44	0.48	0.37	5.58	1.31	0.72	17.36	2.40	1.78	1.78	1.22	0.60	0.69	0.64	1.52	0.55	0.21	1.38	0.47	0.26	4.36	0.67	0.67
Pb	4.33	3.15	2.23	2.00	1.92	0.04	0.03	1.52	0.78	0.43	6.52	1.83	0.05	0.05	1.84	0.04	0.05	1.71	1.89	0.04	0.01	1.87	0.01	0.01	3.98	1.83	1.83
Ga	19.98	2.15	1.52	22.61	16.93	1.64	1.24	14.30	3.25	1.80	18.55	18.54	1.35	1.35	17.53	2.05	2.38	22.21	17.47	2.34	0.90	12.29	1.24	0.68	23.49	1.14	1.14
Zn	117.30	25.23	17.83	123.84	91.30	15.85	11.96	96.63	22.25	12.33	153.19	94.84	4.91	4.91	79.12	10.81	12.50	96.96	86.84	12.11	4.66	74.03	3.22	1.78	121.93	0.61	0.61
Cu	58.27	13.21	9.34	3.57	61.38	7.12	5.37	42.98	10.99	6.09	44.62	73.85	13.38	13.38	51.40	40.21	46.48	182.40	42.09	36.79	14.15	62.17	11.99	6.64	35.05	2.51	2.51
Ni	87.07	31.74	22.43	5.10	431.57	85.57	64.58	271.00	109.91	60.89	284.69	184.04	65.07	65.07	186.96	12.30	14.22	179.69	323.38	98.78	37.99	713.71	124.92	69.21	95.91	17.50	17.50
Sc	29.86	4.82	3.41	22.25	29.14	3.11	2.35	26.91	7.50	4.16	44.44	32.27	1.99	1.99	31.40	1.83	2.11	31.49	22.01	10.34	3.98	11.58	3.05	1.69	27.05	1.40	1.40
V	255.89	51.53	36.42	203.02	234.93	23.30	17.59	245.85	49.17	27.24	301.55	239.79	29.27	29.27	239.17	17.70	20.47	237.79	233.15	19.57	7.53	118.80	16.79	9.30	315.04	9.74	9.74
Ce	56.02	14.05	9.93	78.99	19.03	9.14	6.90	62.79	7.17	3.97	56.65	16.72	10.82	10.82	4.66	4.00	4.62	15.80	7.95	6.60	2.54	6.60	2.19	1.21	71.60	4.58	4.58
Nd	32.43	4.05	2.86	55.71	12.23	6.54	4.93	30.76	2.97	1.65	34.90	12.47	1.59	1.59	2.35	1.18	1.37	7.96	4.20	4.10	1.58	3.21	1.41	0.78	41.53	3.63	3.63
Ba	376.36	170.40	120.42	255.26	226.93	247.80	187.02	433.65	747.28	414.00	501.10	143.44	108.95	108.95	74.21	30.46	35.21	40.45	118.59	67.33	25.90	83.96	96.63	53.53	210.05	22.37	22.37
La	25.13	5.33	3.77	30.06	5.96	3.16	2.38	28.70	4.77	2.65	18.19	2.46	1.55	1.55	3.74	0.15	0.17	3.59	3.74	0.76	0.29	3.52	0.97	0.54	31.18	2.68	2.68
Cr	251.46	92.87	65.63	39.34	609.96	65.80	49.66	614.77	269.35	149.23	721.88	452.46	124.41	124.41	493.80	16.88	19.51	420.81	574.77	105.21	40.46	1179	166.29	92.13	245.47	33.80	33.80

Major elements in weight percent oxide
Trace elements in parts per million
n=number of samples
x=average, s=standard deviation, se=standard error

was to evaluate the geochemical validity of the different greenstone units identified in chapter 3.

Canonical variables 1 and 2 were calculated from the chemical composition of each sample and plotted on a binary diagram to give a graphical representation of the geochemical discrimination among units (Fig. 5.1). Discriminant analysis revealed only two of the eleven units having samples better suited to other units. In unit 6 one of the four samples was grouped with unit 8. In unit 9 one sample was grouped with unit 7 and two samples with unit 6 out of a total of twenty-seven samples. As illustrated in Fig. 5.1 samples of units 6, 7, 8, and 9 are slightly overlapping. The samples were not grouped incorrectly in the first place as substantiated by their mineralogical compositions, they rather exemplify the close geochemical similarities between units 6, 7, 8 and 9.

Elements which best discriminate between the different greenstone units are Nb, Zr, P, V, Ni, Ti, Al, Sr, Mg, Cr and Mn in decreasing order of importance. According to Condie (1981) Nb, Zr, P and V are relatively immobile elements during progressive alteration and greenschist facies metamorphism. The discriminant analysis therefore confirms the classification of the different greenstone units.

5.1.2. MAGMATIC CLASSIFICATION

Chemical classification of the different greenstone units is proposed, because the greenstones were metamorphosed to a degree that precluded classification by conventional mineralogical systems.

Generally the greenstone units are characterized by a low SiO_2 content (34% to 49%) with mg numbers (100 Mg/(Mg + Fe^{2+})) varying between 41 and 84. Their mafic constitution is further depicted by their mineralogical content which mostly comprises ferro-magnesia minerals.

Major and trace element compositions of the greenstone units are comparable to basaltic compositions. Two diagrams were used to illustrate this. The first diagram (Fig. 5.2) is a plot of silica against 'total alkalis' (Na_2O + K_2O) which indicates the fairly precisely defined field occupied by the majority of volcanic rocks (Cox et al.,

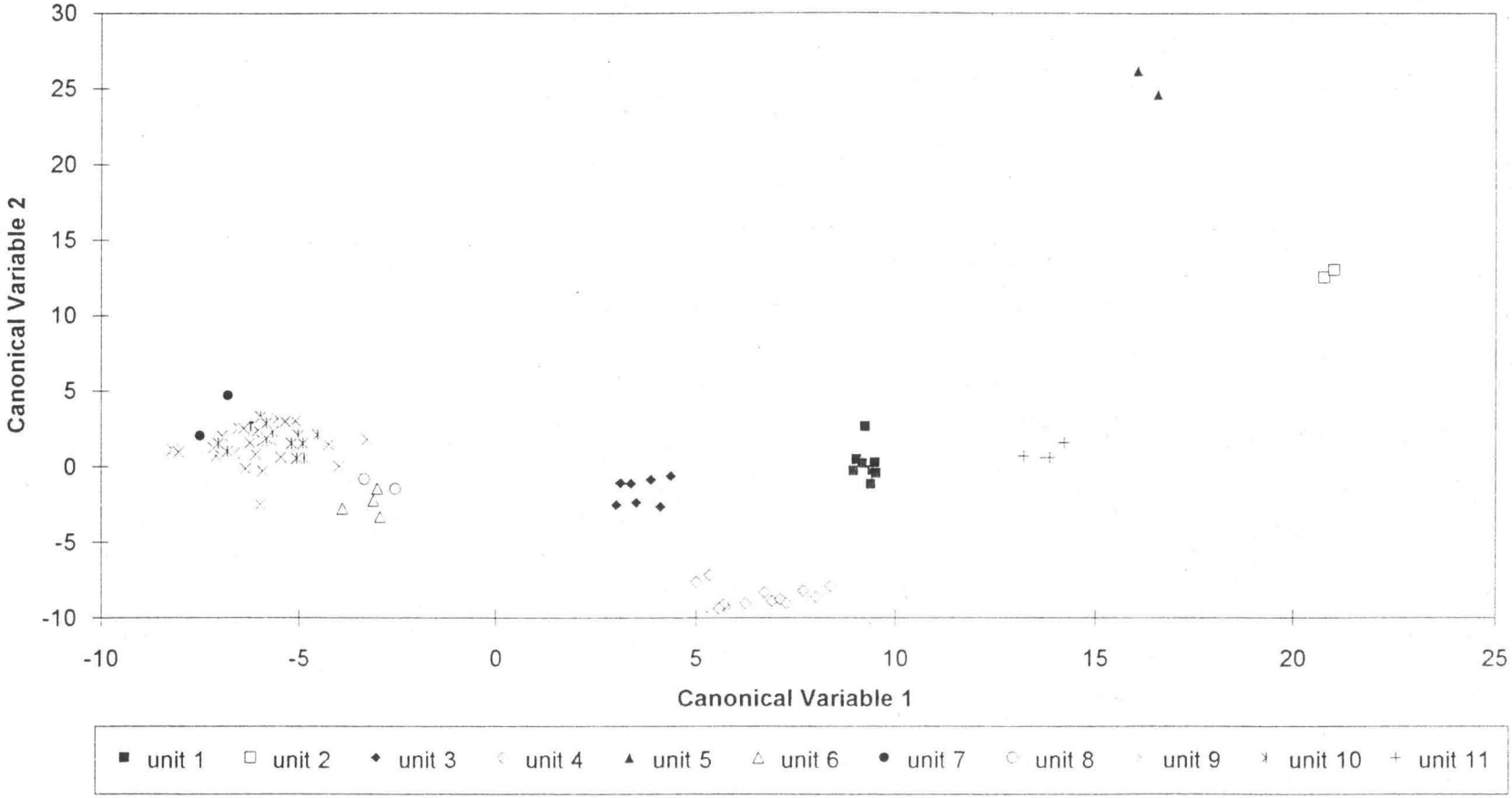

Figure 5.1. Discriminant analysis on major and trace elements of greenstone units of the Bridgetown Formation.

1979). The greenstone units plot mainly in the basaltic field. Units 2 and 7 plot in the trachybasalt field due to their high Na_2O content (unit 2: 5.09 to 6.2%, unit 7: 7.12 to 7.69%). Unit 10, the younger intrusive dyke, has the lowest total alkali content, probably because it consists mostly of augite. Unit 5 and a few samples of unit 1 plot in the andesite field. Not much emphasis will be placed on this diagram, because it utilizes major elements which are known to be mobile during metamorphic and alteration processes. A more reliable diagram to classify different magma series, is the Zr/TiO_2 versus Ce diagram (Fig. 5.3) of Winchester and Floyd (1977). These elements are relatively immobile during secondary alteration processes and greenschist facies metamorphism. Again the greenstones plot extensively in the basaltic field. In this case unit 1 plots mainly in the basaltic field, but unit 5 remains in the andesite field.

The next step is to determine whether these basaltic rocks are subalkaline or alkaline. According to Wilkinson (1986) the appearance of normative quartz or nepheline indicates either subalkaline or alkaline characteristics respectively. In Table 5 (Appendix) norm calculations are expressed as CIPW norms. The units which are mainly nepheline-normative, are units 2, 3, 4, 6 and 7. In the total alkali versus silica diagram (Fig. 5.4) of Irvine and Barager (1971) the nepheline-normative units plot mostly in the alkaline field. The subalkaline field includes units 1, 5, 9, 10 and 11. Another diagram, proposed by Irvine and Barager (1971), to distinguish between alkaline and subalkaline basaltic rocks is the Ol'-Ne'-Q' diagram (Fig. 5.5). The contents of a clinopyroxene-olivine-nepheline-quartz tetrahedron are projected from clinopyroxene onto the basal triangle Ol'-Ne'-Q'. Using the cation norm the coordinates of the ternary diagram become:

Ne'= nepheline + 1/5 * albite

Q' = quartz + 2/5 * albite + 1/4 * orthopyroxene

Ol'= olivine + 3/4 * orthopyroxene

The same tendency is found in this diagram with units 1, 5, 8, 9, 10 and 11 plotting mostly in the subalkaline field and units 2, 3, 4, 6 and 7 in the alkaline field.

Winchester and Floyd (1977) proposed a few graphical representations of immobile element concentrations in volcanic rocks to distinguish between alkaline

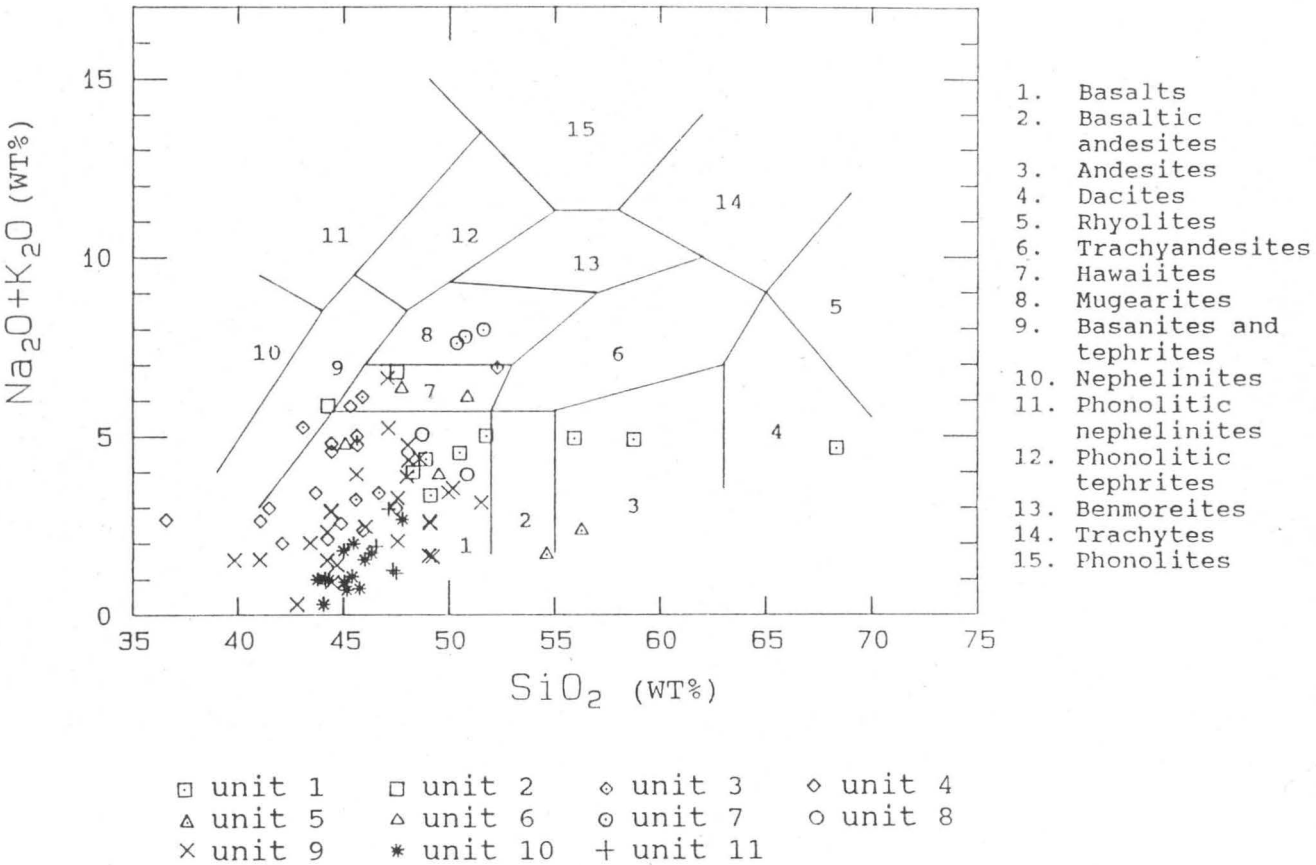

Figure 5.2. Plot of total alkalis versus silica for greenstone units of the Bridgetown Formation which indicates the nomemclature of normal (i.e. non-potassic) volcanic rocks (Cox et al., 1979).

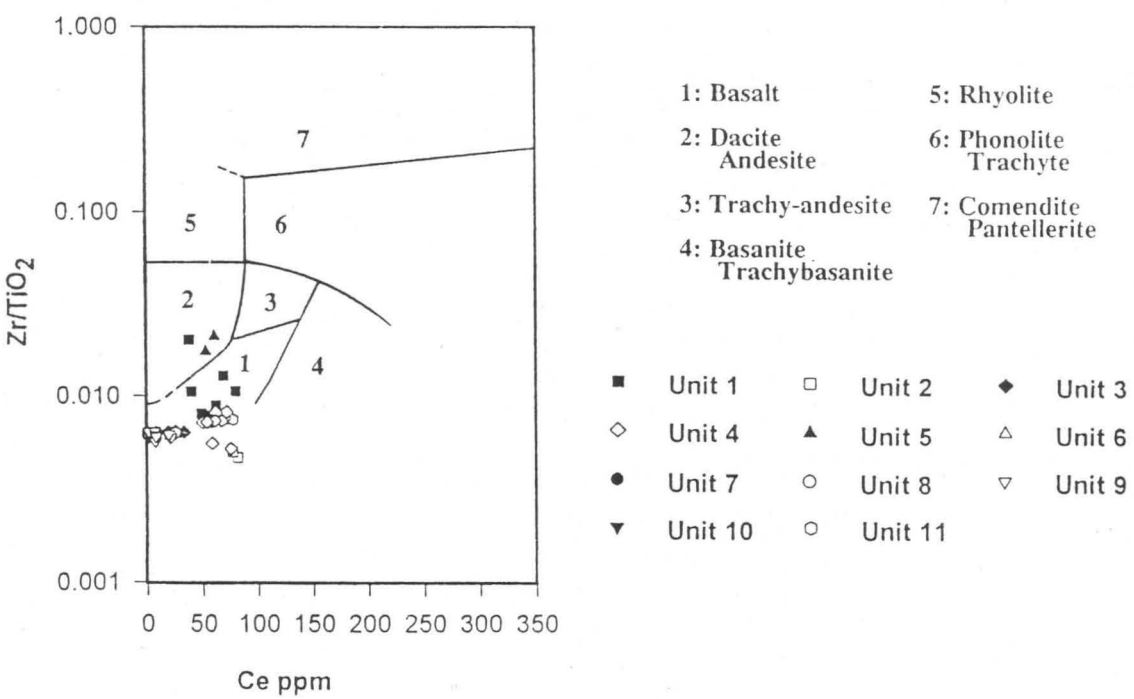

Figure 5.3. Zr/TiO_2 - Ce diagram (Winchester and Floyd, 1977) showing the delimited fields for common volcanic rocks.

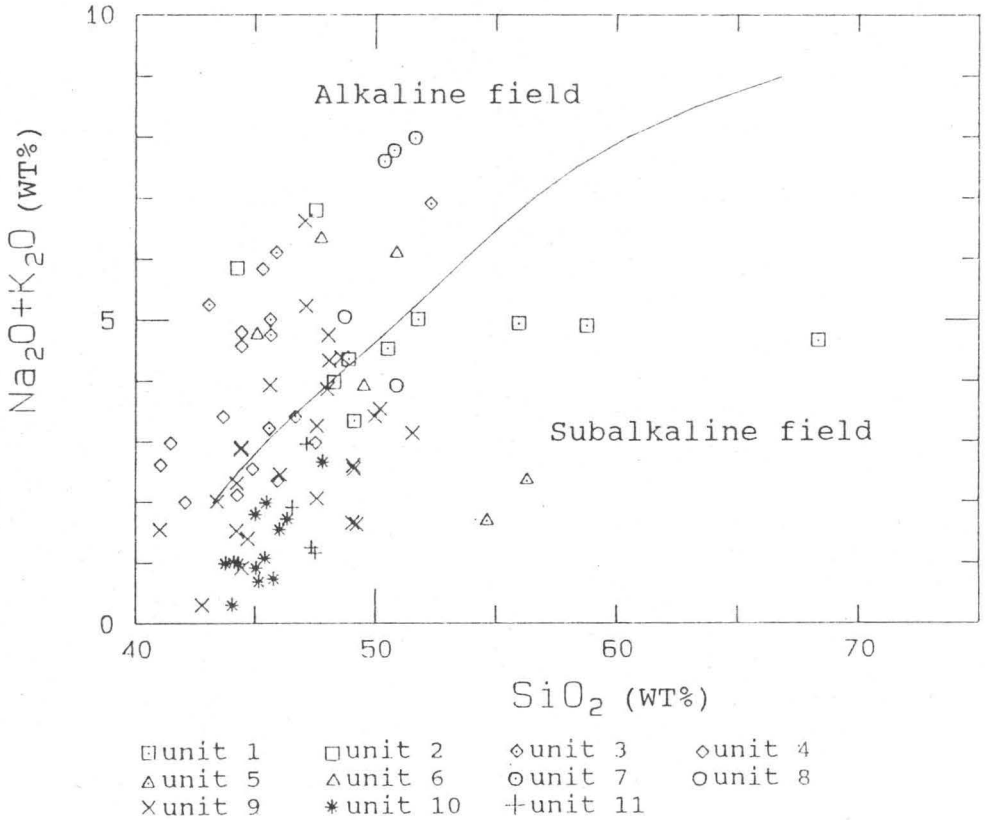

Figure 5.4. Alkalis-silica plot of greenstone units of the Bridgetown Formation. The solid curve is the line chosen by Irvine and Barager (1971) for making a general distinction between alkaline and subalkaline compositions.

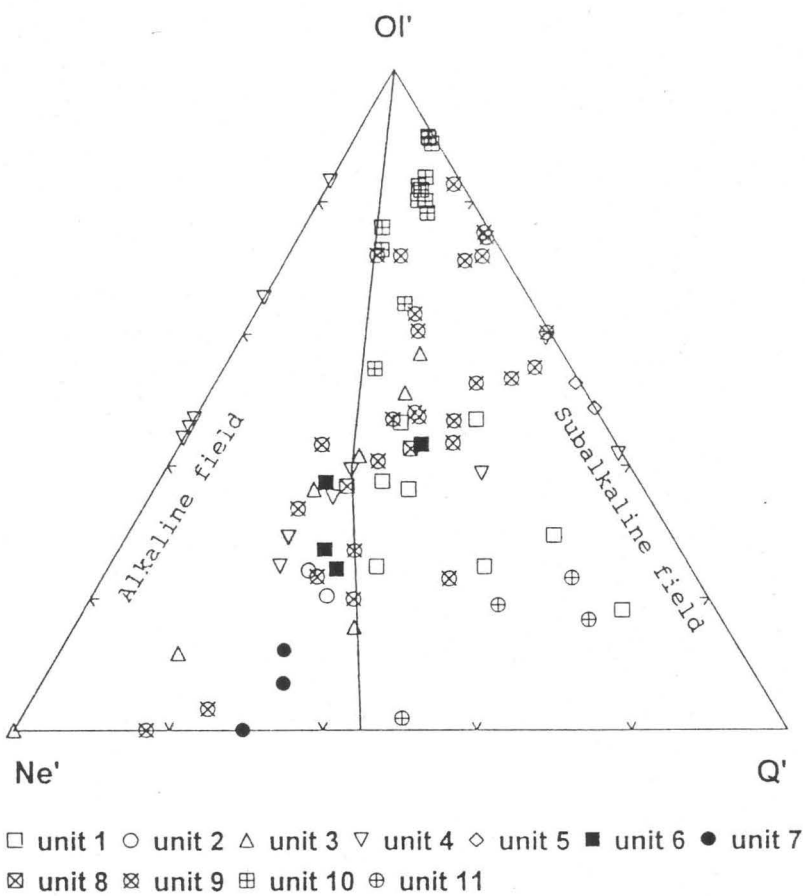

Figure 5.5. Ol'-Ne'-Q' projections (Irvine and Barager, 1971) of greenstone units of the Bridgetown Formation. Plots are in % cation equivalents based on the cation norm.

and subalkaline basaltic rocks where metamorphism or alteration has obscured the original composition. The following diagrams were used: a) SiO_2 versus Zr/TiO_2 (Fig. 5.6 A), b) SiO_2 versus Nb/Y (Fig. 5.6 B), c) Zr/TiO_2 versus Nb/Y (Fig. 5.6 C) and d) Ga/Sc versus Nb/Y (Fig. 5.6 D). The Zr/TiO_2 and Nb/Y ratios reflect the strong concentration of Zr and Nb in alkaline rocks.

These trace element diagrams classify units 7, 9 and 10 (the dyke) as subalkaline basaltic rocks and the other units as mostly alkaline. The trace element diagrams of Winchester and Floyd do not correspond entirely with above mentioned alkaline/subalkaline diagrams of Irvine and Barager (1971), because those diagrams are strongly dependant on the Na_2O content which was highly sensitive to changes imposed by alteration and metamorphism. This is especially evident in unit 7 where albitization was responsible for the high Na_2O content (5.09 to 6.20%) and very low K-content (0.28 to 0.33%).

Alkaline/subalkaline classification of the greenstone units will therefore be based on their relatively immobile trace element content, thus depicting units 7, 9 and 10 as subalkaline and units 1, 2, 3, 4, 5, 6, 8 and 11 as alkaline.

Tholeiitic and calc-alkali basalt series are defined on the basis of the AFM diagram (Irvine and Barager, 1971). In Fig. 5.7 a tholeiitic trend is observed for the subalkaline units (7, 9 and 10). The alkaline units were also included in this diagram to illustrate the general depletion in $Na_2O + K_2O$ in most units. Another chemical difference between calc-alkali and tholeiitic series is their alumina content (Wilkinson, 1986). Calc-alkaline basalts are generally high-alumina types containing 16 to 20% Al_2O_3, whereas their tholeiitic counterparts have only 12 to 16%. Greenstone units 7, 9 and 10 have alumina contents which vary between 9.48 and 16.32%, thus classifying them as low-alumina tholeiitic basalts.

Further division of both the alkaline and subalkaline units into K-poor, "average" and K-rich types can be made by means of an An-Ab'-Or projection (Fig. 5.8, Irvine and Barager, 1971). Plots are based on the cation norm and the coordinates of the ternary diagram are:

An = anorthite

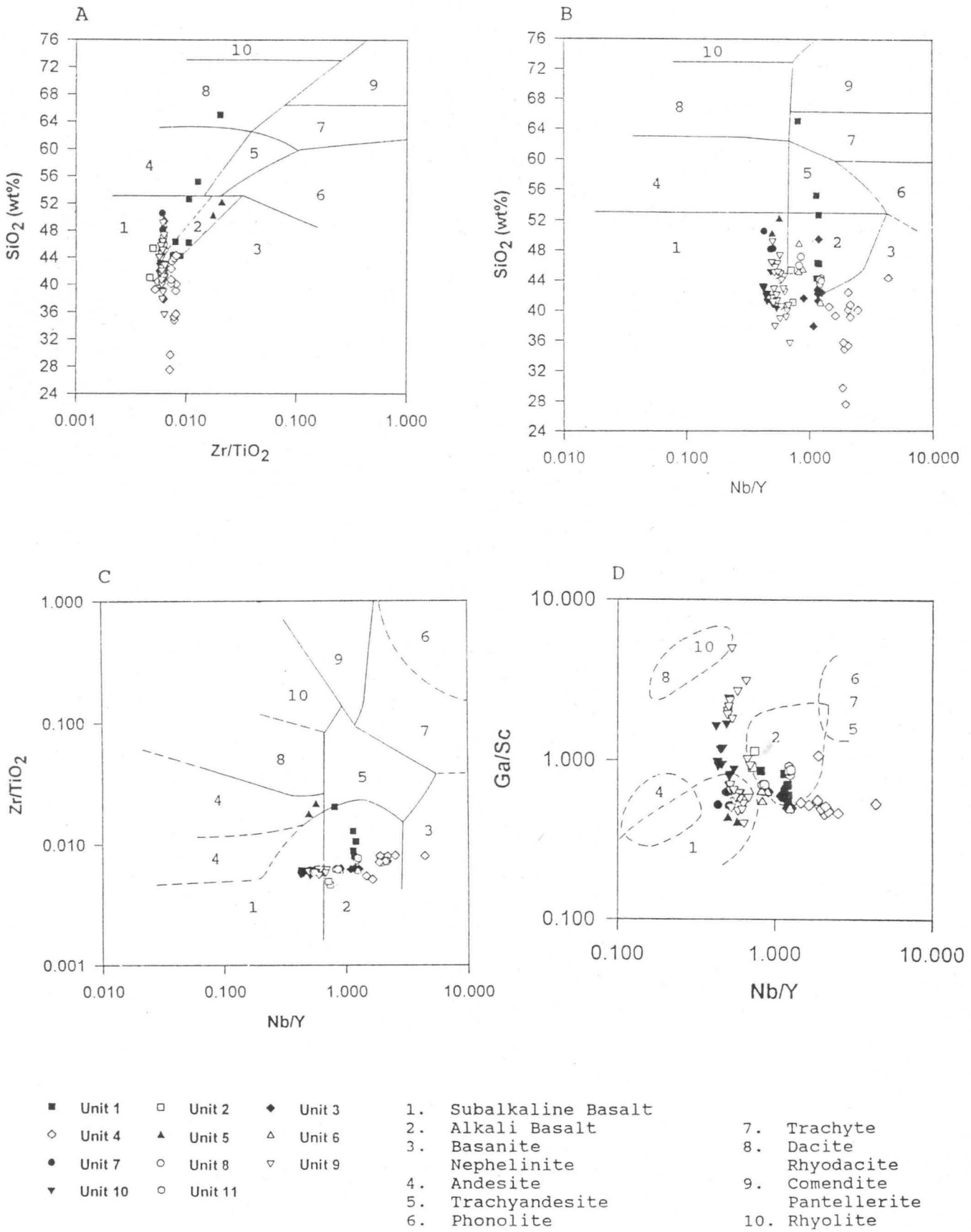

Figure 5.6. Magmatic discrimination diagrams of Winchester and Floyd (1977) using immobile elements. (A) SiO_2 versus Zr/TiO_2. (B) SiO_2 versus Nb/Y. (C) Zr/TiO_2 versus Nb/Y. (D) Ga/Sc versus Nb/Y.

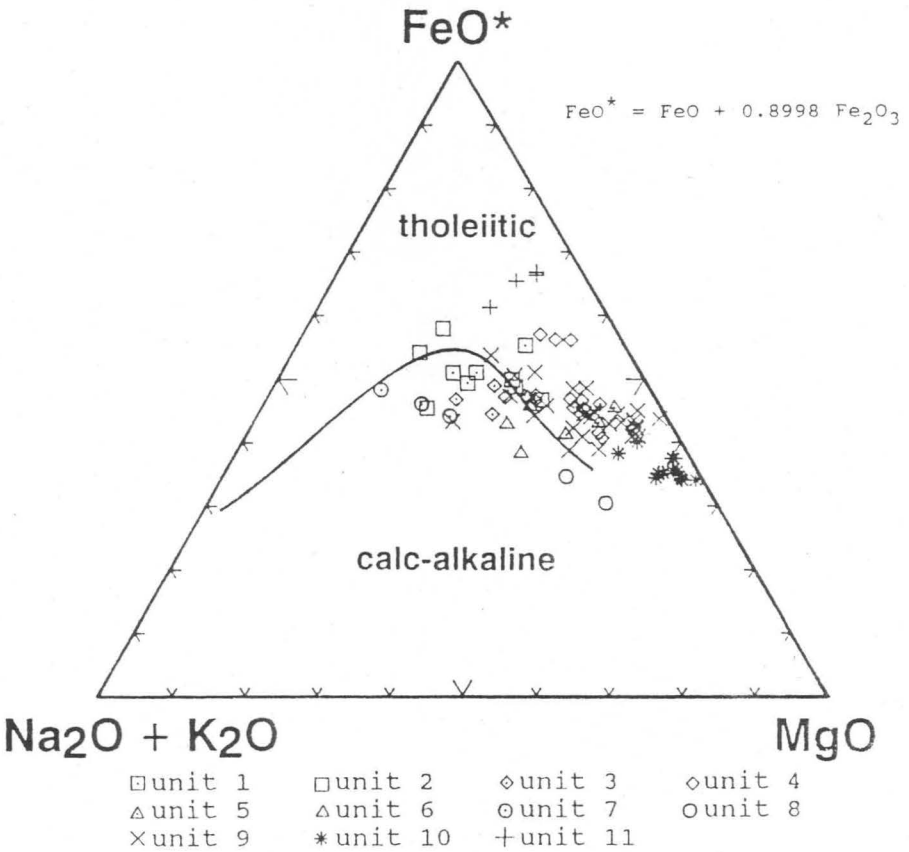

Figure 5.7. AFM diagram of greenstone units of the Bridgetown Formation. The solid curve serves to separate tholeiitic and calc-alkaline compositions.

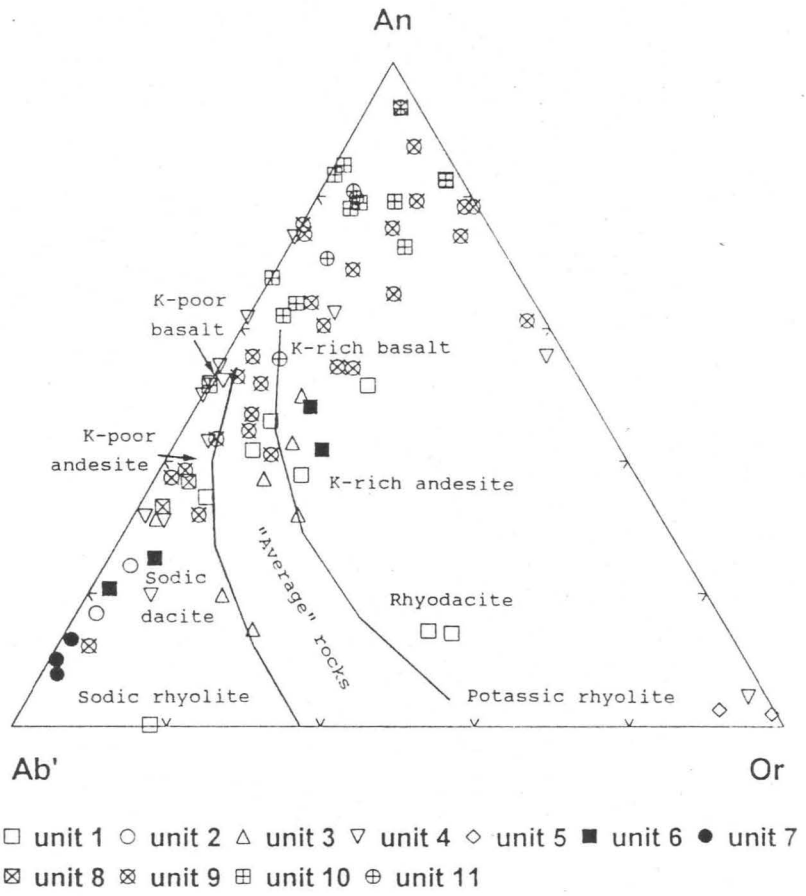

Figure 5.8. An-Ab'-Or projections of greenstone units for distinguishing K-poor, "common" and K-rich variants (Irvine and Barager, 1971). Plots are in % cation equivalents.

Ab' = albite + 5/3 * nepheline

Or = orthoclase

A shortcoming of the diagram is that normative plagioclase composition is strongly dependent on Na_2O and thus may be fairly sensitive to changes imposed by alteration or metamorphism. This is illustrated in Fig. 5.8 where different plots from the same unit are scattered between anorthite and orthoclase. Still, it can be seen that units 5, 10 (the dyke) and 11 are predominantly potassium-rich and that units 2 and 7 are sodic.

The possibility that the basaltic units may be members of a komatiitic suite has to be considered. The pyroxenitic and basaltic members of a komatiitic suite appear to be the result of fractional crystallization of a more magnesian komatiite liquid. Naldrett and Cabri (1976) pointed out that komatiites can be distinguished from tholeiites by plotting Al_2O_3 against the FeO/(FeO + MgO) content of the rock, in which total iron is calculated as FeO. In Fig. 5.9. this is done for the greenstone units. Most units plot in the komatiitic field above the sloping line, except for units 2 and 11. Another distinguishing feature is the relatively low TiO_2 content of komatiites with respect to tholeiites (Naldrett and Cabri, 1976). This is illustrated in a TiO_2-MgO plot (Fig. 5.10) where all the greenstone units plot in the tholeiitic field, except for the younger intrusive dyke (unit 10) which plots in the komatiitic field. Naldrett and Cabri (1976) demonstrated that basaltic komatiites are characterized by high contents of Ni (100 to 181 ppm) and Cr_2O_3 (210 to 800 ppm) compared to "normal" tholeiitic basalts. Greenstone units of the Bridgetown Formation have very high Cr (137 to 1232 ppm, average 521 ppm) and Ni (45.89 to 621.19 ppm, average 268 ppm) contents. The younger intrusive dyke has exceptionally high Cr_2O_3 (890 to 1437 ppm) and Ni (452 to 887 ppm) contents. The chemical discriminatory methods outlined above, can however not be regarded as conclusive evidence for a komatiitic composition. In addition to the chemical criteria, field criteria must also be considered. Field criteria for komatiitic magmatism include 1) the presence of extrusive rocks within an igneous suite 2) the presence of olivine-rich rocks within the suite, and 3) the presence of spinifex textures (Naldrett and Cabri, 1976). Although spinifex textures are absent in greenstones of the Bridgetown Formation, extrusive rocks (unit 1, a

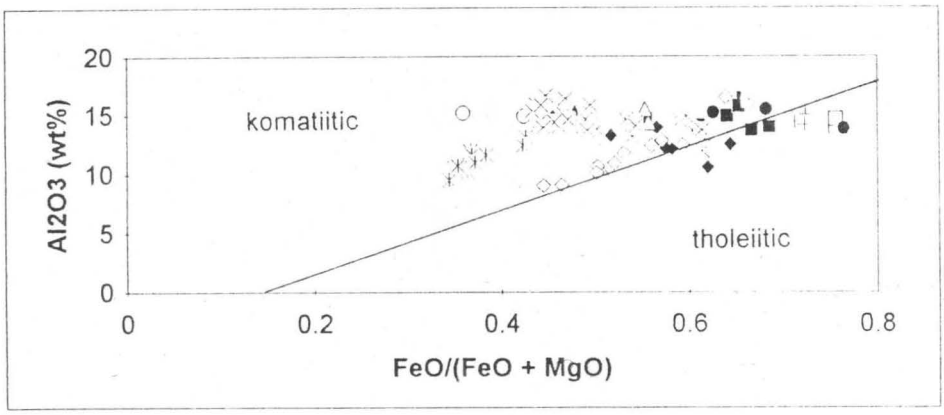

Figure 5.9. Variation of Al_2O_3 with FeO/(FeO + MgO) weight percent ratio in the greenstone units. Note that total Fe is calculated as FeO.

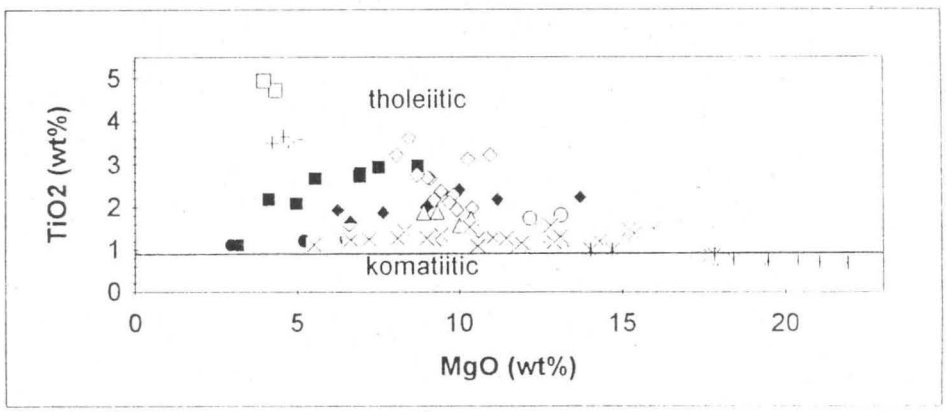

Figure 5.10. Wt percent TiO_2 versus wt percent MgO for greenstone units of the Bridgetown Formation.

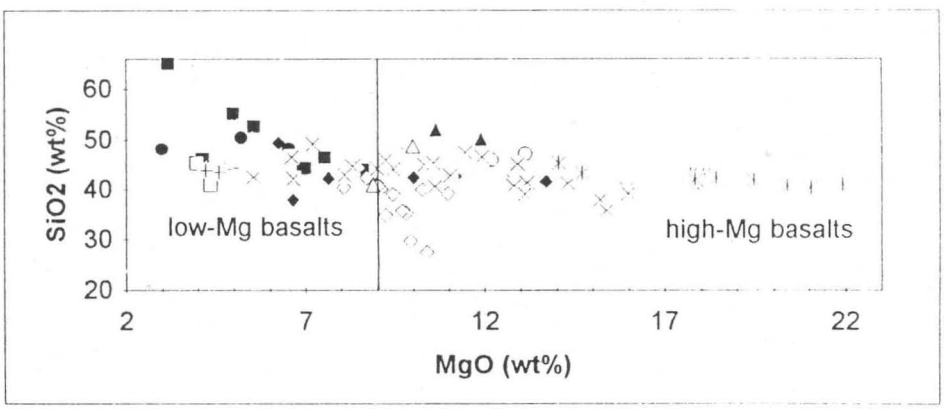

Figure 5.11. SiO_2 versus MgO (wt%) for greenstone units of the Bridgetown Formation. Division between low-Mg and high-Mg basalts are based on those of Redman and Keays (1985).

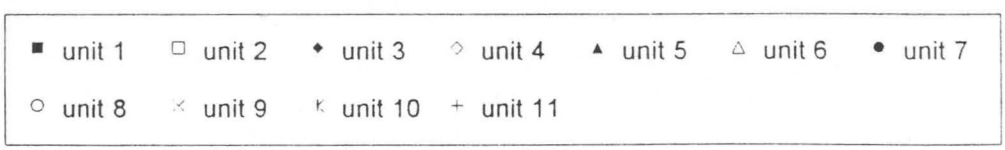

waterlain tuff) are present as well as an olivine-rich unit, unit 10 (the dyke) with 20 to 36% normative olivine (Table 5, Appendix). It is thus concluded that the greenstones of the Bridgetown Formation, or at least some of the units (especially unit 10) can be related to komatiitic magmatism.

Greenstones of the Bridgetown Formation can also be divided into low-Mg basalts and high-Mg basalts according to a SiO_2-MgO diagram of Redman and Keays (1985). In Fig. 5.11 the high-Mg basalts include units 4, 5, 6, 8, 9 and 10 (the dyke) as well as a few samples of unit 3.

In summary, greenstones of the Bridgetown Formation include alkaline (units 1, 2, 3, 4, 5, 6, 8 and 11) and subalkaline (units 7, 9 and 10, the dyke) metabasalts. The subalkaline metabasalts classify as low-alumina tholeiitic metabasalts. Both the alkaline and subalkaline metabasalts include high-Mg (units 4, 5, 6, 8, 9 and 10) and low-Mg (units 1, 2, 3, 7 and 11) rocks. Most of the greenstone units, except for the low-Mg alkaline units (1, 2, 3 and 11) have geochemical characteristics which might indicate komatiitic magmatism.

5.1.3. TECTONOMAGMATIC CLASSIFICATION

Discrimination diagrams based upon incompatible and geochemically immobile elements have been an important tool in determining the tectonomagmatic environment of basaltic rocks. Although their use may be questionable due to the evolution of the crust and mantle through geological time, such discriminants are useful indicators of possible environments of origin for enigmatic rocks.

Three ternary diagrams were used to determine if the different greenstone units are from the same plate-tectonic environment and to identify their petrotectonic origin. They include the Ti/100 - Zr - Y*3 diagram of Pearce and Cann (1973), the Nb*2 - Zr/4 - Y diagram of Meschede (1986) and the TiO_2 - MnO*10 - P_2O_5*10 diagram of Mullen (1983). The elements used as discriminants are virtually immobile during low-temperature alteration and relatively immobile at metamorphic grades up to the greenschist facies.

The Ti/100 - Zr - Y*3 diagram (Fig. 5.12) discriminates between "within-plate" basalts, ocean-floor basalts, low-potassium tholeiites and calc-alkali basalts (Pearce and Cann, 1973). Unfortunately this diagram does not distinguish chemically between ocean island and continental basalts with the result that these are treated as "within-plate basalts". The greenstone units plot predominantly in the within-plate field, except for units 7, 9 and 10 which plot in the ocean-floor basalt field.

The Nb*2 - Zr/4 - Y diagram (Fig. 5.13) of Meschede (1986) distinguishes between different types of mid-ocean ridge basalts ("MORB", including "N-type MORB" from normal mid-ocean ridges and "P-type MORB", from plume-influenced regions), within-plate tholeiites (WPT) and within-plate alkali basalts (WPA). Volcanic arc basalts plot within both WPT and N-type MORB fields and thus cannot be distinguished from these types. The Bridgetown greenstones plot mostly in the within-plate field, except for units 7, 9 and 10 which plot in the P-type MORB field.

The same tendency is found with the Nb/8 - Y/15 - La/10 geotectonic diagram of Cabanis and Lécolle (1989) where the Bridgetown greenstones plot mainly in the non orogenic alkaline basalt field, except for units 7, 9 and 10 which plot in the P-type MORB field. Unit 5 plot separately in the late to post orogenic field.
From the diagrams of Pearce and Cann, Meschede, and Cabanis and Lécolle it is concluded that the subalkaline tholeiitic units (7, 9 and 10, the dyke) are from oceanic environments. This does not exclude the possibility that the units with within-plate characteristics might be ocean island basalts. A useful diagram to distinguish between different oceanic tectonic environments, is the Mn*10 - TiO_2 - P_2O_5*10 diagram (Fig. 5.14) of Mullen (1983). This ternary plot discriminates between the following plate tectonic and petrogenetic environments of volcanic rocks with basaltic to basaltic-andesite composition: mid-ocean ridge (MORB), island arc tholeiite (IAT), calc-alkaline arc (CAB), ocean island tholeiite (OIT), and ocean island alkaline (OIA). In Fig. 5.14. unit 10 (the younger dyke) plots in the island arc tholeiite field, unit 9 in the mid-ocean ridge field and units 1, 2, 3, 4, 5, 6 and 11 in

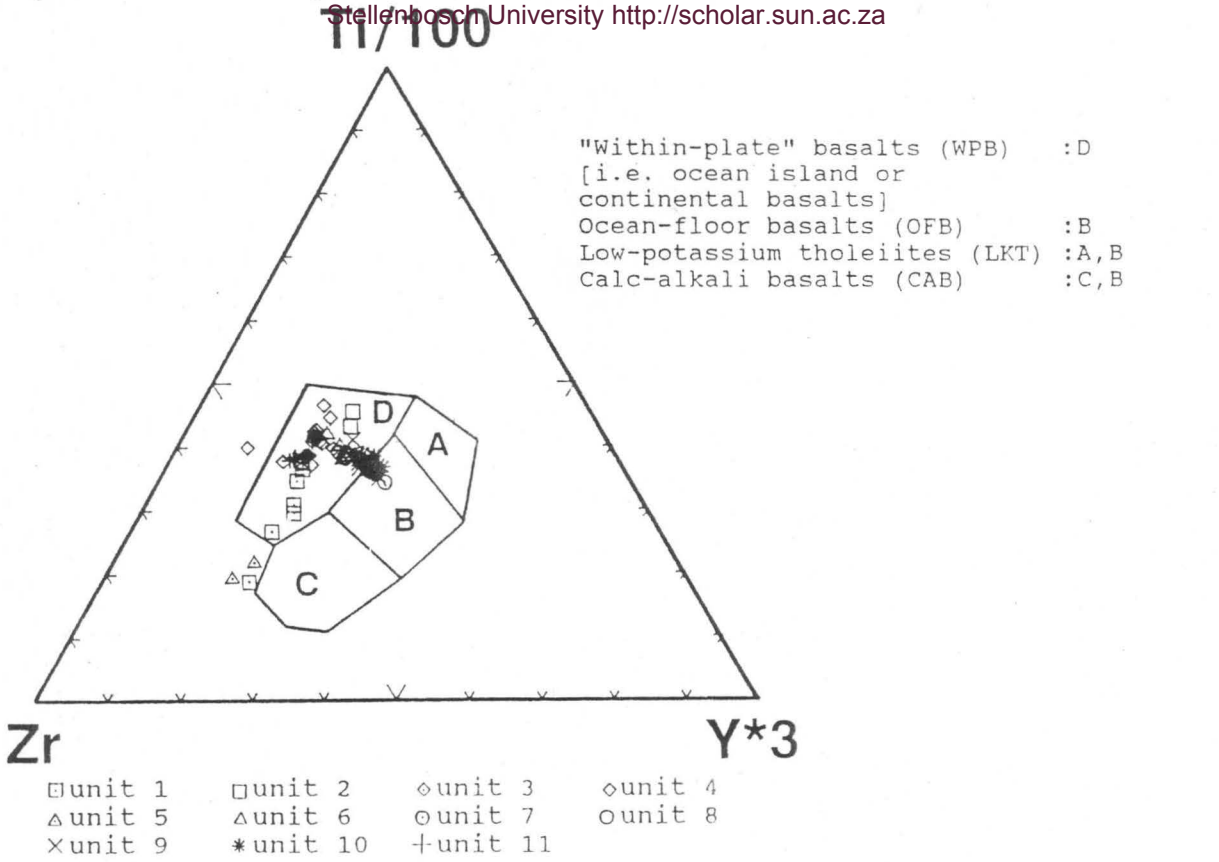

Figure 5.12. Tectonomagmatic discrimination diagram using Ti, Zr and Y (Pearce and Cann, 1973).

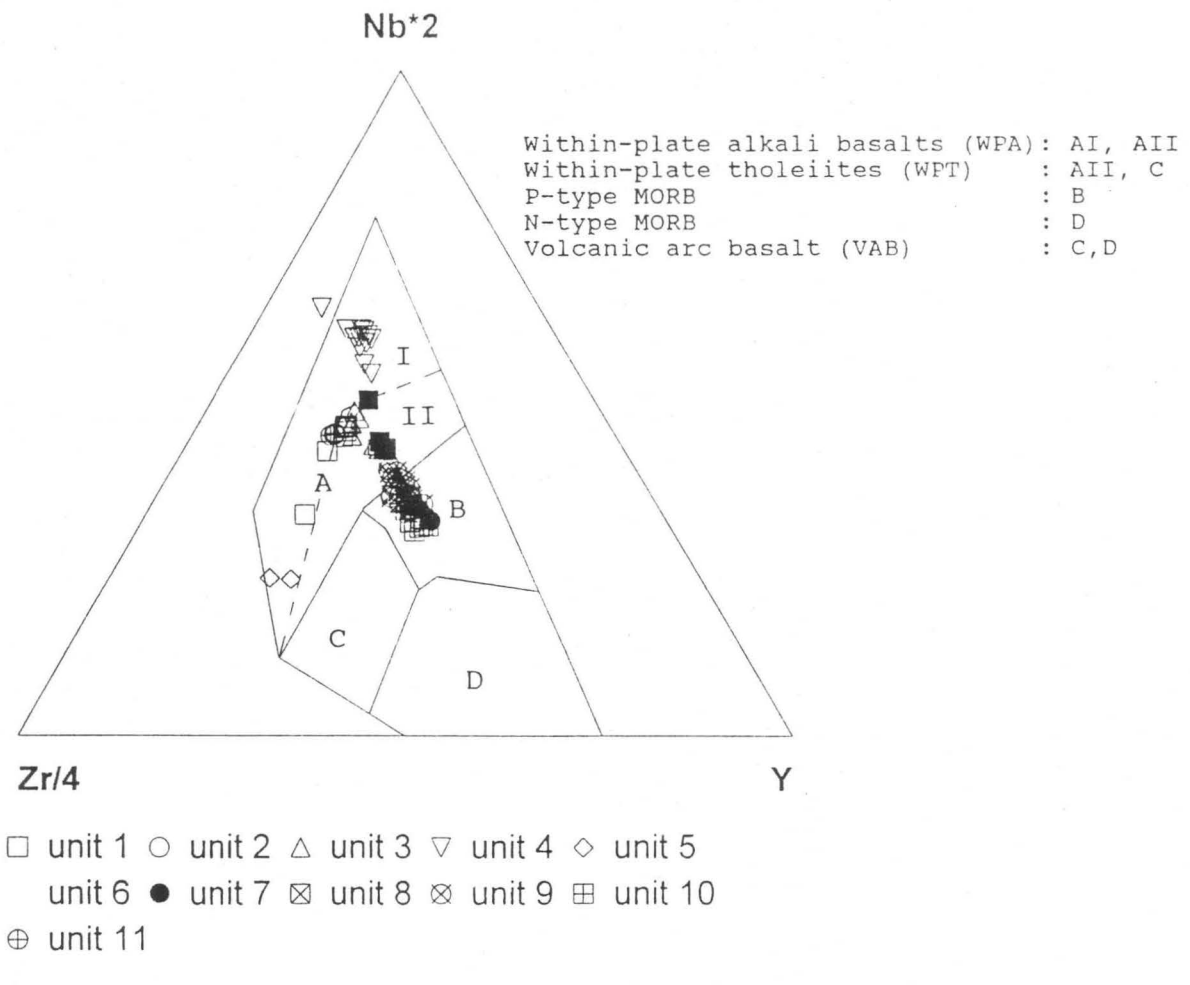

Figure 5.13. Application of the Nb-Zr-Y diagram (Meschede, 1986) to discriminate between magmas from different tectonic environments.

MORB: Mid-Ocean Ridge Basalt
IAT : Island Arc Tholeiite
CAB : Island Arc Calc-Alkaline
OIT : Ocean Island Tholeiite
OIA : Ocean Island Alkalic

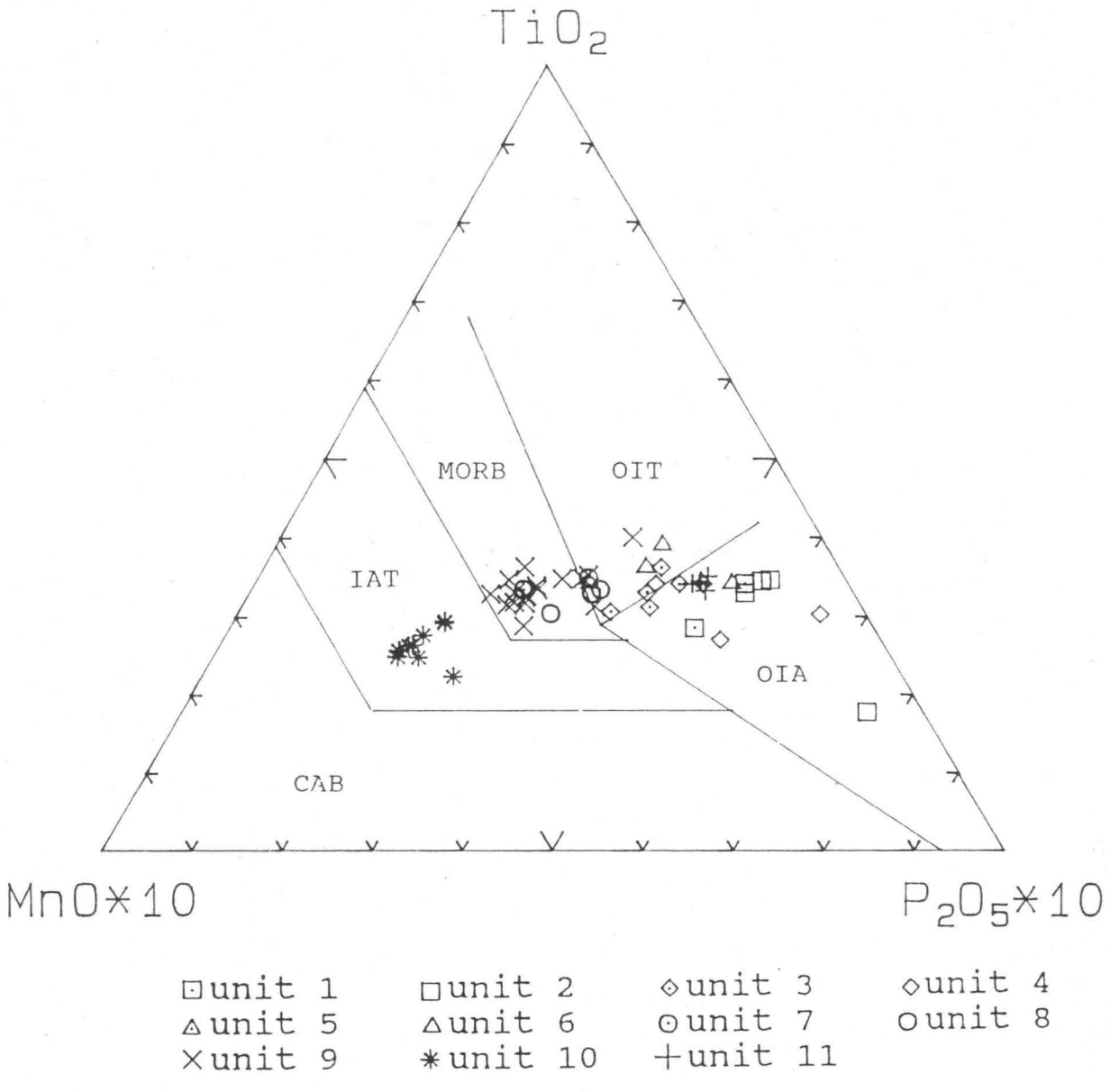

Figure 5.14. MnO*10 - TiO_2 - P_2O_5*10 discriminant diagram for basalts and basaltic andesites of oceanic regions (Mullen, 1983).

the ocean island fields. Units 7 and 8 plot both in the MORB as well as the OIT fields.

So far the elements Ti, Zr, Y, Nb, P and Mn were used to discriminate between different tectonic environments. A different approach is to compare the incompatible element content of the greenstone units with the incompatible element content of selected mafic lavas. This was done by normalizing the incompatible element content of each greenstone unit, an average N-type MORB, E-type MORB (which is equivalent to the N-type MORB) and ocean-island basalt (OIB) to a primitive mantle composition (Fig. 5.15). Average compositions of selected mafic lavas were taken from Sun and McDonough (1989). Normalized data and normalizing factors are listed in Table 6 (Appendix). The elements have been arranged in order of increasing calculated bulk partition coefficient (D) for mantle mineralogies (Wood, 1979). Generally mid-ocean ridge basalts are depleted in incompatible elements relative to oceanic island and continental basalts. E-type MORB are less depleted in incompatible elements than N-type MORB. N-type MORB have a progressive depletion of the incompatible elements with decreasing D relative to the primitive mantle (Wood, 1979). In contrast, the E-type MORB show progressive enrichment of the elements from Y to Nb and then depletion from Nb to Rb.

Three alkaline greenstone units (1, 4 and 11) coincide broadly with the ocean island basalt composition (Fig. 5.15 A, B and C). The negative K, Sr and Rb anomalies (relative to OIB) could be attributed to depletion of these relatively mobile elements during alteration or metamorphism. Units 1, 4 and 11 are enriched in Th ± U relative to the OIB composition which probably indicate crustal contamination.

The three subalkaline units (7, 9 and 10) have similar hyg-element profiles (Fig. 5.15 D, E and F). They are selectively enriched in incompatible elements of low ionic potential (Sr, K, Rb, Ba, Th) with low abundances of elements of high ionic potential (Ce, P, Zr, Ti and Y) relative to N-type MORB, which is distinctive of island arc basalts (Pearce, 1982). The high U and Nb contents are probably due to crustal contamination.

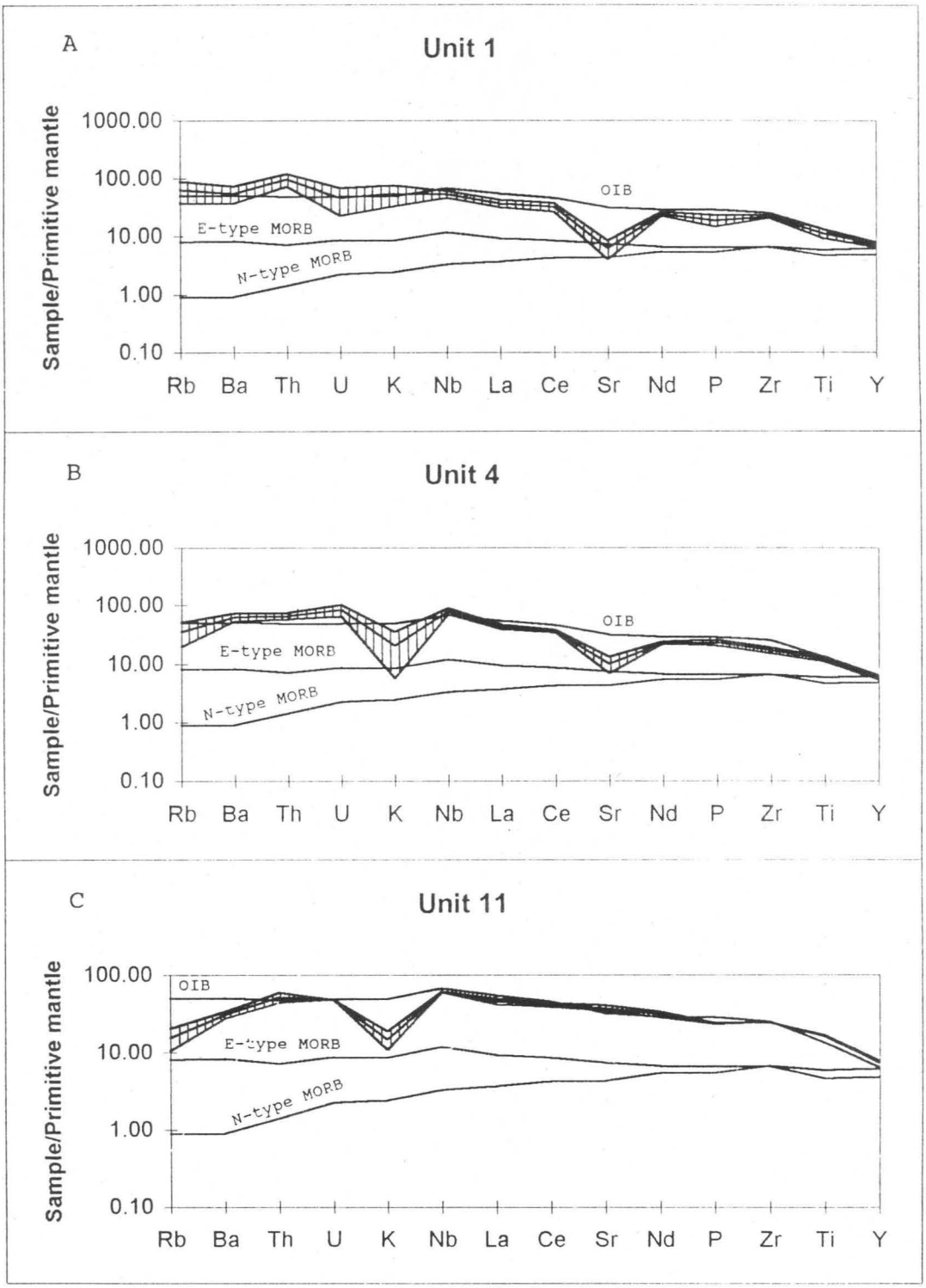

Figure 5.15. Incompatible element abundances, normalized to primitive mantle values, in greenstone units of the Bridgetown Formation, an ocean island basalt (OIB), N-type MORB and E-type MORB. Average compositions of selected mafic magmas and normalizing factors are from Sun and McDonough, 1989.

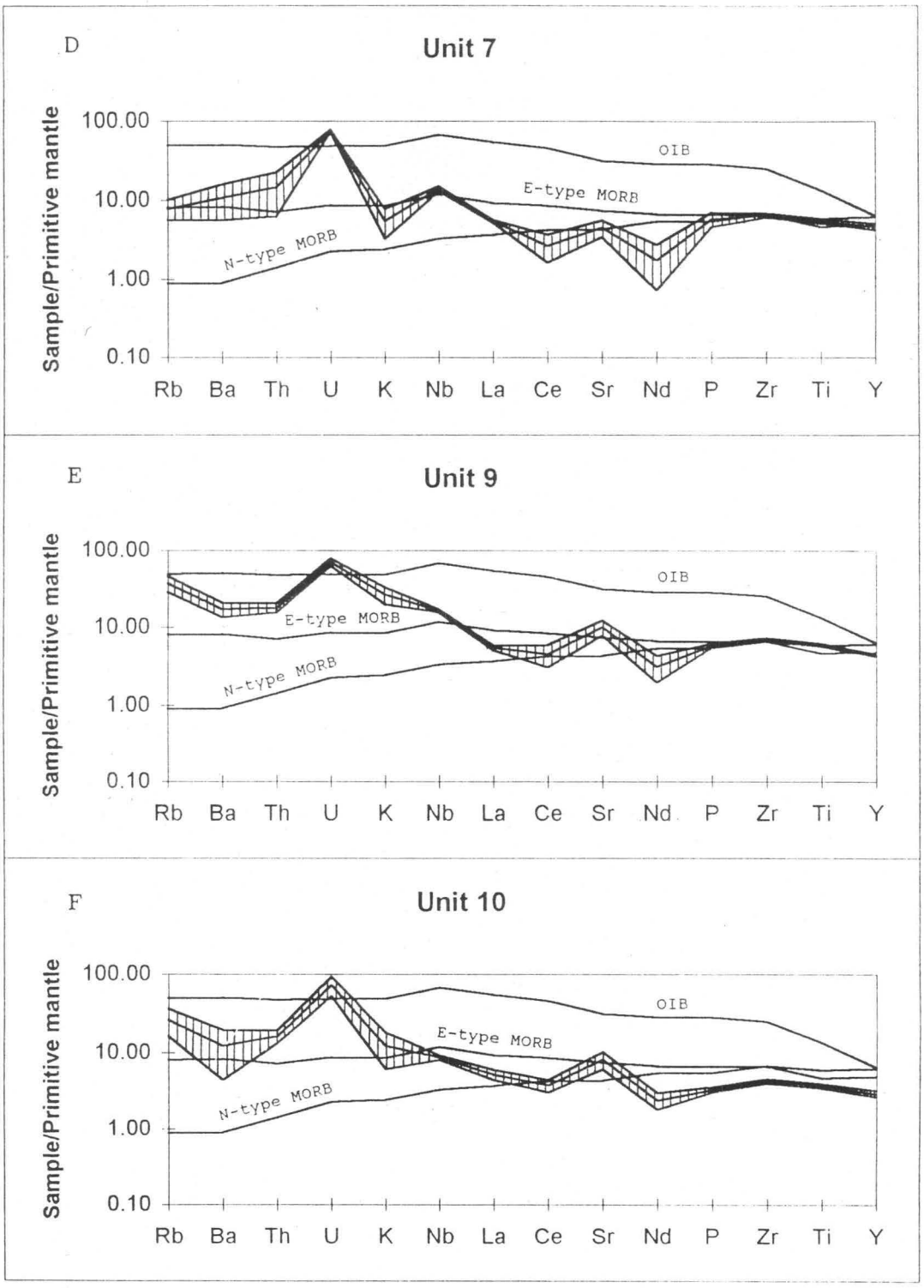

Figure 5.15. (Continued)

Alkaline units 3, 5, 6 and 8 have a 'spiked' hyg-element pattern (Fig. 5.15 G, H, I and J). Marked spikes occur at U, ± Nb and Ce and their Nd-P-Zr-Ti patterns are intermediate between OIB and MORB. They are also depleted in Y and Sc relative to MORB and enriched in U relative to OIB. Although these patterns differ considerably, they show characteristics similar to those found in other intraplate environments (Ewart and Chappell, 1989).

The hyg-element pattern of unit 2 differ considerably from the other greenstone units (Fig. 5.15 K). It has Th, U, Nb, La, Ce and Zr values comparable to those of OIB and is depleted in mobile elements (Ba, Rb, K and Sr) relative to OIB with a distinctively high P, Ti and Y content.

In conclusion alkaline greenstone units have predominantly within-plate characteristics. Incompatible element compositions of units 1, 4 and 11 indicate a possible ocean-island basalt tectonic environment. Subalkaline units 7, 9 and 10 (the younger intrusive dyke) have P-type MORB and island arc basalt characteristics.

5.1.4. MAGMA EVOLUTION

In this section emphasis is placed on the role of partial melting, differentiation and fractional crystallization in determining the observed geochemical patterns for the greenstone units.

Various variation diagrams, plotted in terms of major elements, trace elements and Pearce element ratios were used to determine element relationships in order to model magma evolution.

5.1.4.1. DIFFERENTIATION INDEX

In order to detect compositional variations due to igneous differentiation in greenstone units of the Bridgetown Formation, it is important to select a

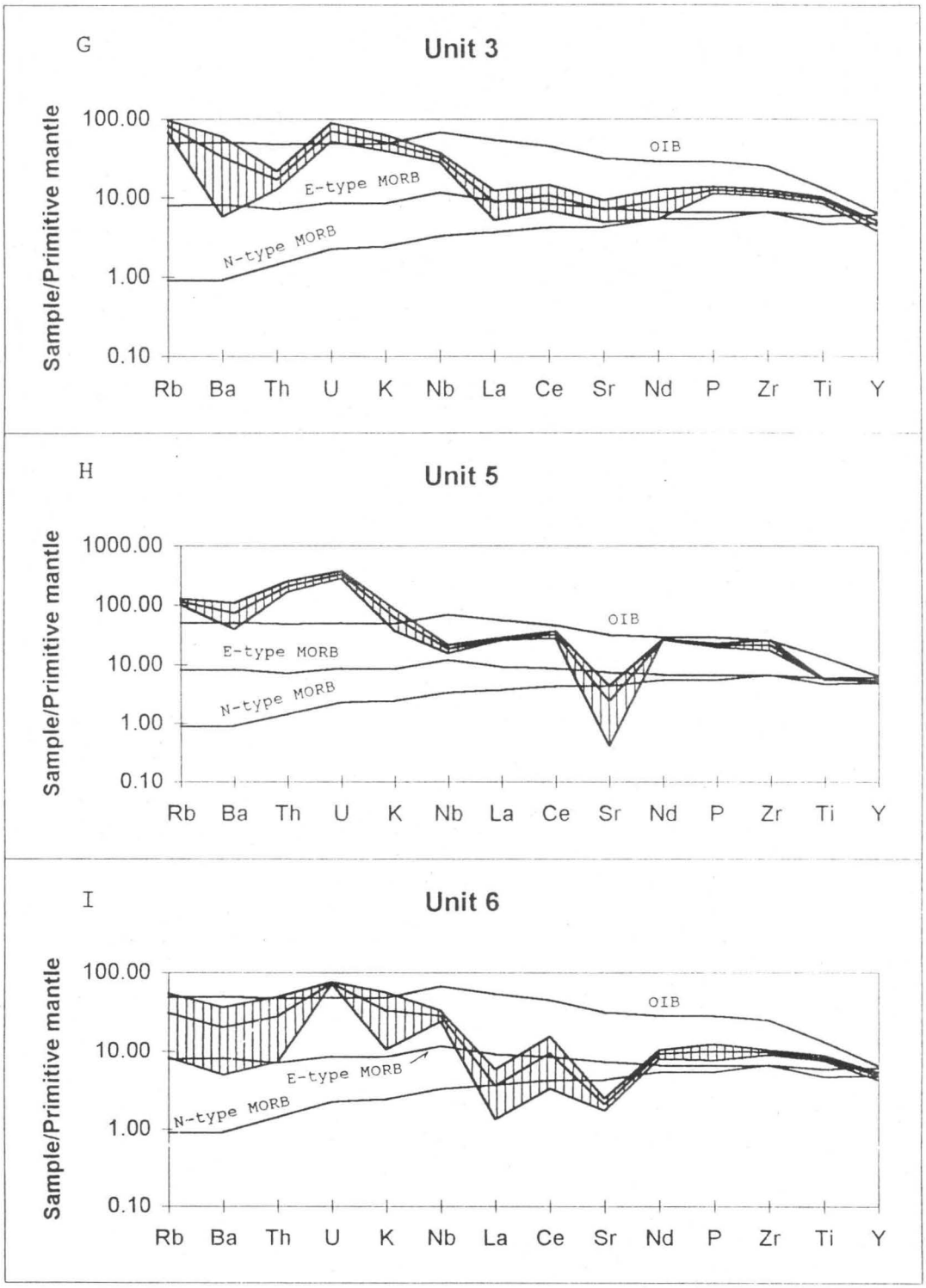

Figure 5.15. (Continued)

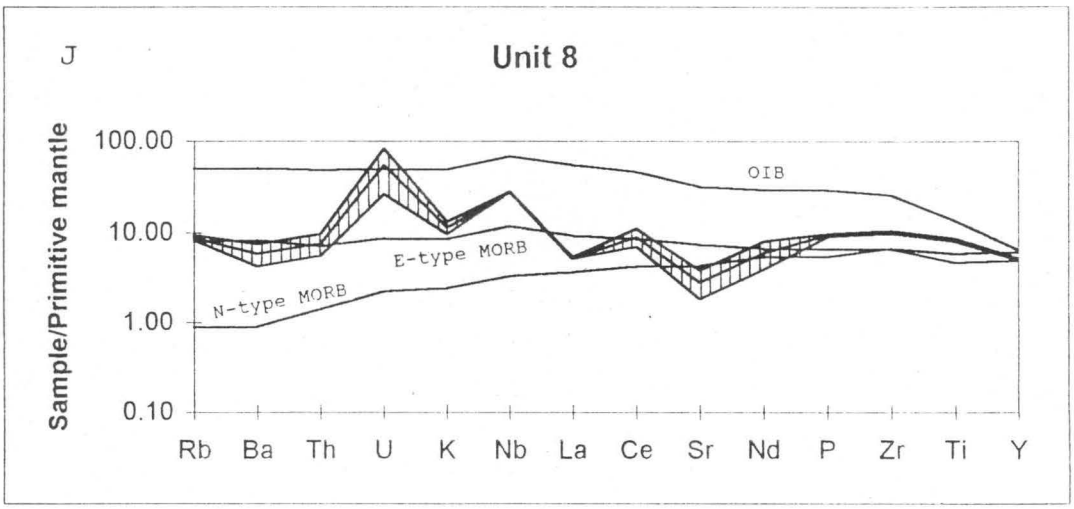

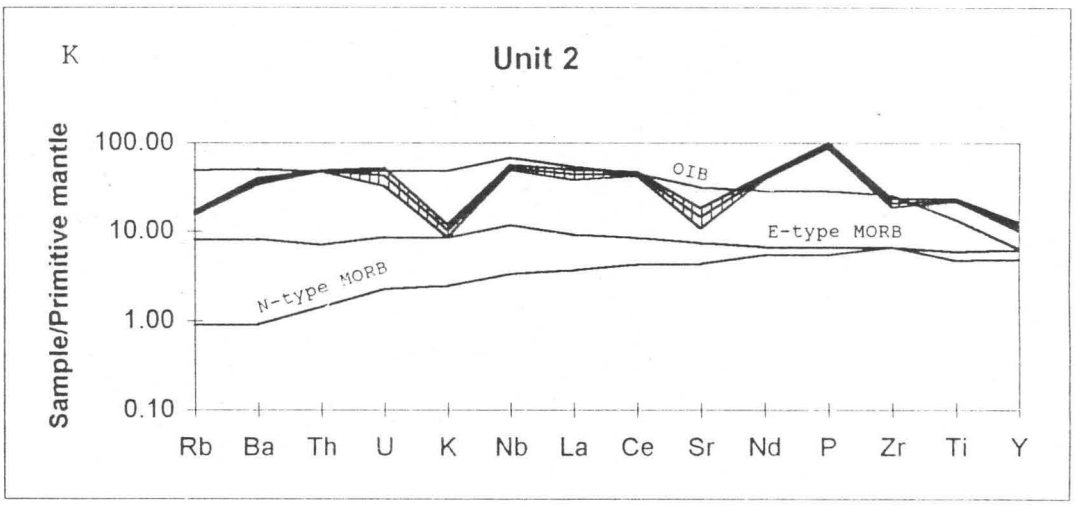


Greenstone unit

Figure 5.15. (Continued)

differentiation index which reflects only igneous variations, rather than those due to metamorphic or alteration processes.

The alkali- and silica-dependent indices were considered inappropriate due to the high mobility of Na_2O, K_2O and silica in the greenstone units. Mg-values ($100Mg/(Mg+Fe^{2+})$), calculated from atomic ratios, were used instead to illustrate differentiation from primitive to more evolved compositions. Mg-values for the different greenstone units are listed in Table 5.2. The greenstone units generally have high mg-values of approximately 70 to 84, except for unit 1 (mg-values: 49 to 63), unit 2 (mg-values: 41.4 to 41.9), unit 5 (mg-value: 67.8 to 68.3) and unit 11 (mg-value: 57 to 69). According to Wilson (1988) primary magmas in equilibrium with typical upper mantle mineralogies (olivine + orthopyroxene + clinopyroxene ± garnet ± spinel) should have mg-values greater than 70, high Ni (>400 ppm), high Cr (>1000 ppm) and SiO_2 not exceeding 50%. The only unit which measures up to these criteria is the younger intrusive dyke (unit 10) which has mg-values of 76 to 84, Cr content of 890 to 1437 ppm, Ni content of 451.6 to 886.6 ppm and SiO_2 content of 40 to 45%. Although units 3, 4, 6, 7, 8 and 9 have very high mg-values, they should not be considered as primary magmas, but rather as basaltic magmas which have undergone little differentiation. The more evolved greenstone units include units 1, 2, 5, and 11.

5.1.4.2. FACTOR ANALYSES

A statistical approach was adopted to evaluate the relationships between elements within a greenstone unit. Factor analysis, which is a multivariant statistical method, was done on the major an trace element chemistry of each unit to determine to which degree certain factors influenced the variance of certain elements within a unit. Units 2, 5 and 8 was omitted due to an insufficient number of samples.

From the factor analyses it is clear that the chemistry of each unit was influenced by various factors. At least one of the following three factors were recognized in each unit:

Factor 1: This factor influenced the variance of the transition elements (Ni, Cr, V, Fe and Sc) as well as Mg to a great extent. This is probably related to olivine and/or

Table 5.2
Mg-values of the Bridgetown greenstone units.

unit	sample	mg-value
1	NS3	60.35
1	NS6	59.03
1	NS7	62.84
1	NS21	54.49
1	NS24	55.94
1	NS28	51.08
1	NS31	48.98
1	NS195	52.89
2	NS10	41.92
2	NS13	41.42
3	NS36	76.16
3	NS37	74.13
3	NS39	73.25
3	NS41	71.74
3	NS44	72.32
3	NS46	72.00
3	NS196	73.43
4	NS173	74.46
4	NS175	76.19
4	NS176	75.34
4	NS178	73.33
4	NS181	75.13
4	NS182	64.40
4	NS183	65.87
4	NS184	76.77
4	NS185	71.55
4	NS187	71.20
4	NS188	77.41
4	NS190	69.99
4	NS191	78.12
5	NS49	67.83
5	NS197	68.32
6	NS57	79.90
6	NS60	80.35
6	NS72	84.60
6	NS76.2	84.42
7	NS64	79.38
7	NS69	77.16
7	NS198	78.44
8	NS74	82.25
8	NS76.1	84.47
9	NS147	79.22
9	NS80	83.00
9	NS82	92.37
9	NS86	82.59
9	NS90	83.04
9	NS92	82.81
9	NS93	82.42
9	NS96	83.63
9	NS97	84.19
9	NS98	81.21
9	NS100	83.66
9	NS102	83.43
9	NS103	81.67
9	NS107	97.77
9	NS109	78.16
9	NS112	79.34
9	NS115	77.42
9	NS121	80.60
9	NS142	81.30
9	NS149	78.35
9	NS151	72.35
9	NS152	70.99
9	NS154	66.11
9	NS157	71.61
9	NS161	70.85
9	NS193	83.85
9	NS194	82.47
10	NS123	76.17
10	NS124	76.37
10	NS126	80.69
10	NS127	84.00
10	NS128	82.08
10	NS129	81.03
10	NS130	81.43
10	NS132	78.31
10	NS134	79.00
10	NS135	78.61
10	NS136	78.35
10	NS138	77.43
10	NS140	77.92
11	NSF/2.5	56.00
11	NSF/2.6	57.05
11	NSF/2.7	53.53
11	NSF/2.8	54.53

pyroxene fractionation during differentiation. Factor 1 was recognized in units 1, 7, 10 and 11.

Factor 2: The variance of incompatible elements such as Nd, Y, Zr, Nb, Ce, P and Ti were determined by factor 2. Factor 2 probably represents incompatible element behaviour during partial melting and differentiation. This factor was recognized in units 1, 3, 9 and 10.

Factor 3: Factor 3 probably represents a metamorphic or alteration event, because it influenced the variance of all the relatively mobile elements such as Ca, Sr, Na, K, Ba and Rb.

Although identification of the different factors are not always successful, it does however indicate the relationship between elements (if they show any correlation or not) which supplied a firm basis to interpret variation diagrams.

5.1.4.3. BINARY VARIATION DIAGRAMS

K_2O, Na_2O, Ba, Rb, Sr and Ca were plotted against SiO_2 to illustrate their scattered variation within the units (Fig. 5.16). It is concluded that these elements, including SiO_2, have suffered some degree of mobilization, probably during prograde metamorphism or alteration processes or both. These events obscure the primary igneous variations of these elements to a great extent.

Fortunately metamorphic and alteration processes had little effect on the variation of Nb, Zr, P, Ti, V and Y. They are relatively immobile elements during low-temperature alteration and metamorphic grades up to the greenschist facies (Condie, 1981). In plots against SiO_2 (Fig. 5.17), they show little scatter within most units. Scattering is more observable in units 1 and 4 which were probably subjected to more severe metamorphic or alteration processes than the other units. This might be related to shearing events which were recognized in borehole core and thin sections (section 3.2.1(vii), unit 1; section 3.2.1(v), unit 4). The incompatible nature of these elements is illustrated by their relatively constant values with SiO_2 variation within a unit. They are also good discriminants between the units as previously concluded from discriminant analysis.

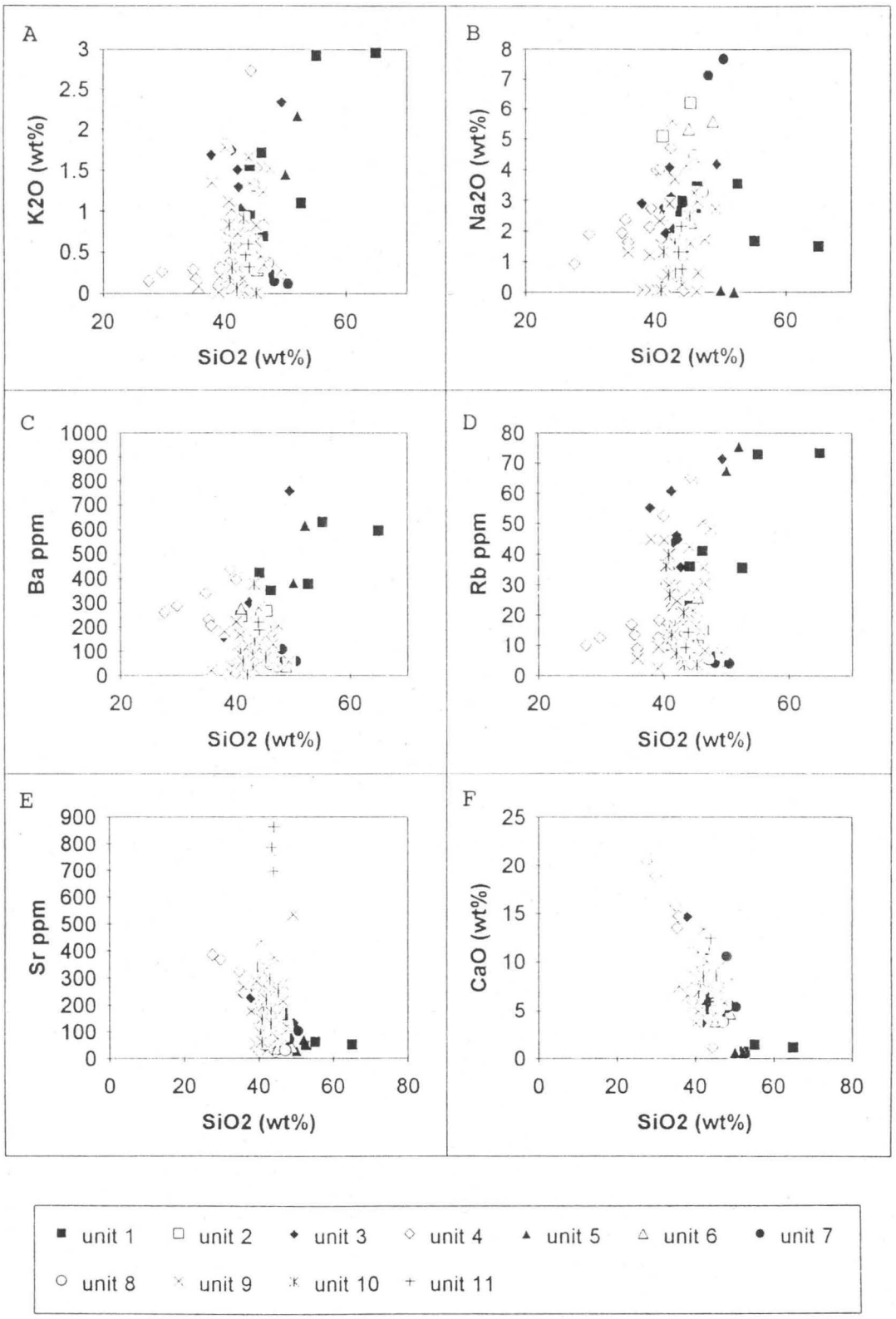

Figure 5.16. Harker variation diagrams of K_2O, Na_2O, Ba, Rb, Sr and CaO for the greenstone units.

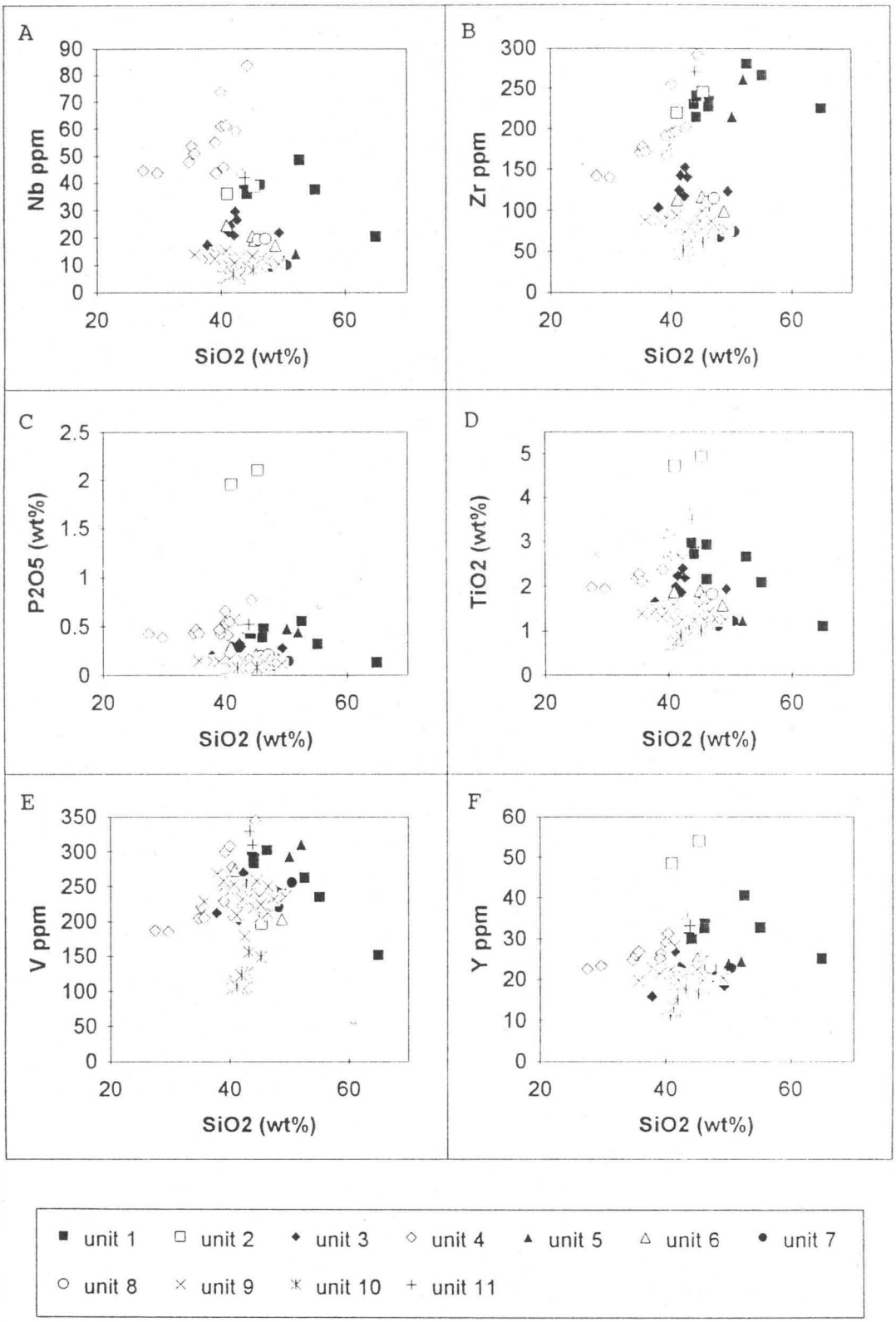

Figure 5.17. Harker variation diagrams of Nb, Zr, P_2O_5, TiO_2, V and Y for the greenstone units.

Correlations between elements, identified in factor analyses, are investigated in this section by plotting binary diagrams in terms of major and trace elements.

Positive correlations are observed between Ni, Cr and MgO (Fig. 5.18). These correlations are not present within every unit due to scattered variation within certain units, but a general positive correlation is still discernable. This might be interpreted as olivine and/or pyroxene fractionation during differentiation. Unit 10 (the dyke) has the highest Ni, Cr and MgO content. These elements show little scattering and a positive linear trend within unit 10 indicates internal fractionation and differentiation. The dyke, which is younger than the other greenstone units, was subjected to a lower degree of alteration, consequently preserving the primary igneous relations of Ni, Cr and Mg. The dyke is the only unit which contains primary igneous minerals (augite) which were not completely altered.

Positive correlations are also observed between the incompatible elements Nb, Zr, P, Y, Ce and Ti (Fig 5.19).

Correlations clearly exist between P_2O_5 and Ce for most units which can be interpreted as monazite fractionation (Fig. 5.19 A). Units 9, 8, 7, 6, 5, 4, 3 and 11 plot on the same regression line which probably indicates similar fractionation paths for these two elements. Unit 2 plots way above this path due to its exceptionally high P_2O_5 content (1.96 to 2.10%).

Collinear relationships are observed when plotting P_2O_5, Nb, Zr and TiO_2 against each other. In the P_2O_5-Nb diagram (Fig. 5.19 B), all the units except units 5 and 2 plot on the same linear trend. In the P_2O_5-Zr diagram (Fig. 5.19 C) a linear trend is defined by units 10, 9, 8, 7, 6, 4 and 3. In Fig. 5.19 D, Zr and Nb also correlate on a a well-defined trend which includes units 10, 9, 8, 7, 6 and 3. P_2O_5, Nb and Zr also show a collinear relation with Ti for units 10, 9, 8, 7, 6, 3, ±1 (Fig. 5.20). Although units 1 and 4 usually plot above or below the various linear trends, it should be taken into account that Nb, Zr, P_2O_5 and Ti were more mobile in these two units than in the other units. It can therefore be concluded that units 3, 6, 7, 8, 9, 10, 11 ± 1 and 4 followed a similar fractionation path for the incompatible elements P_2O_5, Zr, Nb and Ti. These elements are probably mineralogically related, occurring together in either primary or metamorphic minerals. For example Nb can be incorporated in

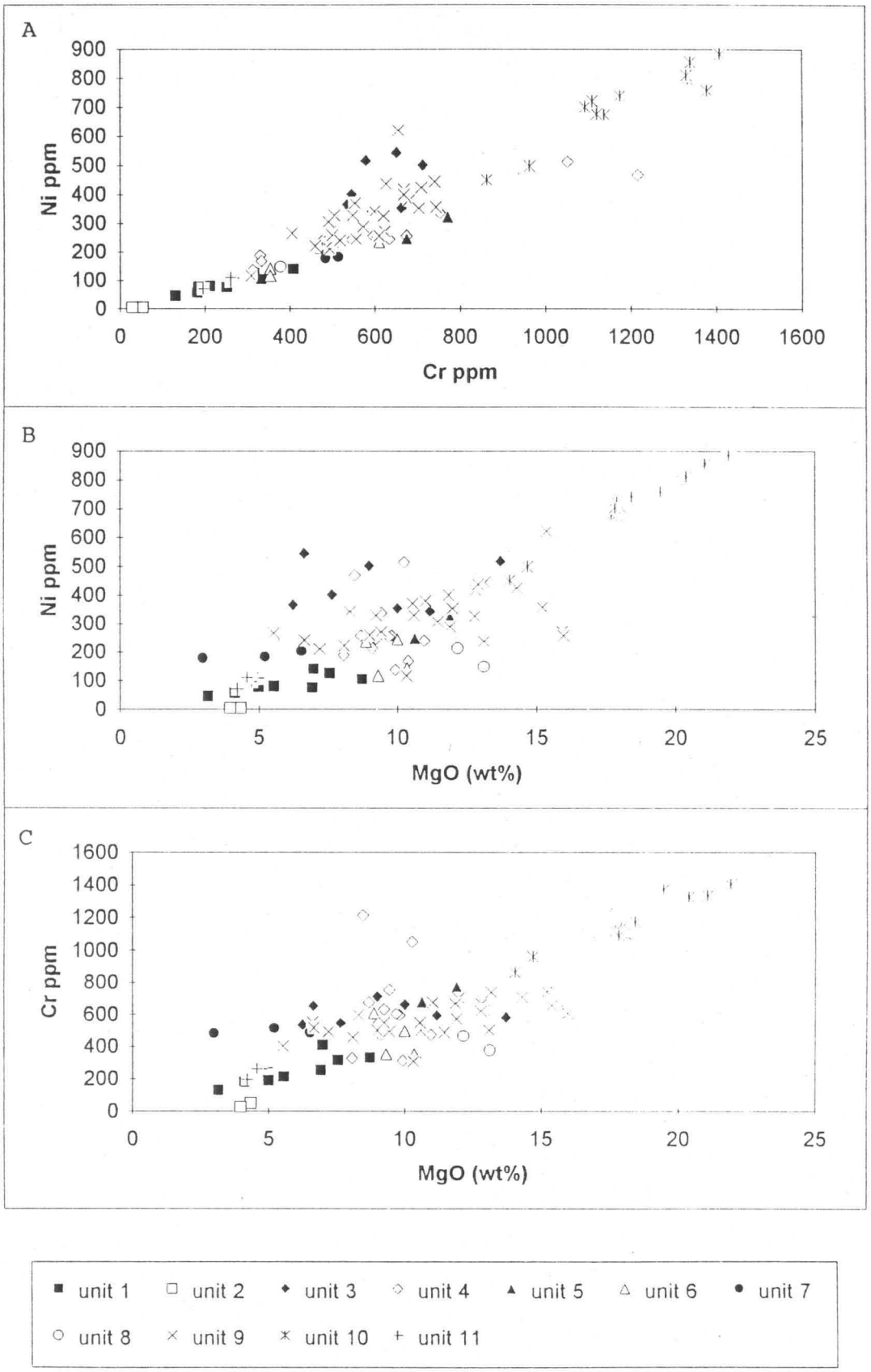

Figure 5.18. Variation diagrams of Ni, Cr and MgO for the greenstone units.

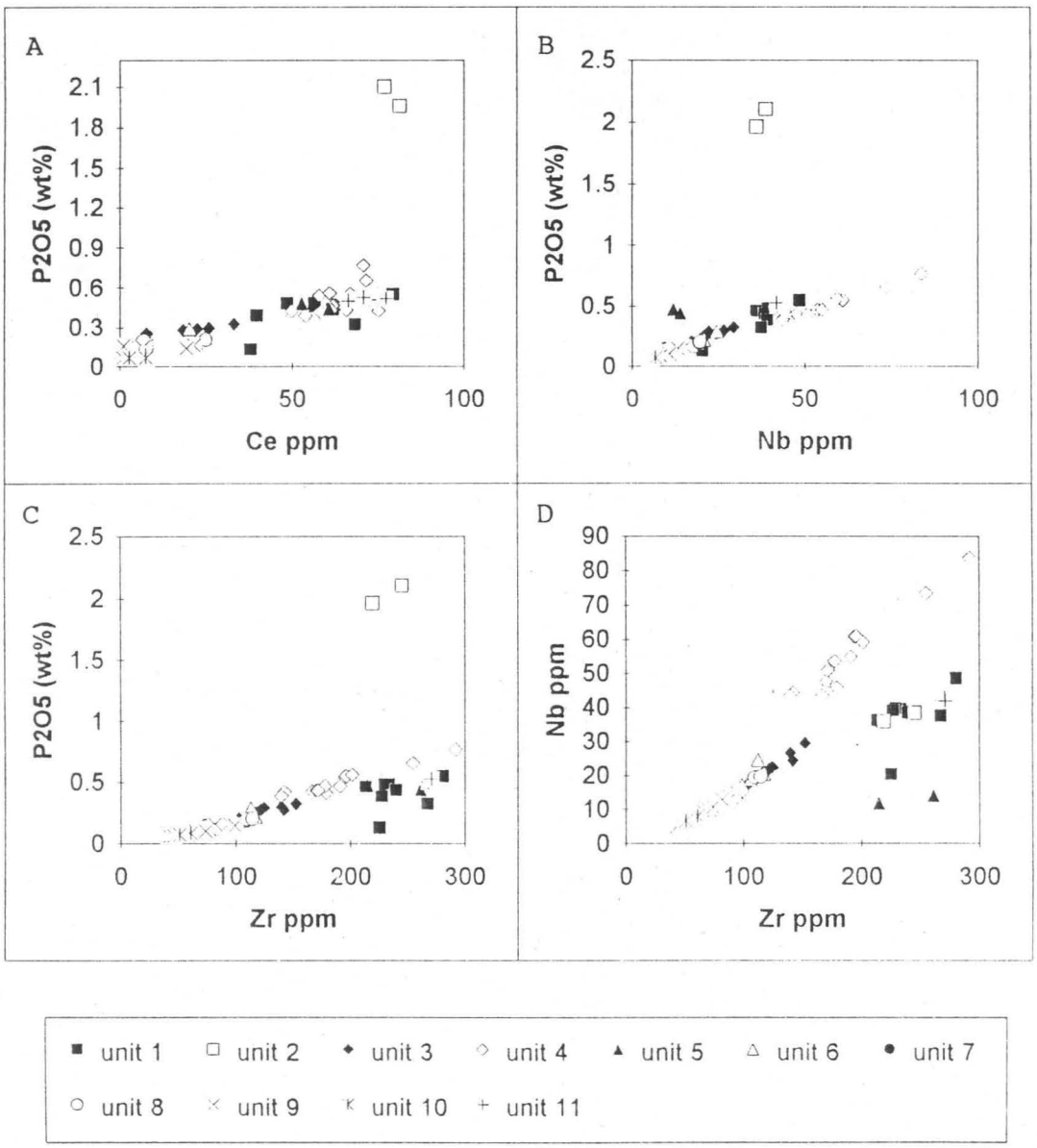

Figure 5.19. Variation diagrams of P_2O_5, Ce, Nb and Zr for the greenstone units.

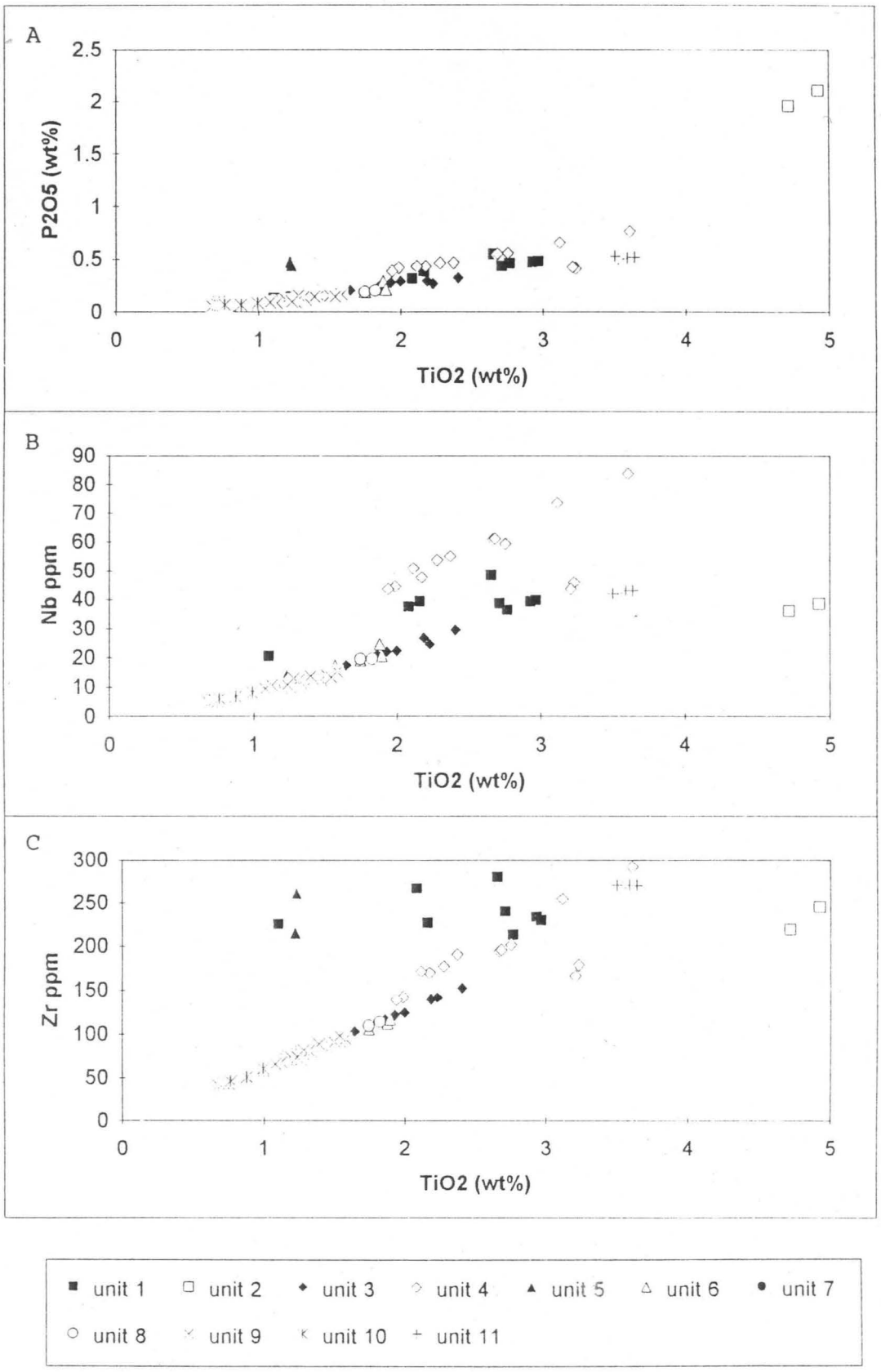

Figure 5.20. Variation diagrams of P_2O_5, Nb and Zr versus TiO_2 for the greenstone units.

ilmenite, zircon and titanite (Wedepohl, 1987b) explaining the Nb-Zr-Ti relationship. Titanite was petrographically recognized in all these units. Ilmenite is present in units 1, 3, 10 and 11. Although zircon was not petrographically identified in any of these units, it is assumed that it occurs as cryptocrystalline grains in units 1, 3, 4, 6, 8 and 11, as indicated by their high whole rock zirconia contents (108 to 270 ppm).

Some units show positive correlations of Y with Nb, Zr, P_2O_5 and Ti (Fig. 5.21). Yttrium and Nb are commonly present in zircon and titanite (Deer et al., 1992) which explains the Y-Nb-Zr-Ti relationship. The Y-P_2O_5 relationship may be interpreted as xenotime fractionation, although xenotime has not been recognized in any of these units.

The more evolved units have higher P_2O_5, Ce, Nb, Zr, Y and Ti contents than the more primary magmas. This is due to the incompatible nature of these elements which tend to concentrate in the more evolved magmas.

The fact that alkaline units 3, 6, 8, 11 ± 1 and 4, and subalkaline tholeiitic units 7, 9 and 10 followed similar fractionation paths for the elements Nb, Zr, Y, Ti and P may indicate that the alkaline and subalkaline units originated from the same source material. Ito and Kennedy (1974) found that by varying the conditions of melting, either a tholeiitic or an alkali basalt could be produced. For instance, the initial melting product of a spinel-lherzolite is a tholeiitic melt (such as units 7 and 9) at low pressures (<15kbars); an alkali basaltic melt (such as units 1, 3, 4, 6, 8 and 11) at higher pressures; and a high degree of partial melting will give rise to a liquid of picritic or komatiitic composition such as unit 10, the dyke (Takahashi and Kushiro, 1983). Similarly Jaques and Green (1980) found that melting of spinel-peridotite at 15 kbars gave alkali olivine basalt melt at <15% melting, olivine-tholeiite at 20 to 30% melting, and picritic to komatiitic liquid at 40 to 60% melting.

5.1.4.4. PEARCE ELEMENT RATIO DIAGRAMS

The major shortcoming of binary variation diagrams is that magmatic systems are complex with more than two variables, requiring multidimensional representation. Pearce (1968) recognized that provided there is at least one conserved element in a

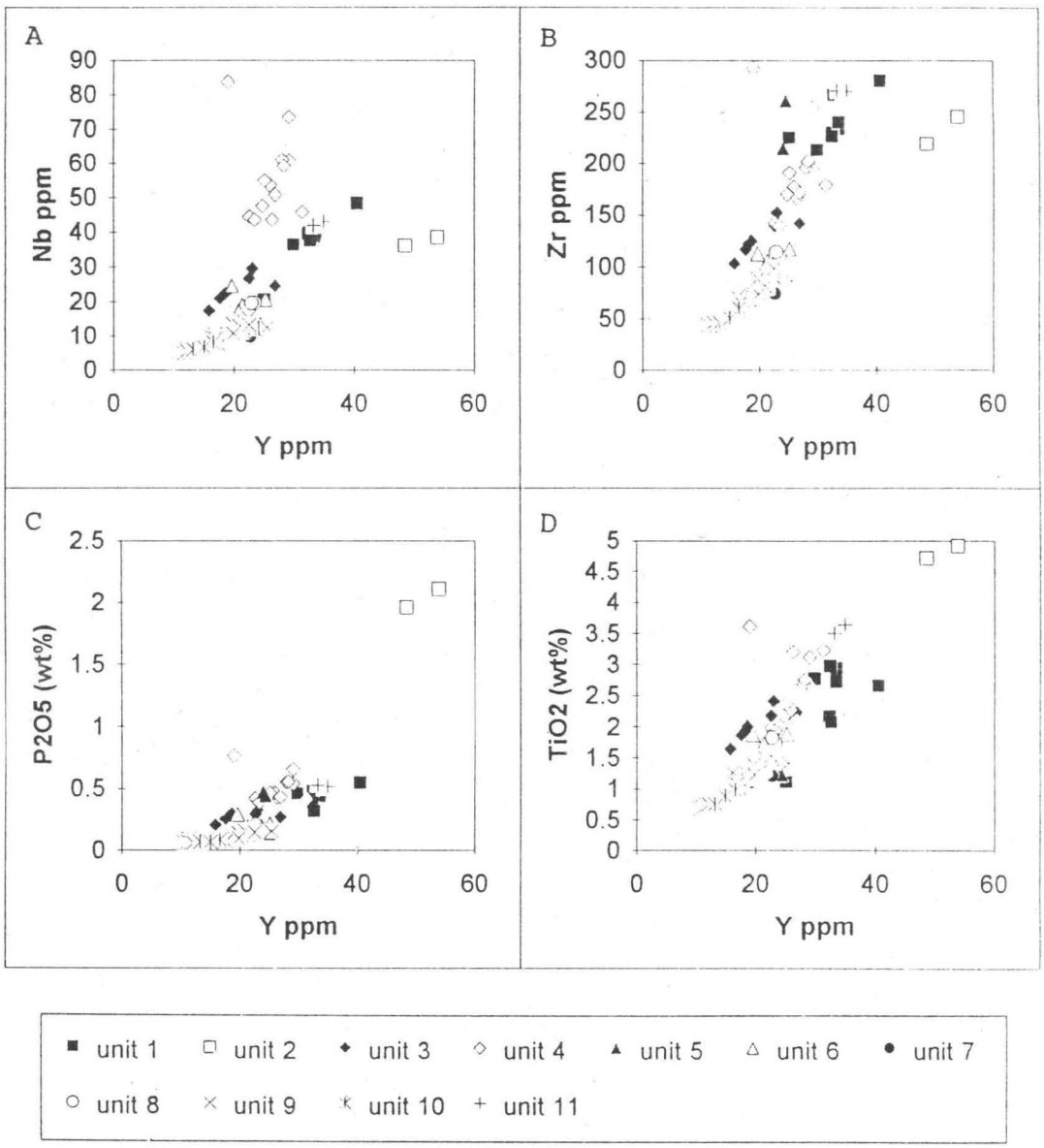

Figure 5.21. Variation diagrams of Nb, Zr, P_2O_5 and TiO_2 versus Y for the greenstone units.

magmatic system, a simple transformation of the compositional data can be used to reveal the exact relationships between the nonconserved elements. This transformation is done by calculating Pearce element ratios from the element numbers (e_1), where

$$e_i = (W_i * A_i)/M_i$$

and W_i, A_i and M_i are the weight percent, cation number and molecular weight of the oxide i. The corresponding Pearce element ratio is

$$R_i = e_i/e_z$$

The subscript z refers to the conserved element.
Pearce element ratios can be used to test hypotheses concerning igneous differentiation processes. It can be employed to recognize cogenetic rock analyses, the minerals involved in differentiation and the compositional proportions of the involved phases.

To investigate differentiation processes based upon measured lava compositions, implies that samples are of a single magmatic lineage. Pearce element ratios, constructed from conserved constituents, can be used to test this premise (Nicholls, 1988). Stanley and Russell (1989) suggested that K, Ti and P are usually not involved in the early crystallization of basaltic magmas. Due to the fact that K was relatively mobile in the greenstones during metamorphic and alteration processes, Y and Nb will be used alternatively as common denominators. In plots of Y and Nb against SiO_2 (Fig. 5.17 F and 5.17 A) it can be seen that both elements are relatively constant with SiO_2 variation within a specific unit. Yttrium also shows little variation between units. This leads to the assumption that Y, and to a lesser extent Nb, were not involved in early crystallization processes of the basalts. If true, P/Y, Ti/Y, P/Nb and Ti/Nb should be single-valued for all related basaltic lavas.

Fig 5.22 A is a P/Y versus Ti/Y plot for greenstone units of the Bridgetown Formation. Basalts derived from the same magma should plot around a single point. Units 1, 2, 4 and 5 plot as separate groups. Overlapping is found between units 7, 9 and 10; units 3 and 11; and units 6 and 8.

The same tendency is found in the P/Nb versus Ti/Nb diagram (Fig 5.22 B). Again units 1, 2, 4 and 5 plot as separate groups with overlapping between units 3 and 11, and units 6 and 8. The only difference is that overlapping between units 7, 9 and 10 is minimal. Grouping of units 6 and 8 as the same magmatic lineage, is supported by the occurrence of unit 8 as small bands within unit 6.

The dispersion in Ti/Y and Ti/Nb data, especially for units 1 and 4, implies that Ti was either mobile within these units or that Ti was not conserved totally, perhaps because of substitution into clinopyroxene or oxides. It is already known that the incompatible elements within units 1 and 4 show some degree of mobility, therefore dispersion of Ti/Y and Ti/Nb data within these units are mainly ascribed to metamorphic and/or alteration processes.

Consequently it is deduced that greenstone units 1 to 11 are related to a maximum of 9 magmatic lineages (Fig 5.22 B) and a minimum of 7 magmatic lineages (Fig 5.22 A).

Molemineral indices, as given by Stanley and Russell (1989), could not be transformed into Pearce ratios in order to determine the minerals involved in differentiation, due to the high mobility of K, Na, Ca and Si in the greenstones. However, all the previous mentioned correlations (Fig. 5.18, 5.19, 5.20 and 5.21) were reconfirmed, by converting the elements into Pearce ratios and thereby excluding the closure problem.

5.1.4.5. RARE EARTH ELEMENT GEOCHEMISTRY

Twenty seven greenstone samples (Table 4, Appendix) were chosen for REE-analysis. Each greenstone unit is represented by two or more samples, except for unit 8 which is represented by one sample. Samples were analyzed by ICP-AES which is discussed under analytical methods in the appendix. Average REE values

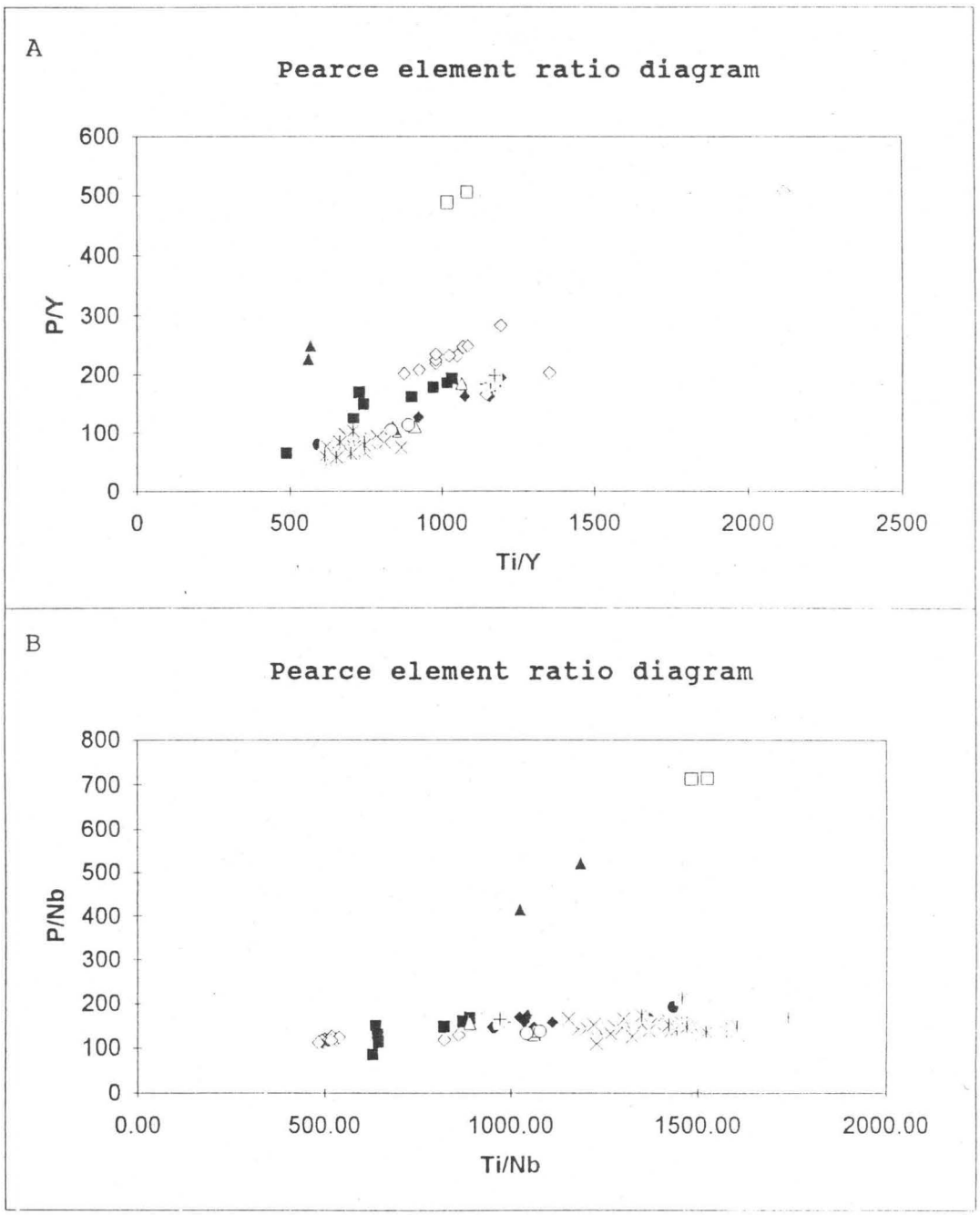

Figure 5.22. Conserved element plots using (A) P/Y versus Ti/Y, and (B) P/Nb versus Ti/Nb.

for each unit were normalized to the chondrite values recommended by Henderson (1984, Table 4).

REE profiles for each greenstone unit are presented in Figures 5.23. and 5.24. REE patterns for most units are subparallel, except for units 1, 3 and 5 which were plotted on a separate diagram (Fig. 5.24).

All the REE-profiles are HREE-depleted with approximately 4 to 54 times chondrite for HREE's and 7 to 154 times chondrite for LREE's. Units with the highest mg-values tend to have the lowest total REE concentrations. For instance, unit 2 has the highest total REE content and the lowest average mg-value of 41.7, whereas unit 10 has the lowest total REE content and the highest average mg-value of 79. Also, the subalkaline units (7, 9 and 10) have a lower total REE content than the alkaline units (1, 2, 3, 4, 5, 6, 8 and 11). Eu anomalies are small to almost absent with (Eu^N/Eu^*)-1 ratios ($Eu^* = Sm^N/2 + Gd^N/2$) ranging from -0.3 (unit 5) to 0.03 (unit 2).

Units 6, 7, 8 and 9 have very similar total REE concentrations, LREE slopes (La/Sm = 1.7 to 2.1), HREE slopes (La/Yb = 3.4 to 6.8) as well as mg-values (Table 5.2). Units 6, 7 and 8 occur in contact with each other in borehole BW2 (Site B), and adjacent to unit 9 (Fig. 3.3).

In Figure 5.24. it is evident that the REE profile of units 5 and 1 differ slightly from the other profiles. Unit 5 is the only profile with a negative slope between La and Nd. Unit 1 on the other hand has the highest La/Sm value (4.2) of all the greenstone units.

Three major factors control the distribution of REE's in igneous rocks: the composition of the source; the degree and conditions of partial melting of the source; and fractional crystallization (Henderson, 1984). The LREE-enriched pattern of the greenstone units could be the result of various factors such as a LREE-enriched source, fractionation involving garnet (garnet has high partition coefficients for the HREE) and concentration of LREE in minerals such as titanite, allanite, apatite and monazite (Henderson, 1984). Titanite is relatively abundant in the Bridgetown greenstones. Very small to almost absent Eu anomalies indicate that removal of plagioclase to produce negative Eu anomalies did not play a significant role. The

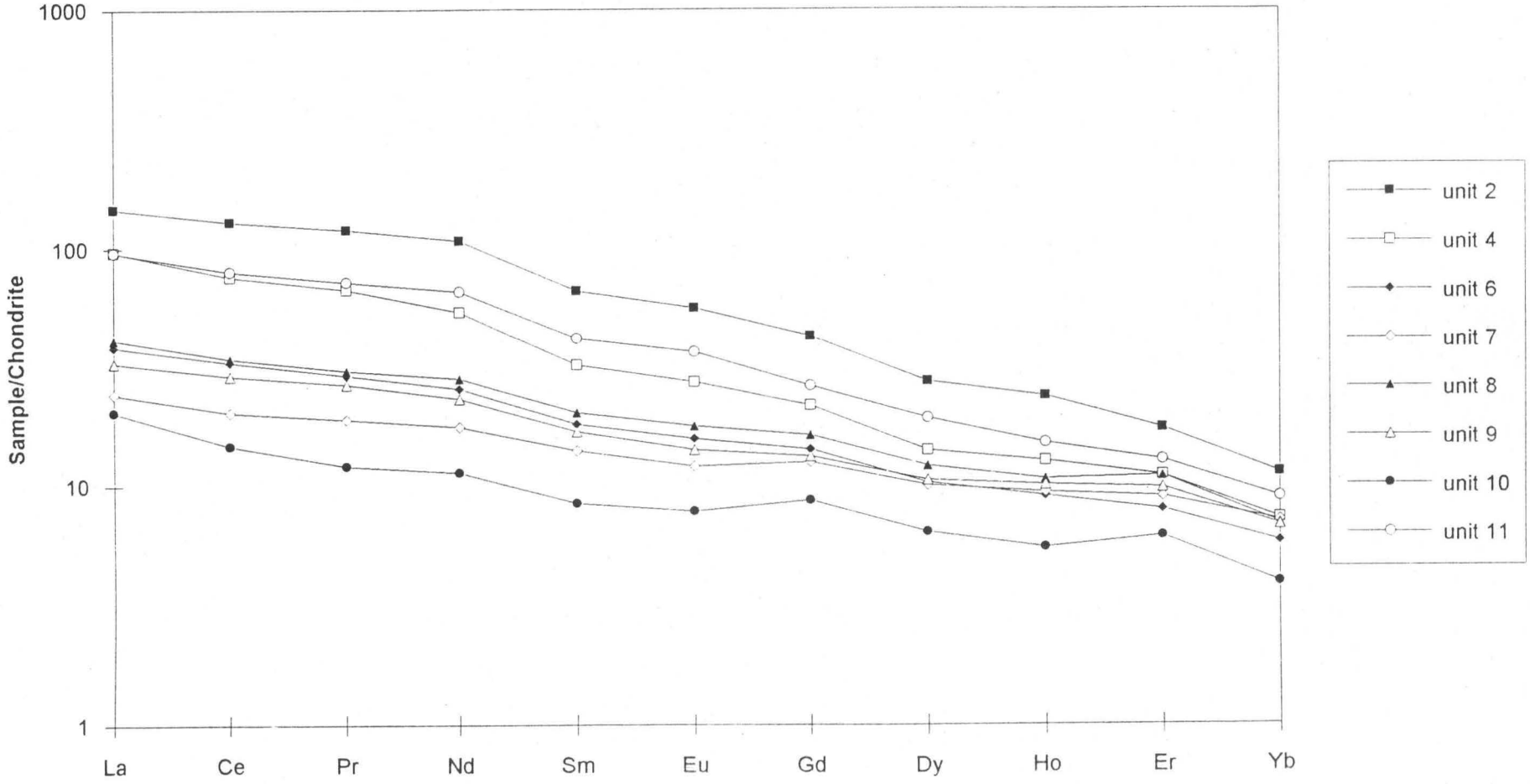

Figure 5.23. Chondrite-normalized REE patterns for greenstone units of the Bridgetown Formation.

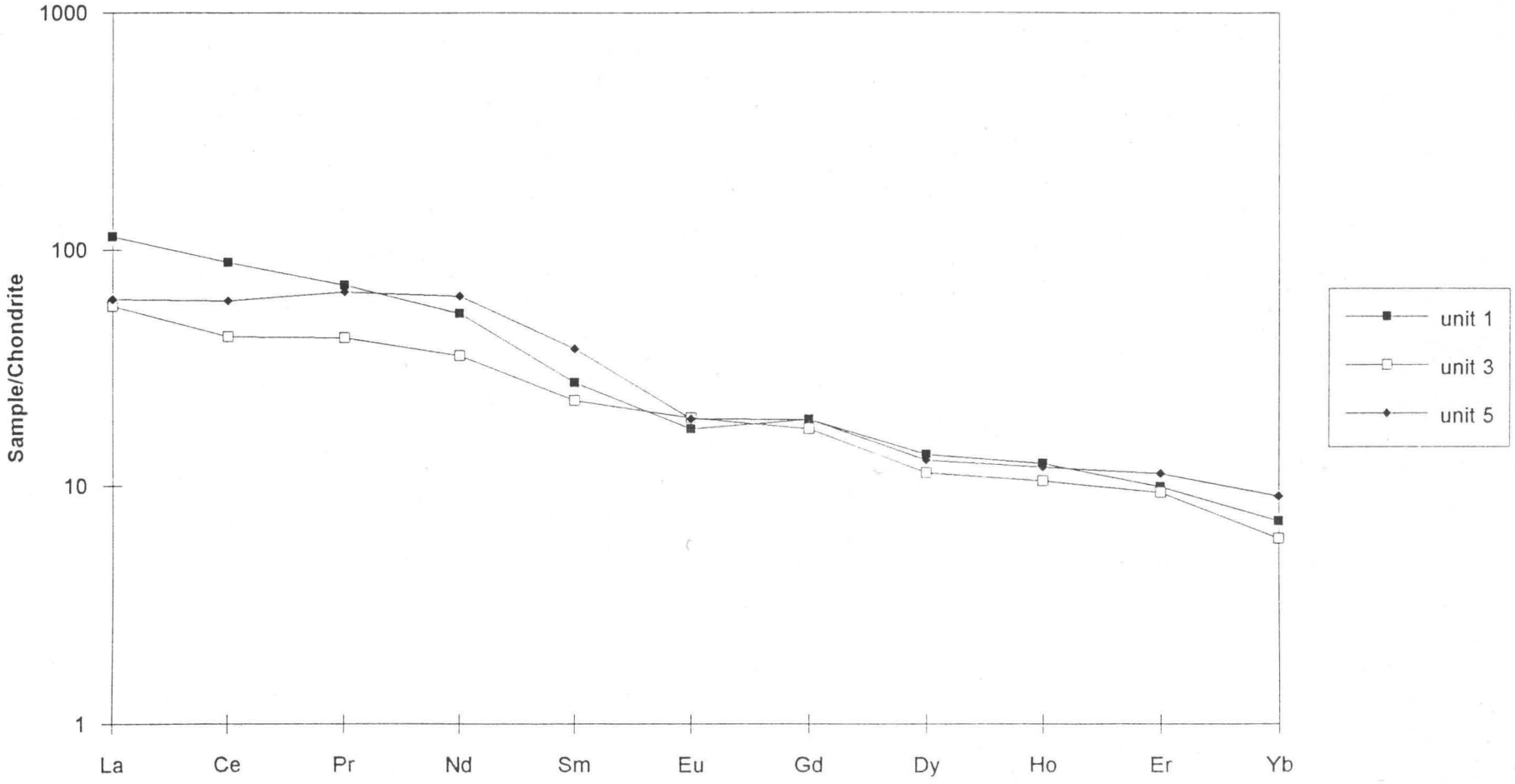

Figure 5.24. Chondrite-normalized REE patterns for greenstone units of the Bridgetown Formation.

negative correlation of total REE content and mg-value indicates that an increase in REE concentration occurs with differentiation.

LREE-enriched patterns for basaltic rocks are found in various tectonomagmatic environments. Although it is not possible to define a specific tectonic environment on account of a LREE-enriched pattern, a few tectonomagmatic environments can be eliminated, being characterized by LREE-depleted to flat patterns. They include N-type mid-ocean ridge basalts and ocean plateau volcanics (Henderson, 1984).

In conclusion, REE-profiles of the alkaline and subalkaline magmas show some similarities:
i) both are LREE-enriched,
ii) both have small to almost absent Eu anomalies, and
iii) their LREE and HREE slopes do not differ much (excluding units 1, 3 and 5).
This supports the theory that the alkaline and subalkaline magmas originated from the same source material. The source material was probably LREE-enriched. During partial melting of a LREE-enriched source, incompatible elements (including REEs) will be highly enriched in initial melt fractions which are usually silica-undersaturated (e.g. alkali basalts), compared with products of a higher degree of melting (e.g. tholeiitic basalts; Hall, 1987). Pearce element ratio diagrams (Fig 5.22) indicated that the different units are not necessarily from the same magmatic lineage. Unit 10, the younger dyke, is the product of a high degree of partial melting of the same source material, already depleted in REEs.

5.1.5. DISCUSSION

A geochemical investigation of the greenstones confirmed the existence of different greenstone units within the Bridgetown Formation. Although the greenstone units vary considerably in composition, two major magma types were identified:
a) an alkaline magma (units 1, (2), 3, 4, 5, 6, 8 and 11), and
b) a subalkaline tholeiitic magma (units 7, 9 and 10).

Geochemically the units belonging to the alkaline magma classify as basaltic, except for unit 5 which classifies as andesitic. The alkaline units have chemistries similar to within-plate basaltic rocks. The incompatible element composition of units 1, 4 and 11 coincides broadly with an ocean island basalt composition. The alkaline units include poorly differentiated magmas with high mg-values (units 3, 4, 6 and 8) as well as more evolved magmas with relatively low mg-values (units 1, 5 and 11). Conserved Pearce element ratio plots indicated that units 3 and 11; and units 6 and 8 are comagmatic. Unit 11 is probably a differentiation product of unit 3. Grouping of units 6 and 8 into one unit is supported by similar REE patterns, overlapping between the units in discriminant analyses, and the occurrence of unit 8 as small bands within unit 6.

Unit 5 differs geochemically and mineralogically (section 3.2.1.(x)) from the other alkaline units. Its composition is andesitic and not basaltic; its REE profile differs from the other units having a negative La/Nd slope; and in binary element variation diagrams it seldom exhibits collinear relationships with the other units. Unit 5 represents either a metamorphosed intermediate volcanic rock or a mafic metavolcanic rock, contaminated by a sedimentary component. The possibility of unit 5 being a pure metasedimentary unit is excluded on account of its high MgO (11,26%), Ni (284,69 ppm) and Cr (721,88 ppm) content.

Unit 2 also exhibits few geochemical similarities with the other alkaline units. It has a much higher Na_2O (5.64%), P_2O_5 (2.03%), TiO_2 (4.82%), Y (51,19 ppm) and total REE content, and is depleted in Ni (a mere 5,1 ppm) and Cr (39,34 ppm) relative to the other alkaline units. In binary element variation diagrams it seldom exhibits collinear relationships with the other greenstone units. Although high Na_2O and P_2O_5 values, and low Ni and Cr values are often found in nephelenites and basanites, classification diagrams of Winchester and Floyd (1977; Figs. 5.3 and 5.6), based on the Zr, TiO_2, Ce, Y and Nb contents of unit 2, indicate that unit 2 does not have a nephelenitic or basanitic composition. It is therefore concluded that unit 2 is a metasedimentary unit. The high Na_2O content indicates a marine origin. According to Wedepohl (1987a) the Na_2O content of argillaceous marine sediments can be as high as 6,9%. On an ACF diagram, with fields of various magmatic and sedimentary rocks indicated (see Fig. 4.4, section 4.1), unit 2 plots on the boundary

between basaltic rocks and graywackes. This suggests that unit 2 may also comprise a mafic volcanic component (such as thin mafic tuff layers).

The subalkaline units (7, 9 and 10) classify as low-alumina tholeiitic basalts with ocean-floor basalt (P-type MORB) and island arc basalt characteristics. Their high mg-values (78 to 80) indicate that they have undergone little differentiation.

Unit 10, the younger intrusive dyke, is characterized by a very high Ni, Cr and MgO content, coupled with very low concentrations of Ti, Zr, Y and REE.

A common source material for the alkaline and subalkaline units is supported by the following:

a) The alkaline and subalkaline units (excluding units 2 and 5) followed similar fractionation paths for the incompatible elements Nb, Zr, Y, Ti and P. These elements exhibit collinear relationships and all the units (except units 2 and 5) plot on the same linear trend.

b) The alkaline and subalkaline units have similar REE profiles. In both cases REE profiles are LREE-enriched with very small to almost absent Eu anomalies; and with similar LREE and HREE slopes.

By varying the conditions of melting, both tholeiitic and alkali basalts can be produced from the same source material (Hall, 1987). Alkaline units 3, 4 and 6(=8) were formed at high pressures (>15kbars) or low degrees of partial melting (3 to 7%). Some of the melting products have undergone differentiation to produce more evolved alkaline units (e.g. units 1 and 11). For example, unit 11 is a differentiation product of unit 3. Tholeiitic units 7 and 9 were formed at low pressures (<15kbars) or greater degrees of partial melting (20 to 30%). Unit 10, the younger intrusive dyke, is the product of a high degree of partial melting (>40%) at low pressures of the same source which has been depleted in its initial melt fractions.

It is concluded that the alkaline and subalkaline units are not from different tectonic environments, rather they represent products of varying conditions of melting of the same source material.

Table 5.3
Major and trace element content of graphitic schists and muscovite-quartz schists of the Bridgetown Formation

Rock-type	graphitic schist							muscovite-quartz schist				Turekian & Wedepohl, 1961
Location	Bh AW1				Bh AE2			Tweevlei outcrop				
Depth (m)	17.06	17.47	18.1	18.69	24.28	28.57	29					
Colour	grey	grey	dark grey	black	light grey	black	black	dark grey	dark grey	dark grey	dark grey	Avg Shale
SAMPLE	NS17	NS18	NS19	NS20	NS51	NS54	NS55	NSF/2.1	NSF/2.2	NSF/2.3	NSF/2.4	
SiO_2	63.23	60.25	54.53	52.20	67.58	60.59	58.20	61.28	62.84	63.37	63.69	58.50
TiO_2	0.99	0.99	1.45	2.08	0.87	0.97	0.94	0.72	0.73	0.72	0.72	0.46
Al_2O_3	14.36	15.23	15.03	14.73	12.84	14.39	13.85	15.62	15.47	15.13	15.13	8.00
Cr_2O_3	0.02	0.03	0.02	0.03	0.02	0.02	0.02	0.01	0.01	0.01	0.01	0.01
FeO	4.03	6.29	2.24	2.52	3.55	2.19	2.63	2.25	2.07	2.16	2.07	-
Fe_2O_3	1.67	1.14	7.20	7.44	2.02	4.86	3.73	4.61	4.51	4.09	4.39	4.70
MgO	4.31	4.65	3.73	3.86	2.56	2.32	2.83	3.60	3.46	3.29	3.31	1.50
MnO	0.03	0.03	0.02	0.03	0.21	0.03	0.07	0.03	0.03	0.02	0.02	0.09
CaO	0.24	0.25	0.36	0.56	0.26	0.54	1.76	0.16	0.15	0.17	0.17	2.21
Na_2O	0.73	0.75	0.03	0.04	0.11	0.16	0.15	0.08	0.08	0.08	0.08	0.96
K_2O	4.03	3.69	4.31	4.23	4.54	4.96	4.73	4.05	3.97	3.97	3.88	2.66
P_2O_5	0.17	0.18	0.28	0.44	0.18	0.16	0.15	0.10	0.10	0.10	0.10	-
H_2O-	0.15	0.12	0.48	0.55	0.11	0.23	0.38	0.63	0.60	0.61	0.64	-
CO_2	0.08	0.10	0.20	0.52	0.85	0.53	2.88	-	-	-	-	-
C	0.13	0.13	1.42	1.86	0.12	1.86	1.98	-	-	-	-	1.60
S	0.58	0.28	3.02	3.24	1.02	2.62	2.13	-	-	-	-	0.24
TOTAL	98.70	98.69	98.19	98.47	99.34	99.15	99.08	98.30	99.10	98.65	99.05	-
Mo	1	1	4	8	1	3	4	1	1	1	1	3
Nb	17	17	25	37	14	16	15	13	14	13	14	-
Zr	207	206	214	260	176	191	179	152	160	168	163	-
Y	34	36	44	43	32	39	38	29	29	30	30	-
Sr	18	19	13	16	46	60	110	18	17	14	14	-
U	4	2	1	2	3	4	3	2	4	4	5	-
Rb	135	124	174	162	148	166	153	157	155	155	154	-
Th	13	12	11	10	10	14	12	13	15	14	14	-
Pb	17	16	23	22	15	15	19	18	19	20	21	20
Ga	20	21	23	24	18	21	20	22	23	23	23	16
Zn	159	173	94	128	119	64	67	167	148	150	142	95
Cu	48	51	40	36	39	38	34	44	41	49	49	45
Ni	75	69	192	264	43	30	29	48	50	44	48	68
Sc	10	20	21	18	14	19	19	20	18	18	19	-
W	52	24	100	109	44	117	115	-	-	-	-	-
V	141	142	172	212	140	174	163	131	128	124	127	130
Ce	-	-	-	-	-	-	-	72	77	66	74	-
Nd	-	-	-	-	-	-	-	36	34	32	34	-
Ba	650	576	892	842	881	926	865	968	870	569	559	580
La	-	-	-	-	-	-	-	38	37	43	39	-
Cr	-	-	-	-	-	-	-	87	90	88	86	90

Major elements in weight percent oxide
Trace elements in parts per million

5.2. GRAPHITIC SCHISTS AND MUSCOVITE-QUARTZ SCHISTS

Major and trace element geochemical analyses were performed on graphitic schists and muscovite-quartz schists associated with greenstones of the Bridgetown Formation. The data is represented in Table 5.3.

Two graphitic schist lenses, occurring in boreholes AW2 and AE2 (Fig. 3.4) in greenstone units 1 and 5 respectively, were investigated.

In borehole AW2 graphitic schist was intersected from a depth of 15 to 19 metres. The physical features and major and trace element chemistry of four samples from this zone are listed in Table 5.3.

Although the contacts between greenstone unit 1 and the graphitic schist are relatively sharp, the graphitic schist is darker coloured away from the contacts. The darker graphitic schist zones also contain more pyrite than the lighter coloured zones. Chemical analyses show that the dark grey to black samples (NS19 and NS20) have a higher carbon, sulfur, P_2O_5, CaO, CO_2 and TiO_2 content than the grey coloured samples (NS17 and NS18). The dark coloured samples also have a slightly higher Ba, Nb, Ni, Pb, Rb, V, W and Zr content, but are depleted in SiO_2, MgO and Na_2O relatively to the grey coloured samples.

In borehole AE2 graphitic schist was intersected between 23.2 and 30 metres. The contact with greenstone unit 5 is characterized by alternating greenstone and graphitic schist bands. Further away from the contact the greenstone component becomes less and the graphitic schist becomes darker coloured. Major and trace element chemistry and colour descriptions of three graphitic schist samples, taken at different depths, are listed in Table 5.3. The two black samples (NS54 and NS55) have a lower SiO_2 content and a higher carbon, sulfur, CaO, CO_2, TiO_2, Sr, V and W content than the light grey sample (NS51).

It is concluded that in both graphitic schist lenses the darker colour is related to a higher carbon content. Organic carbon would have enabled sulfate reducing bacteria to produce hydrogen sulfide (Leventhal, 1983). Some of the sulfide reacted with iron to form pyrite, which explains the high pyrite content in the dark zones and

a general increase in the sulfur content with an increase in the carbon content. In borehole AW2 metals such as Ni, Pb and W also exhibit higher concentrations with an increase in the carbon content. Metals may be chemically concentrated by adsorption on organic matter or by metal-organic complexing (Vine and Tourtelot, 1970). The high CaO and CO_2 content in the C-rich samples reflect the higher calcite content in these samples. The lower contents of MgO, SiO_2 and Na_2O in the C-rich samples probably reflect the smaller proportion of detrital minerals.

A small muscovite-quartz schist outcrop on the farm Tweevlei (Sheet A) was also submitted for major and trace element analyses. The chemical compositions of four whole rock samples are shown in Table 5.3. Generally the major and trace element content of the muscovite-quartz schist is comparable to those of the graphitic schists. Although carbon and sulfur contents of the muscovite-quartz schist are not available, the absence of sulfides is probably indicative of a low sulfur content.

According to Vine and Tourtelot (1970) the term "black shale" includes a wide range of dark-coloured fine-grained rocks. The term implies that the rock owes its dark colour to the presence of organic matter. The average chemical composition of black shales agrees closely with estimates for shale averages. Estimates of elemental abundance in an average shale is given in Table 5.3 (Turekian and Wedepohl, 1961). The major difference between the average black shale and the average shale is the content of organic carbon. The organic carbon content in the average black shale is about 3 percent, which is significantly higher than the 0.65 percent estimated by Green (1959) for the average shale. The carbon content of the Bridgetown graphitic schists varies between 0.12 and 1.98 percent which falls between the average shale and average black shale. It is predicted that the carbon content of the muscovite-quartz schist at Tweevlei is even lower, because it is not as dark as the graphitic schists. The graphitic schists and the muscovite-quartz schist have a much higher SiO_2, Al_2O_3, K_2O and MgO content than the average shale, probably due to a larger proportion of detrital minerals. Their metal content is comparable to those of the average shale; therefore it is concluded that the graphitic

schists and muscovite-quartz schist of the Bridgetown Formation are metal-poor schists.

Rare earth element (REE) distributions in the graphitic schists and the muscovite-quartz schist at Tweevlei are shown in Fig. 5.25.

The graphitic schists are represented by samples NS20 and NS55 from boreholes AW2 and AE2 respectively. They are characterized by a high carbon content compared to other samples of the same graphitic schist. Although samples NS20 and NS55 are from two different graphitic schist lenses, their chondrite-normalized patterns are almost identical. The REE-profiles are HREE-depleted with about 100 * chondrite for light (L)REEs, 10 * chondrite for heavy (H)REEs and negative Eu anomalies. These features are typical of the uniform chondrite-normalized REE distribution pattern of cratonic shales (Taylor and McLennan, 1985). The term 'cratonic shale' refers to shales with a continental crust provenance.

The muscovite-quartz schist at Tweevlei (sample NSF/2.1) has a slightly lower total REE content than the graphitic schists, but its REE-profile is also similar to the REE distribution of cratonic shales (Fig. 5.25).

The relatively higher total REE content in the graphitic schists is probably related to the higher carbon content. REEs may be chemically concentrated in organic carbon rich shales by adsorption on organic matter or by REE-organic complexing (Vine and Tourtelot, 1970).

So far researchers have not come to an agreement on why cratonic shales are depleted in HREEs with Eu anomalies. Condie (1991) suggested that no single mineral controls the Eu anomaly in shales. Taylor and Mclennan (1985) consider the uniformity of the Eu anomaly and the REE distributions in most cratonic shales as an indication of thorough mixing of the detritus during weathering and sediment transport. The REE pattern in cratonic shales reflect the average REE pattern of the sources, regardless of the ratio of clays to heavy minerals in the shales.

In conclusion, the two graphitic schist lenses are geochemically very similar. They probably were metal-poor black shales which were converted to graphitic schists during polyphase deformation and prograde metamorphism up to the lower

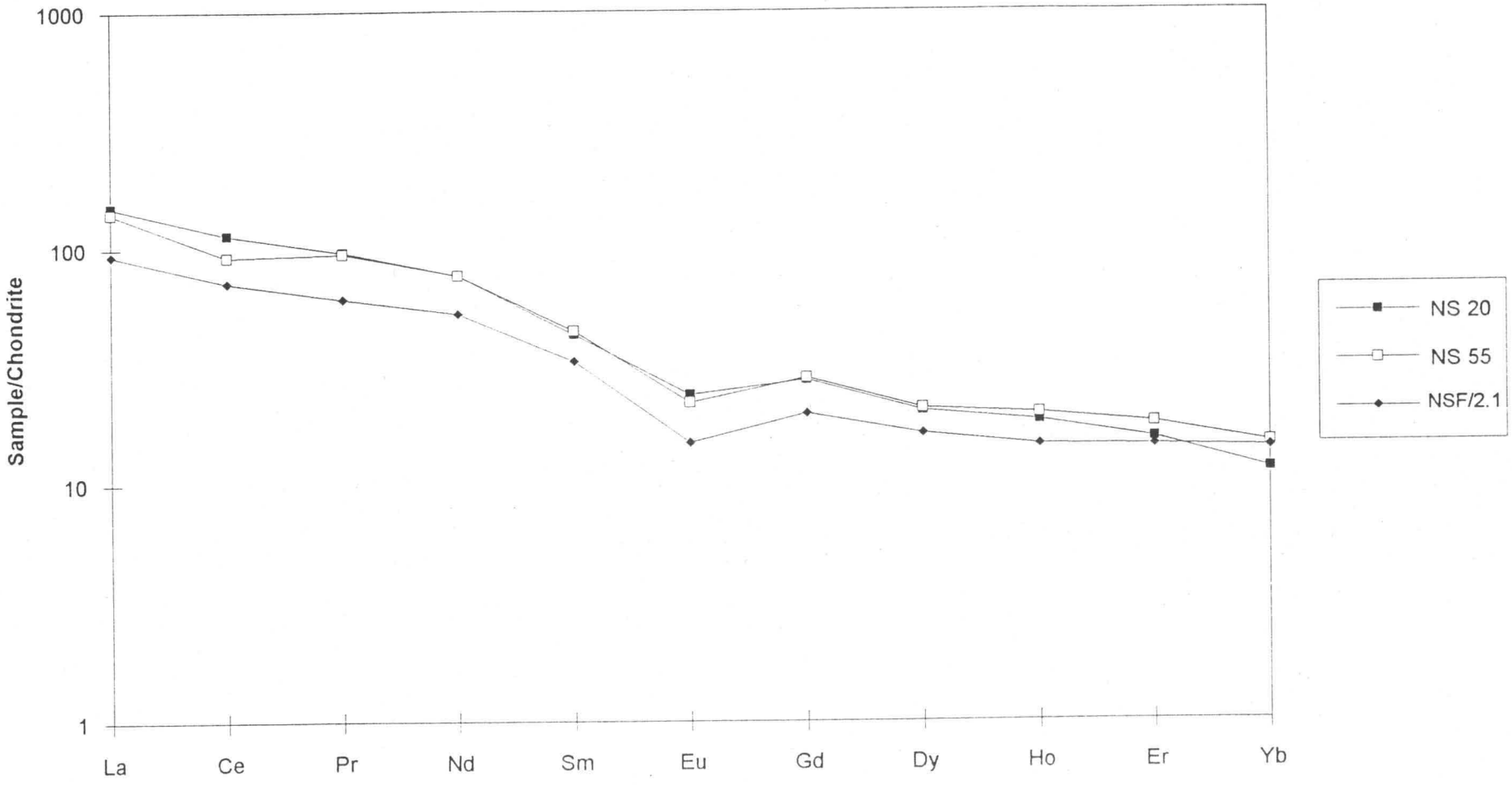

Figure 5.25. Chondrite-normalized REE patterns for graphitic schists (NS 20 and NS 55) and the muscovite-quartz schist (NSF/2.1).

greenschist facies. The muscovite-quartz schist at Tweevlei has also reached the lower greenschist facies during regional metamorphism, but were subjected to only two deformation events. The shale's elemental composition resembles those of a metal-poor "ordinary" shale and not a black shale. Both the graphitic schists and the muscovite-quartz schist have chondrite-normalized REE distributions similar to those of cratonic shales. The significance of this conclusion with regards to the greenstones is discussed in section 9.1.

5.3. DOLOMITES

In this section we examine the major and trace element composition of the dolomites to establish their origin and association with the greenstones. Ten dolomite samples were included in this study. Six samples are from dolomite lenses which alternate with greenstone unit 4 in borehole CE1 (Fig. 3.6) and the other four were sampled at the Bridgetown dolomite quarry (Sheet A).

The origin of the Bridgetown dolomites and their association with the greenstones are still enigmatic and controversial. De Villiers (1969) and Jacobs (1974) suggested that the Bridgetown dolomite is not a sedimentary rock, but a product of subsequent replacement of the greenstone; the latter providing the magnesia necessary for the formation of dolomite. This interpretation was purely based on field evidence and it has the problem of explaining the relatively thick (>70m thick) and massive occurrence of dolomite on the farms Bridgetown and Volgelstruisdrift.

In section 3.2.4 possible ghost limestone textures in the dolomite were described in thin section. The thin section was taken from the largest dolomite lens in borehole CE1 (Fig. 3.6). The occurrence of relict limestone textures in dolomite indicates that the dolomite was formed by replacement processes, with the mineral dolomite replacing calcite, Mg-calcite or aragonite (Boggs, 1992). Replacement presumably occurred as Mg-bearing subsurface waters migrated through oolitic carbonate sediments, possibly over periods of tens to hundreds of millions of years. The general absence of relict limestone textures in the Bridgetown dolomites is probably due to destruction of these textures as a result of recrystallization during regional

metamorphism. This, however, does not exclude the possibility that the Bridgetown dolomites may also consist of primary precipitated dolomite.

Part of the "dolomite problem" involves coming up with a satisfactory explanation to account for the large amounts of Mg that had to be imported into preexisting calcium carbonate sediments to bring about dolomitization. Due to the fact that seawater is the only common and abundant magnesium-rich fluid on Earth, seawater must have furnished the primary source of Mg for dolomitization (Boggs, 1992). Mg-rich basalts in contact with the carbonates probably were a supplementary source of Mg to subsurface waters. Boggs (1992) proposed a few mechanisms to force large quantities of Mg-bearing water through precursor carbonate sediment. They include 1) burial compaction, 2) topography-driven (or gravity-driven) flow, 3) thermal convection, and 4) hydrothermal flow.

Chemical analyses of the Bridgetown dolomites (Table 5.4) reveal that they have a MgO content of 17.8 to 20.6% and a CaO content of 26.4 to 30.7% which is the approximate MgO and CaO content found in the mineral dolomite (Deer et al., 1992). The Bridgetown dolomites are accordingly of high purity with minor impurities of Fe_2O_3t (0.27 to 2.03%), Al_2O_3 (0.02 to 2.08%) and SiO_2 (0.05 to 4.08%). Highly jointed samples usually have the highest content of impurities, indicating secondary enrichment. Small amounts of Fe^{2+} and Mn are also present in the lattice positions of dolomite (Morse and Mackenzie, 1990). Trace elements such as K, Rb, Sr and Na are found principally in illite and authigenic potash feldspar with some Na bound in carbonate phases. Silica is found in the dolomites as chert and secondary quartz veins. The ten dolomite samples show no anomalous metal enrichment. The dolomite lenses in borehole CE1 have a slighty higher Cr and Zn content than samples from the Bridgetown quarry. This is probably the result of secondary enrichment, with the greenstones furnishing the Cr and Zn to circulating waters.

In summary, the Bridgetown dolomites are of high purity when it is not admixed with chert or quartz. Highly jointed dolomite usually have the highest content of impurities, indicating secondary enrichment. The presence of relict limestone textures in some dolomite samples indicate subsurface dolomitization of precursor

Table 5.4
Major and trace element chemistry of the Bridgetown dolomites.

Location	Bh E1	Bh E1	Bh E1	Bh E1	Bh E1	Bh E1	Quarry	Quarry	Quarry	Quarry
Sample	NS162	NS164	NS166	NS168	NS169	NS177	NSF/1.1	NSF/1.2	NSF/1.3	NSF/1.4
SiO_2	0.23	0.57	2.32	3.42	0.05	4.08	0.05	0.05	0.82	0.05
TiO_2	0.01	0.03	0.01	0.09	0.01	0.23	0.01	0.01	0.03	0.01
Al_2O_3	0.21	0.44	0.24	2.08	0.02	0.88	0.02	0.01	0.54	0.02
FeO	0.07	0.36	0.18	0.27	0.18	0.72	0.18	0.27	0.36	0.18
Fe_2O_3	0.68	0.46	0.80	1.73	0.07	0.08	0.06	<0.09	0.93	<0.06
MgO	20.46	20.52	17.76	18.37	20.57	18.98	20.55	20.51	19.89	20.33
MnO	0.07	0.08	0.08	0.17	0.05	0.06	0.03	0.05	0.17	0.02
CaO	30.27	29.93	26.43	29.27	30.69	30.37	28.84	29.05	28.63	28.97
Na_2O	0.08	0.08	0.08	0.08	0.08	0.08	0.08	0.08	0.08	0.08
K_2O	0.01	0.01	0.01	0.13	0.01	0.01	0.01	0.01	0.01	0.01
P_2O_5	0.01	0.05	0.01	0.02	0.08	0.01	0.01	0.01	0.04	0.02
H2O-	0.23	0.13	0.37	0.15	0.16	0.23	0.17	0.11	0.21	0.11
TOTAL	98.40	98.40	92.75	98.50	97.80	98.50	96.85	96.70	97.05	96.15
Mo	1.01	0.96	0.80	0.97	1.03	4.44	0.75	0.63	0.50	0.68
Nb	0.51	0.13	0.11	1.99	0.13	3.67	0.50	0.50	0.91	0.50
Zr	4.29	8.61	5.03	21.39	2.22	19.22	1.58	1.02	9.98	2.08
Y	2.97	6.46	3.57	10.09	4.66	4.31	2.00	2.25	3.49	1.97
Sr	108.26	88.13	99.58	81.18	80.59	470.29	43.01	34.24	87.75	47.13
U	0.10	0.14	2.93	1.44	1.39	0.63	1.00	1.00	1.83	1.00
Rb	3.41	3.09	2.81	16.00	0.12	1.52	1.00	1.00	1.00	1.00
Th	1.42	1.37	1.37	1.42	1.37	1.41	1.50	1.50	1.50	1.50
Pb	1.68	1.63	1.63	1.68	1.62	1.67	1.50	1.50	1.50	1.50
Ga	1.37	1.33	1.33	0.29	1.33	1.38	1.50	1.50	2.13	1.50
Zn	5.80	10.59	5.15	31.11	1.93	12.67	2.28	1.50	9.00	1.50
Cu	2.94	2.79	2.82	2.94	2.85	2.98	2.50	2.50	2.50	2.50
Ni	3.42	3.44	3.36	1.48	3.38	16.84	2.50	2.50	2.50	2.50
Sc	1.65	1.83	1.65	1.83	1.88	1.86	1.50	1.50	1.50	1.50
V	4.32	8.41	6.68	28.14	0.50	12.56	1.50	1.50	5.09	1.50
Ce	7.21	7.17	6.58	2.36	7.22	17.75	4.50	4.50	11.64	4.50
Nd	3.80	3.78	3.47	4.65	3.80	0.52	4.00	4.00	6.25	4.00
Ba	7.38	23.60	44.59	174.08	7.39	1083.57	4.50	10.99	4.50	4.50
La	4.18	4.13	3.75	0.07	4.21	4.33	4.00	4.00	4.00	4.00
Cr	68.43	68.43	68.43	68.43	68.43	68.43	2.50	2.50	3.58	2.50

Major elements in weight percent oxide.
Trace elements in parts per million.

limestones. High-Mg basalts probably were a supplementary source of Mg to subsurface waters, explaining the dolomite-greenstone association in the Bridgetown Formation. Direct precipitation or dolomitization is not totally excluded.

5.4. CHERTS

Cherts associated with greenstones and dolomite of the Bridgetown Formation vary considerably in colour, texture, deformation and nature of occurrence. Major and trace element analyses were done on the different types of chert to determine if there is any significant differences in their major and trace element content.

The samples include white to grey massive chert, oolitic chert and massive jasper. Their location and chemistry are listed in Table 5.5.

The white to grey massive chert and the oolitic chert are very pure cherts with a SiO_2 content of 96 to 99%. They also include minor amounts of Al, Fe, Ba and Zr which are probably present in detrital impurities. All the other elements (including the REE's) have concentrations near or below their detection limits. In section 3.2.5(ii) we discussed the possibility of the oolitic cherts being replacement products of oolitic carbonates. If the oolitic cherts represent replacement cherts then the high SiO_2 content of these samples indicate that they are completely silicified; the ooids as well as the carbonate matrix have been fully replaced by silica.

Oxygen isotope analysis was done on two chert samples. An oolitic chert sample (NSF/12) from the farm Volgelstruisdrift has a $\delta^{18}O$(SMOW) value of 26.39 per mil and a massive chert sample (NSF/14) from the farm Tweevlei has a $\delta^{18}O$(SMOW) value of 23.4 per mil. According to Hoefs (1987) cherts have the highest $^{18}O/^{16}O$ ratios found in rocks. This is due to the large oxygen isotope fractionation factor between quartz and water at low temperatures. Their oxygen isotope composition can vary between 20 to 44 per mil, which is much higher than the oxygen isotope composition of hydrothermal quartz. The $\delta^{18}O_{quartz}$ values of mesothermal vein systems, generally cluster between 15 to 16 per mil (Rushton et al., 1993). It is concluded that formation of the massive and oolitic cherts of the Bridgetown

Table 5.5. Major and trace element chemistry of cherts of the Bridgetown Formation.

SAMPLE	NSF/3.1	NSF/3.2	NSF/3.4	NSF/3.5	NSF/3.6	NSF/7	NSF/12
SiO_2	88.49	97.34	97.35	96.56	97.69	98.00	98.00
TiO_2	0.01	0.01	0.01	0.01	0.01	0.01	0.01
Al_2O_3	0.11	0.02	0.28	0.02	0.47	0.12	0.01
Cr_2O_3	0.00	0.00	0.00	0.00	0.00	0.00	0.00
Fe_2O_3·	9.89	1.72	0.52	0.09	0.12	0.02	0.19
MgO	0.03	0.03	0.04	0.03	0.02	0.04	0.03
MnO	0.01	0.01	0.01	0.01	0.01	0.11	0.03
CaO	0.00	0.00	0.00	0.00	0.02	0.02	0.00
Na_2O	0.08	0.08	0.08	0.08	0.08	0.08	0.08
K_2O	0.01	0.01	0.01	0.01	0.01	0.01	0.01
P_2O_5	0.14	0.02	0.01	0.01	0.16	0.04	0.03
H_2O-	0.11	0.08	0.09	0.05	0.27	0.07	0.04
TOTAL	99.10	99.40	98.65	96.85	99.15	99.50	99.50
Mo	15	1	1	1	1	1	1
Nb	1	1	1	1	1	1	1
Zr	86	95	15	4	4	1	2
Y	1	1	2	1	1	4	2
Sr	9	1	1	1	37	6	11
U	1	1	1	1	1	1	1
Rb	1	1	1	1	1	1	1
Th	2	2	2	2	2	2	2
Pb	2	2	2	2	2	2	2
Ga	2	2	2	2	2	2	2
Zn	2	2	2	2	2	2	2
Cu	3	3	3	3	3	3	3
Ni	90	3	4	3	3	35	3
Sc	2	2	2	2	2	2	2
V	35	10	7	2	3	2	2
Ce	5	5	5	5	5	5	5
Nd	4	6	4	4	4	4	4
Ba	5	5	89	5	98	18	114
La	4	5	4	4	4	4	5
Cr	9	11	4	5	6	9	7

Major elements in weight percent oxide. Fe_2O_3 * = total Fe

Trace elements in parts per million.

Sample	Description	Location
NSF/3.1	Jasper	De Pont
NSF/3.2	Grey massive chert	De Pont
NSF/3.4	Chert with ooids	Palestina
NSF/3.5	Chert with ooids	Palestina
NSF/3.6	White to grey massive chert	Tweevlei
NSF/7	Chert with ooids	Vogelstruisdrift
NSF/12	Chert with ooids	Vogelstruisdrift

Formation are not related to a hydrothermal event. If replacement of carbonates by silica did occur, it must have taken place at low temperatures.

Replacement cherts can occur in shallow platform carbonates as well as in open-ocean or deep-sea carbonates. Maliva and Siever (1988) refer to the mechanism for forming deep-sea oolitic replacement cherts as a maturation process whereby chert evolves from originally dispersed biogenic opal-A (amorphous silica) through an intermediate stage to quartz porcellanite or chert. These cherts are typically characterized by quartz-replaced lepisheres, which provide good textural evidence for an opal-CT precursor. Opal-CT is a low-temperature cristobalite, disordered by interlayered tridymite lattices (Boggs, 1992). Kanauth (1979) suggested that the mixing zone where meteoric groundwaters mix with seawater in a coastal area may be a favourable geochemical environment for the formation of shallow or platform replacement cherts. Silica is supplied in this environment by the dissolution of sponge spicules or other forms of biogenic opal-A within the sediment pile and is then transported into the zone of mixing, where replacement of $CaCO_3$ occurs. Opal-A is first transformed to opal-CT, which then replaces the carbonate and is later diagenetically altered to quartz chert. Replacement of carbonates by silica to form replacement cherts accordingly takes place at low temperatures.

The jasper-rich chert has a SiO_2 content of 88.5% and a total Fe_2O_3 content of 9.9%. Most of the iron occur in red disseminated hematite. Minor amounts of Al, Mo, Zr, Ni and V are also present. The relatively high Ni content (89.5 ppm) and the presence of jasper-rich chert lenses in the greenstones might indicate a possible volcanogenic (exhalative) origin for the jasper-rich cherts.

In conclusion, oxygen isotope analysis proved that the massive quartz bodies, associated with the dolomite and greenstones, are cherts and not superficially silicified rocks. The oolitic cherts are replacement products of oolitic carbonates. Silica was presumably added to the environment through reaction of seawater with hot volcanic rocks, while silica-secreting organisms were responsible for removal of silica from the ocean water. The jasper-rich cherts and jaspilites are probably products of exhalative volcanism.

5.5. CONCLUSION

In Table 5.6 geochemical characteristics of each lithological unit of the Bridgetown Formation are illustrated with respect to the non-facing stratigraphy.

Two general trends are observed in this greenstone sequence relative to the adopted stratigraphic interpretation.

i) an increase in the more evolved magmas, and

ii) the ratio of sedimentary units, pyroclastic material and chemical precipitates to mafic flows increases upwards.

These trends are often found in greenstone successions. An example is the Archaean Swaziland Sequence of the Barberton greenstone belt, South Africa, which exhibits a general decrease in the ultramafic rocks and an increase in the felsic rocks, sediments and pyroclastics towards the top.

Reconstruction of the sequence of events is complicated by the following: 1) it is not clear whether boundaries between lithologies are stratigraphic or tectonic, and 2) additional metavolcanic and metasedimentary units, other than those encountered, can be expected in this highly heterogeneous greenstone body.

The following can be deduced:

1) Both alkaline and tholeiitic magmatism occurred. Their chronological relationship is unclear. Unit 10, the tholeiitic dyke, represents the youngest magmatic event.

The alkaline and tholeiitic magmas originated from the same source material, being products of varying conditions of melting.

2) Alkaline magmatism occurred contemporaneously with deposition of sediments and chemical precipitates (e.g. carbonates and cherts). Some degree of mixing of the basaltic rocks and the sediments has taken place.

Table 5.6. Geochemical characterization of lithological units of the Bridgetown Formation.

Formation	Lithology (non-facing)	Geochemical characterization
Bridgetown	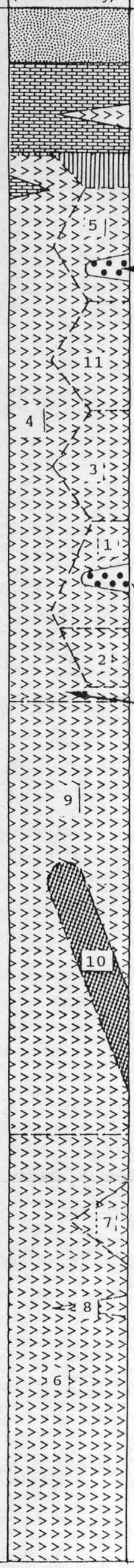	Oolitic, massive and jasper-rich cherts Dolomite with small greenstone bodies (>>>>) Metal-poor muscovite-quartz schist with a continental crust provenance Unit 5: a metamorphosed intermediate volcanic rock or a metabasalt, contaminated by a sedimentary component Metal-poor graphitic schist lens with a continental crust provenance Unit 11: - alkaline metabasalt - within-plate tectonomagmatic fingerprint (OIB) - more evolved magma with low mg-value (56) - differentiation product of unit 3 Unit 3: - alkaline metabasalt - within-plate tectonomagmatic fingerprint - poorly differentiated magma with high mg-value (73) - formed at high pressures (>15 kbars) or low degrees of partial melting (3 to 7%) of a LREE-enriched source Unit 1: - metatuff with an alkaline basaltic composition - within-plate tectonomagmatic fingerprint (OIB) - more evolved magma with low mg-value (56) Metal-poor graphitic schist lens with a continental crust provenance Unit 2: - metasedimentary unit with a mafic volcanic component - marine origin Unit 4: - alkaline metabasalt with dolomite lenses (≡≡≡) - within-plate tectonomagmatic fingerprint (OIB) - poorly differentiated magma with high mg-value (73) - formed at high pressures (>15 kbars) or low degrees of partial melting (3 to 7%) of a LREE-enriched source. Unit 9: - subalkaline, low-alumina, tholeiitic metabasalt - ocean-floor basalt (P-type MORB) fingerprint - poorly differentiated magma with high mg-value (80%) - formed at low pressures (<15 kbars) or high degrees of partial melting (20 to 30%) of a LREE-enriched source Unit 10: - subalkaline, low-alumina, tholeiitic metabasite - ocean-floor basalt (P-type MORB) and island arc basalt fingerprint - poorly differentiated magma with high mg-value (79) - formed at low pressures (<15 kbars) and high degrees of partial melting (>40%) of a source, depleted in its initial melt fractions. Unit 7: - subalkaline, low-alumina, tholeiitic metabasalt - ocean-floor basalt (P-type MORB) fingerprint - poorly differentiated magma with high mg-value (78) - formed at low pressures (<15 kbars) or high degrees of partial melting (20 to 30%) of a LREE-enriched source Unit 6: (=unit 8) - alkaline metabasalt - within-plate tectonomagmatic fingerprint - poorly differentiated magma with high mg-value (82) - formed at high pressures (>15 kbars) or low degrees of partial melting (3 to 7%) of a LREE-depleted source

6. GEOCHEMISTRY OF BANDED CHERT, CHLORITE SCHIST AND QUARTZ VEINS AT SPITSKOP

The geochemistry of some rock types at Spitskop was investigated to evaluate the possibility of them being hosts to anomalous gold and arsenic, found in adjacent streams during a regional stream sampling project. The rock types investigated include a) banded chert which covers the top of Spitskop and its south-eastern flank, b) a small chlorite schist outcrop, exposed in a road-cutting through the south-eastern flank of Spitskop and c) quartz veins of different ages which cross-cut the chlorite schist, banded chert and quartz-feldspar-sericite schists. An attempt was also made to compare the banded chert and chlorite schist at Spitskop with cherts and greenstones of the Bridgetown Formation.

6.1. BANDED CHERT

Two banded chert samples were analyzed for major and trace elements (Table 6.1). One of the samples (NSF/6) was also analyzed for Au, Ag, As and Sb.

The Au and Sb content of NSF/6 are below their respective detection limits, but minor amounts of Ag (0.7 ppm) and As (35 ppm) were detected. Although sample NSF/6 does not contain any gold mineralization; the possibility of gold mineralization in the banded chert body should not be totally excluded on account of one sample.

The major and trace element content of the banded chert differ considerably from the element content of the cherts associated with the main greenstone body. Its SiO_2 and Fe_2O_3t content are intermediate between those of the relatively pure cherts and the jasper-rich chert. The major chemical difference is the anomalous high Ni (549 to 694 ppm) and Cr (1835 to 2268 ppm) content in the banded chert. In section 3.4.3. chromite grains and Cr-rich micas (biotite and chlorite) were identified in small irregular discontinuous cracks in the banded chert. These minerals are responsible for the high Cr-values in the banded chert. Thus far the high Ni-values could not be linked to specific minerals in the banded chert. A very high Ba value (1093 ppm) was also detected in sample NSF/11.

Table 6.1. Whole rock major and trace element chemistry of rock types at Spitskop.

	banded chert	banded chert	chlorite schist	steatite
SAMPLE	NSF/11	NSF/6	NSF/9	NSF/10
SiO_2	94.45	93.27	53.82	58.96
TiO_2	0.01	0.01	0.40	0.01
Al_2O_3	0.29	0.37	17.47	1.15
Cr_2O_3	0.29	0.31	0.01	0.37
FeO	0.45	0.45	5.40	1.35
Fe_2O_3	3.60	3.80	1.75	8.01
MgO	0.18	0.03	11.03	25.07
MnO	0.08	0.02	0.10	0.04
CaO	0.00	0.00	0.07	0.00
Na_2O	0.08	0.08	4.39	0.08
K_2O	0.01	0.01	0.01	0.01
P_2O_5	0.01	0.00	0.01	0.01
H_2O-	0.13	0.28	0.14	0.41
TOTAL	99.50	99.40	99.50	99.50
Mo	1	1	1	1
Nb	1	2	1	1
Zr	32	63	12	2
Y	4	4	12	5
Sr	23	1	68	1
U	1	1	1	1
Rb	1	1	3	1
Th	2	2	2	2
Pb	2	24	2	2
Ga	2	2	16	2
Zn	13	28	46	49
Cu	3	3	33	14
Ni	694	549	268	3691
Sc	6	8	59	7
V	22	29	286	51
Ce	5	5	5	5
Nd	4	4	4	4
Ba	1093	8	35	5
La	5	4	4	4
Cr	1835	2268	54	2221

Major elements in weight percent oxide.
Trace elements in parts per million.

The high contents of Ni, Cr ± Ba and its association with a chlorite schist indicate a possible hydrothermal-volcanogenic origin for the banded chert. It, however, does not show chemical similarities with hematite cherts or banded iron formations associated with volcanogenic massive sulfide deposits (e.g.. the Kuroko-type, the Cyprus-type and the Besshi-type). The Fe, Cu, Pb, Zn and Mn content of the Spitskop banded chert is much lower than in these types.

6.2. CHLORITE SCHIST

The greenschist body at Spitskop consists of a dark olive-green chlorite schist with albite porphyroclasts, and small irregular light grey to pale-blue talc-rich bodies. Major and trace element analyses, done on one chlorite schist sample and one talc-rich sample, are listed in Table 6.1.

The major and trace element content of the chlorite schist does not agree with the element content of any of the greenstone units described so far. It has a much higher SiO_2, Al_2O_3 and Sc content and is depleted in Fe_2O_3t, CaO, most of the incompatible elements and all the REE's relative to the other greenstone units. It has a flat chondrite normalized REE pattern (Fig. 6.1) which is depleted in total REE's (<10*chondrite).

If the assumption is made that the chlorite schist is magmatic, it would classify as a subalkaline basaltic andesite according to its $Na_2O + K_2O$ and SiO_2 content (Cox et al., 1979 and Irvine and Barager, 1971).

The talc-rich sample has a SiO_2 content of 59% and a MgO content of 25% which is slightly lower than the average SiO_2 and MgO content of the mineral talc which is 62.6% and 30,2% respectively (Deer et al., 1992). XRD analysis on one of the samples confirmed that it consists mainly of talc. The high Fe_2O_3t content (9.5%) of the talc-rich sample is probably related to the presence of oxidized material which occurs as small speckles in the sample. The talc-rich sample has extremely high contents of Ni (3691 ppm) and Cr (2221 ppm).

The occurrence of small Ni- and Cr-rich talc bodies in association with a chlorite schist may indicate the possible presence of an ultramafic body at Spitskop. An example of such a lithological association in literature, is the Roxbury serpentinites

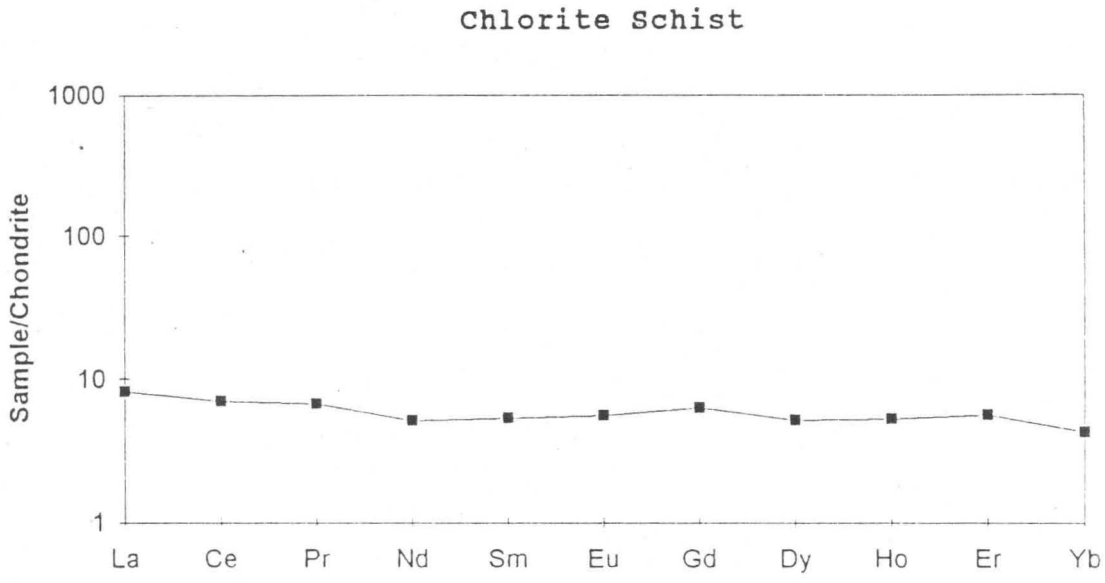

Figure 6.1. Chondrite-nomalized REE pattern for a chlorite schist at Spitskop.

in Vermont (Jahns, 1967). Although serpentinite is predominant, other rock types form well-defined units within the ultramafic bodies. The distribution of the major units is illustrated in Fig. 6.2 and the principal features of the rock types are summarized as follows:

a) The blackwall zone.

This zone consists of highly foliated dark coloured chlorite-rich rocks that form thin, sharply defined, and nearly continuous rinds about the ultramafic bodies. They range in thickness from a knife edge to a few metres wide. The outer margins of the exterior rinds grade abruptly into country rock, and commonly are flanked by local concentrations of porphyroblastic albite, and less commonly porphyroblastic muscovite. The inner margins grade into steatite, talc-carbonate rock or sheared serpentinite.

b) Steatite.

It is a massive to microsheared, compact, pale-blue to light grey rock, consisting mainly or almost wholly of fine-grained talc. It occurs typically along the inner margins of the blackwall zone as irregular lenses, rarely more than 1 metre thick.

c) Talc-carbonate rocks and veins.

They consist of massive to mildly sheared aggregates of talc and carbonate minerals, generally with carbonate porphyroblasts and commonly veined by younger carbonates. This rock extends from the inner margins of steatite masses and blackwall zones into serpentinite. They range from bulb- or fingerlike projections to pods and thin tabular masses. The talc-carbonate veins are mostly joint controlled.

d) Serpentinite.

Massive to highly sheared, pale-green to very dark-greenish-grey aggregates of serpentine minerals. It comprises the interiors of the ultramafic bodies.

The chlorite schist and the talc-rich masses at Spitskop are comparable to the outer margin of the blackwall zone associated with the Roxbury serpentinites (Fig. 6.2). Small fingerlike zones of dolomite, talc and chlorite occur along joints in the Spitskop banded chert. They may be related to the talc-carbonate kind of rocks associated with the Roxbury serpentinites.

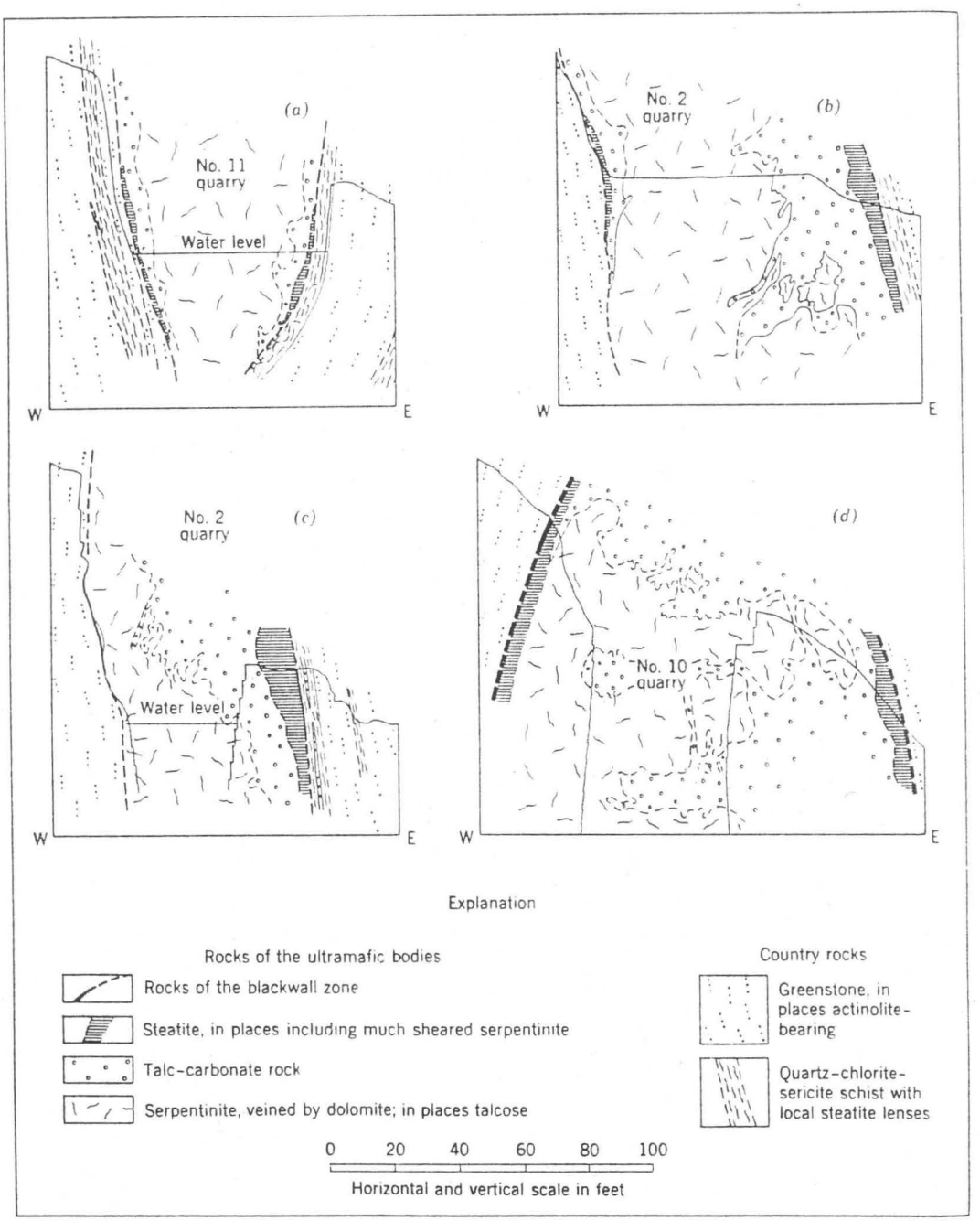

Figure 6.2. Geological sketch sections through typical ultramafic bodies, Roxbury district, showing distribution of major rock types (Jahns, 1967).

Thus, there are some indications that a metamorphosed ultramafic body might be present at Spitskop. As previously mentioned (section 3.4.4), Ni-rich talc is often associated with reactions between quartzites, in this case the banded chert, and ultramafic rocks (De Waal, 1970). If so, then the high Ni- and Cr-values in the banded chert is probably related to secondary enrichment processes involving interaction of SiO_2-satured and CO_2-bearing metamorphic fluids with the ultramafic body (Evans and Guggenheim, 1988); resulting in precipitation of minerals such as chromite, Cr-rich chlorite and biotite, talc and dolomite along fractures and joints in the banded chert.

6.3. QUARTZ VEINS

Banded chert, chlorite schist and quartz-feldspar-sericite schists at Spitskop are cut by numerous quartz veins of different ages.

Although many of the quartz veins at Spitskop have boxwork textures, only a few massive quartz bodies contain visible sulfide mineralization in outcrop. These relatively pure, milky quartz bodies occur in quartz-feldpar-sericite schists on the northern flank of Spitskop. They have been subjected to more than one episode of brittle deformation and are mineralized with galena, pyrite and sphalerite. Major and trace element analyses on one sample (Table 6.2) show anomalous high contents of Pb (41735 ppm; present as galena), Zn (1573 ppm, present as sphalerite), As (346 ppm), Ag (325 ppm), Th (121 ppm) and Sb (44 ppm) with traces of Au (70 ppb). The low total is due to the high sulfur content present as galena, sphalerite and pyrite in this sample.

Fluid inclusion studies on these quartz bodies revealed three primary inclusion populations (Spathelf, unpubl.) They can be divided into a) H_2O - NaCl, b) H_2O - NaCl - CO_2 and c) CO_2 inclusions. Their melting and homogenization temperatures and their densities are given in Table 6.3. The H_2O-NaCl (Th = 160°C) population is found throughout the Western Cape Province, in all the lithologies (R. Scheepers, pers. comm., 1995). It represents either a regional metamorphic overprint in the Malmesbury Group or is related to orogenesis of the Cape Fold Belt. The H_2O-

Table 6.2. Whole rock major and trace element chemistry of mineralized quartz at Spitskop.

SAMPLE	NSF/5
SiO_2	90.95
TiO_2	0.01
Al_2O_3	0.30
Cr_2O_3	0.00
FeO	0.27
Fe_2O_3	1.12
MgO	0.01
MnO	0.01
CaO	0.25
Na_2O	0.08
K_2O	0.01
P_2O_5	0.70
H_2O-	0.08
TOTAL	94.70
Mo	3
Nb	1
Zr	79
Y	33
Sr	46
U	1
Rb	1
Th	121
Pb	41736
Ga	55
Zn	1573
Cu	26
Ni	3
Sc	2
V	5
Ce	74
Nd	10
Ba	5
La	4
Cr	9
As	346
Ag	325
Sb	44
Au	70

Major elements in weight percent oxide.
Trace elements in parts per million.
Gold in parts per billion.

Table 6.3. Th, Tm and density of fluid inclusions in mineralized quartz at Spitskop.

Population	Th (°C)	Tm (°C)	Density (g/cm^3)
H_2O-NaCl	160	-1.60	0.922
H_2O-NaCl-CO_2	270	-0.60	0.782
CO_2	15	-55	0.822

$NaCl\text{-}CO_2$ (Th = 270°C) population might be related to the main sulfide mineralization. According to Pisutha-Arnond and Ohmoto (1983) the formation of black ore minerals (sphalerite, galena and pyrite) during intensifying stages of hydrothermal activity occur at T = 200°C to 330°C. Pb-Zn-(Ag) vein mineralization in Alcudia Valley, Spain, are associated with low salinity (<11,7 wt% eq. NaCl), medium temperature (204 to 370°C; frequency maximum in the interval 240 to 260°C) aqueous-carbonic fluids (H_2O-NaCl and H_2O-NaCl-CO_2; Palero et al., 1991). According to Banks et al. (1993), gold transport is often associated with late stage, low temperature H_2O-salt fluids.

Oxygen isotope analyses were done on quartz veins of different ages and the banded chert to determine their genetic relationship. The $\delta^{18}O$(SMOW) values and sample descriptions are given in Table 6.4.; and the sample locations are shown in Figure 6.3.

The $\delta^{18}O$ values of the quartz veins vary between 13.53 and 17.92 per mil. According to Rushton et al. (1993) these values are typical of most mesothermal vein systems. Mechanisms which have been invoked to account for generation of the mineralizing fluids involved in mesothermal vein genesis include (1) lateral secretion, (2) mantle degassing-granulitization, (3) meteoric water circulation, (4) metamorphic devolatilization and (5) an orthomagmatic origin (Rushton et al., 1993). It is not possible to determine which one of these mechanisms was responsible for generation of fluids involved in vein genesis at Spitskop, by using $\delta^{18}O_{quartz}$ data alone. Plots of $\delta D_{inclusion\ fluids}$ versus calculated $\delta^{18}O_{fluid}$ can be used to determine if the isotopic composition of quartz vein fluids lies inside the magmatic and metamorphic water fields which overlap each other (Rushton et al., 1993). Unfortunately isotope analyses were not done on the quartz vein fluids.

The genetic model for the origin of mesothermal fluids which is most widely accepted is the generation of H_2O and CO_2 during prograde metamorphism under greenschist facies conditions (Kerrich and Fyfe, 1981). The fluids are focused along and channeled into major crustal structures, and migrate upward along the structures losing volatiles and precipitating ore and gangue minerals.

Table 6.4. Oxygen isotope composition of quartz veins and banded chert at Spitskop.

No.	$\delta^{18}O$(SMOW)	Description
N1	15.50	Sheared milky quartz body in banded chert.
N2	13.53	Massive milky quartz body in banded chert.
N4	17.92	Milky quartz vein in banded chert.
N6	14.02	Milky quartz body, containing a few small oxidized sulfide grains.
N7	14.90	Massive, relatively pure milky quartz body in banded chert.
N8	14.71	Brittle deformed grey quartz in banded chert.
N9.1A	14.4	Milky quartz vein, cutting through a cherty matrix which has a gossan-like appearance.
N9.4	13.8	Milky quartz vein, cutting through a cherty matrix which has a gossan-like appearance.
N11	16.81	Clear grey quartz vein in banded chert.
N13	14.60	Massive milky quartz vein in chlorite schist.
N3	15.90	Banded chert.
N10	15.45	Banded chert.

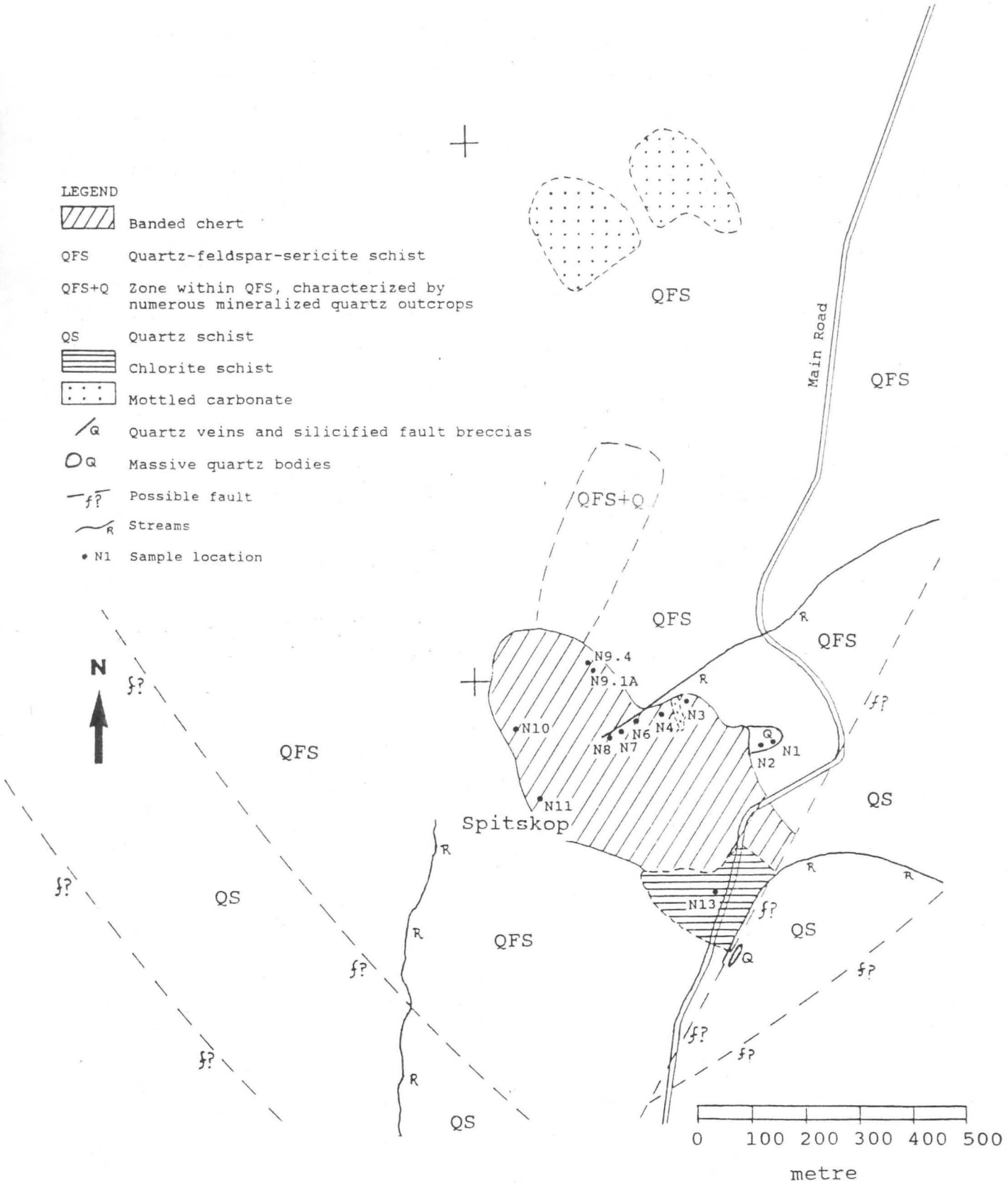

Figure 6.3. Locality map of samples taken for oxygen isotope analyses.

The two banded chert samples exhibit $\delta^{18}O$ values of 15.45 and 15.90 per mil alternatively. These $\delta^{18}O$ values are very low for cherts, which might indicate the following:

a) it is not a chert; or

b) its $\delta^{18}O$ values were strongly affected by either regional metamorphism, contact metamorphism (if there proves to be an igneous body underneath) or a hydrothermal event.

6.4. CONCLUSION

Small Ni- and Cr-rich talc bodies, chlorite schist with albite porphyroblasts and small fingerlike dolomite-talc-chlorite bodies at Spitskop are units often associated with serpentinites. The possibility exists that a metamorphosed ultramafic body is present in the interiors of Spitskop, probably underlying the banded chert.

The banded chert which covers the top of Spitskop and its southeastern flank is probably not a chert. It is either the result of silica leaching of the metamorphosed ultramafic body, or it represents a sheared quartzite. The high Ni- and Cr-values in the banded chert is related to secondary enrichment processes, involving interaction of SiO_2-satured and CO_2-bearing metamorphic fluids with the ultramafic body, resulting in precipitation of minerals such as chromite, Cr-rich biotite and chlorite, talc and dolomite along fractures and joints in the banded chert.

Gold mineralization at Spitskop is hosted in quartz veins which developed at zones of competency contrasts in all the lithologies in the region. Although many of the quartz veins at Spitskop have boxwork textures, only a few massive quartz bodies contain visible sulfide mineralization (galena, pyrite and sphalerite) in outcrop. Au-analysis on one sample revealed only traces of gold (70 ppb) in these bodies. These Pb-Zn-(Ag)-bearing massive quartz bodies contain at least three different populations of mesothermal fluids (H_2O-NaCl, H_2O-NaCl-CO_2 and CO_2-rich fluids) which originated during and/or after greenschist facies metamorphism. The fluids migrated along major crustal structures, losing volatiles and precipitating ore and gangue minerals. Sulfide mineralization is probably related to the H_2O-NaCl-CO_2

(Th = 270°C) population. At least one of the three populations contained traces of gold. The fluids are probably the products of metamorphic devolatilization, but an orthomagmatic origin is not totally excluded.

7. ECONOMIC POTENTIAL OF THE AREA BETWEEN SPITSKOP AND WINKELHAAKSVLEI

During a regional stream sampling project which covered the Malmesbury Group, gold and arsenic anomalies were detected in streams draining Spitskop. This warranted further investigation of the area around Spitskop. Greenstones and associated rock types of the Bridgetown Formation, outcropping directly southeast of Spitskop, were also included in this investigation to determine their mineralization potential.

7.1. BRIDGETOWN FORMATION

The economical viability of each lithological component of the Bridgetown Formation will be discussed.

7.1.1. GREENSTONES

Although the greenstones exhibit some features which would favour mineralization, such as quartz veins in brittle-ductile shear zones; the only mineralization present is pyrite in units 1 and 2 and a few disseminated pyrrhotite grains in unit 11.

The greenstones contain no anomalous base metal values, except for unit 10 (the younger intrusive dyke) which has a Ni content of 452 to 887 ppm and a Cr content of 890 to 1437 ppm. This greenstone unit has geochemical characteristics of magmas often enriched in PGE's (Saini-Eidukat et al., 1993). These magmas are enriched in MgO and Cr and depleted in Ti, Ta, Nb and HREE's compared to tholeiites. It is suggested that further studies on the dyke should include PGE-analysis.

The cores of twelve boreholes (locations in Fig. 3.3) were sampled from top to bottom for Au. The samples had a maximum length of 1 metre. Four hand specimens of unit 11 were also included for Au-analysis. A total of 277 greenstone samples were analyzed for gold by means of Graphite Furnace Atomic Absorption Analysis. The highest value obtained was a mere 27 ppb.

7.1.2. GRAPHITIC SCHISTS AND MUSCOVITE-QUARTZ SCHIST

Graphitic schist lenses, encountered in boreholes AW2 and AE2 (Fig. 3.4), are well-mineralized with pyrite, but their metal content is comparable to those of an 'average shale' (section 5.2). The graphitic schist lenses were also submitted for low level gold analyses (Graphite Furnace Atomic Absorption Analysis). The highest value obtained was 3.5 ppb.

A dark muscovite-quartz schist, outcropping on the farm Tweevlei, also classifies as a metal-poor schist, having a metal content similar to those of an 'average shale'. Gold-analysis, done on four samples, revealed a Au-content of less than 10 ppb.

According to Pasava (1993) shales which host economically important PGE accumulations are rift-related metal-rich shales. The possibility of the graphitic schists and the muscovite-quartz schist bearing economically important PGE concentrations is ruled out, due to the fact that they are metal-poor schists.

7.1.3. DOLOMITES

Dolomite is currently being mined on the farm Bridgetown, mostly for agricultural use. The dolomite is of high purity as previously mentioned in section 5.3. The width of the main dolomite body varies from a few metres to approximately 800m. Dolomite was encountered up to depths of 70 metres in boreholes drilled by PPC on the farm Vogelstruisdrift (M. Taylor, pers. comm., 1994). Structurally the boreholes were drilled into the western limb of a broad synform (Sheet A). It is concluded that the dolomite reserves are far bigger than was first estimated.

So far no anomalous metal enrichments were found in dolomites of the Bridgetown Formation. Samples which were analyzed for metals (including Au), are from the Bridgetown quarry (Sheet A) as well as a few dolomite lenses intersected in borehole CE1 (Fig. 3.6). Fifty-two dolomite samples from the Bridgetown quarry and

exploration boreholes drilled into the dolomite, in the vicinity of the quarry, were analyzed for base metals by Lime Sales Ltd. (M. Taylor, pers. comm., 1994). These analyses rendered no base metal enrichments in the dolomite.

On the farm Tweevlei, a limonitic zone outcrops next to the dolomite (Sheet A). The zone is 5 to 20 metres wide and has a nodular appearance. Some of the nodules contain red iron-rich soil. Two samples from the limonitic zone were analyzed for base metals by Lime Sales Ltd. (M. Taylor, pers. comm., 1994). One of the samples contained anomalous Zn (663.8 ppm) and Ni (803.4 ppm). This limonitic zone is probably the product of secondary enrichment processes similar to those associated with gossan formation.

7.1.4. CHERTS

Various chert outcrops (their descriptions and locations are listed in Table 1 and Sheet A) were analyzed for metals, including Au. They contain no anomalous metal enrichment and classify as relatively pure cherts.

7.2. SPITSKOP AREA

Stream sediment sampling in the Spitskop area revealed gold and arsenic anomalies in streams draining Spitskop. The location of the streams and anomalous stream sediment samples are indicated on the geological map of Fig. 7.1. Gold was also panned in the stream draining the southern flank of Spitskop.

The next step was to pinpoint the Au and As anomalies by means of soil sampling. Hundred-and-twenty soil samples (100g each) were taken on a 200m grid which included Spitskop and the surrounding area. One of the gridlines, traversing the highest point of Spitskop, was sampled every 100 metres. These samples were analyzed for Au and As by means of fire assay. Contoured gold and arsenic concentrations in the soil samples are shown on Figures 7.1 and 7.2 respectively in relation to the geology and topography of the Spitskop area.

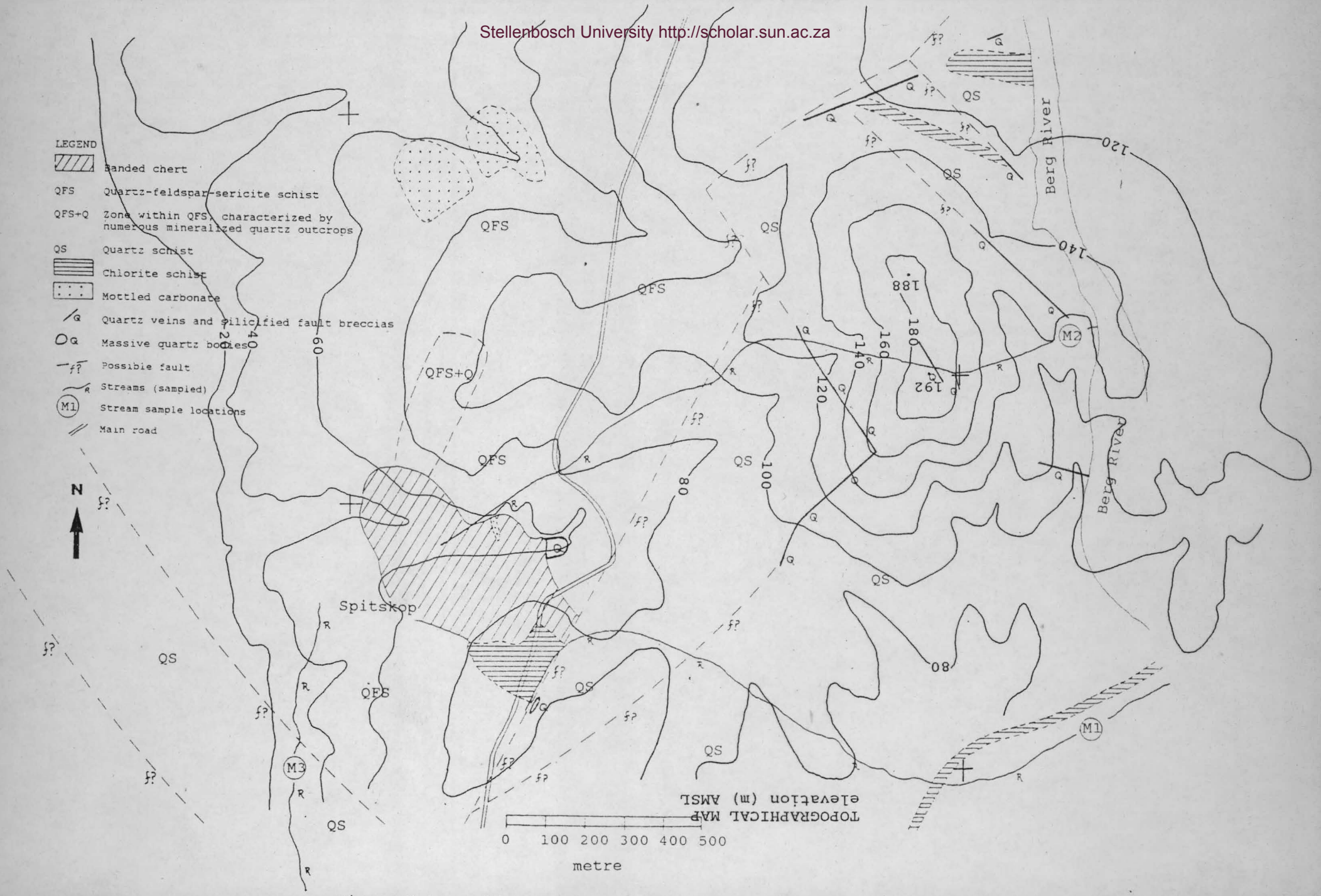

Figure 7.1 Gold anomalies (in soil samples) in relation

GOLD CONCENTRATIONS IN SOIL SAMPLES

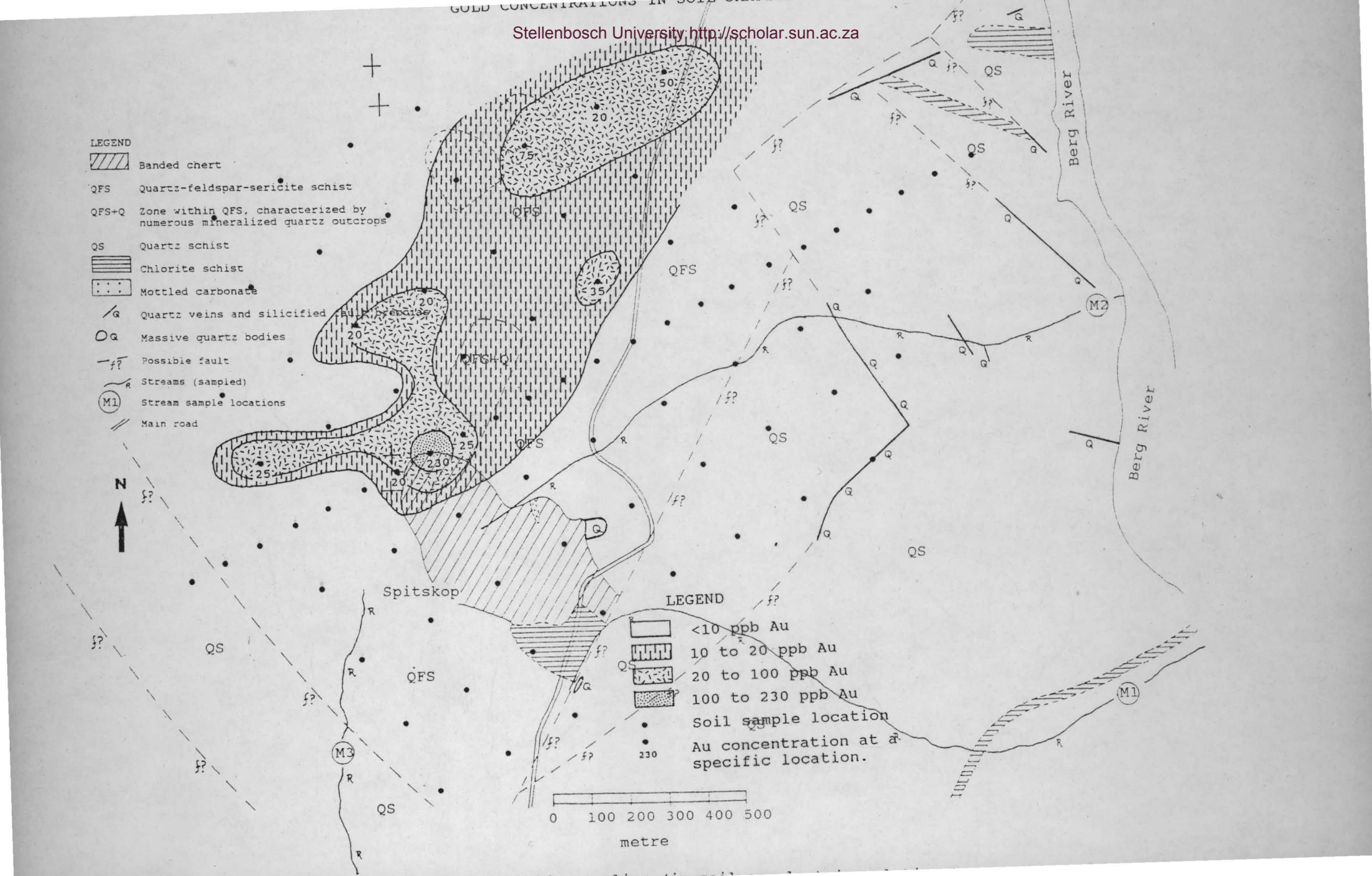

GOLD CONCENTRATIONS IN SOIL SAMPLES

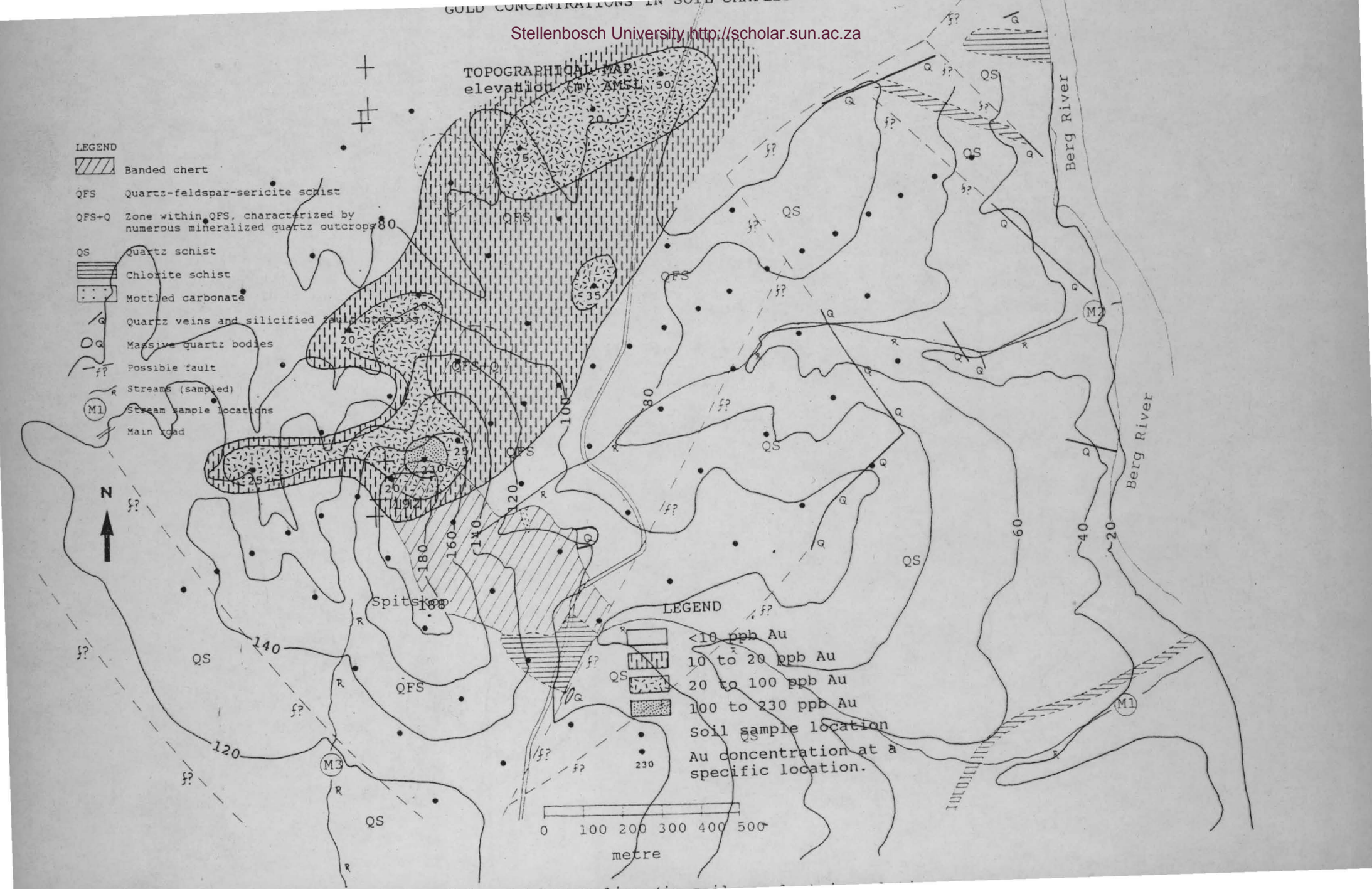

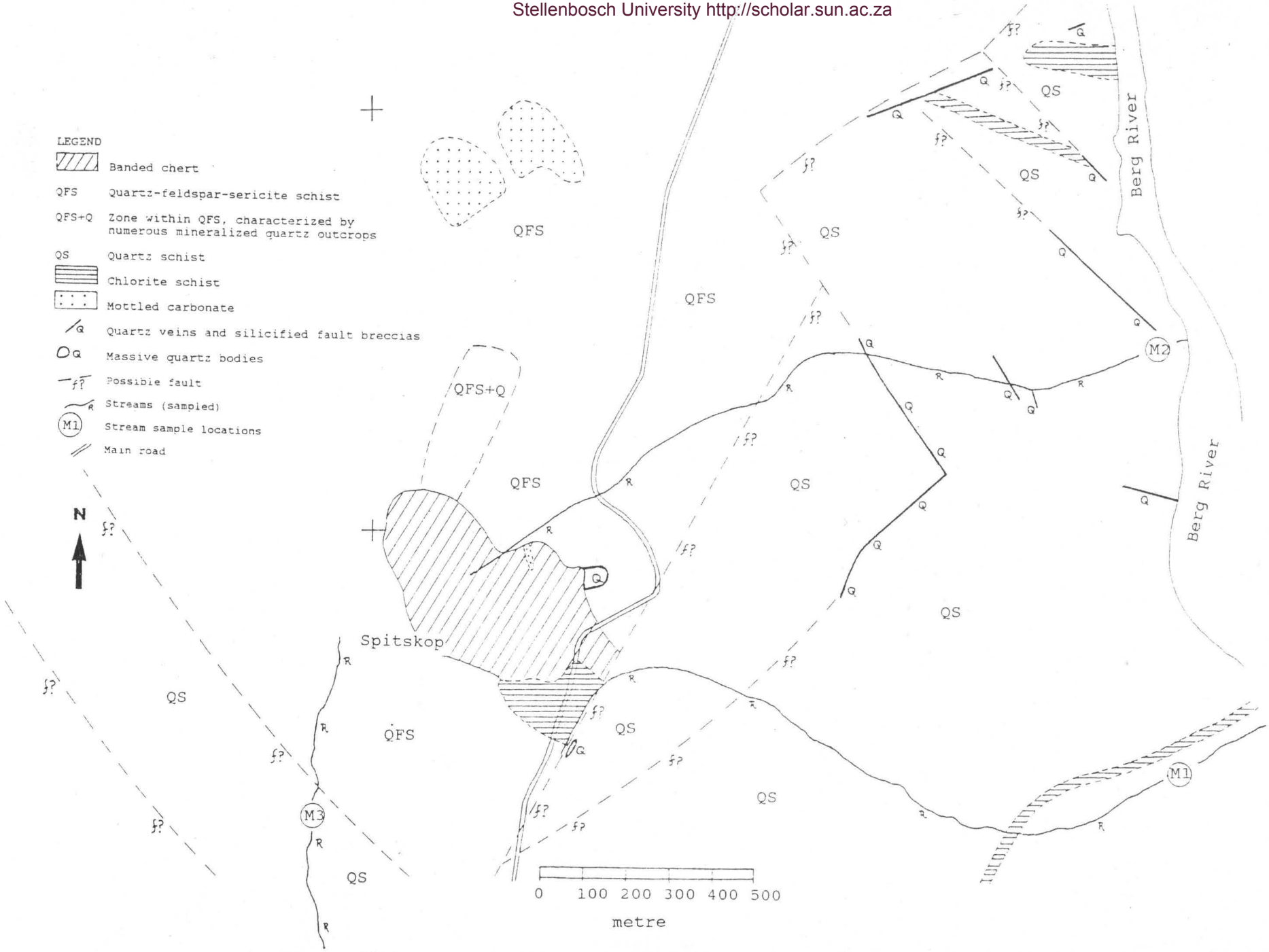

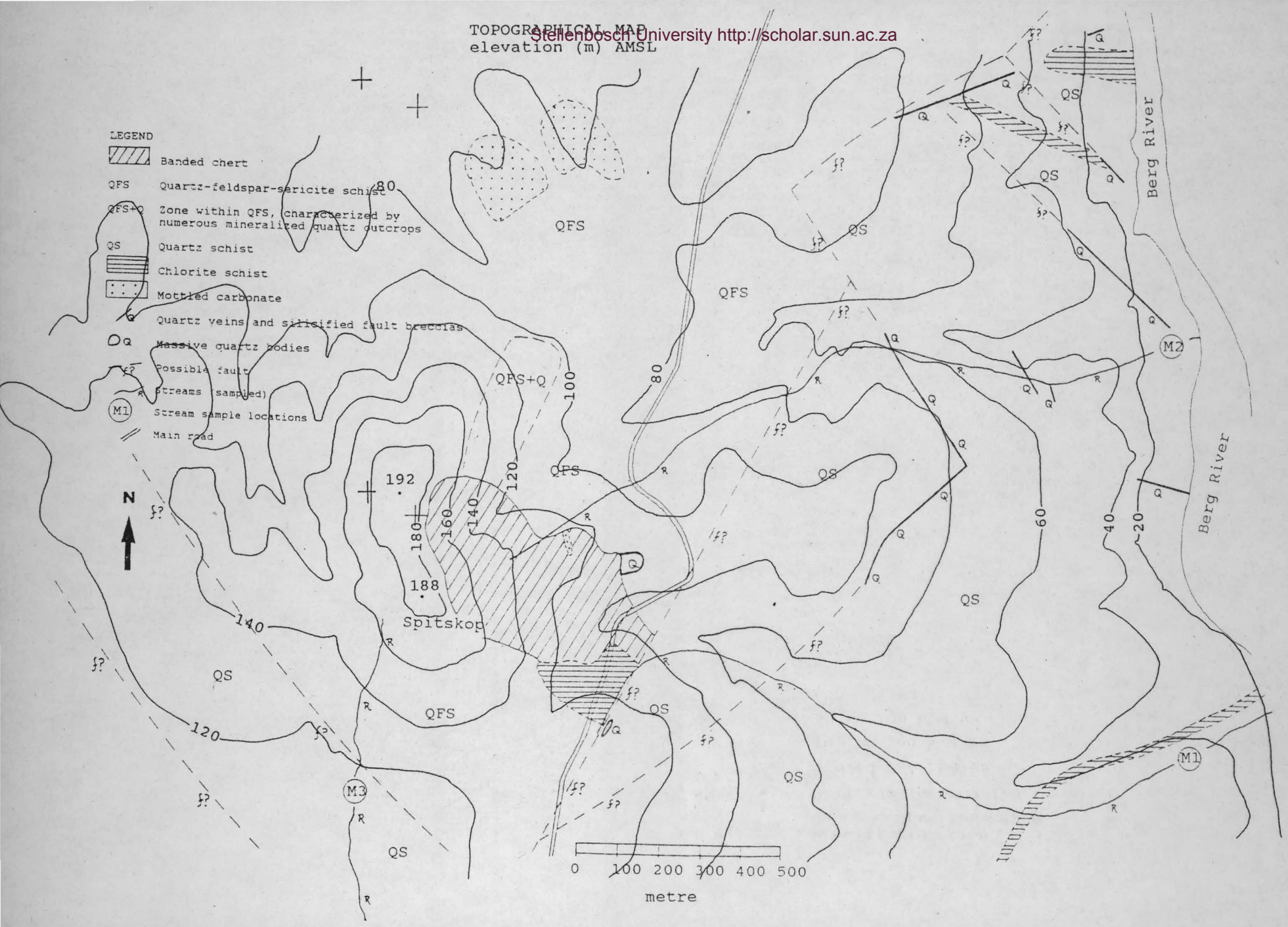

Figure 7.2. Arsenic anomalies (in soil samples) in relation

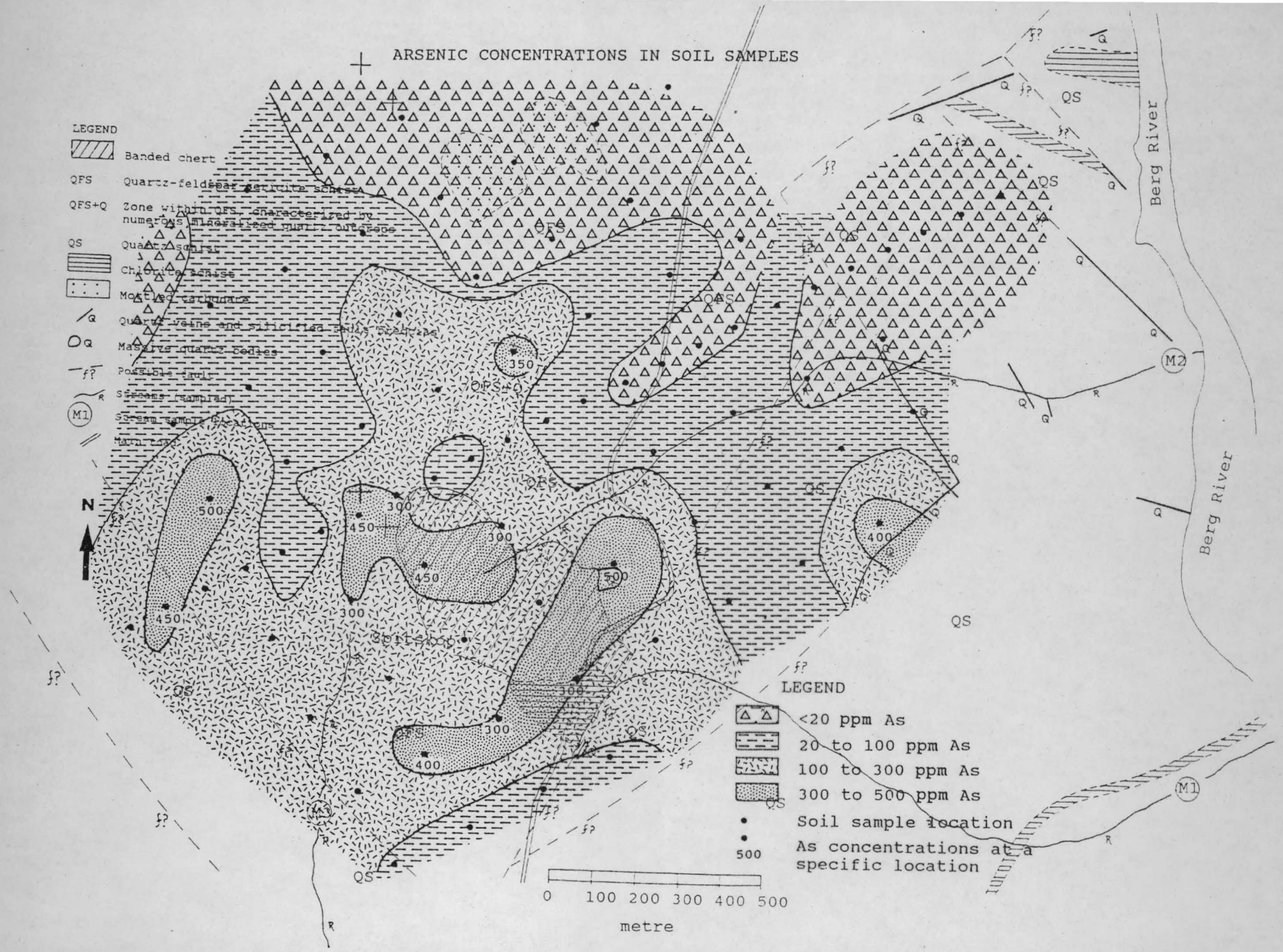

Figure 7.2. Arsenic anomalies (in soil samples) in relation

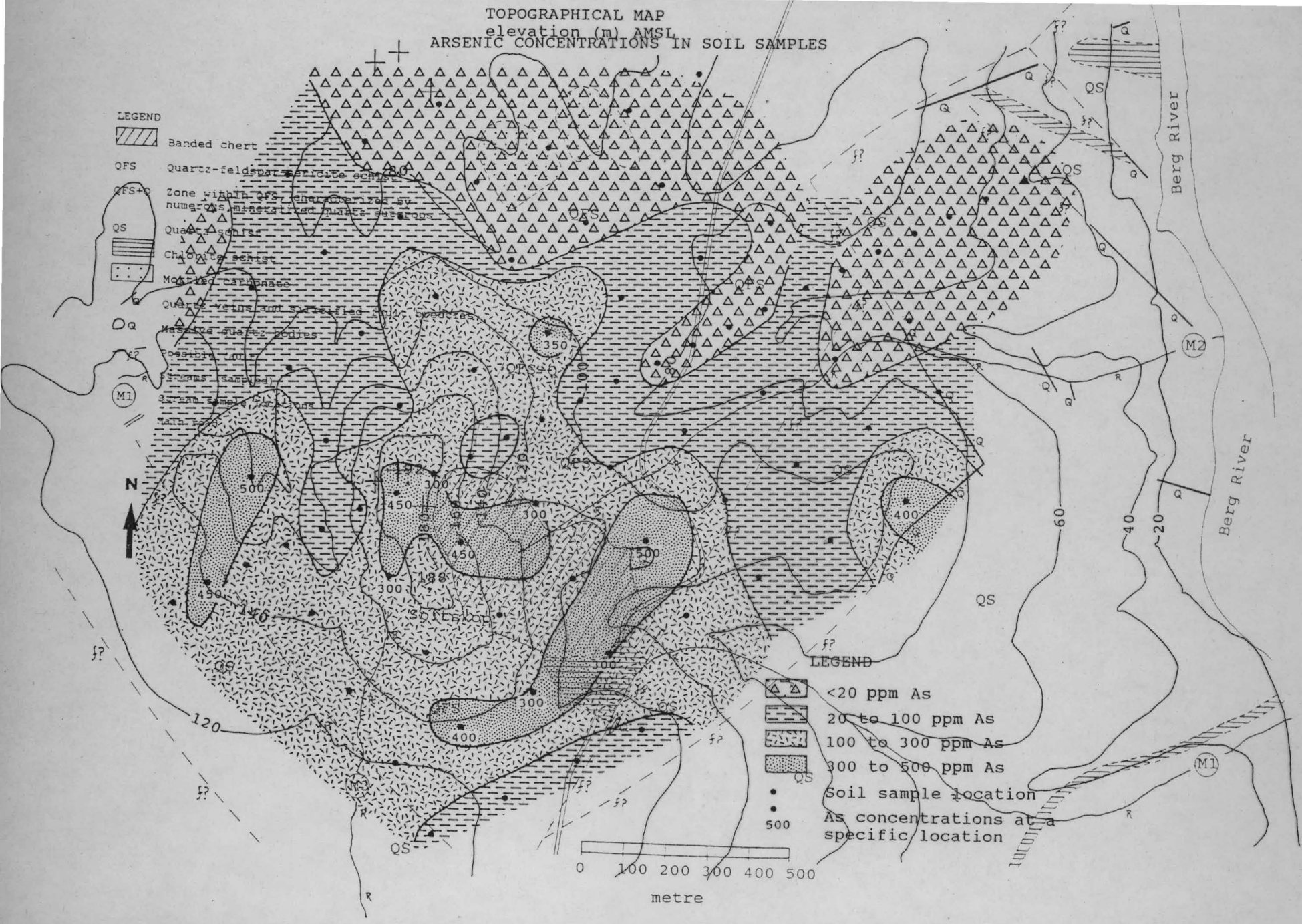

Figure 7.2. Arsenic anomalies (in soil samples) in relation

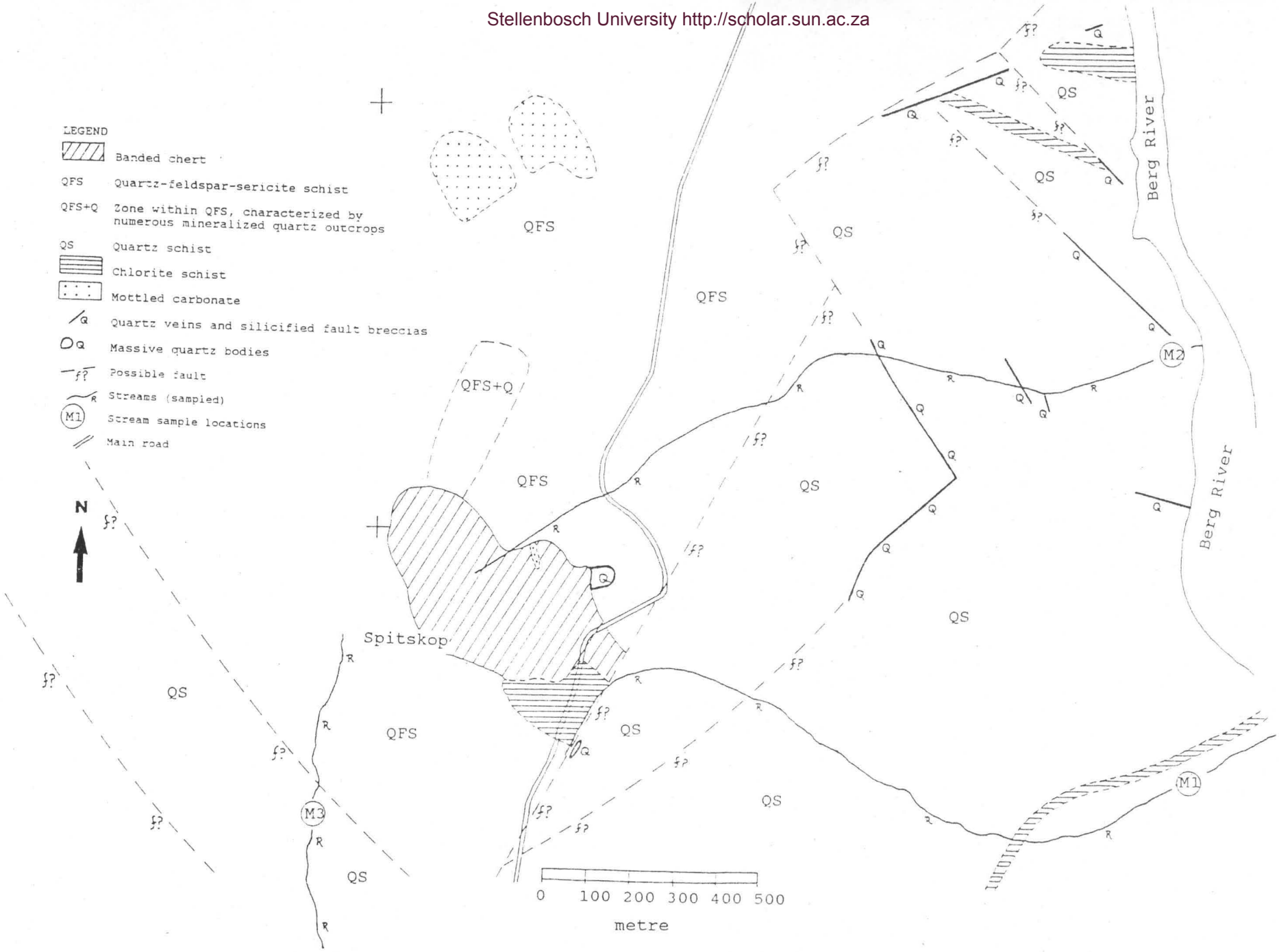

Figure 7.2. Arsenic anomalies (in soil samples) in relation

The highest gold concentration (230 ppb) was found in soil next to the highest point of Spitskop in the banded chert. In this area the chert is cut by numerous clear and milky quartz veins of different ages. The cherty matrix has a gossan-like appearance, probably due to the removal of sulfides during weathering. Neither the quartz veins nor the cherty matrix contains sulfide mineralization in the outcrop. A similar outcrop also occurs 120m east of the highest point, on the northeastern flank of Spitskop. At this outcrop Au-values of approximately 10 to 25 ppb were detected in soil samples.

Numerous massive quartz bodies outcrop in the quartz-feldspar-sericite schist 110m northeast of the highest point (Fig. 7.1). These quartz outcrops have been subjected to more than one episode of brittle deformation and are mineralized with galena, pyrite and sphalerite. One whole rock analysis was done on a quartz outcrop (Table 6.2). These quartz bodies have a very high Pb (41735 ppm, present as galena), Zn (1573 ppm, present as sphalerite), As (325 ppm) and Ag (325 ppm) content with traces of Au (70 ppb). Soil samples taken adjacent to the quartz bodies have gold concentrations of 10 to 20 ppb.

Various quartz veins at Spitskop, which were submitted for oxygen isotope analyses, were also analyzed for Au and As (locations: Fig. 6.3). None of these samples contain anomalous Au or As concentrations.

Au values between 20 and 75 ppb were detected in soil samples in the region of a mottled carbonate outcrop (Fig. 7.1). So far these anomalies could not be related to a specific geological feature and require further investigation.

It is concluded that gold mineralization in the Spitskop area is hosted in clear to milky quartz veins which developed along zones of competency contrasts in all the lithologies in the area. The possibility of gold mineralization in the massive quartz bodies which outcrop in the quartz-feldspar-sericite schist, on the northern flank of Spitskop, should not be excluded on account of one sample. According to Banks et al. (1993) Iberian granite-hosted quartz veins with Au mineralization have some uniform characteristics. The quartz veins display multistage and complex deformation, with each deformational stage being characterized by specific metal deposition. Au is usually associated with arsenopyrite but is later than the sulfide

precipitation. Au transport is associated with late stage, low salinity, low temperature H_2O-salt fluids. The fact that the massive quartz outcrops at Spitskop suffered a multistage deformational history of intense microfracturing and fluid injection (including low temperature H_2O-salt fluids; see section 6.3) as well as the presence of sulfides, render it a good candidate for gold mineralization.

Various mechanisms for transport and deposition of gold in quartz veins have been postulated. Most of the auriferous veins in literature are associated with shear zones which exhibit a complex history of ductile and brittle deformation; for example quartz veins from the Central Pyrenees, Spain (Arcos and Solder, 1991); and an Archaean lode-gold deposit near Kalgoorlie, Western Australia (Gebre-Mariam et al., 1991). Au-bearing fluids circulating through the shear zones do not have fixed properties. It can vary from CO_2-poor brines with high salinity (Arcos and Solder, 1991) to H_2O-CO_2-N_2-rich fluids (Giuliani et al., 1991). Nevertheless, gold has high solubility and mobility in the solutions from which crystallization of sulphide-arsenic parageneses is possible (Pal'Yanova and Kolonin, 1991). The chloride complex $AuCl_2^-$ dominates in acid solutions at a temperature above 300°C and with chloride-ion concentration more than 2mol/kg H_2O. The hydrosulphide complex AuHS prevails in acid solutions and $Au(HS)_2^-$ are the dominant species in the near-neutral to alkaline solutions (Pal'Yanova and Kolonin, 1991). Further studies on the Au-bearing fluids at Spitskop is necessary before any physical-chemical conditions can be postulated for transport and deposition of the gold.

It is important to note that the only soil sample with more than 100 ppb Au, was sampled on the line with 100 metre sample intervals. Furthermore, if the gold is hosted in quartz veins, gold in the soil profile might be highly localized. It is therefore predicted that if soil sampling is done on smaller intervals (e.g. every 50 metres) more areas with high Au anomalies will be defined. The presence of Au in stream sample M1 indicates that there should be some additional Au concentrations located at or near the southern or southeastern flanks of Spitskop.

Generally high arsenic values were found in soil samples at Spitskop, ranging between 100 to 500 ppm (Fig. 7.2). The highest As concentrations (300 to 450 ppm)

occur at the following locations: a) adjacent to a quartz ridge which outcrops in the quartz schist, b) along a NE-SW striking fault zone with massive quartz bodies which have experienced brittle deformation, c) the top of Spitskop (including the area of high Au concentrations) and adjacent eastern and western flanks of Spitskop, d) along a possible NW-SE striking fault which defines the quartz schist/quartz-feldspar-sericite schist contact and contains numerous quartz veins, and e) adjacent to a massive quartz outcrop in the quartz-feldspar-sericite schist (north of Spitskop). It is therefore concluded that As anomalies are associated with quartz bodies or veins which have been subjected to some degree of shearing. Although high As values do not always correlate with high Au values, it should be taken into account that As is more mobile than Au and will display less localized concentrations.

Other geological features at Spitskop, which might have some economical significance, is the occurrence of small Ni- and Cr-rich talc bodies in association with a chlorite schist and an overlying Ni- and Cr-rich banded chert. The talc bodies occur as small irregular lenses in the chlorite schist (rarely more than 1 metre thick) and has a Ni content of 3691 ppm and a Cr content of 2221 ppm. As previously mentioned in sections 6.2 the occurrence of these Ni- and Cr-rich lithologies probably indicate the presence of an unexposed, highly altered and low-grade metamorphosed ultramafic body at Spitskop.

7.3. DISCUSSION

It is suggested that further exploration in the area between Spitskop and Winkelhaaksvlei should be focused on the area around Spitskop. So far no mineralization has been found in the greenstones and associated rock types of the Bridgetown Formation.

Au and As anomalies at Spitskop definitely warrant further investigation. The following exploration program is proposed for the Spitskop area:

a) A detailed soil sampling program.

b) Detailed structural and geological mapping of the Spitskop area.

c) Channel sampling of brittle deformed quartz veins and massive quartz bodies associated with Au and As anomalies.

d) Drilling is recommended if a) and c) prove to be successful.

8. COMPARATIVE STUDY

To obtain a better understanding of the Bridgetown Formation, it is necessary to compare it with age related formations consisting of similar rock types elsewhere. The few examples which are discussed in this chapter, are all associated with Late Proterozoic - Early Palaeozoic Pan-African mobile belts. A comparison with the following three examples is particularly instructive: a) lavas and tuffs at Bloubergstrand (Saldania Belt), b) mafic and intermediate igneous rocks intrusive into the Malmesbury Group (Saldania Belt), and c) the Marmora Terrane of the Gariep Belt. A short descriptive summary of other Pan-African volcano-sedimentary assemblages is also given.

8.1. LAVAS AND TUFFS AT BLOUBERGSTRAND

Lavas and tuffs which are exposed at Bloubergstrand (Fig. 8.1) were first described by Haughton (1933). The Blouberg volcanics are part of the Tygerberg Formation which lies in the Tygerberg terrane of the Malmesbury Group.

Von Veh (1983) described the volcanics as andesitic lava with red tuff, and the adjacent rocks as siltstone, mudstone, arkosic wacke and sandstone.

Jacobs (1974) did a petrographical and geochemical study on the volcanics and divided them into sheared amygdaloidal lavas, massive lavas and lithic tuffs. The sheared amygdaloidal lavas are characterized by their greenish colour and their high content of large flattened amygdales (4mm in length) which are filled with calcite, quartz and minor chlorite. The lava consists of short plagioclase laths, sericite, quartz and iron oxides. The sheared lavas grade into the massive lavas which are characterized by their reddish or grey colour and smaller and fewer amygdales. Mineralogically these lavas are identical to the sheared lavas. The lithic tuffs are also reddish in colour. Lithic fragments, consisting of quartz and feldspar, are set in a glassy matrix.

According to chemical classification diagrams of Winchester and Floyd (1977; SiO_2 versus Nb/Y) and Irvine and Barager (1971; Ol'-Ne'-Q' and AFM diagram) the

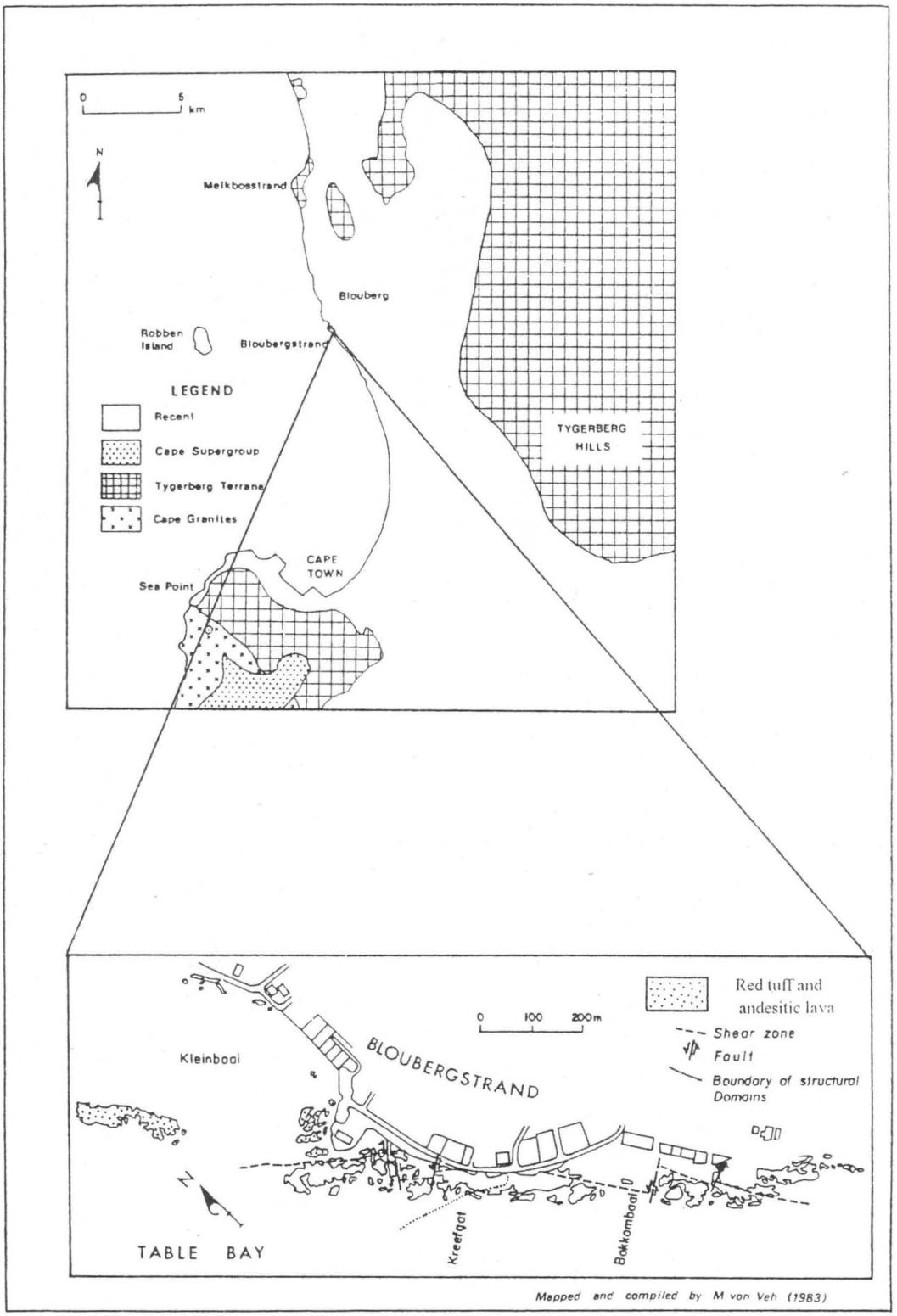

Figure 8.1. Locality map of lavas and tuffs at Bloubergstrand.

Blouberg lavas classify as calc-alkaline andesitic rocks; whereas the Bridgetown metavolcanics classify as alkaline and tholeiitic metabasaltic rocks.

It is concluded that the Bridgetown metavolcanics and the Blouberg volcanics represent two unrelated magmatic events.

8.2. MAFIC AND INTERMEDIATE IGNEOUS ROCKS INTRUSIVE INTO THE MALMESBURY GROUP

Jordaan (1990) and Jordaan et al. (1994) described a few mafic and intermediate igneous rocks associated with the Cape Granite Suite. Two of these bodies are situated on the west coast at the town of Yzerfontein and on the farm Mud River (Fig. 8.2). Their main constituents are monzonite and monzogabbro respectively. Four more bodies, consisting of three small plutons and a set of dykes occur inland near the town of Malmesbury (Fig. 8.2). The dykes consist of porhyritic granodiorite and the plutons of gabbro and gabbro-norite. According to Jordaan et al. (1994), geochemical and isotopic differences exist between the coastal and inland bodies. On the modified TAS-diagram of Middlemost (1991), the coastal bodies correspond to a transalkaline suite and the inland bodies to a subalkaline suite. On an AFM diagram the coastal bodies belong to a calcalkaline series while the inland bodies are tholeiitic. The Ti/100-Zr-Y*3 tectonomagmatic diagram of Pearce and Cann (1973), illustrates that the coastal bodies correspond to calcalkaline basalts and the inland bodies plot in the ocean-floor basalt field. Furthermore, the inland bodies have a higher initial $^{87}Sr/^{86}Sr$ ratio of 0.7087, compared to the ratio of 0.7047 for the coastal bodies.

Jordaan et al. (1994) defines the Yzerfontein and Mud River plutons as mafic and intermediate counterparts of a potassic transalkali (high K-calcalkaline) series, with the younger I-type Cape granites being the felsic end members. The mafic plutons at Malmesbury, however belong to a tholeiitic series and are the possible source rocks for the A-type granites of the Cape granite Suite. Jordaan (1990) also suggested the possibility of the mafic rocks at Malmesbury being related to an older parent basaltic magma.

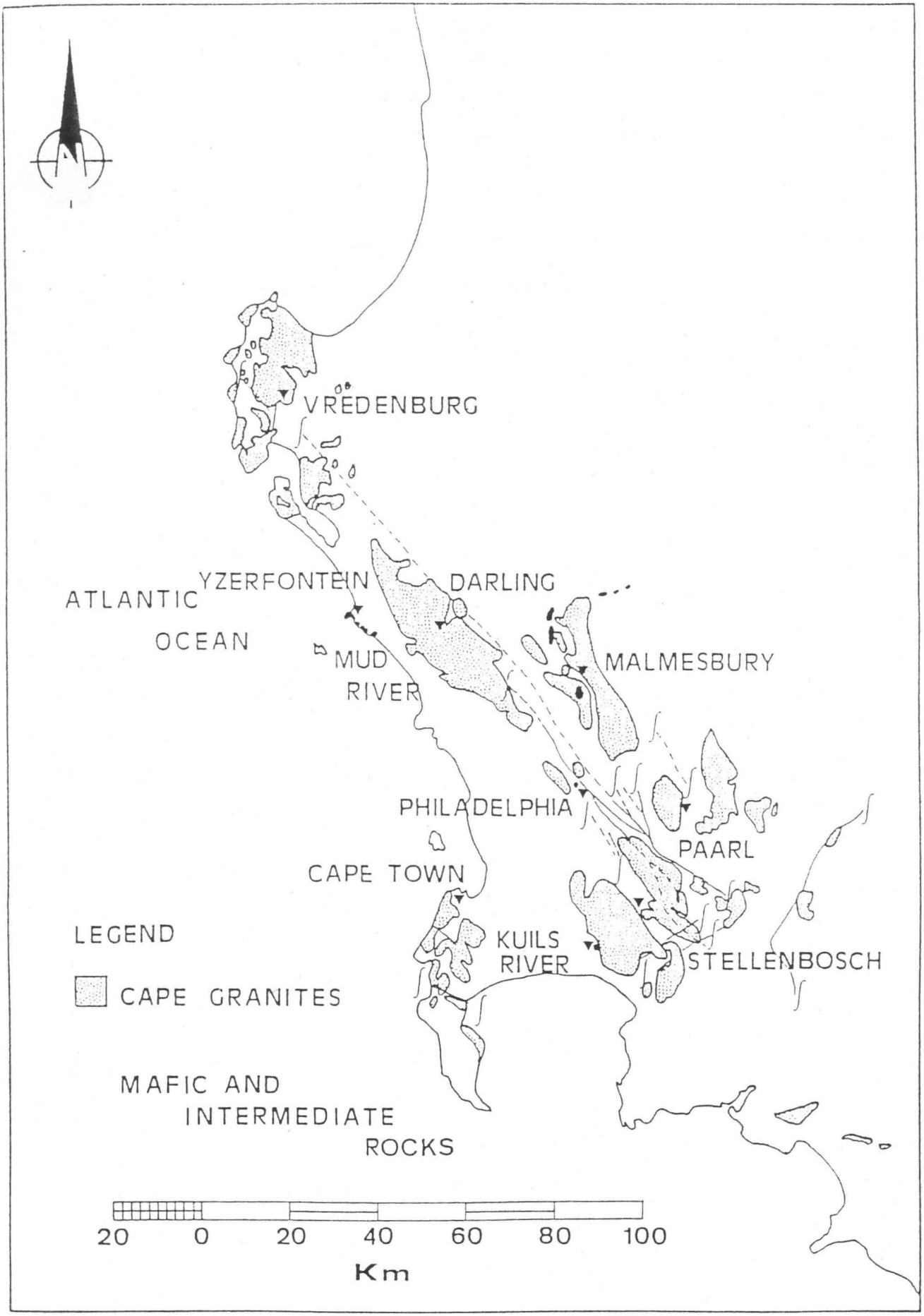

Figure 8.2. Locality map of mafic and intermediate igneous intrusions; spatially associated with the Cape Granite Suite in the southwestern Cape Province (Jordaan, 1990).

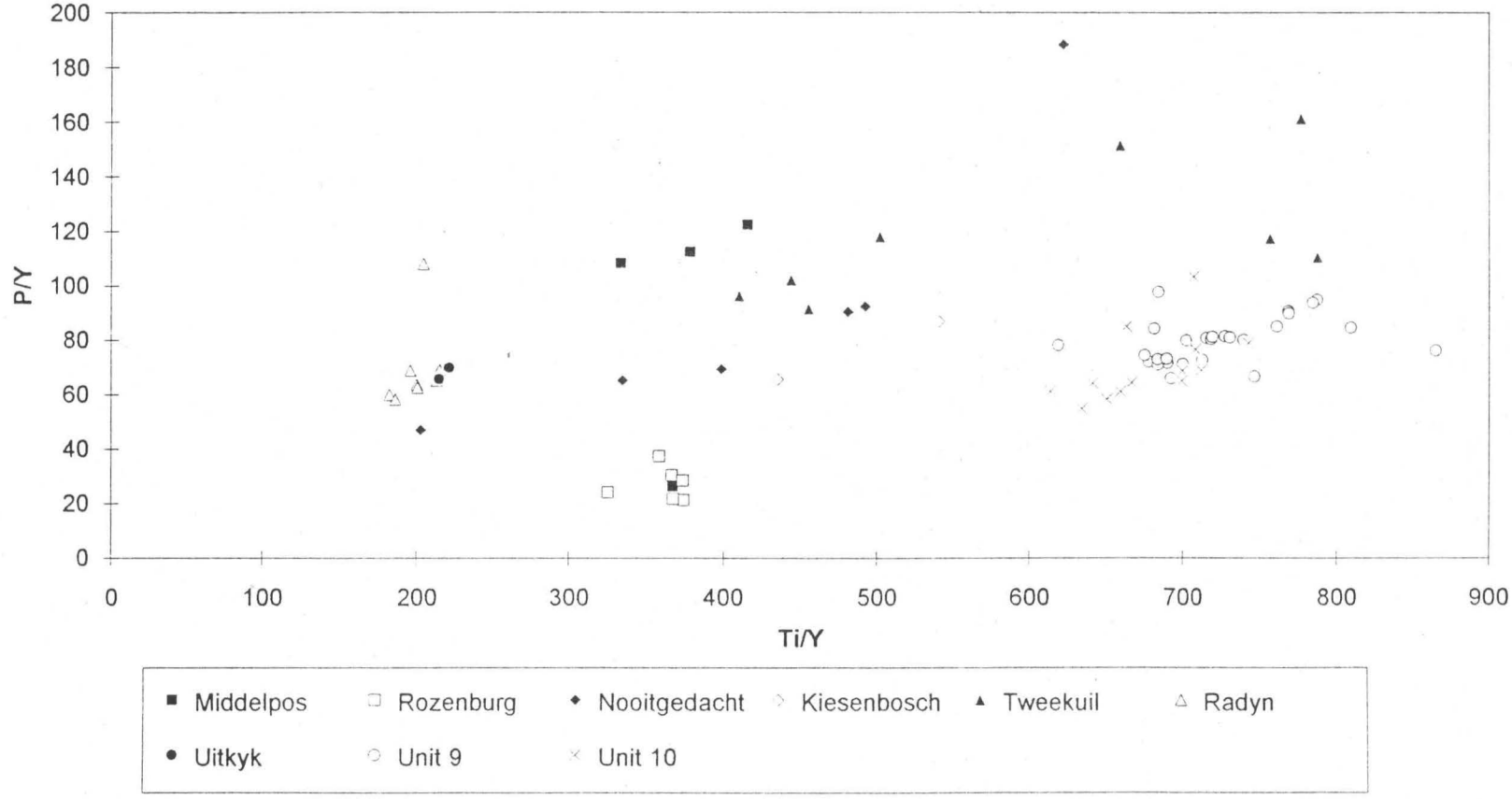

Figure 8.3. A P/Y versus Ti/Y plot for greenstone units 9 and 10 of the Bridgetown Formation and the Malmesbury mafic rocks from different localities.

It is therefore necessary to compare the greenstones of the Bridgetown Formation to the Malmesbury mafics in order to determine whether there is any magmatic association. Greenstone units of the Bridgetown Formation which show geochemical similarities with the Malmesbury mafics, are unit 9 and the younger intrusive dyke (unit 10). These two units classify as subalkaline tholeiitic basalts (section 5.1.2) with ocean-floor basalt characteristics according to the Ti/100-Zr-Y*3 diagram of Pearce and Cann (1973).

Pearce element ratios constructed from conserved constituents (P, Ti and Y) will be used to test if units 9 and 10 have comagmatic relationships with the Malmesbury mafics. Fig. 8.3. is a P/Y versus Ti/Y plot for greenstone units 9 and 10, and Malmesbury mafics from different localities. TiO_2, P_2O_5 and Y values were taken from Jordaan (1990). Basalts derived from the same magma should plot around a single point. Although some scattering of the data points occur, it is clear that greenstone units 9 and 10 plot separately from the other mafic rocks. Another interesting feature is that granodiorite dyke samples from the farms Radyn and Uitkyk cluster around the same point. Data clustering near the x-axis represents gabbro norite from the farm Rozenburg.

It is concluded that the tholeiitic greenstone units of the Bridgetown Formation are not from the same magmatic lineage as tholeiitic mafic rocks outcropping near Malmesbury. It is further deduced that more than one magmatic lineage was responsible for the variety of mafic plutonic rocks in the Malmesbury area.

8.3. MARMORA TERRANE OF THE GARIEP SUPERGROUP

The Late Proterozoic Gariep Belt forms part of a system of Pan-African mobile belts in equatorial and southern Africa and is believed to be linked to the Saldania Belt of the Western Cape Province. The Gariep Supergroup (Gariep Belt) consists of two major tectonostratigraphic units, the eastern Port Nolloth Zone and the western Marmora Terrane (Hartnady et al., 1990; Fig. 8.4.). The Marmora Terrane can be subdivided into three sub-terranes namely the Schakalsberge Complex, the Oranjemund Complex and the Chameis Complex (Hartnady and Von Veh, 1990).

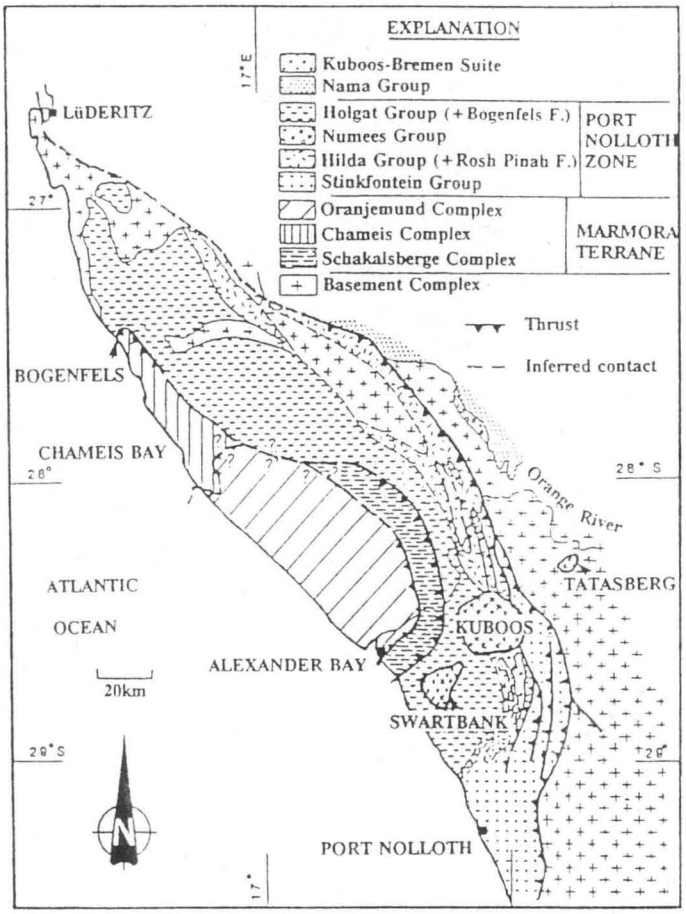

Figure 8.4. Geological map of the Gariep Belt. Modified by Gresse and Scheepers (1993), after Hartnady and Von Veh (1990).

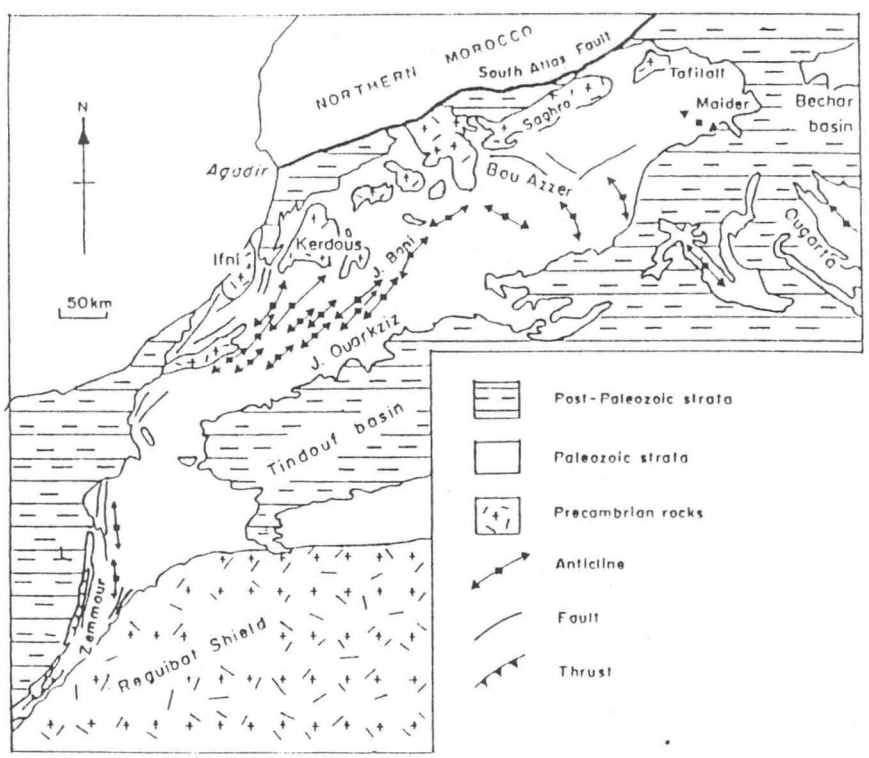

Figure 8.5. Tectonic sketch map of the Moroccan Anti-Atlas (Petters, 1991; redrawn from Piqué and Michard, 1989).

The Schakalsberg Complex, composed of metabasic lavas of the Grootderm Formation and an overlying cherty and stromatolitic dolomite sequence of the Gais Formation, was thrusted over the Port Nolloth Zone along the southeast-vergent Schakalsberge Thrust (Frimmel and Hartnady, 1992a; Fig. 8.4). In the Chameis Complex ultramafic and mafic blocks (0.1 to 100 m size) occur within a highly tectonised, metasedimentary sequence comprising interbedded chloritic, talcose, quartzitic, quartzo-feldspathic, dolomitic, graphitic and ferruginous schists (Frimmel and Hartnady, 1992b). Ultramafics include serpentinised metapyroxenites and metaperidotites, and mafic rock types include massive and layered metagabbros, metadolorites and metabasalts. Mafic and ultramafic bodies in the Marmora Terrane are considered to represent a tectonic melange zone (Frimmel and Hartnady, 1992b) where mafic and ultramafic blocks were tectonically emplaced in a metasedimentary envelope. Locally a sequence with pyroxenites and peridotites at the base, overlain by massive and layered gabbro, followed by basalts and hyoclastite and tuff horizons can be recognized (Frimmel et al., 1995). Post-orogenic alkaline plutons along the Bremen-Kuboos line have a Rb/Sr age of 530 ± 12 Ma and a U/Pb age of 520 ± 12 Ma (Allsopp et al., 1979) thus setting a minimum age limit for obduction of the Marmora Terrane onto the Port Nolloth foreland (Frimmel and Hartnady, 1992a).

Similar to the Bridgetown Formation, the Grootderm Formation is overlain by a dolomite sequence. The Grootderm Formation has also been intensely recrystallized to greenschist facies mineral assemblages containing chlorite, albite, epidote, actinolite and calcite (Smith and Hartnady, 1984). In many areas extrusive structures such as massive flows, volcanic breccias and pillow lavas are well preserved. These structures are also preserved in metavolcanics of the Bridgetown Formation at Voëlvlei Dam. Unfortunately, to date, no geochemical work has been done on the Voëlvlei metavolcanics to prove their association with the Berg River metavolcanics of the Bridgetown Formation. Geochemically mafic rocks of the Gariep Supergroup show some resemblance to greenschists of the Bridgetown Formation, outcropping along the Berg River. In both cases the mafic rocks are basaltic in composition, enriched in LREE's and can be subdivided into within-plate metabasalts and P-type ocean-floor metabasalts (Smith and Hartnady, 1984; Frimmel et al., 1995).

Although the Bridgetown Formation does not contain any ultramafics, as found in the Chameis Complex, the possibility exists that an unexposed metamorphosed ultramafic body might be present at Spitskop (see section 6.2).

8.4. OTHER PAN-AFRICAN VOLCANO-SEDIMENTARY ASSEMBLAGES

It is important to note that the majority of volcano-sedimentary assemblages associated with Late Proterozoic - Early Palaeozoic Pan-African mobile belts have been described as ophiolite complexes. The following examples will be discussed briefly:

a) The Bou Azzer Ophiolite of the Moroccan Anti-Atlas (Fig. 8.5).

b) Ophiolitic rocks of the Mozambique Belt (Kenya and Tanzania, Fig. 8.6).

c) Volcano-sedimentary and ophiolite assemblages of the Arabian-Nubian Shield (Fig. 8.6).

The Bou Azzer Ophiolite includes from bottom to top, serpentinized peridotites, discordant layered gabbros, large stocks of quartz-diorite, discordant layered gabbros, basic lavas with pillow lavas and volcano-sedimentary rocks (Leblanc, 1981). In the volcano-sedimentary succession there is an interlayered sequence of graywackes and calc-alkaline volcanics with subordinate spilitic pillow lavas which range in composition from basalt to dacite. Jaspilites and calcareous tuffs occur among the sediments and arkosic sandstones at the top of the volcano-sedimentary sequence. The ophiolite was obducted and dismembered into several sheets which were thrusted against the continental margin during the Pan-African deformation at about 685 Ma (Petters, 1991). Deformation was accompanied by greenschist facies metamorphism, and was followed by post-kinematic granodiorite intrusion at about 615 Ma.

The central zone of the Mozambique belt contains imbricated slices of mafic and ultramafic rocks (Fig 8.6). Their ophiolitic characteristics survived the high-grade metamorphism and intense deformation in the mobile belt (Petters, 1991). Berhe (1990) linked ophiolites of Sekerr, Baragoi and Moyale of northern Kenya with

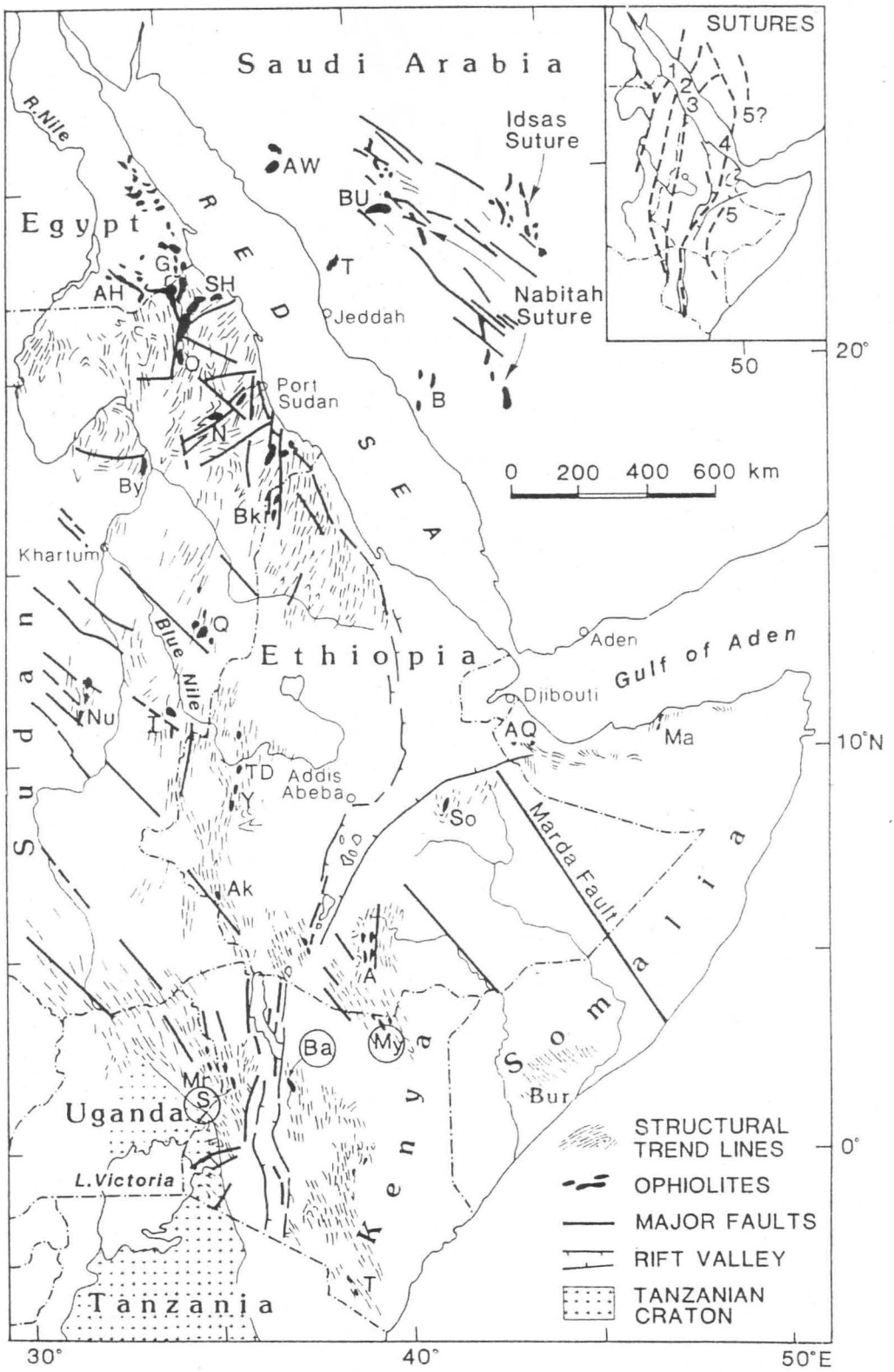

Figure 8.6. Ophiolite belts of the northern Mozambique belt and the Arabian-Nubian shield (Berhe, 1990).

Place names are: AW, Jebel al Wask; BU, Bir Umq; T, Jebel Thurwah; B, Bishah; SH, Sol Hamed; G, Gebel Gerf; O, Onib; AH, Allaqi-Heini B.; N, Nakasib; Bk, Barka; Q, Quala al Nahal; Nu, Nuba; By, Bayuda; I, Ingessana; TD, Tulu Dimtu; Y, Yubdo; Ak, Akobo; So, Soka; A, Adola; My, Moyale; AQ, Abdul Qadr; Ma, Mait; Mr, Moroto; S, Sekerr; Ba, Baragoi; T, Taita Hills.

ophiolites of the Arabian-Nubian Shield by means of geochemical and structural data (Fig. 8.6).

The Sekerr ophiolites consist of a sequence of andesitic meta-volcanics, pillow lavas, layered gabbros, hornblende schists, serpentinites with podiform chromite, basic dykes, marble lenses and narrow bands of quartzites which are believed to have been original chert layers, psammites and mica schists which were probably tuffs; and pyroclastic and turbiditic sediments (Vail, 1988). Trace element data indicate a back-arc basin origin between 1.0 Ga and 663 Ma ago (Berhe, 1990).

The Baragoi ophiolites include metamorphosed mantle dunites and sheeted dykes (Petters, 1991). Trace element data indicate a transition between mid-ocean ridge basalts and island-arc tholeiites. Two separate suites of ophiolitic rocks in the Baragoi area yielded ages of 796 Ma and 609 Ma.

The Moyale ophiolite includes serpentinized harzburgite and gabbros with trace elements showing a back-arc tectonic setting (Berhe, 1990). It occurs as thrust slices among continental shelf meta-pelites (Petters, 1991).

Beyond the Kenya-Tanzania province the Mozambique belt splits into two segments which are separated by a large wedge of low-grade volcano-sedimentary rocks containing ophiolites, the so-called Arabian-Nubian Shield (Fig. 8.6). The volcano-sedimentary and ophiolite assemblages constitute the Red Sea fold and thrust belt (Petters, 1991). The volcano-sedimentary assemblage consists of basaltic to andesitic calc-alkaline volcanics of oceanic margin and island-arc settings, and associated pyroclastic volcanogenic and shallow-water shales, siltstones and limestones (Vail, 1988). The ophiolites are closely associated with the volcano-sedimentary assemblages and consist of serpentinized pyroxenites and peridotites, layered gabbros, sheeted dyke complexes, pillow lavas and rare siliceous bands and plagiogranite.

8.5. DISCUSSION

The Bridgetown metavolcanics have no magmatic association with either the Bloubergstrand volcanics or mafic and intermediate plutonic rocks in the

Malmesbury Group. However, some physical and geochemical similarities exist between the Bridgetown Formation and the age related Grootderm Formation of the Marmora Terrane (Gariep Supergroup) which is considered to represent ophiolitic material.

Many of the volcano-sedimentary assemblages in Late Proterozoic - Early Palaeozoic Pan-African mobile belts have been described as possible ophiolite complexes. Some of them show distinctive ophiolite assemblages and others seem to represent partial or dismembered ophiolites. Their existence indicates major collision events during the Pan-African. Against this background, the Bridgetown Formation should be evaluated carefully as possible ophiolitic material in the Saldania Belt. An in depth discussion on this aspect is given in chapter 9 under the title "genetic considerations".

9. GENETIC CONSIDERATIONS

Various authors (Rabie, 1974a; De Villiers, 1969 and Hartnady et al., 1974) considered the greenstones of the Bridgetown Formation to be both intrusive and extrusive. The rather common occurrence of ophiolite complexes in Pan-African mobile belts (section 8.5), increases the possibility that the Bridgetown Formation might be ophiolitic. Dunlevey (1988 and 1992) suggested that the Bridgetown Formation may be an ophiolite complex. It is therefore necessary to compare each lithological component of the Bridgetown Formation with a typical ophiolite assemblage.

The term "ophiolite" has been defined by a consensus statement of those present at the GSA Penrose Conference, 1972 (Lord, 1991). "Ophiolite", refers to a distinctive assemblage of mafic to ultramafic rocks. In a completely developed ophiolite the rock types occur in the following sequence, starting from bottom to top:

(i) an ultramafic complex, consisting of variable proportions of harzburgite, lherzolite and dunite, usually with a metamorphic tectonic fabric (more or less serpentinised).

(ii) a gabbroic complex, normally with cumulus textures commonly containing cumulus peridotites and pyroxenites and usually less deformed than the ultramafic complex.

(iii) a mafic sheeted dyke complex.

(iv) a mafic volcanic complex, commonly pillowed.

Associated rock types include:

(1) an overlying sedimentary sequence typically including ribbon cherts, thin shale interbeds, and minor limestones;

(2) podiform bodies of chromite generally associated with dunite;

(3) sodic felsic intrusive and extrusive rocks.

An ophiolite may be incomplete, dismembered or metamorphosed, in which case it should be called a partial, dismembered, or metamorphosed ophiolite. Although ophiolite generally is interpreted to be oceanic crust and upper mantle, the use of the term should be independent of its supposed origin (GSA Penrose Conference, 1972).

Ore deposits often associated with ophiolite complexes include stratabound massive sulfides within the pillow lava section, podiform chromite within peridotites, iron and nickel laterites which develop on peridotites, asbestos within serpentinized peridotites and PGE mineralization within the ultramafic and gabbroic complexes (Coleman, 1977).

The following components of the Bridgetown Formation might be correlated with some of the above mentioned ophiolite components:

(i) The occurrence of Ni- and Cr-rich banded chert and talc masses in association with a chlorite schist may indicate the possible presence of a metamorphosed ultramafic complex at Spitskop.

(ii) An igneous body at Brewelskloof, near the town Worcester, is in concordant contact with the upper part of the Brandwacht Formation (Hartnady et al., 1974). There has been some speculation that it may be an overthrust part of the adjacent Swartland terrane (Hartnady et al., 1984). This body has been described as a diorite (map compiled by the University of Stellenbosch, 1948); a biotite eucrite (De Villiers et al., 1968); and a meta-andesite (Hoal, 1978; Hartnady et al., 1984). The igneous body is highly altered and is characterized by the greenschist facies assemblages quartz-albite-chlorite-biotite-epidote (Hoal, 1978). The decussate growth of biotite post-dates the formation of a penetrative regional foliation (S_1). Large quartz- and calcite-filled 'amygdales', enveloped by the foliated matrix, are present. Geochemical analyses on the igneous rocks at Brewelskloof was done by Byers (1975). He classified the rocks as calc-alkaline. The andesitic nature was confirmed by Hoal (1978) by means of the Zr/TiO_2 - Nb/Y discrimination diagram of Winchester and Floyd (1977). The igneous body is well-mineralized with disseminated pyrite which occurs as late euhedral growths overprinting S_1. Gold-anomalies have been detected in streams draining the area. It is evident that little is known about this body. Further petrographical and geochemical investigation of this rock type is necessary for positive identification. Although this body is not regarded as part of the Bridgetown Formation, the possibility of it representing the high level gabbroic complex of an ophiolite should be considered.

iii) Greenstones outcropping along the Berg River and at Voëlvlei Dam may represent the mafic volcanic complex of an ophiolite sequence. The greenstones along the Berg River comprises tuffs with an alkaline basaltic composition, and alkaline and tholeiitic metabasalts, interlayered with metasediments, as well as a younger intrusive tholeiitic metabasite. Although few volcanic textures (e.g. graded bedding in tuffs) were recognized in the greenstones along the Berg River, volcanic flow textures, volcanic breccias and pillow structures have been described in the Voëlvlei metavolcanics. To date, no geochemical work has been done on the Voëlvlei metavolcanics. It is therefore recommended that a comparative study should be done between greenstones along the Berg River and greenstones at Voëlvlei Dam. To date, no massive sulfide deposits have been found in this mafic volcanic complex.

(iv) Rock types associated with the Bridgetown greenstones include jasper-rich cherts, massive and oolitic cherts, thin muscovite-quartz schist and graphitic schist interbeds and dolomite.

Although certain features of the Bridgetown Formation resemble those of an ophiolite sequence, this study does not permit a final conclusion to be reached on this matter. The following conceptual model, showing the Bridgetown Formation as part of a dismembered ophiolite, is presented here to illustrate the possible sequence of geological events that led to its formation (Fig. 9.1).

1) During the interval 900 to 700 Ma, continental rift and drift led to the formation of the Adamastor Ocean west of the Khalahari Craton (Hartnady, 1991; Unrug, 1993). Malmesbury sediments were deposited on the rift margin and oceanic crust generated during spreading (Fig. 9.1A; Siegfried, 1993; De Beer et al., 1982).

2) During rifting and deposition of the Malmesbury sediments plume related intraplate volcanism occurred on cold oceanic crust, probably halfway between the spreading centre and the eastern rift margin (Fig. 9.1 B). Volcanic activity was related to upwelling thermochemical plumes derived from the deep mantle. The sequence of eruptive stages is modeled after Hawaiian volcanism (Clague, 1987). The initial deep water stage of Hawaiian volcanism is characterized by lenticular,

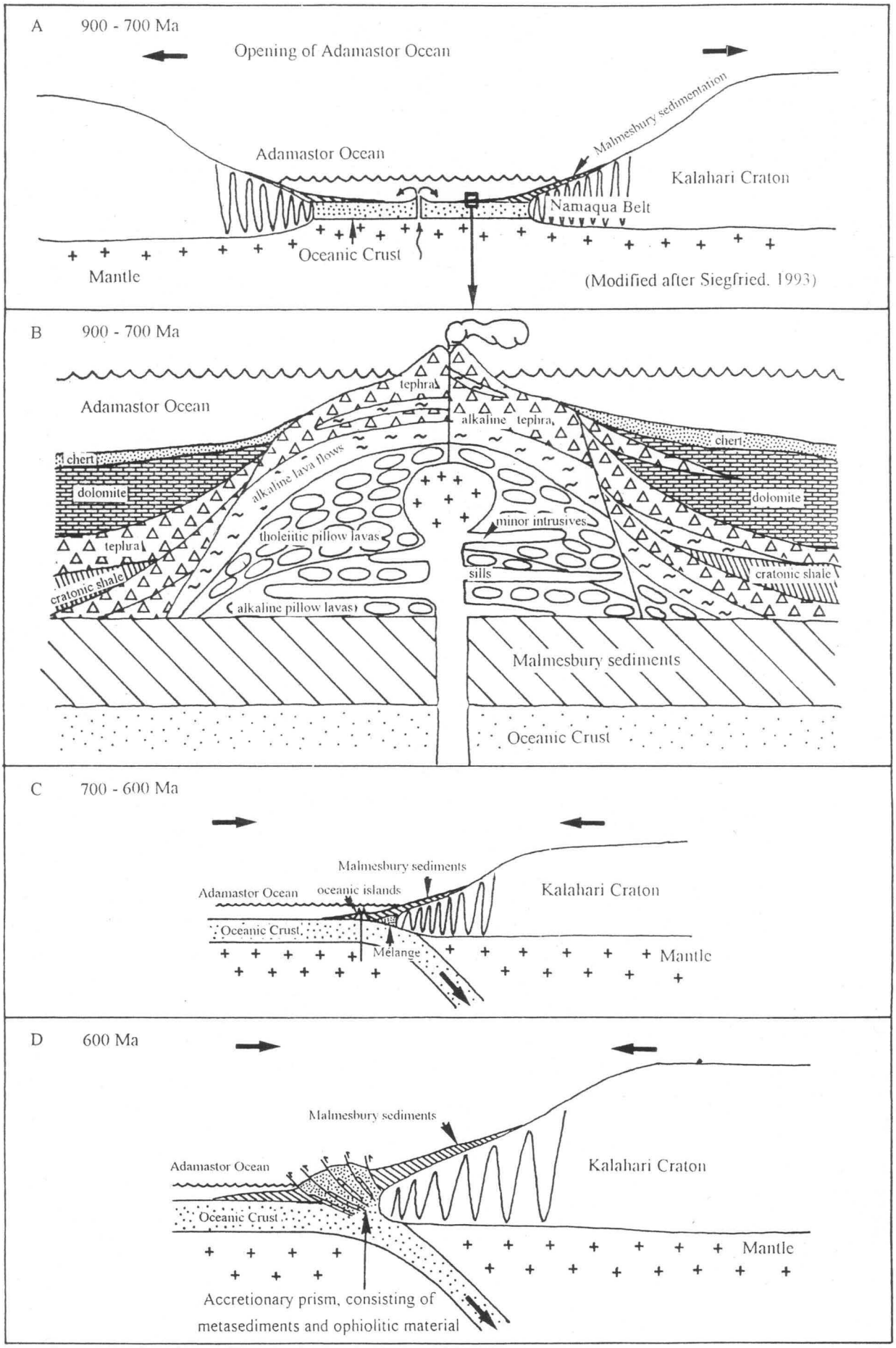

Figure 9.1. Diagrammatic representation of the sequence of events during the evolution of the Bridgetown Formation.

massive flow and pillow basalts which build up steep slopes, surrounded by minor pillow breccias on the flanks. As the seamount builds up, a critical water depth is reached when gases in the lava are explosively released. At this stage the products of explosive volcanism (e.g. ash, lapilli and pumice) increase markedly relative to the proportion of lava flows. A thick tephra cap to the deep water lavas below is produced, and slumping of such material produces an apron of volcaniclastic debris. Compositionally Hawaiian volcanism is characterized by four sequential eruptive growth stages: early submarine (alkalic), main submarine to subaerial edifice (tholeiitic), post-caldera (alkalic) and post-erosional (high alkalic; Floyd, 1991). The Hawaiian stratigraphy shows some resemblance to the present stratigraphic interpretation of the Bridgetown Formation, namely a basal unit of alkaline metabasalt (unit 6), an intermediate unit of tholeiitic metabasalt (units 7 and 9) and an upper unit of alkaline metabasalt (units 4, 3 and 11) interlayered with metatuff (unit 1) of alkaline basaltic composition. The correlation between the Hawaiian volcanic stratigraphy and the present stratigraphic interpretation of the Bridgetown Formation volcanics supports the inferred upward facing direction of the Bridgetown Formation. In the case of the Bridgetown Formation the shallow water alkaline stage (post-caldera) occurred contemporaneously with deposition of shales, carbonates and oolitic and massive chert. Carbonates in contact with the Mg-rich basaltic rocks underwent dolomitization due to a supplementary source of Mg to subsurface waters.

3) Closure of the oceanic basin through subduction on one or more sides occurred between 700 to 600 Ma. Eastward subduction underneath the Kalahari Craton, partly overlain by sediments of the Malmesbury Group, is postulated (Fig. 9.1C). Malmesbury sediments, scraped off the oceanic crust, accumulated as mélange in the subduction trench.

4) The oceanic crust probably included seamounts of oceanic islands which were also presented to the subduction mechanism. It is proposed that during convergence these hot mechanically weak segments of oceanic crust and upper mantle, laced with magma chambers, were dismembered and tectonically emplaced in an accretionary prism zone.

10. SUMMARY

A detailed geological and geochemical study was conducted on the Bridgetown Formation of the Malmesbury Group, outcropping along the Berg River, 20km east of the town Moorreesburg.

a) The Bridgetown Formation consists of the following rock types, starting from the inferred bottom:

i) A basal unit consisting mainly of poorly differentiated alkaline metabasalt with a within-plate tectonomagmatic fingerprint.

ii) An intermediate unit consisting of poorly differentiated tholeiitic metabasalt, intruded by a younger tholeiitic metabasite with a low degree of differentiation. Both have ocean-floor basalt (P-type MORB) and island arc basalt fingerprints.

iii) An upper unit consisting of poorly differentiated as well as more evolved alkaline metabasalts, interlayered with metatuffs with an alkaline basaltic composition, metasedimentary rocks with a marine origin, and graphitic schists and muscovite-quartz schists, both with a continental crust provenance.

iv) An overlying metasedimentary sequence including dolomite, massive and oolitic chert, jasper and jaspilite.

The stratigraphy and the geochemistry of the Bridgetown metavolcanics resemble Hawaiian volcanism which comprises four eruptive growth stages: early submarine (alkalic), main submarine to subaerial edifice (tholeiitic), post-caldera (alkalic) and post-erosional (highly alkalic).

The Bridgetown Formation probably also comprises an unexposed lower metamorphosed ultramafic unit. Indications of the presence of a metamorphosed ultramafic unit were found at Spitskop, situated directly northwest of the main greenstone body. Small Ni- and Cr-rich talc bodies, Ni- and Cr-rich banded chert, chlorite schist with albite porphyroblasts, and small fingerlike dolomite-talc-chlorite bodies at Spitskop are units often associated with serpentinites.

This meta-volcano-sedimentary sequence exhibit the following general trends:

i) an increase in the more evolved magmas, and

ii) the ratio of sedimentary rocks, pyroclastic material and chemical precipitates to mafic flows increases stratigraphically upwards.

b) The metasediments and metavolcanics of the Bridgetown Formation, as well as metasedimentary rocks in contact with the Bridgetown Formation, have suffered polyphase deformation. A well-defined foliation with a general NNW-SSE strike is present in all the rock types (excluding chert and dolomite). The foliation was regionally folded into antiformal structures and locally into small near-upright tight folds. Faulting within the Bridgetown Formation is obscured by poor exposure of the metavolcanics which are very susceptible to weathering. The Bridgetown Formation is included in the Boland tectonic domain by placing the Piketberg-Wellington fault zone 5km west of Heuningberg, subparallel to the Berg River. This agrees with Rabie's (1974b) original subdivision of the tectonic domains.

c) The Bridgetown Formation has experienced metamorphism up to the lower greenschist facies, which coincides with the metamorphic grade of the surrounding metasediments. The Bridgetown Formation and the surrounding Malmesbury beds have been subjected to the same regional metamorphic event which was probably contemporaneous with the main deformation event.

Metavolcanic rocks of the Bridgetown Formation consist of the following metamorphic minerals: albite (An_{0-2}), actinolite, epidote, calcite, chlorite, titanite, magnetite, ilmenite and muscovite. Some quartz is always present. Many combinations of these minerals occur depending on the chemical composition of the original rock, the degree of deformation of the rock and the degree of alteration. Unit 10, the younger tholeiitic dyke, is the only unit which contains relict igneous minerals (e.g. augite).

d) The Bridgetown metavolcanics have no magmatic association with either the Bloubergstrand volcanics or mafic and intermediate plutonic rocks in the Malmesbury Group. However, some physical and geochemical similarities exist between the Bridgetown Formation and the age related Grootderm Formation of the Marmora Terrane (Gariep Supergroup) which is considered to represent ophiolitic

material. Many volcano-sedimentary assemblages in the Late Proterozoic - Early Palaeozoic Pan-African mobile belts have been described as possible ophiolite complexes. The Bridgetown meta-volcano-sedimentary sequence bear some stratigraphic resemblances to a dismembered, metamorphosed ophiolite.

e) The presence of both tholeiitic metabasalts with P-type MORB and island arc basalt characteristics, and alkaline metabasalts with within-plate basalt characteristics is the result of varying conditions of melting of the same source material in an ocean island tectonic environment.

During deposition of the Malmesbury sediments into an ocean basin, plume related intraplate volcanism occurred on cold oceanic crust. The proposed sequence of eruptive stages resembled Hawaiian volcanism. The initial deep water stage was characterized by alkaline magmatism, followed by a main tholeiitic edifice and post-caldera alkaline magmatism. Post-caldera alkaline magmatism occurred contemporaneously with deposition of sediments and chemical precipitates (e.g. carbonates and cherts). Carbonates in contact with the Mg-rich basaltic rocks underwent dolomitization due to a supplementary source of Mg to subsurface waters.

Closure of the proposed oceanic basin through subduction underneath the Kalahari Craton, occurred 600 to 700 Ma ago. During this process segments of dismembered oceanic crust, including seamounts of oceanic islands, were tectonically emplaced in an accretionary prism zone and incorporated in the Malmesbury Group as small greenstone bodies.

f) To date, no ophiolite-type mineralization has been found in metavolcanic and metasedimentary rocks of the Bridgetown Formation. However, the younger intrusive metabasite (unit 10) has geochemical characteristics of magmas often enriched in PGE's. These magmas are enriched in MgO and Cr and depleted in Ti, Ta, Nb and HREE's compared to tholeiites. It is suggested that further studies on the metabasite should include PGE-analysis.

In the Spitskop area the following geological features may have some economic significance:

i) Au- and As-bearing brittle deformed clear to milky quartz veins which developed along zones of competency contrasts in all the lithologies in the Spitskop area. To date, very few gold analyses have been done on the quartz veins and they require further investigation.

ii) Pb-Zn-(Ag)-bearing quartz bodies. Although Au-analysis on one sample revealed only traces of gold (70 ppb), the possibility of gold mineralization in these bodies should not be excluded on account of one sample.

iii) Small irregular talc bodies with an exceptionally high Ni (3691 ppm) and Cr (2221 ppm) content. These bodies are probably associated with a serpentinized ultramafic body which may have Ni, Cr and PGE mineralization potential.

ACKNOWLEDGEMENTS

The author whishes to thank and acknowledge the following persons and institutions for assistance during the compilation of this thesis:

Dr. R. Scheepers acting as internal promoter as well as for his constructive comments and friendship.

Prof. A. Rozendaal for acting as internal examiner.

Dr. P.G. Gresse for acting as external examiner.

Financial support for this project was provided by Delta Gold N.L. and Scorpio Mining N.L., Australia.

Dr. L.E. Pretorius of Scorpio Mining N.L. who introduced me to this project.

The Geological Survey, Bellville, for supplying and cutting borehole core of the Bridgetown Formation.

Terry Lemmon of Masasa Mines (Private) Limited for conducting gold, Hf and Ta analyses.

Technical assistance at the University of Stellenbosch was provided by J. Smit (preparation of samples), D. Hendrikse (thin sections), S. Smit (requisitions), J. Swart (figures for conference), R. O'Brien (computer assistance, electron microprobe, ICP) and A. Uttley (XRF).

Dr. C. Harris of the University of Cape Town for oxygen isotope analyses.

The Director of the Council of Geoscience for giving permission for the following analyses which were conducted by:

T. Cloete of the Geological Survey, Pretoria: SEM-EDAX analyses,
H.C.C. Cloete, J.H. Elsenbroek, A.Schoeman and J. Trojak of the Geological Survey, Pretoria: major and trace element analyses on graphitic schist samples,
W.D. Havenga: microprobe analyses.

M. Taylor for information and discussions concerning the Bridgetown Formation.

Marthinus Afrika for assistance during field work.

My sister, Jeané, for drawing the map of the Bridgetown Formation.

My parents for their support and encouragement.

The Lord, who makes everything possible.

REFERENCES

Allsopp, H.L., Köstlin, E.O., Welke, H.J., Burger, A.J., Kröner, A., Blignault, H.J., 1979. Rb-Sr and U-Pb geochronology of Late Precambrian-Early Paleozoic igneous activity in the Richtersveld (South Africa) and southern South West Africa. Trans. Geol. Soc. S. Afr. 82, 185-204.

Arcos, D., Solder, A., 1991. Gold transport conditions in shear zones from the Central Pyrenees, Spain. In: Pagel, M., Leroy, J.L. (eds.) Sources, Transport and Deposition of Metals. Rotterdam/Brookfield: Balkema, 633-636.

Banks, D.A., Yardley, B.W.D., Miller, M.F., Shepherd, T.J., Cathelineau, M., Boiron, M.C., Urbano, R., Florida, P., Palomero, F.G., Pereira, E.S., Noronha, F., Barriga, F., 1993. Fluid inclusion chemistry of Hercynian, granite-hosted vein Au-mineralization. In: Torres, A.J., Gervilla, R., Gervilla, F. (eds.) Current Research in Geology applied to Ore Deposits. University of Granada: Spain, 403-406.

Barker, A.J., 1989. Introduction to metamorphic textures and microstructures. Glasgow and London: Blackie, 162 pp.

Berhe, S.M., 1990. Ophiolites in northeast and East Africa: implications for Proterozoic crustal growth. J. geol. Soc. London. 147, 41-57.

Boggs, S., 1992. Petrology of Sedimentary Rocks. New York: Macmillan Publishing Company, 707 pp.

Borthwick, J., Harmon, R.S., 1982. A note regarding ClF_3 as an alternative to BrF_5 for oxygen isotope analysis. Geochim. Cosmochim. Acta 46, 1665-1668.

Burger, A.J., Coertze, F.J., 1973. Radiometric age measurements on rocks from Southern Africa to the end of 1971. Bull. Geol. Surv. S. Afr. 58, 46 pp.

Byers, D., 1975. A geochemical study of the greenstones in the Worcester district. Unpubl. Honours Project, University of Cape Towm.

Cabanis, B., Lécolle, M., 1989. Le diagramme La/10 - Y/15 - Nb/8: Vn outil pour la discrimination des séries volcaniques et la mise eu évidence des processus de mélange et/ou de contamination crustale. C.R. Acad. Sci., Paris, 309 (serie II), 2023-2029.

Cas, R.A.F., Wright, J.V., 1987. Volcanic Successions: Modern and Ancient. London: Allen & Unwin, 527 pp.

Clague, D.A., 1987. Hawaiian alkaline volcanism. In: Fitton, J.G., Upton, B.G.J. (eds.) Alkaline Igneous Rocks, Geol. Soc. London, Spec. Publ., 30, 227-252.

Coleman, R.G., 1977. Ophiolites. Springer-Verlag, 229 pp.

Condie, K.C., 1981. Archaean Greenstone belts. In: Windley, B.F. (ed.) Developments in Precambrian Geology 3. Elsevier, 434 pp.

Condie, K.C., 1991. Another look at rare earth elements in shales. Geochim. Cosmochim. Acta 55, 2527-2531.

Cox, K.G., Bell, J.D., Pankhurst, R.J., 1979. The Interpretation of Igneous Rocks. London: George Allen & Unwin, 450 pp.

De Beer, J.H., Van Zijl, J.S.V., Gough, D.I., 1982. The Southern Cape conductive belt: its composition, origin and tectonic significance, Tectonophysics 83, 205-225.

Deer, W.A., Howie, R.A., Zussman, J., 1986. Rock-forming Minerals: Disilicates and Ring Silicates, VIB, Longman Scientific & Technical, 629 pp.

Deer, W.A., Howie, R.A., Zussman, J., 1992. An Introduction to the Rock-Forming Minerals. Longman Scientific & Technical, 696 pp.

De Villiers, J.E., Jansen, H., Mulder, M.P., 1968. Geologie van die Gebied tussen Worcester en Hermanus. Toel. bl. 3319C en 3419A, Geol. Opn. S.-Afr.

De Villiers, J.E., 1969. The geology of the country between Riebeek-Kasteel and Moorreesburg. Ann. Geol. Surv. S. Afr. 7, 29-41.

De Villiers, J.E., 1979. Note on deformation and metasomatism in rocks of the Koringberg-Hermon area. Trans. Geol. Soc. S. Afr. 82, 179-181.

De Waal, S.A., 1970. Nickel minerals from Barberton, South Africa: III. Willemseite, A nickel-rich talc. Am. Mineral. 55, 31-42.

Dunlevey, J.N., 1988. Evolution of the Saldanian Orogeny and development of the Cape Granite Suite. Suid-Afrikaanse Tydskrrif vir Wetenskap 84, 565-567.

Dunlevey, J.N., 1992. Pan-African crustal evolution of south-western Africa. J.Afr. Earth Sci. 15, 2207-2216.

Elthon, D., 1982. Metamorphism in oceanic spreading centers. In: Emiliani, C. (ed.), The Sea: The Oceanic Lithosphere. New York: Wiley, 7, 285-303.

Evans, B.W., Guggenheim, S., 1988. Talc, Pyrophyllite, and related minerals. In: Baily, S.W. (ed.) Hydrous Phyllosilicates. Reviews in Mineralogy, 19. Mineral. Soc. of Am., 225-280.

Ewart, A., Chappell, B.W., 1989. East Australian Petrology and Geochemistry. In: Johnson, R.W. (ed.) Intraplate Volcanism in Eastern Australia and New Zealand. Cambridge: Cambridge University Press, 189-246.

Fernandes, J.A.D., Tommasi, A., Porcher, C.C., 1992. Deformation patterns in the southern Brazilian branch of the Dom Feliciano Belt, a reappraisal. J. of S. Am. Earth Sci. 5, 77-96.

Floyd, P.A., 1991. Oceanic Basalts. Blackie, Van Abstrand Reinhold, 456 pp.

Frey, M., 1987. Low Temperature Metamorphism. Glasgow London: Blackie, 351 pp.

Frimmel, H.E., Hartnady, C.J.H., 1992a. The Significance of Blue Amphiboles for the Metamorphic History of the Pan-African Gariep Belt, Namibia. Precambr. Res. Unit, Univ. of Cape Town, no. 5, 1-27.

Frimmel, H.E., Hartnady, C.J.H., 1992b. Blue amphiboles and their significance for the metamorphic history of the Pan-African Gariep Belt, Namibia. J. Metam. Geol. 10, 651-669.

Frimmel, H.E., Koller, F., Watkins, R.T., Faure, K., 1995. Tectonic History of Mafic and Ultramafic Rocks in the Gariep Belt. Extended Abstract Centennial Geocongress, Geological Society of South Africa, Vol 1, 226-229.

Gebre-Mariam, M., Groves, D.I., Ho, S.E., McNaughton, N.J., Vearncombe, J.R., 1991. The Archaean lode-gold deposit at Racetrack, near Kalgoorlie, Western Australia: A transitional mesothermal-epithermal hydrothermal system. In: Pagel, M., Leroy, J.L. (eds.) Sources, Transport and Deposition of Metals. Rotterdam/Brookfield: Balkema, 661-664.

Giret, A., Bonin, B., Leger, J., 1980. Amphibole compositional trends in oversaturated and undersaturated alkaline plutonic ring-complexes. Can. Min. 18, 481-495.

Giuliani, G., Fortes, P.T.F.O., Olivo, G.R., Ronchi, L.H., Santos, M.M., Marini, O.J., 1991. Contrasting Archaean-Proterozoic-hosted gold deposit types and associated gold-bearing fluids. In: Pagel, M., Leroy, J.L. (eds.) Sources, Transport and Deposition of Metals. Rotterdam/Brookfield: Balkema, 665-668.

Goodwin, A.M., 1962. Structure, stratigraphy and origin of iron formations, Michipi Coten area, Ontario, Canada. Geol. Soc. Am. Bull. 73, 561-586.

Govindaraju, K., Mevell, G., 1987. Fully Automated Dissolution and Separation Methods for Inductively Coupled Plasma Atomic Emission Spectrometry Rock Analysis. Application to the Determination of Rare Earth Elements. Journal of Analytical Atomic Spectrometry 2, 615-621.

Green, J., 1959. Geochemical table of the elements for 1959. Geol. Soc. America Bull. 70, no. 9, 1127-1183.

Gresse, P.G., Scheepers, R., 1993. Neoproterozoic to Cambrian (Namibian) rocks of South Africa: a geochronological and geotectonic review. J. Afr. Earth Sci. 16, no. 4, 375-393.

Hall, A., 1987. Igneous Petrology. Longman Scientific & Technical, 573 pp.

Hartnady, C.J.H., 1969. Structural analysis of some pre-Cape formations in the western Cape Province. Bull. Precambr. Res. Unit, Univ. Cape Town, 6, 70 pp.

Hartnady, C.J., Newton, A.R., Theron, J.N., 1974. The stratigraphy and structure of the Malmesbury Group in the southwestern Cape In: Kröner, A. (ed.) Contributions to the Precambrian geology of southern Africa. Precambr. Res. Unit., Univ. Cape Town, Bull. 15, 193-213.

Hartnady, C.J.H, Von Veh, M.W., Booth, P.W.K., 1984. Boland Terrane Tectonostratigraphy: Conference on Middle to Late Proterozoic Lithosphere Evolution, Excursion Guidebook. Precambr. Research Unit, Univ. Cape Town.

Hartnady, C.J.H, Halbich, I.W., 1985. Structural correlation on the Swartland Dome between Riebeeck Kasteel, Malmesbury and Moorreesburg: Excursion guidebook of the Geol. Soc. of S. Afr., W.P. Branch.

Hartnady, C.J.H., Ransome, I.G.D., Frimmel, H.E., 1990. Accreted composite terranes - an example from the Gariep orogenic belt. Abstracts Geocongress '90, Geol. Soc. S. Afr., Cape Town, 218-221.

Hartnady, C.J.H., Von Veh, M.W., 1990. Tectonostratigraphic and structural history of the Late Proterozoic-Early Paleozoic Gariep Belt, Cape Province, South Africa. Guidebook Geocongress '90, Geol. Soc. of S. Afr., PO1, 1-49.

Hartnady, C.J.H., 1991. Supercontinents and Geotectonic Megacycles. Precambr. Res. Unit, Inform. Circ., No 1., Part 2, 1-6.

Haughton, S.H., 1933. Geology of Cape Town and adjoining country. Geol. Surv. S.Afr. Expl. sheet 247.

Heiken, G., Wohletz, K., 1985. Volcanic ash. University of California Press, 245 pp.

Henderson, P., 1984. Rare Earth Element Geochemistry. Amsterdam: Elsevier, 499 pp.

Hesse, R., 1989. Silica Diagenesis: Origin of Inorganic and Replacement Cherts. Earth-Science Rev. 26, 253-284.

Hey, M.H., 1954. A new review of the chlorites. Miner. Mag. 30, 277-292.

Hoal, B.G., 1978. The Pre-Cape Brewelskloof - Meiringsberg Area north of Worcester: Structural analysis, petrography, geochemistry and application of white mica geothermometry and geobarometry. Unpubl. Honours Project, University of Cape Town, 56 pp.

Hoefs, J., 1987. Stable Isotope Geochemistry. Springer-Verlag, 236 pp.

Irvine, T.N., Baragar, W.R.A., 1971. A Guide to the Chemical Classification of the Common Volcanic Rocks. Can. J. of Earth Sci. 8, 523-544.

Ito, K., Kennedy, G.C., 1974. The composition of liquids formed by partial melting of eclogites at high temperatures and pressures. J. Geol. 82, 383-392.

Jacobs, R., 1974. Orientation survey of the lavas at Bloubergstrand, the greenstones of the Bridgetown Complex and some dike rocks. Unpubl. Honours Project, University of Cape Town, 73 pp.

Jahns, R.H., 1967. Serpentinites of the Roxbury District, Vermont. In: Wyllie, P.J. (ed.) Ultramafic and Related Rocks. New York: John Wiley, 137-160.

Jaques, A.L., Green, D.H., 1980. Anhydrous melting of peridotite at 0-15 kb pressure and the genesis of tholeiitic basalts. C.M.P. 73, 287-310.

Jordaan, L.J., 1990. The Geology and Geochemistry of Mafic and Intermediate Igneous Rocks associated with the Cape Granites. Unpubl. M.Sc. thesis, University of Stellenbosch, 216 pp.

Jordaan, L.J., Scheepers, R., Barton, E.S., 1994. The correlation between the isotope distribution and geochemistry of mafic to intermediate igneous rocks from the South African West Coast. Mineral. Mag., VM Goldschmidt Conference: Edinburgh, 58A, 456-457.

Kanauth, L.P., 1979. A model for the origin of chert in limestone. Geology 7, 274-277.

Kerrich, R.W., Fyfe, W.S., 1981. The gold-carbonate association: Source of CO_2 and CO_2-fixation reactions in Archaean lode gold deposits. Chem. Geol. 33, 265-294.

Landis, C.A., 1971. Graphitization of dispersed carbonaceous material in metamorphic rocks. Contrib. Mineral. Petrol. 30, 34-45.

LeBlanc, M., 1981. The late Proterozoic ophiolites of Bou Azzer (Morocco): evidence for Pan-African plate tectonics. In: Kröner, A. (ed.) Precambrian plate tectonics. Amsterdam: Elsevier, 435-451.

Leventhal, J. 1983. Interpretation of organic carbon and sulfur relationships in Black Sea sediments as indicators of environment of deposition. Geochim. Cosmochim. Acta 47, 133-137.

Liou, J.G., Kuniyoshi, S., Ito, K., 1974. Experimental studies of the phase relations between greenschist and amphibolite in a basaltic system. Am. J. Sci. 274, 613-632.

Lord, R.A., 1991. Platinum-Group Element Mineralization in the Shetland Ophiolite Complex. Unpubl. Ph.D. Thesis, Department of Earth Sciences, The Open University.

Lytwyn, J.N., Casey, J.F., 1993. The geochemistry and petrogenesis of volcanics and sheeted dikes from the Hatay (Kizildag) Ophiolite, southern Turkey: possible formation with the Troodos Ophiolite, Cyprus, along fore-arc spreading centers. Tectonophysics 223, 237-272.

Maliva, R.G., Siever, R., 1988. Diagenetic replacement controlled by force of crystallization. Geology 16, 688-691.

Maynard, J.B., 1983. Geochemistry of sedimentary ore deposits. New York: Springer-Verlag, 305 pp.

Meschede, M. 1986. A method of discriminating between different types of mid-ocean ridge basalts and continental tholeiites with the Nb-Zr-Y diagram. Chem. Geol. 56, 207-218.

Middlemost, E.A.K., 1991. Towards a comprehensive classification of igneous rocks and magmas. Earth-Science Reviews 31, 73-87.

Morimoto, N., 1989. Nomenclature of pyroxenes. Can Min. 27, 143-156.

Morse, J.W., Mackenzie, F.T., 1990. Geochemistry of Sedimentary Carbonates. Elsevier, 521 pp.

Mullen, E.D., 1983. $MnO/TiO_2/P_2O_5$: a minor element discriminant for basaltic rocks of oceanic environments and its implications for petrogenesis. Earth and Plan. Sci. Lett. 62, 53-62.

Naldrett, A.J., Cabri, L.J., 1976. Ultramafic and Related Mafic Rocks: Their Classification and Genesis with Special Reference to the Concentration of Nickel Sulfides and Platinum-Group Elements. Econ. Geol. 71, 1131-1158.

Nicholls, J., 1988. The statistics of Pearce element diagrams and the Chayes closure problem. Contrib. Min. Petrol. 99, no. 1, 36-43.

Nockolds, S.R., 1954. Bull Geol. Am. 66, 1007-1032.

Norrish, K., Hutton, J.T., 1969. An accurate X-ray spectroscopic method for analysis of a wide range of geological samples. Geochim. Cosmochim. Acta 33, 431-453.

Palero, F.J., Mangas, J., Both, R.A., Arribas, A., 1991. Metallogeny of sheared Zn-Pb vein deposits of Alcudia Valley, Cicudad Real, Spain. In: Pagel, M., Leroy, J.L. (eds.) Source, Transport and Deposition of Metals. Balkema/Rotterdam/Brookfield, 213-217.

Pal'Yanova, G.A., Kolonin, G.R., 1991. Physical-chemical model of transport and deposition of gold together with sulphides. In: Pagel. M., Leroy, J.L. (eds.) Source, Transport and Deposition of Metals. Rotterdam/Brookfield: Balkema, 693-696.

Pasava, J., 1993. Rift-related marine black shales, an important source of PGE. In: Hach, P.F., Torres, A.J., Gervilla, R., Gervilla, F. (eds.) Current Research in Geology applied to ore deposits. Granada: Universidad de Granada, 209-212.

Pearce, T.H., 1968. A contribution to the theory of variation diagrams. Contrib. Min. Petrol. 19, no. 2, 142-157.

Pearce, J.A., Cann J.R., 1973. Tectonic setting of basic volcanic rocks determined using trace element analyses. Earth and Plan. Sci. Lett. 19, 290-300.

Pearce, J.A., 1982. Trace element characteristics of lavas from destructive plate boundaries. In: Thorpe, R.S. (ed.) Andesites: orogenic andesites and related rocks. Chichester: Wiley, 525-548.

Peck, L.C., 1964. Systematic analysis of silicates. U.S. Geol. Surv. Bull. 1170, 39-42.

Petters, S.W., 1991. Regional Geology of Africa. Springer-Verlag, 723 pp.

Pique, A., Michard, A., 1989. Moroccan Hercynides: A synopsis. The Paleozoic sedimentary and tectonic evolution at the northern margin of West Africa. Amer. J. Sci. 289, 286-330.

Pisutha-Arnond, V., Ohmoto, H., 1983. Thermal History, and Chemical and Isotopic Compositions of the Ore-Forming Fluids Responsible for the Kuroko Massive Sulfide Deposit in the Hokuroku District of Japan. In: Ohmoto, H., Skinner, B.J. (eds.) The Kuroko and Related Volcanogenic Massive Sulfide Deposits, Econ. Geol. Monograph 5, 523-558.

Rabie, L.P., 1974a. Geological map of the Moorreesburg-Wellington area. Ann. Univ. Stellenbosch, 49 A (5).

Rabie, L.P., 1974b. Structural map of the Moorreesburg-Wellington area. Ann. Univ. Stellenbosch, 49 A (6).

Redman, B.A., Keays, R.R., 1985. Archaean basic volcanism in the Eastern Goldfields Province, Yilgarn Block, Western Australia. Precambr. Res. 30, 113-152.

Ronov, A.B., Khlebnikova, Z.V., 1957. Geochemistry 6, 527-552.

Rozendaal, A., Scheepers, R., 1994. Metallogenesis and Exploration Potential of the Neoproterozoic Saldanian Belt in the Southwestern Cape Province, South Africa, Expl. and Min. Geol. 3, 419-438.

Rozendaal, A., Gresse, P.G., Scheepers, R., De Beer, C.H., 1994. Structural setting of the Riviera W-Mo deposit, Western Cape, South Africa, S. Afr. J. Geol. 97(2), 184-195.

Rushton, R.W., Nesbitt, B.E., Meuhlenbachs, K., 1993. A fluid inclusion and stable isotope study of Au quartz veins in the Klondike District, Yukon Territory, Canada: A section through a mesothermal vein system. Econ. Geol. 88, 647-678.

Saini-Eidukat, B., Thalhammer, O.A.R., Alapieti, T., Halkoaho, T., Iljina, M., 1993. Controls on PGE mineralization in the Early Paleozoic Kemi-Koillismaa-Oulanka mafic intrusion belt, Fennoscandian Shield. In: Hach, P.F., Torres, A.J., Gervilla, R., Gervilla, F. (eds.) Current Research in Geology applied to ore deposits. Granada: Universidad de Granada, 555-557.

Scheepers, R., Rozendaal, A., 1992. Relationship of the Riviera W-(Mo-Cu) deposit to magmatism in the southwestern Cape Province, South Africa. Abstr. Geocongress 1992, Geol. Soc. S. Afr., 339-341.

Schoch, A.E., Leygonie, F.E., Burger, A.J., 1975. U-Pb ages for Cape granites from the Saldanha Batholith: a preliminary report. Trans. Geol. Soc. S. Afr. 78, 97-100.

Siegfried, H.P., 1993. The Malmesbury batholith and its relationship to granitic plutons in the Swartland tectonic domain. Unpubl. Ph.D. thesis, University of Stellenbosch, 137 pp.

Smith, H.S., Hartnady, C.J.H., 1984. Geochemistry of Grootderm Formation lavas: Indication of tectonic environment of extrusion. Abstract International Conference on Middle to Late Proterozoic Lithosphere Evolution. Precambr. Res. Unit, Univ. of Cape Town.

Stanley, C.R., Russell, J.K., 1989. Pearce.Plot: A Turbo-Pascal Program for the Analysis of Rock Compositions with Pearce Element Ratio Diagrams. Computors & Geosciences 15, no. 6, 905-926.

Sun, S.-s., McDonough, W.F., 1989. Chemical and isotopic systematics of oceanic basalts: implications for mantle composition and processes. In: Saunders, A.D., Norry, M.J. (ed.) Magmatism in the Ocean Basins. Geol. Soc. Spec. Publ. No. 42, 313-345.

Takahashi, E., Kushiro, I., 1983. Melting of a dry peridotite at high pressures and basalt magma genesis. Amer. Min. 68, 859-879.

Theron, J.N., 1990. Geology of Sheet 3318 Cape Town. Geol. Surv. S. Afr.

Turpin, L., 1984. Altérations hydrothermales et caratérisation isotopique (O-H-C) des minéraux et des fluides dans le massif uranifère de St. Sylvestre - Extension à d'autres gisements intragranitiques d'uranium francais. Docteur De Troisieme Cycle, L Institut National Polytechnique de Lorraine, 189 pp.

Taylor, G.H., 1971. Cabonaceous matter: a guide to the genesis and history of ores. Soc. Min. Geol. Japan, spec. Issue 3, 283-288.

Taylor, S.R., McLennan, S.M., 1985. The Continental Crust: Its Composition and Evolution. Oxford: Blackwell, 312 pp.

Turekian, K.K., Wedepohl, K.H., 1961. Distribution of the elements in some major units of the Earth's crust. Geol. Soc. Amer. Bull. 72, no.2, 175-191.

Unrug, 1993. The Supercontinent cycle and Gondwanaland assembly: Component cratons and suturing events timing. J. Geodynamics (in Press.).

Vail, J.R., 1988. Tectonics and evolution of the Proterozoic basement of northeastern Africa. In: El Gaby, S., Greiling, R.O. (eds.) The Pan-African belt of northeast Africa and adjacent areas, Braunschweig: Vieweg, 195-226.

Van der Merwe, W.J., 1983. Department of Environment Affairs: Berg River-Saldanha government water scheme. Report on engineering geological feasibility investigations at three alternative alignments for the proposed Vogelstruisdrift Dam (Kantey & Templer consulting engineers and engineering geologists), Unpubl. Report, 18 pp.

Vine, J.D., Tourtelot, E.B., 1970. Geochemistry of Black Shale Deposits - A Summary Report. Econ. Geol., 65, 253-272.

Visser, H.N., Theron, J.N., 1973. Explanation of Sheet 3218 Clanwilliam, Geol. Surv. S. Afr.

Visser, H.N., De Villiers, J.E., Theron, J.N., Hill, R.S., 1981. Die geologie van die gebied tussen Ceres en Moorrreesburg. Toeligting blad 3318B (Malmesbury) en 3319A (Ceres). Ooplêerverslag Geol. Opn. S.-Afr. 177, 129 pp.

Von Veh, M.W., 1983. Aspects of the sedimentation, structure and tectonic evolution in the Tygerberg terrane, southwestern Cape Province. Bull. Precambr. Res. Unit, Univ. Cape Town 32.

Wedepohl, K.H. (exec. ed.), 1987a. Handbook of Geochemistry (Elements H to Al). Springer-Verlag Berlin. Heidelberg. New York., Vol 11/1, 11-K-1 to 11-K-2.

Wedepohl, K.H. (exec. ed.), 1987b. Handbook of Geochemistry (Elements Kr to Ba). Springer-Verlag Berlin. Heidelberg. New York., Vol 11/4, 41-A-1 to 41-I-1.

Wilkinson, J.F.G., 1986. Classification and Average Chemical Compositions of Common Basalts and Andesites. Petrology 27, 31-62.

Wilson, M., 1988. Igneous Petrogenesis: A Global Tectonic Approach. London: Unwin Hyman, 466 pp.

Winchester, J.A., Floyd, P.A., 1977. Geochemical discrimination of different magma series and their differentiation products using immobile elements. Chem. Geol. 20, 325-343.

Winkler, H.G.F, 1976. Petrogenesis of Metamorphic Rocks. New York Heidelberg Berlin: Springer-Verlag, 334 pp.

Wood, D.A., 1979. A variably veined suboceanic upper mantle - Genetic significance for mid-ocean ridge basalts from geochemical evidence. Geology 7, 499-503.

APPENDIX

1. ANALYTICAL TECHNIQUES

1.1. SAMPLE PREPARATION

Borehole core from twelve boreholes were halved and samples of approximately 20 cm in length were collected from one of the halves. Samples of approximately 20 kg were also collected in the field and reduced to fist size by sledgehammer. Samples were further crushed by jawcrusher and roller mill. Representative samples of 200 g were selected by coning and quartering and powdered in a Siebtechnik swing-mill.

1.2. MAJOR AND TRACE ELEMENT ANALYSIS

Major and trace element analyses were done by X-ray fluorescence (XRF) on a Philips 1410 spectrometer, located in the Department of Geology at The University of Stellenbosch. Major element analyses were done on Norrish fusion pennies which were made according to the technique described by Norrish and Hutton (1969). Trace elements and chromium were determined on powder briquets, consisting of a Moviol solution and 8 g of powdered sample. Water content was determined by weighing and overnight drying of samples at 100°C. Loss on ignition was measured by roasting samples at 1000°C. Spectrometer data were corrected for absorption and matrix effects by microcomputer.
Major and Trace element analyses (including C_{org}- and sulfur-content) of graphitic samples were done by J.H. Elsenbroek at the Geological Survey in Pretoria.

1.3. FEO ANALYSIS

Fe^{2+} was determined according to the method described by Peck (1964). The sample (0.5 g) and water (1 ml) are added to a 50 ml platinum crucible to form a slurry. A mixture of water (5 ml), HF (5 ml) and H_2SO_4 (5 ml) is added to the slurry which is then heated to dissolve the sample. Dilute 100 ml of the dissolving solution to 300 ml and add 2 drops of 0,2% sodium diphenylamine sulfonate indicator. Lower

crucible with content into dissolving solution and tritrate resultant solution against the potassium dichromate solution until a purple colour is retained for 30 seconds. FeO is calculated as follows: ml $K_2Cr_2O_7$ * 0.9 = FeO%

1.4. RARE EARTH ELEMENTS

Rare earth elements (La, Ce, Pr, Nd, Sm, Eu, Gd, Dy, Ho, Er and Yb) of selected crushed whole rock samples were analyzed by means of Inductively Coupled Plasma Atomic Emission Spectroscopy (ICP-AES) at the University of Stellenbosch. Sample preparation was done according to the method of Govindaraju and Mevelle (1987). Powdered whole rock material (0.5 g) in a platinum crucible are heated for two hours at 800°C. After cooling, $LiBO_2$ (1.5 g) is added and the contents is mixed well. The contents is then transformed into a fusion bead by melting (over a gas burner) and quick cooling. The platinum crucible and the bead are placed in a 150 ml glass beaker containing a magnetic stirring rod. A 100 ml volume of complexing solution is added. The complexing solution is prepared by mixing 50 g of oxalic acid, 500 ml of 14.5 M HCL, 25 ml of H_2O_2 and distilled water to make up the volume. The contents of the beakers are stirred magnetically for 3 hours or overnight. Subsequently, clear solutions are obtained.

Rare earth elements were extracted by using resin columns (Amberlite 120 GC, 100-200 mesh). The columns are prepared by pumping through 10 ml 5 M HCL. The sample solution (35 ml) is pumped through the resin, followed by 10 ml 2 M HNO_3 to extract all residue Ca and Mg. An eluting solution (10 ml of 7.25 M HCL) is used to extract the REE's. The REE solution is dried, and later dissolved in 5 ml 4 M HCL for ICP analysis.

Analyses were done by a Philips ICP - plasma source and a RSV optical spectrometer. Samples and standards were counted on 16 channels. A multi-element standard and spectrometric blank were also included to correct peak shifts. The precision obtained is better than 5%.

1.5. OXYGEN ISOTOPE ANALYSIS

Oxygen isotope analyses performed by Dr. C. Harris at the University of Cape Town. Mineral separates were obtained by sieving and initial magnetic sorting, followed by handpicking. The separates were cleaned in warm 20% HCL to aid identification of impurities and to remove iron oxides. Oxygen isotope analyses were made according to well-established procedures using ClF_3 as reagent (Borthwick and Harmon, 1982). The results are reported in units of per mil relative to Vienna standard mean ocean water (V-SMOW).

1.6. MICROPROBE ANALYSIS

Microprobe analyses were performed at the University of Cape Town, using standard procedures. A Camebax Microbeam electron microprobe (Model MBX) was used.

Acceleration voltage	:15 KV
Beam current	:40 nA
Peak counting time	:10 seconds
Background counting time	:5 seconds
Corrections	:ZAF correction factors
Standards	:Set of mineral and synthetic standards

1.7. COMPUTER ANALYSIS

The statistical package BMDP was run on a VAX main frame computer to perform discriminant analysis and factor analyses. The following programs were used for word processing and data reduction: AS-EASY-AS V.5, MS WORD V.5, and microsoft WINDOWS V.4.1 (EXCEL V.5). CIPW norm calculations and values for magmatic classification diagrams were done with the PETMIN program.

2. TABLES AND FIGURES

NO.	UNIT	ROCKTYPE	BH NO.	LOCATION
NS3	1	greenstone	AW1	Vogelstruisdrift
NS6	1	greenstone	AW1	Vogelstruisdrift
NS7	1	greenstone	AW1	Vogelstruisdrift
NS21	1	greenstone	AW2	Vogelstruisdrift
NS24	1	greenstone	AW2	Vogelstruisdrift
NS28	1	greenstone	AW2	Vogelstruisdrift
NS31	1	greenstone	AW2	Vogelstruisdrift
NS195	1	greenstone	AW2	Vogelstruisdrift
NS10	2	greenstone	AW1	Vogelstruisdrift
NS13	2	greenstone	AW1	Vogelstruisdrift
NS36	3	greenstone	AE1	Matjiesrivier
NS37	3	greenstone	AE1	Matjiesrivier
NS39	3	greenstone	AE1	Matjiesrivier
NS41	3	greenstone	AE1	Matjiesrivier
NS44	3	greenstone	AE1	Matjiesrivier
NS46	3	greenstone	AE1	Matjiesrivier
NS196	3	greenstone	AE1	Matjiesrivier
NS173	4	greenstone	CE1	Toorkrans
NS175	4	greenstone	CE1	Toorkrans
NS176	4	greenstone	CE1	Toorkrans
NS178	4	greenstone	CE1	Toorkrans
NS181	4	greenstone	CE1	Toorkrans
NS182	4	greenstone	CE1	Toorkrans
NS183	4	greenstone	CE1	Toorkrans
NS184	4	greenstone	CE1	Toorkrans
NS185	4	greenstone	CE1	Toorkrans
NS187	4	greenstone	CE1	Toorkrans
NS188	4	greenstone	CE1	Toorkrans
NS190	4	greenstone	CE1	Toorkrans
NS191	4	greenstone	CE1	Toorkrans
NS49	5	greenstone	AE2	Matjiesrivier
NS197	5	greenstone	AE2	Matjiesrivier
NS57	6	greenstone	BW2	Vogelstruisdrift
NS60	6	greenstone	BW2	Vogelstruisdrift
NS72	6	greenstone	BW2	Vogelstruisdrift
NS76.2	6	greenstone	BW2	Vogelstruisdrift
NS64	7	greenstone	BW2	Vogelstruisdrift
NS69	7	greenstone	BW2	Vogelstruisdrift
NS198	7	greenstone	BW2	Vogelstruisdrift
NS74	8	greenstone	BW2	Vogelstruisdrift
NS76.1	8	greenstone	BW2	Vogelstruisdrift
NS86	9	greenstone	BW1	Vogelstruisdrift
NS90	9	greenstone	BW1	Vogelstruisdrift
NS92	9	greenstone	BW1	Vogelstruisdrift
NS93	9	greenstone	BW1	Vogelstruisdrift
NS96	9	greenstone	BW1	Vogelstruisdrift
NS97	9	greenstone	BW1	Vogelstruisdrift
NS98	9	greenstone	BW1	Vogelstruisdrift
NS100	9	greenstone	BW1	Vogelstruisdrift
NS102	9	greenstone	BW1	Vogelstruisdrift
NS103	9	greenstone	BW1	Vogelstruisdrift
NS107	9	greenstone	BE1	Toorkrans
NS109	9	greenstone	BE1	Toorkrans
NS112	9	greenstone	BE1	Toorkrans
NS115	9	greenstone	BE1	Toorkrans
NS121	9	greenstone	BE1	Toorkrans
NS142	9	greenstone	CW1	Vogelstruisdrift
NS147	9	greenstone	CW1	Vogelstruisdrift
NS149	9	greenstone	CW1	Vogelstruisdrift
NS151	9	greenstone	CW1	Vogelstruisdrift

Table 1. Locality and description table.

NO.	UNIT	ROCKTYPE	BH NO.	LOCATION
NS152	9	greenstone	CW1	Vogelstruisdrift
NS154	9	greenstone	CW1	Vogelstruisdrift
NS157	9	greenstone	CW1	Vogelstruisdrift
NS161	9	greenstone	CW1	Vogelstruisdrift
NS80	9	greenstone	BC1	Berg River
NS82	9	greenstone	BC1	Berg River
NS193	9	greenstone	BC1	Berg River
NS194	9	greenstone	BC1	Berg River
NS123	10	greenstone	BE2	Toorkrans
NS124	10	greenstone	BE2	Toorkrans
NS126	10	greenstone	BE2	Toorkrans
NS127	10	greenstone	BE2	Toorkrans
NS128	10	greenstone	BE2	Toorkrans
NS129	10	greenstone	BE2	Toorkrans
NS130	10	greenstone	BE2	Toorkrans
NS132	10	greenstone	BE2	Toorkrans
NS134	10	greenstone	BE2	Toorkrans
NS135	10	greenstone	BE2	Toorkrans
NS136	10	greenstone	BE2	Toorkrans
NS138	10	greenstone	BE2	Toorkrans
NS140	10	greenstone	BE2	Toorkrans
NSF/2.5	11	greenstone		Drie Heuwels
NSF/2.6	11	greenstone		Drie Heuwels
NSF/2.7	11	greenstone		Drie Heuwels
NSF/2.8	11	greenstone		Drie Heuwels
NS17		graphitic schist	AW2	Vogelstruisdrift
NS18		graphitic schist	AW2	Vogelstruisdrift
NS19		graphitic schist	AW2	Vogelstruisdrift
NS20		graphitic schist	AW2	Vogelstruisdrift
NS51		graphitic schist	AE2	Matjiesrivier
NS54		graphitic schist	AE2	Matjiesrivier
NS55		graphitic schist	AE2	Matjiesrivier
NSF/2.1		shale		Tweevlei
NSF/2.2		shale		Tweevlei
NSF/2.3		shale		Tweevlei
NSF/2.4		shale		Tweevlei
NS162		dolomite	CE1	Toorkrans
NS164		dolomite	CE1	Toorkrans
NS166		dolomite	CE1	Toorkrans
NS168		dolomite	CE1	Toorkrans
NS169		dolomite	CE1	Toorkrans
NS177		dolomite	CE1	Toorkrans
NSF/1.1		dolomite		Bridgetown
NSF/1.2		dolomite		Bridgetown
NSF/1.3		dolomite		Bridgetown
NSF/1.4		dolomite		Bridgetown
NSF/3.1		chert		De Pont
NSF/3.2		chert		De Pont
NSF/3.4		chert		Palestina
NSF/3.5		chert		Palestina
NSF/3.6		chert		Tweevlei
NSF/7		chert		Vogelstruisdrift
NSF/12		chert		Vogelstruisdrift
NSF/11		banded chert		Spitskop
NSF/6		banded chert		Spitskop
NSF/9		chlorite schist		Spitskop
NSF/10		steatite		Spitskop
NSF/5		quartz		Spitskop

Table 1 (cont.)

Figure 1. Sample positions in borehole core (Site A).

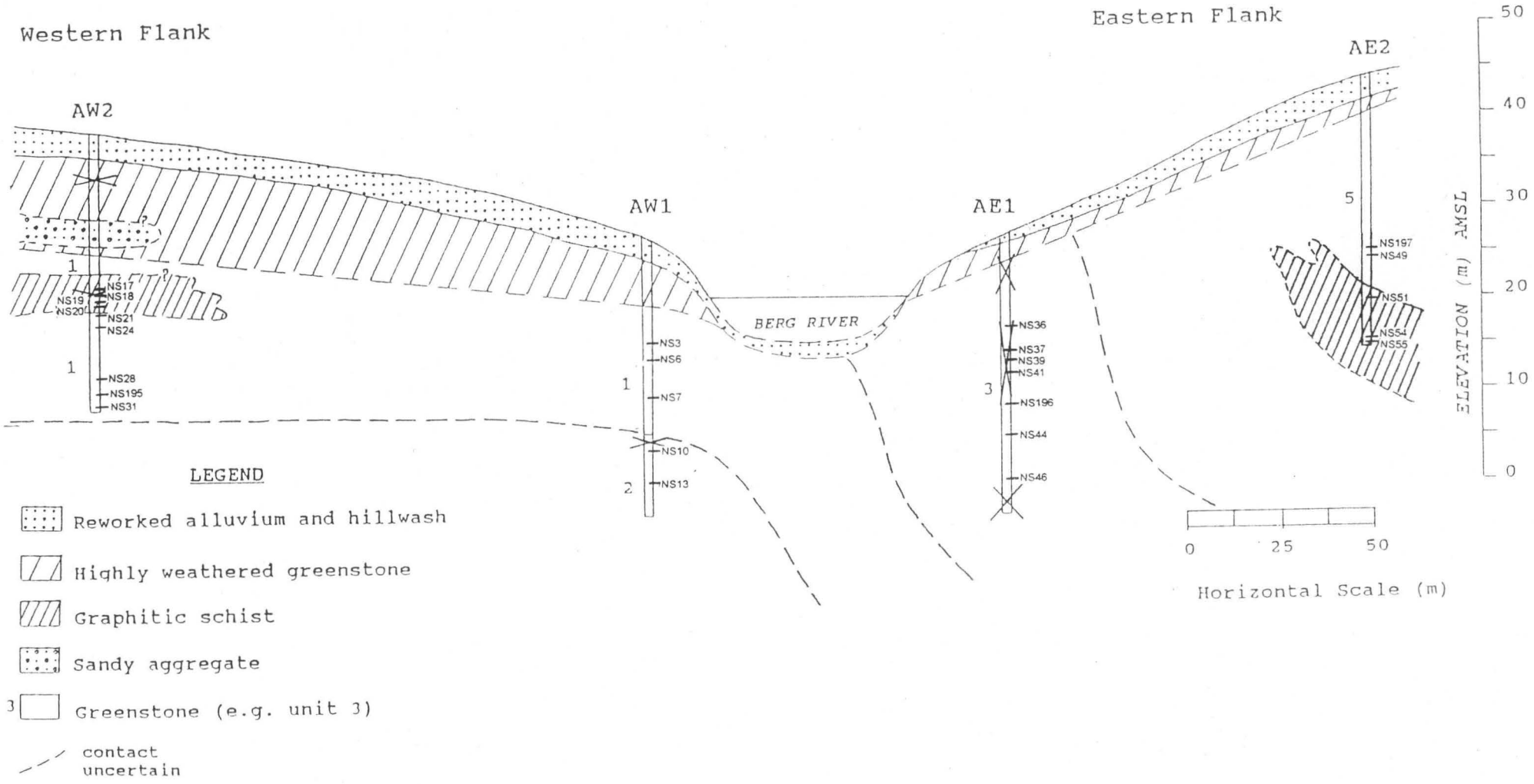

Figure 2. Sample positions in borehole core (Site B).

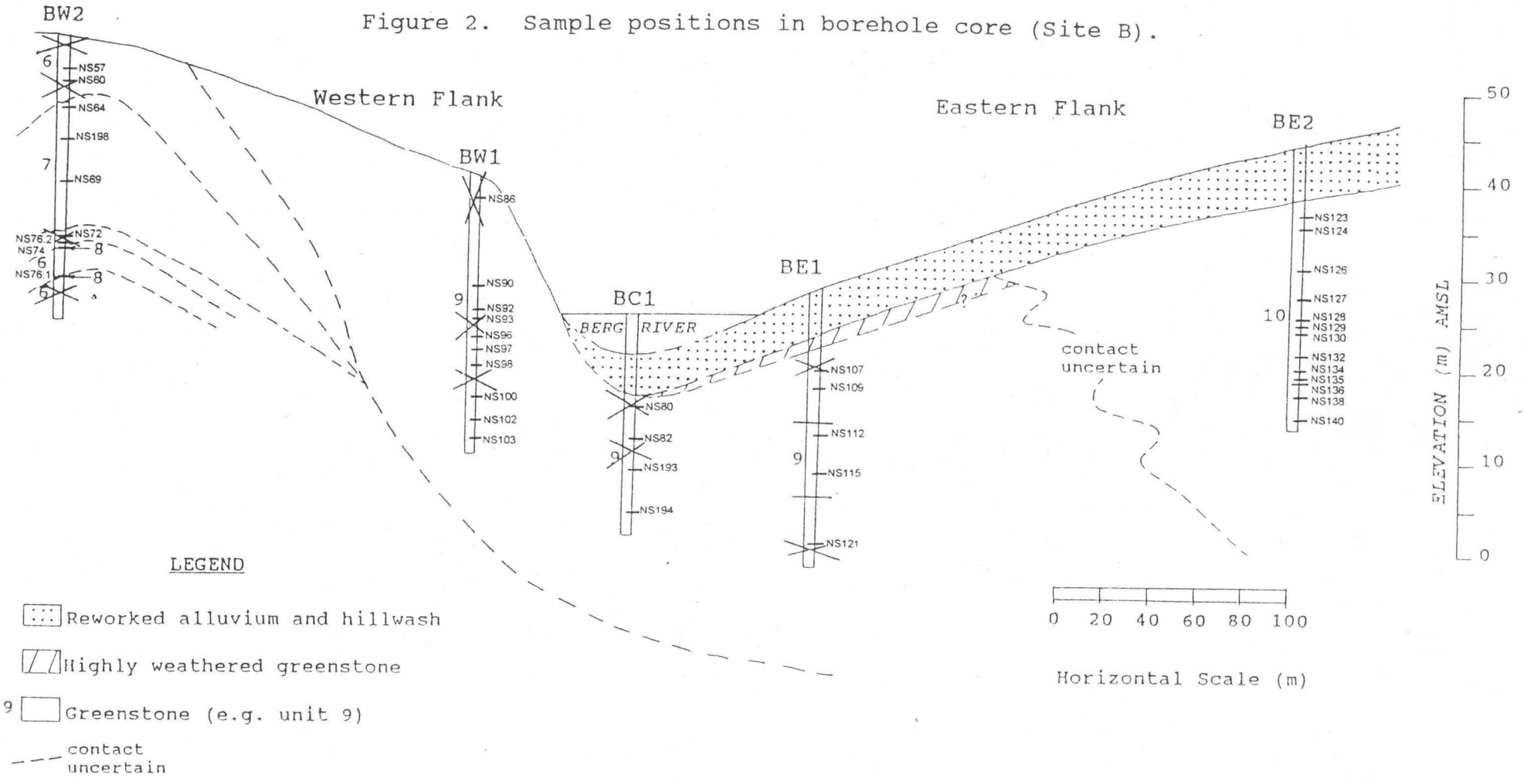

Figure 3. Sample positions in borehole core (Site C).

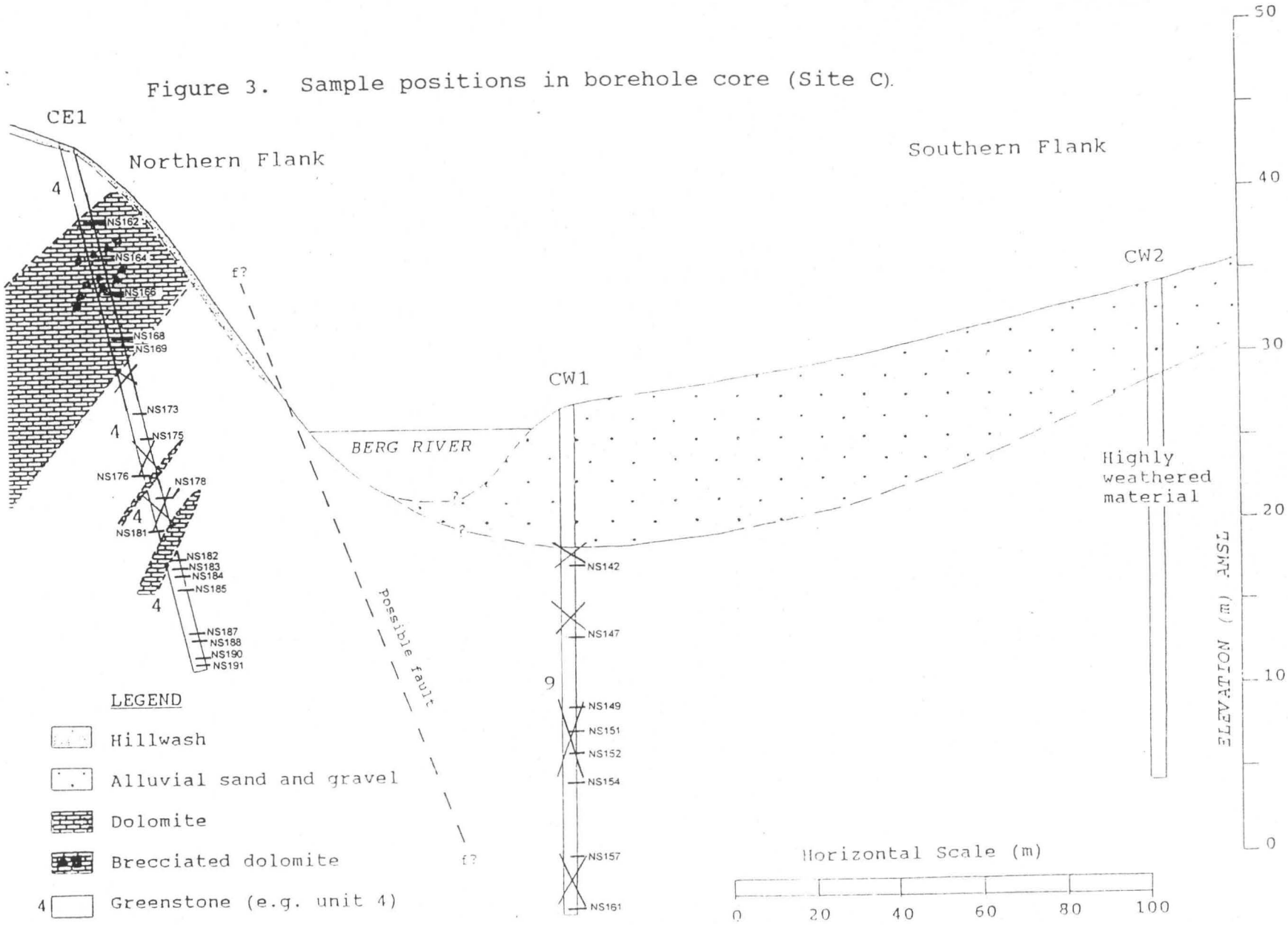

Unit	No.	SiO_2	TiO_2	Al_2O_3	Fe_2O_3	FeO	MnO	MgO	CaO	Na_2O	K_2O	P_2O_5	H_2O-	H2O+	TOTAL
1	NS3	46.30	2.93	14.64	2.55	8.82	0.07	7.53	4.19	3.46	0.69	0.48	0.25	6.45	99.40
1	NS6	44.16	2.77	14.00	2.52	8.62	0.10	6.97	6.80	2.98	0.95	0.46	0.18	8.17	99.70
1	NS7	43.80	2.96	14.60	1.83	9.18	0.08	8.71	5.47	2.66	0.95	0.48	0.25	7.73	99.80
1	NS21	52.63	2.65	16.36	2.66	8.26	0.03	5.55	0.74	3.55	1.10	0.55	0.68	4.07	99.80
1	NS24	44.19	2.71	14.89	2.88	9.72	0.09	6.93	5.14	1.45	1.55	0.43	0.30	7.51	98.95
1	NS28	64.96	1.10	13.65	1.03	5.40	0.03	3.16	1.15	1.48	2.96	0.13	0.18	3.12	98.95
1	NS31	46.16	2.16	13.88	1.45	7.65	0.15	4.12	8.77	2.76	1.71	0.39	0.28	8.87	99.20
1	NS195	55.16	2.08	15.67	1.62	7.90	0.05	4.98	1.48	1.68	2.92	0.32	0.19	4.25	99.20
2	NS10	41.02	4.72	13.90	3.05	10.71	0.23	4.34	7.34	5.09	0.33	1.96	0.23	5.62	99.75
2	NS13	45.33	4.92	14.53	2.61	9.99	0.17	3.96	5.28	6.20	0.28	2.10	0.33	3.45	100.30
3	NS36	41.54	2.23	14.76	4.21	7.65	0.12	13.71	3.71	1.93	1.00	0.27	1.31	6.72	100.10
3	NS37	42.13	1.86	12.07	6.52	4.75	0.17	7.64	10.81	4.09	1.51	0.25	0.21	7.89	100.60
3	NS39	37.85	1.64	10.54	7.22	4.32	0.18	6.64	14.68	2.92	1.69	0.20	0.21	11.52	100.20
3	NS41	42.31	2.40	13.92	6.69	7.02	0.13	10.00	5.46	3.10	1.30	0.33	0.19	6.01	99.75
3	NS44	41.22	2.00	12.15	6.71	6.12	0.15	8.98	8.18	2.77	1.75	0.29	0.23	8.19	99.50
3	NS46	49.42	1.93	12.50	7.69	4.32	0.09	6.23	5.52	4.19	2.34	0.28	0.15	4.63	99.85
3	NS196	42.66	2.18	13.18	5.26	7.20	0.15	11.17	6.21	2.08	1.03	0.29	0.26	7.30	99.85
4	NS173	40.46	3.23	12.43	9.01	4.93	0.20	8.07	7.29	1.30	0.77	0.42	0.94	9.72	99.40
4	NS175	39.26	3.21	11.79	6.98	6.10	0.22	10.96	7.88	2.75	0.31	0.43	0.46	8.61	99.70
4	NS176	34.81	2.17	9.94	4.56	5.38	0.20	9.22	15.82	1.93	0.29	0.43	0.39	13.98	99.85
4	NS178	35.28	2.28	10.66	3.95	6.35	0.18	9.80	13.53	2.36	0.17	0.47	0.29	13.04	99.15
4	NS181	39.08	2.37	10.90	5.17	5.56	0.18	9.43	11.67	2.12	0.10	0.47	0.45	11.31	99.55
4	NS182	44.31	3.61	16.44	7.33	8.33	0.06	8.46	1.17	0.05	2.73	0.77	0.38	5.36	100.10
4	NS183	40.04	3.12	14.28	6.81	9.47	0.14	10.26	3.79	0.08	1.83	0.66	0.31	8.55	100.50
4	NS184	35.69	2.11	10.07	5.02	5.22	0.17	9.68	14.71	1.62	0.07	0.43	0.29	14.03	99.80
4	NS185	40.08	2.67	12.37	5.71	6.44	0.16	9.09	9.00	3.99	0.13	0.54	0.35	8.11	99.45
4	NS187	40.74	2.68	12.81	6.10	6.50	0.15	9.02	8.73	4.03	0.37	0.55	0.32	7.81	100.60
4	NS188	27.53	1.98	8.99	3.24	5.40	0.16	10.39	20.43	0.92	0.15	0.42	0.31	18.43	99.00
4	NS190	42.35	2.75	12.39	6.68	6.64	0.18	8.69	7.74	4.71	0.74	0.56	0.32	6.40	101.00
4	NS191	29.73	1.94	9.08	4.04	4.95	0.15	9.92	18.90	1.89	0.27	0.39	0.30	16.83	99.00
5	NS49	50.07	1.22	14.00	1.32	10.05	0.40	11.89	0.68	0.08	1.46	0.48	0.47	6.96	100.20
5	NS197	52.04	1.23	15.26	1.05	8.78	0.21	10.63	0.63	0.01	2.17	0.44	0.48	6.29	100.30
6	NS57	45.35	1.74	14.32	5.73	4.64	0.08	10.35	5.61	2.27	1.31	0.19	0.25	7.67	100.10
6	NS60	40.87	1.88	14.33	8.08	3.87	0.07	8.88	8.08	2.52	1.79	0.29	0.25	8.65	100.05
6	NS72	48.74	1.57	14.08	7.32	3.24	0.13	9.99	4.74	5.58	0.25	0.17	0.25	4.47	101.00
6	NS76.2	45.06	1.89	15.45	9.38	3.06	0.11	9.31	3.92	5.32	0.65	0.22	0.23	5.58	100.55
7	NS64	48.20	1.24	15.14	8.78	3.02	0.10	6.52	5.30	7.12	0.15	0.13	0.30	5.23	101.65
7	NS69	50.50	1.21	15.37	9.32	2.75	0.10	5.21	5.40	7.69	0.11	0.14	0.19	3.05	101.45
7	NS198	48.09	1.11	13.81	9.14	1.46	0.12	2.98	10.56	7.13	0.23	0.10	0.23	5.75	100.95
8	NS74	45.98	1.75	14.82	4.77	4.68	0.20	12.17	5.06	4.45	0.31	0.20	0.19	5.04	100.20
8	NS76.1	47.11	1.82	15.10	3.38	4.30	0.16	13.13	3.79	3.26	0.37	0.21	0.22	6.85	100.20
9	NS147	40.59	1.27	13.80	6.32	4.95	0.16	10.59	10.98	2.33	0.29	0.13	0.13	0.25	98.80
9	NS80	44.02	1.34	14.62	8.10	3.44	0.12	9.42	9.46	0.24	1.66	0.13	0.29	5.98	99.30
9	NS82	44.66	1.45	14.43	11.88	1.22	0.12	8.29	7.64	4.13	0.82	0.15	0.16	5.21	100.40
9	NS86	42.90	1.29	15.06	7.52	4.14	0.16	11.02	8.69	1.69	0.60	0.12	0.20	4.48	98.45
9	NS90	41.65	1.33	16.32	7.35	4.66	0.14	12.81	7.60	1.29	0.89	0.12	0.20	5.16	100.15
9	NS92	46.27	1.16	14.14	7.16	4.43	0.13	11.98	7.42	0.03	1.53	0.11	0.19	4.48	99.65
9	NS93	41.41	1.23	15.03	7.22	5.00	0.13	13.16	9.03	0.19	0.66	0.12	0.23	4.93	99.00
9	NS96	45.16	1.17	14.43	6.34	4.50	0.14	12.91	7.10	2.51	0.58	0.11	0.24	4.30	100.10
9	NS97	46.36	1.12	14.40	6.87	3.96	0.13	11.84	6.43	2.95	1.23	0.11	0.21	4.21	100.35
9	NS98	40.08	1.54	15.88	6.44	6.57	0.15	15.94	3.73	0.08	1.77	0.14	0.30	7.61	101.00
9	NS100	46.46	1.16	14.05	6.75	4.14	0.12	11.89	8.18	0.65	0.89	0.11	0.19	4.43	99.60
9	NS102	47.42	1.26	14.61	6.82	4.05	0.10	11.45	5.83	1.72	1.52	0.13	0.21	4.35	100.00
9	NS103	37.97	1.47	16.61	6.91	6.08	0.15	15.20	6.56	0.08	1.35	0.15	0.19	6.63	100.10
9	NS107	41.21	1.19	15.33	11.48	0.58	0.13	14.29	7.43	0.40	1.02	0.12	0.34	5.77	99.45
9	NS109	49.26	1.26	14.87	7.88	3.58	0.14	7.19	8.31	2.72	0.28	0.12	0.23	4.09	100.40
9	NS112	46.50	1.42	16.16	11.08	3.06	0.19	6.60	7.04	4.25	0.35	0.16	0.23	3.08	100.55
9	NS115	39.20	1.50	15.81	4.83	8.30	0.13	15.97	5.42	0.08	0.20	0.16	0.33	7.49	100.35
9	NS121	45.86	1.24	14.26	7.75	3.96	0.14	9.23	9.32	3.24	0.45	0.11	0.26	4.13	100.50
9	NS142	35.72	1.39	14.37	7.35	6.30	0.14	15.38	7.51	1.29	0.08	0.15	0.27	7.76	98.50
9	NS149	42.52	1.12	11.96	6.74	2.72	0.12	5.52	13.56	5.62	0.36	0.09	0.31	9.85	100.90
9	NS151	40.78	1.58	15.82	4.22	8.71	0.16	12.79	4.91	1.54	1.12	0.17	0.27	6.69	99.85
9	NS152	39.00	1.31	13.88	1.04	9.54	0.16	13.10	7.88	1.21	0.01	0.14	0.24	10.64	99.30
9	NS154	42.95	1.28	13.13	2.32	7.38	0.12	8.08	10.05	3.69	0.18	0.16	0.34	9.68	100.25
9	NS157	44.17	1.26	14.04	4.79	6.35	0.12	8.99	7.85	0.95	1.34	0.10	0.40	8.09	99.20
9	NS161	45.01	1.54	14.58	2.58	7.56	0.08	10.31	4.72	2.54	0.63	0.15	0.25	8.01	98.85
9	NS193	45.22	1.08	13.71	7.29	3.62	0.11	10.55	8.09	1.58	0.82	0.10	0.19	5.98	98.85
9	NS194	42.14	1.23	13.69	8.91	2.52	0.15	6.65	13.37	2.90	0.73	0.10	0.18	7.84	100.75
10	NS123	43.24	1.00	13.06	3.02	8.19	0.16	14.70	8.26	1.59	0.01	0.08	0.86	4.77	100.00
10	NS124	45.20	0.99	12.40	2.82	7.74	0.16	14.04	8.60	2.51	0.01	0.08	0.66	4.31	100.55
10	NS126	41.80	0.72	10.08	3.20	8.30	0.16	19.46	8.17	0.54	0.31	0.09	1.29	5.66	100.95
10	NS127	40.94	0.72	10.29	4.91	6.87	0.16	20.25	7.66	0.38	0.55	0.08	0.60	5.68	100.05
10	NS128	40.35	0.70	10.54	3.51	8.19	0.17	21.06	6.69	0.08	0.83	0.07	1.30	6.17	100.70
10	NS129	40.86	0.68	9.48	2.60	9.14	0.17	21.91	7.56	0.08	0.20	0.06	0.54	6.19	100.60
10	NS130	40.79	0.71	10.69	3.17	8.28	0.16	20.38	6.90	0.08	0.83	0.07	0.71	6.21	100.05
10	NS132	43.14	0.73	11.44	1.85	8.84	0.16	17.91	8.16	0.53	0.92	0.06	0.27	4.75	99.90
10	NS134	42.88	0.75	11.93	2.12	8.55	0.15	18.05	7.94	1.57	0.30	0.06	0.34	5.05	100.80
10	NS135	42.29	0.76	11.57	2.02	8.93	0.16	18.42	7.92	0.69	0.31	0.06	0.23	5.06	99.60
10	NS136	41.22	0.76	10.99	1.97	8.82	0.16	17.92	8.03	1.32	0.32	0.07	0.27	4.88	97.85
10	NS138	42.96	0.86	11.54	2.07	9.20	0.17	17.71	8.59	0.65	0.04	0.07	0.28	4.90	100.25
10	NS140	41.98	0.88	11.59	2.30	9.00	0.16	17.83	8.52	0.57	0.07	0.07	0.22	4.81	99.15
11	NSF/2.5	44.31	3.59	14.61	5.71	6.93	0.18	4.95	11.62	0.78	0.39	0.51	0.25	3.00	97.70
11	NSF/2.6	44.08	3.53	14.39	5.94	6.35	0.15	4.73	12.04	0.76	0.32	0.50	0.40	3.46	97.40
11	NSF/2.7	43.46	3.64	14.96	5.48	7.07	0.17	4.57	11.73	1.31	0.47	0.52	0.26	2.85	97.35
11	NSF/2.8	43.89	3.50	14.09	5.26	6.26	0.17	4.21	12.43	2.15	0.60	0.53	0.22	4.11	98.15

Major elements in weight percent oxide.

Table 2. Whole rock major element chemistry of greenstone units.

Unit	No.	Mo	Nb	Zr	Y	Sr	U	Rb	Th	Pb	Ga	Zn	Cu	Ni	Sc	V	Ce	Nd	Ba	La	Cr
1	NS3	1.67	39.15	233.30	33.55	152.42	0.18	15.06	6.68	1.87	20.60	107.03	50.94	121.79	35.20	301.60	48.55	29.78	166.17	19.27	314.75
1	NS6	1.08	36.12	213.28	29.86	203.07	1.61	22.97	5.24	1.89	17.54	97.75	58.68	138.65	33.01	290.22	56.30	31.75	219.17	18.00	407.13
1	NS7	1.09	39.55	229.46	32.46	191.90	1.60	19.13	5.19	1.87	20.68	99.68	54.78	102.49	34.05	301.50	56.57	29.86	242.43	22.55	331.86
1	NS21	0.41	48.44	280.12	40.56	49.50	1.54	35.76	8.20	8.18	20.03	173.30	89.71	80.21	28.77	262.63	79.30	41.84	378.56	33.82	212.12
1	NS24	1.30	38.47	239.69	33.53	144.69	0.61	36.15	6.85	0.34	21.16	110.61	52.65	74.66	32.88	282.77	61.67	32.33	425.95	25.56	249.75
1	NS28	0.02	20.35	225.11	25.10	53.44	1.42	73.53	12.57	6.26	18.86	101.79	47.04	45.89	21.87	151.53	37.83	29.04	595.38	30.36	130.01
1	NS31	0.44	39.11	226.83	32.39	192.16	0.02	41.24	7.91	6.31	17.15	115.66	56.94	56.41	24.25	222.31	39.60	32.98	351.20	24.41	181.33
1	NS195	0.42	37.46	266.85	32.71	63.44	0.55	73.09	12.13	7.92	23.82	132.59	55.42	76.45	28.88	234.55	68.32	31.83	632.01	27.06	184.75
2	NS10	1.42	35.95	218.99	48.50	342.03	0.08	10.31	4.05	2.02	24.19	135.19	3.63	5.17	21.17	209.59	81.25	54.19	243.95	28.00	51.32
2	NS13	2.69	38.59	245.06	53.88	265.56	1.69	9.84	4.10	1.98	21.03	112.49	3.51	5.04	23.33	196.44	76.73	57.23	266.57	32.11	27.37
3	NS36	1.02	24.35	141.54	26.89	44.73	1.57	44.04	1.56	1.84	18.05	119.18	72.01	515.64	28.28	202.66	18.40	18.43	69.94	10.67	578.19
3	NS37	0.14	20.84	116.69	17.64	147.40	1.66	46.22	1.64	1.94	16.82	86.15	55.69	401.07	29.04	226.57	7.60	9.95	140.55	4.18	543.98
3	NS39	0.33	17.18	102.85	15.80	227.80	1.69	55.26	1.67	1.97	14.86	75.96	52.66	542.39	24.78	211.55	7.97	0.38	161.91	4.40	650.04
3	NS41	0.32	29.38	151.99	23.06	204.15	1.67	45.04	0.34	1.95	17.48	101.46	67.07	352.26	34.59	269.25	32.89	20.31	301.33	10.47	660.30
3	NS44	1.33	22.19	124.40	18.63	169.63	1.66	60.79	1.64	1.94	18.89	91.02	65.99	502.19	27.17	241.46	22.37	12.98	66.38	4.04	711.62
3	NS46	1.20	21.91	121.94	18.29	133.15	0.32	71.47	1.60	1.90	14.55	72.29	56.19	364.94	28.82	239.03	18.33	10.07	758.07	3.95	533.71
3	NS196	1.54	26.51	139.56	22.59	122.54	1.63	36.01	1.62	1.92	17.83	93.04	60.02	342.48	31.32	253.98	25.65	13.47	90.30	3.99	591.88
4	NS173	0.05	45.79	178.93	31.33	59.41	1.67	30.32	4.68	1.96	15.61	104.96	40.38	189.14	28.56	278.38	58.39	32.42	71.27	26.92	328.44
4	NS175	0.01	43.45	166.61	26.39	257.24	1.68	18.24	4.06	1.97	16.02	95.80	51.19	238.51	30.40	299.82	75.20	27.25	2890.61	22.79	475.55
4	NS176	0.08	47.67	170.20	24.74	324.38	1.65	16.91	5.50	1.93	11.95	81.17	41.25	246.79	22.82	204.16	65.82	31.90	340.25	33.56	632.93
4	NS178	1.49	53.68	177.54	25.92	248.92	1.63	13.43	5.30	1.91	12.52	80.27	37.41	257.60	27.03	221.20	62.53	32.25	230.83	34.20	595.30
4	NS181	0.95	54.94	191.07	25.15	245.29	1.62	12.52	4.79	1.90	12.51	84.39	48.11	336.37	25.38	228.96	61.86	29.48	438.77	27.81	752.67
4	NS182	0.20	83.75	292.02	18.97	23.73	1.70	65.19	8.04	0.13	22.22	130.72	62.49	470.16	41.27	344.38	70.69	34.04	112.79	31.14	1214.54
4	NS183	0.47	73.49	254.63	29.06	25.05	1.73	52.59	6.63	0.06	16.81	145.43	50.31	514.04	35.77	308.53	71.36	33.64	80.05	33.00	1050.32
4	NS184	0.21	50.81	171.44	26.87	246.20	1.64	8.87	4.60	1.92	13.78	83.55	39.08	253.54	12.82	205.08	61.28	32.15	207.88	27.18	605.56
4	NS185	1.01	60.92	194.44	29.06	195.86	1.66	9.74	6.73	1.94	14.43	94.85	43.14	213.51	28.26	247.45	57.72	30.55	395.93	29.21	475.55
4	NS187	0.09	61.02	195.98	27.95	180.47	0.47	14.18	6.78	1.94	14.35	100.61	45.31	243.59	29.80	247.53	66.90	33.48	186.84	31.46	543.98
4	NS188	0.17	44.47	142.00	22.58	384.76	1.65	9.99	4.01	1.93	9.19	72.60	25.69	167.68	18.38	187.48	49.88	25.86	262.94	21.88	331.86
4	NS190	1.06	59.34	201.52	28.25	161.68	3.79	23.63	6.97	0.29	15.74	111.38	52.87	255.90	30.40	237.50	60.81	31.76	130.76	33.82	673.99
4	NS191	0.14	43.56	139.51	23.35	369.39	1.66	12.39	4.42	1.94	10.74	70.41	21.43	136.19	18.97	185.63	53.79	25.07	288.44	20.13	311.33
5	NS49	0.08	11.95	214.57	23.96	29.47	6.29	67.51	15.61	5.75	18.56	173.96	43.02	323.01	42.91	292.93	52.67	35.04	384.92	17.76	769.78
5	NS197	0.50	13.95	260.80	24.41	70.65	7.25	75.70	19.11	7.29	18.53	132.42	46.21	246.38	45.97	310.17	60.63	34.75	617.29	18.61	673.99
6	NS57	0.09	19.07	105.67	21.35	37.31	1.52	26.02	0.27	1.79	19.51	94.35	62.88	140.53	31.01	233.63	21.74	12.67	183.45	3.73	352.39
6	NS60	1.05	24.52	112.68	19.64	54.38	1.62	36.95	1.61	1.90	17.39	88.07	89.95	234.86	35.24	273.05	19.98	11.43	277.78	1.88	608.98
6	NS72	1.02	17.17	98.58	20.68	46.38	1.53	5.04	3.65	1.79	17.36	98.36	62.78	244.41	31.59	203.24	0.72	11.14	36.77	3.71	496.08
6	NS76.2	0.50	20.68	117.08	25.18	37.96	1.57	10.91	4.08	1.83	19.89	98.56	79.78	116.36	31.25	249.23	24.44	14.64	75.76	0.53	352.39
7	NS64	0.18	10.52	76.03	20.63	72.72	1.54	4.46	1.53	1.81	17.36	90.59	97.81	201.00	33.30	220.54	6.91	1.52	54.46	3.64	485.82
7	NS69	0.05	9.82	73.49	22.77	104.99	1.56	3.98	0.53	1.83	15.56	77.64	29.20	181.62	29.65	255.77	7.03	3.71	58.89	3.68	513.19
7	NS198	0.07	9.33	67.44	19.20	106.41	1.61	6.26	1.59	1.89	19.66	69.13	27.18	178.06	31.23	241.21	0.05	1.83	109.29	3.91	482.40
8	NS74	1.36	19.47	109.44	23.38	88.38	0.83	5.75	1.00	1.75	22.36	94.58	118.01	211.60	31.74	230.25	6.82	1.96	46.07	3.63	465.29
8	NS76.1	0.39	19.64	114.37	22.85	30.42	1.42	5.37	0.28	1.66	22.06	99.34	246.78	147.78	31.24	245.32	24.78	13.96	34.84	3.54	376.34
9	NS147	0.36	11.89	77.50	19.80	438.76	1.64	10.83	1.62	1.92	17.39	84.13	70.16	328.82	27.50	213.83	7.51	1.60	63.74	4.00	502.92
9	NS80	0.44	11.87	79.38	20.43	375.93	1.63	42.43	1.61	1.91	17.06	80.97	0.47	270.13	28.33	248.73	20.04	0.17	279.44	4.02	492.66
9	NS82	0.44	13.18	86.32	20.95	99.16	1.62	21.72	1.60	1.90	16.26	86.24	84.02	342.59	29.86	258.02	7.37	3.89	156.82	3.96	598.72
9	NS86	0.15	11.03	80.01	21.19	144.56	1.63	16.80	1.61	1.90	18.86	95.65	12.83	379.10	28.83	227.43	7.40	3.91	111.29	3.93	677.41
9	NS90	0.18	11.10	80.58	21.47	300.53	1.63	29.35	1.61	1.90	21.52	106.87	14.78	417.28	30.22	253.85	0.19	0.43	121.65	0.01	667.14
9	NS92	0.07	9.51	71.30	17.38	214.17	1.62	50.82	1.60	1.89	17.06	82.52	4.24	353.23	27.01	230.58	0.27	1.17	200.83	3.94	701.36
9	NS93	0.24	10.28	73.17	18.65	349.36	1.65	23.14	1.63	1.93	16.94	83.58	3.52	445.23	30.16	244.71	1.15	0.68	86.45	3.91	738.99
9	NS96	1.01	10.00	73.37	19.08	170.33	1.59	18.22	1.57	1.86	14.22	90.11	3.35	437.95	27.68	207.57	7.24	1.32	76.10	3.80	626.09
9	NS97	0.90	9.85	67.16	17.76	86.83	1.58	35.77	1.57	1.86	16.75	86.26	0.06	399.21	26.88	211.48	7.19	3.80	155.61	3.77	667.14
9	NS98	0.21	14.12	92.29	21.14	112.65	1.60	44.71	1.59	1.88	23.13	89.79	120.29	272.40	22.34	243.99	20.55	9.56	222.05	3.69	622.67
9	NS100	0.17	9.41	70.50	18.92	278.29	1.61	30.13	1.59	1.88	17.16	74.66	3.39	289.18	8.35	222.49	7.35	0.65	126.22	3.87	571.35
9	NS102	0.05	11.30	79.49	19.52	117.83	1.58	48.25	1.57	1.85	15.88	80.07	3.29	306.88	5.81	231.59	0.93	9.74	206.88	3.79	489.24
9	NS103	0.44	12.05	89.01	22.78	176.33	1.64	44.79	1.62	1.92	20.00	96.16	17.13	357.60	3.95	268.38	20.05	11.76	184.03	3.88	742.41

Trace elements in parts per million.

Table 3. Whole rock trace element chemistry of greenstone units

Unit	No.	Mo	Nb	Zr	Y	Sr	U	Rb	Th	Pb	Ga	Zn	Cu	Ni	Sc	V	Ce	Nd	Ba	La	Cr
9	NS107	1.34	10.07	74.10	19.58	270.21	1.56	24.54	1.58	1.87	18.74	87.75	12.77	424.11	7.88	209.33	2.27	1.14	141.62	3.86	708.20
9	NS109	0.04	10.27	77.35	20.33	536.61	1.62	7.63	0.41	1.89	16.71	77.38	69.59	210.39	7.61	235.48	7.41	3.91	57.48	3.94	492.66
9	NS112	0.08	12.65	86.70	25.47	91.84	1.67	8.19	0.06	1.96	15.58	97.27	53.82	245.45	7.94	250.63	7.44	0.53	57.57	3.93	554.24
9	NS115	0.01	14.23	90.72	21.72	285.99	1.62	9.51	1.60	1.89	20.07	92.29	70.06	257.31	6.31	251.70	2.48	8.81	37.72	3.77	608.98
9	NS121	0.07	10.50	72.93	19.68	85.06	1.63	14.55	1.61	1.91	17.19	82.03	24.86	330.35	9.33	222.74	7.52	3.97	74.71	4.00	547.40
9	NS142	0.17	13.72	88.40	19.69	268.64	1.65	5.60	1.63	1.92	18.89	123.49	12.13	621.19	20.05	229.41	1.90	3.79	21.74	3.81	653.46
9	NS149	0.98	10.62	67.45	16.75	104.21	1.57	7.89	1.55	1.84	11.43	67.14	53.91	266.27	28.00	178.88	7.48	0.46	83.01	4.06	403.71
9	NS151	0.02	15.27	94.34	22.41	169.12	1.62	29.88	1.60	1.89	19.22	100.19	98.16	327.03	32.50	253.01	21.47	10.38	168.79	3.79	619.25
9	NS152	1.18	12.49	81.32	21.45	55.60	1.57	2.42	1.56	1.84	18.06	74.04	72.13	237.89	37.00	257.67	19.40	14.61	7.24	3.85	499.50
9	NS154	1.03	12.89	81.71	20.82	150.07	0.03	5.50	0.52	1.83	15.72	72.49	92.14	220.53	31.55	231.61	1.16	1.11	30.69	3.89	458.45
9	NS157	0.58	9.73	71.47	16.24	153.49	1.59	28.35	1.58	1.86	16.36	78.97	92.84	259.88	27.95	220.90	7.29	3.86	151.78	3.85	499.50
9	NS161	1.51	13.24	98.89	22.48	74.95	1.53	16.66	1.52	1.79	19.46	100.08	54.35	117.55	30.60	235.19	6.67	7.64	91.26	3.59	307.91
9	NS193	1.25	9.43	65.94	16.85	277.94	0.34	28.70	3.33	1.85	14.91	79.82	35.97	371.95	24.66	224.45	7.24	3.83	163.57	3.82	550.82
9	NS194	1.13	10.82	73.89	19.82	336.58	0.70	24.62	1.63	1.93	17.15	74.71	56.01	241.69	25.82	231.28	7.78	0.53	123.58	4.24	516.61
10	NS123	0.08	7.35	57.65	17.48	185.46	1.60	3.76	1.59	1.88	13.73	77.61	83.48	499.57	8.28	156.68	7.42	3.92	145.53	3.88	961.37
10	NS124	0.23	8.08	60.74	16.55	250.33	1.55	3.77	1.57	1.85	13.96	69.62	83.86	451.60	8.19	149.29	7.46	1.42	73.96	3.81	862.15
10	NS126	0.09	5.73	40.35	11.30	70.16	1.60	16.20	1.58	1.87	11.32	77.46	65.87	756.94	16.03	114.90	7.52	3.97	36.26	3.82	1375.34
10	NS127	0.25	6.21	45.29	12.10	92.15	1.60	26.95	1.58	1.87	11.14	76.03	60.10	797.55	13.48	109.28	7.44	3.93	41.36	3.77	1330.87
10	NS128	0.16	5.72	42.99	10.48	94.61	0.42	36.23	1.50	1.85	10.86	73.26	60.04	857.61	12.19	104.98	0.81	0.85	84.60	3.73	1337.71
10	NS129	0.29	5.45	40.93	10.78	60.79	3.42	14.95	1.57	1.86	11.17	71.16	59.55	886.59	4.54	114.40	7.54	3.95	6.96	3.76	1406.13
10	NS130	0.27	5.67	43.73	11.14	147.42	1.58	39.97	0.24	1.85	10.53	70.36	64.47	810.33	13.10	110.11	7.34	3.88	89.48	3.69	1327.44
10	NS132	1.14	5.70	45.46	13.21	129.47	1.61	20.85	1.59	1.88	12.57	74.30	66.69	674.09	13.50	117.77	2.68	3.96	379.71	3.85	1135.85
10	NS134	0.43	4.99	42.84	11.65	299.10	1.58	13.33	1.56	1.84	13.08	71.88	66.98	704.93	13.15	106.10	7.54	3.99	84.75	3.75	1105.06
10	NS135	0.03	5.59	46.01	12.14	226.13	1.59	14.03	1.57	1.86	12.17	73.82	43.45	739.15	10.10	103.78	7.49	3.95	54.64	0.29	1173.49
10	NS136	0.27	6.02	46.07	13.20	200.80	1.60	13.41	1.58	1.88	11.91	70.83	49.19	721.83	12.50	106.63	7.45	3.93	59.40	3.70	1108.48
10	NS138	1.33	6.26	51.39	14.56	231.85	1.61	5.72	1.59	1.88	13.42	76.05	50.27	676.67	13.75	127.04	7.59	0.06	29.89	3.83	1118.75
10	NS140	1.25	6.69	51.06	14.96	221.99	0.01	7.35	0.38	1.88	13.92	79.92	54.28	701.38	11.75	123.45	7.50	3.95	4.96	3.80	1091.38
11	NSF/2.5	1.04	42.92	270.79	34.34	775.25	1.00	7.96	4.81	5.88	23.02	122.72	33.15	107.63	28.09	311.10	72.32	40.29	195.68	34.92	266.86
11	NSF/2.6	1.38	42.10	267.97	34.21	863.41	1.00	7.46	4.22	3.99	24.47	121.89	33.40	95.18	26.68	309.42	66.19	38.05	188.10	28.56	260.01
11	NSF/2.7	1.52	43.05	270.04	34.93	786.45	1.00	9.23	4.94	4.54	24.36	121.89	35.03	109.40	28.20	329.61	77.27	46.60	236.99	30.46	260.01
11	NSF/2.8	1.48	41.92	270.77	33.20	696.22	1.00	14.32	3.47	1.50	22.09	121.23	38.60	71.43	25.22	310.00	70.63	41.17	219.42	30.77	195.01

Trace elements in parts per million

Table 3 (cont.)

ROCKTYPE	NO.	La	Ce	Pr	Nd	Sm	Eu	Gd	Dy	Ho	Er	Yb
Greenstones												
unit 1	NS3	34.04	68.94	8.52	32.85	5.66	1.54	5.36	4.78	0.92	2.28	1.52
unit 1	NS7	33.54	69.81	8.62	33.13	5.68	1.49	5.54	4.64	0.96	2.04	1.48
unit 1	NS28	38.20	75.49	8.90	30.59	4.66	0.82	3.94	3.70	0.80	1.94	1.44
$\bar{x}$		35.26	71.41	8.68	32.19	5.34	1.28	4.95	4.37	0.89	2.09	1.48
unit 2	NS10	47.86	106.45	13.67	55.58	9.25	2.84	7.90	6.56	1.22	2.56	1.52
unit 2	NS13	42.86	103.18	15.53	73.64	16.44	5.35	14.04	11.02	2.18	4.68	3.18
$\bar{x}$		45.36	104.82	14.60	64.61	12.84	4.10	10.97	8.79	1.70	3.62	2.35
unit 3	NS37	15.21	32.24	4.38	19.07	4.22	1.37	4.58	3.52	0.72	2.02	1.26
unit 3	NS41	20.76	45.44	6.57	28.58	6.28	1.97	5.92	4.84	1.00	2.56	1.64
unit 3	NS46	17.79	26.34	4.61	16.55	2.99	0.95	3.08	2.60	0.54	1.32	0.86
$\bar{x}$		17.92	34.67	5.19	21.40	4.49	1.43	4.53	3.65	0.75	1.97	1.25
unit 4	NS175	27.15	56.51	7.47	29.21	5.40	1.76	4.88	3.96	0.76	1.98	1.12
unit 4	NS187	33.56	66.30	8.58	32.78	5.85	1.84	5.24	4.30	0.88	2.00	1.42
unit 4	NS190	29.23	61.42	8.51	35.04	7.54	2.40	6.74	5.24	1.08	2.90	1.98
$\bar{x}$		29.98	61.41	8.18	32.35	6.26	2.00	5.62	4.50	0.91	2.29	1.51
unit 5	NS49	19.02	48.56	8.10	36.53	7.19	1.36	5.20	4.04	0.86	2.36	1.72
unit 5	NS197	19.37	49.73	8.08	39.82	7.71	1.47	4.72	4.22	0.86	2.38	2.06
$\bar{x}$		19.19	49.15	8.09	38.17	7.45	1.41	4.96	4.13	0.86	2.37	1.89
unit 6	NS57	11.11	26.82	3.66	15.84	3.73	1.28	4.10	3.56	0.72	1.86	1.24
unit 6	NS60	14.13	30.88	4.12	17.12	3.75	1.15	3.48	3.24	0.66	1.56	1.26
unit 6	NS72	10.29	22.10	2.82	12.96	3.10	1.02	3.38	3.10	0.56	1.54	1.12
$\bar{x}$		11.84	26.60	3.53	15.31	3.53	1.15	3.65	3.30	0.65	1.65	1.21
unit 7	NS64	6.07	14.30	2.04	9.75	2.67	0.87	3.24	3.18	0.70	2.00	1.62
unit 7	NS69	8.95	18.42	2.58	11.40	2.79	0.89	3.22	3.24	0.64	1.74	1.34
$\bar{x}$		7.51	16.36	2.31	10.58	2.73	0.88	3.23	3.21	0.67	1.87	1.48
unit 8	NS74	12.74	27.62	3.71	16.90	3.96	1.30	4.20	3.88	0.76	2.28	1.44
unit 9	NS80	9.94	23.47	3.47	14.84	3.83	1.19	3.94	3.96	0.88	2.38	1.74
unit 9	NS90	10.08	22.71	3.29	13.67	3.36	1.04	3.62	3.46	0.76	2.18	1.44
unit 9	NS151	10.44	23.62	2.97	13.09	2.67	0.87	2.70	2.74	0.52	1.58	1.08
$\bar{x}$		10.15	23.27	3.24	13.87	3.29	1.03	3.42	3.39	0.72	2.05	1.42
unit 10	NS123	7.97	12.57	1.62	7.56	1.86	0.65	2.60	2.32	0.46	1.42	1.00
unit 10	NS127	5.92	11.55	1.26	6.13	1.36	0.46	1.66	1.62	0.32	1.06	0.62
unit 10	NS132	5.07	11.46	1.52	6.70	1.71	0.59	2.44	2.19	0.40	1.36	0.82
$\bar{x}$		6.32	11.86	1.47	6.80	1.64	0.57	2.23	2.04	0.39	1.28	0.81
unit 11	NSF2.6	29.51	62.59	8.43	37.22	7.21	2.41	6.20	5.60	0.98	2.24	1.66
unit 11	NSF2.7	30.09	66.17	9.17	41.73	8.99	2.93	7.34	6.72	1.18	3.08	2.04
$\bar{x}$		29.80	64.38	8.80	39.47	8.10	2.67	6.77	6.16	1.08	2.66	1.85
graphitic schist	NS20	46.65	92.41	11.79	45.98	8.38	1.75	7.10	6.54	1.32	3.24	2.38
graphitic schist	NS55	43.87	74.60	11.63	45.95	8.65	1.62	7.26	6.68	1.42	3.76	3.08
shale	NSF2.1	29.05	57.85	7.47	31.55	6.43	1.10	5.12	5.24	1.04	3.02	2.94
chlorite schist	NSF9	2.53	5.66	0.82	3.10	1.04	0.41	1.64	1.68	0.38	1.18	0.90

REE values in ppm.

$\bar{x}$ = average

Chondrite Values (Henderson, 1984)

La	Ce	Pr	Nd	Sm	Eu	Gd	Dy	Ho	Er	Yb
0.31	0.808	0.122	0.6	0.195	0.0735	0.259	0.322	0.0718	0.21	0.209

Table 4. Whole rock rare earth element chemistry.

SAMPLE	UNIT	Q	OR	AB	AN	LC	NE	KAL	C	DI	HY	WO	OL
NS3	1	0.41	4.08	29.3	17.7	0	0	0	1.73	0	28.1	0	0
NS6	1	0	5.61	25.2	22	0	0	0	0	7.07	12.9	0	7.55
NS7	1	0	5.61	22.5	24	0	0	0	0.4	0	19.7	0	9.16
NS21	1	15.5	6.5	30	0.08	0	0	0	9.3	0	22.5	0	0
NS24	1	4.61	9.16	12.3	22.7	0	0	0	2.51	0	28.4	0	0
NS28	1	34.9	17.5	12.5	4.86	0	0	0	6.23	0	15.2	0	0
NS31	1	0	10.1	23.4	20.4	0	0	0	0	16.9	10.7	0	0.54
NS195	1	20.1	17.3	14.2	5.25	0	0	0	7.82	0	22.2	0	0
NS10	2	0	1.95	33.3	14.1	0	5.3	0	0	7.84	0	0	12.3
NS13	2	0	1.65	48.3	11	0	2.24	0	0	1.22	0	0	12.9
NS36	3	0	5.91	16.3	16.6	0	0	0	4.4	0	26	0	10.9
NS37	3	0	8.92	10.2	10.1	0	13.2	0	0	32.7	0	0	3.08
NS39	3	0	1.07	0	10.7	7	13.4	0	0	35.7	0	6.28	0
NS41	3	0	7.68	26.2	20.2	0	0	0	0	3.71	2.62	0	17.2
NS44	3	0	10.3	16.7	15.6	0	3.67	0	0	18.2	0	0	11.7
NS46	3	0	13.8	35.5	8.39	0	0	0	0	13.4	7.56	0	1.23
NS196	3	0	6.09	17.6	23.6	0	0	0	0	4.23	17.8	0	9.67
NS173	4	5.13	4.55	11	25.8	0	0	0	0	5.93	17.4	0	0
NS175	4	0	1.83	23.3	18.9	0	0.01	0	0	13.6	0	0	15.1
NS176	4	0	0	0	17.6	1.34	8.85	0	0	32.6	0	0	7.47
NS178	4	0	0	0	18	0.79	10.8	0	0	33.4	0	0	9.65
NS181	4	0	0.59	15.5	19.9	0	1.32	0	0	27.4	0	0	9.17
NS182	4	19.1	16.1	0.42	0.77	0	0	0	13.1	0	24.5	0	0
NS183	4	7.89	10.8	0.68	14.5	0	0	0	6.86	0	32.4	0	0
NS184	4	0	0	0	20	0.32	7.43	0	0	38.5	0	0	5.88
NS185	4	0	0.77	20.5	15.5	0	7.18	0	0	20.2	0	0	11.4
NS187	4	0	2.19	20.9	15.8	0	7.14	0	0	18.9	0	0	11.6
NS188	4	0	0	0	20	0	4.22	0.5	0	0	0	0	20.8
NS190	4	0	4.37	23.9	10.5	0	8.63	0	0	19.1	0	0	10.7
NS191	4	0	0	0	15.5	1.25	8.66	0	0	9.01	0	0	16.5
NS49	5	18.9	8.63	0.68	0.24	0	0	0	12.2	0	45.7	0	0
NS197	5	21.5	12.8	0.08	0.25	0	0	0	12.8	0	40.1	0	0
NS57	6	0.08	7.74	19.2	25	0	0	0	0	1.23	26.3	0	0
NS60	6	0	10.6	16.8	22.5	0	2.43	0	0	12.2	0	0	11.5
NS72	6	0	1.48	45.6	12.6	0	0.88	0	0	7.61	0	0	15
NS76.2	6	0	3.84	38.7	16.4	0	3.44	0	0	1.29	0	0	15.8
NS64	7	0	0.89	43.1	8.91	0	9.28	0	0	12.9	0	0	7.2
NS69	7	0	0.65	48.3	7.1	0	9.08	0	0	14.6	0	0	4.34
NS198	7	0	1.36	36.4	5	0	13	0	0	16	0	10.9	0
NS74	8	0	1.83	36.6	19.6	0	0.55	0	0	3.33	0	0	21.8
NS76.1	8	0	2.19	27.6	17.4	0	0	0	2.95	0	30.1	0	3.49
NS147	9	0	1.71	13.9	26.3	0	3.14	0	0	21.4	0	0	13
NS80	9	4.95	9.81	2.03	33.9	0	0	0	0	9.47	19.1	0	0

Table 5. C.I.P.W. norms.

SAMPLE	UNIT	AC	MT	IL	HEM	TI	AP	CC	PERO	WUS	RU
NS3	1	0	3.7	5.56	0	0	1.11	0	0	0	0
NS6	1	0	3.65	5.26	0	0	1.07	0	0	0	0
NS7	1	0	2.65	5.62	0	0	1.11	0	0	0	0
NS21	1	0	3.86	5.03	0	0	1.27	0	0	0	0
NS24	1	0	4.18	5.15	0	0	1	0	0	0	0
NS28	1	0	1.49	2.09	0	0	0.3	0	0	0	0
NS31	1	0	2.1	4.1	0	0	0.9	0	0	0	0
NS195	1	0	2.35	3.95	0	0	0.74	0	0	0	0
NS10	2	0	4.42	8.96	0	0	4.54	0	0	0	0
NS13	2	0	3.78	9.34	0	0	4.87	0	0	0	0
NS36	3	0	6.1	4.24	0	0	0.63	0	0	0	0
NS37	3	0	9.45	3.53	0	0	0.58	0	0	0	0
NS39	3	0	9.76	3.11	0.49	0	0.46	0	0	0	0
NS41	3	0	9.7	4.56	0	0	0.76	0	0	0	0
NS44	3	0	9.73	3.8	0	0	0.67	0	0	0	0
NS46	3	0	8.62	3.67	1.74	0	0.65	0	0	0	0
NS196	3	0	7.63	4.14	0	0	0.67	0	0	0	0
NS173	4	0	7.18	6.13	4.06	0	0.97	0	0	0	0
NS175	4	0	10.1	6.1	0	0	1	0	0	0	0
NS176	4	0	6.61	4.12	0	0	1	0	0	0	0
NS178	4	0	5.73	4.33	0	0	1.09	0	0	0	0
NS181	4	0	7.5	4.5	0	0	1.09	0	0	0	0
NS182	4	0	10.6	6.86	0	0	1.78	0	0	0	0
NS183	4	0	9.87	5.93	0	0	1.53	0	0	0	0
NS184	4	0	7.28	4.01	0	0	1	0	0	0	0
NS185	4	0	8.28	5.07	0	0	1.25	0	0	0	0
NS187	4	0	8.84	5.09	0	0	1.27	0	0	0	0
NS188	4	0	4.7	3.76	0	0	0.97	0	0	0.4	0
NS190	4	0	9.69	5.22	0	0	1.3	0	0	0	0
NS191	4	0	5.86	3.68	0	0	0.9	0	0	0	0
NS49	5	0	1.91	2.32	0	0	1.11	0	0	0	0
NS197	5	0	1.52	2.34	0	0	1.02	0	0	0	0
NS57	6	0	8.31	3.3	0	0	0.44	0	0	0	0
NS60	6	0	7.25	3.57	3.08	0	0.67	0	0	0	0
NS72	6	0	6.32	2.98	2.96	0	0.39	0	0	0	0
NS76.2	6	0	4.74	3.59	6.11	0	0.51	0	0	0	0
NS64	7	0	6.47	2.36	4.32	0	0.3	0	0	0	0
NS69	7	0	5.68	2.3	5.4	0	0.32	0	0	0	0
NS198	7	0	1.88	2.11	7.84	0	0.23	0	0	0	0
NS74	8	0	6.92	3.32	0	0	0.46	0	0	0	0
NS76.1	8	0	4.9	3.46	0	0	0.49	0	0	0	0
NS147	9	0	9.16	2.41	0	0	0.3	0	0	0	0
NS80	9	0	7.59	2.54	2.86	0	0.3	0	0	0	0

Table 5 (cont.)

SAMPLE	UNIT	Q	OR	AB	AN	LC	NE	KAL	C	DI	HY	WO	OL
NS82	9	0	4.85	29.2	18.4	0	3.11	0	0	14.4	0	0	9.79
NS86	9	0	3.55	14.3	31.7	0	0	0	0	8.25	18.1	0	3.86
NS90	9	0	5.26	10.9	36.1	0	0	0	0	0.63	17.5	0	10.3
NS92	9	7.01	9.04	0.25	33.9	0	0	0	0	1.69	29.6	0	0
NS93	9	0	3.9	1.61	38.2	0	0	0	0	4.54	31.3	0	0.58
NS96	9	0	3.43	21.2	26.4	0	0	0	0	6.34	14.8	0	11.1
NS97	9	0	7.27	25	22.4	0	0	0	0	6.82	10.5	0	11.1
NS98	9	0	10.5	0.68	17.6	0	0	0	7.39	0	42.3	0	1.34
NS100	9	5.71	5.26	5.5	32.8	0	0	0	0	5.51	27.4	0	0
NS102	9	2.5	8.98	14.6	27.7	0	0	0	0	0.32	28.4	0	0
NS103	9	0	7.98	0.68	31.6	0	0	0	3.45	0	22.6	0	13.1
NS107	9	0	6.03	3.38	36.1	0	0	0	0.35	0	29.2	0	4.45
NS109	9	6.97	1.65	23	27.5	0	0	0	0	10	13.3	0	0
NS112	9	0	2.07	36	24	0	0	0	0	7.7	6.53	0	4.44
NS115	9	0	1.18	0.68	25.8	0	0	0	5.99	0	44.9	0	2.75
NS121	9	0	2.66	27.4	23	0	0	0	0	17.5	3.94	0	7.66
NS142	9	0	0.47	10.9	33.2	0	0	0	0	2.43	1.11	0	27.9
NS149	9	0	2.13	13.6	6.35	0	18.4	0	0	29.7	0	9.29	0
NS151	9	0	6.62	13	23.3	0	0	0	3.55	0	20	0	15.8
NS152	9	0	0.06	10.2	32.4	0	0	0	0	4.66	10.6	0	25
NS154	9	0	1.06	19.7	18.7	0	6.24	0	0	24.3	0	0	13.1
NS157	9	2.69	7.92	8.04	30.1	0	0	0	0	6.54	25.1	0	0
NS161	9	0	3.72	21.5	22.4	0	0	0	1.5	0	29.7	0	3.84
NS193	9	2.62	4.85	13.4	27.9	0	0	0	0	9.02	22.1	0	0
NS194	9	0	4.31	11.1	22.2	0	7.27	0	0	33.9	0	0	0.61
NS123	10	0	0.06	13.5	28.5	0	0	0	0	9.59	15.1	0	20.2
NS124	10	0	0.06	21.2	22.5	0	0	0	0	15.7	5.7	0	23.2
NS126	10	0	1.83	4.57	24.2	0	0	0	0	12.6	16.7	0	26.8
NS127	10	0	3.25	3.22	24.8	0	0	0	0	10.1	17.2	0	25.7
NS128	10	0	4.91	0.68	26	0	0	0	0	5.39	17.6	0	31.1
NS129	10	0	1.18	0.68	24.9	0	0	0	0	9.72	19.1	0	32
NS130	10	0	4.91	0.68	26.4	0	0	0	0	5.9	19.3	0	28.9
NS132	10	0	5.44	4.48	26.1	0	0	0	0	11.2	15	0	27.3
NS134	10	0	1.77	13.3	24.6	0	0	0	0	11.5	3.17	0	35.3
NS135	10	0	1.83	5.84	27.6	0	0	0	0	9.07	16.5	0	27.9
NS136	10	0	1.89	11.2	23.1	0	0	0	0	13	2.16	0	35.8
NS138	10	0	0.24	5.5	28.5	0	0	0	0	11	20.9	0	23
NS140	10	0	0.41	4.82	28.9	0	0	0	0	10.4	19	0	24.3
NSF/2.	11	10.5	2.3	6.6	35.2	0	0	0	0	15.2	7.57	0	0
NSF/2.	11	11.1	1.89	6.43	34.9	0	0	0	0	17	5.03	0	0
NSF/2.	11	6.89	2.78	11.1	33.6	0	0	0	0	16.9	6.1	0	0
NSF/2.	11	3.64	3.55	18.2	27	0	0	0	0	24.7	0.53	0	0

Table 5 (cont.)

SAMPLE	UNIT	AC	MT	IL	HEM	TI	AP	CC	PERO	WUS	RU
NS82	9	0	0.12	2.75	11.8	0	0.35	0	0	0	0
NS86	9	0	10.1	2.45	0.54	0	0.28	0	0	0	0
NS90	9	0	10.7	2.53	0	0	0.28	0	0	0	0
NS92	9	0	10.4	2.2	0	0	0.25	0	0	0	0
NS93	9	0	10.5	2.34	0	0	0.28	0	0	0	0
NS96	9	0	9.19	2.22	0	0	0.25	0	0	0	0
NS97	9	0	9.94	2.13	0.01	0	0.25	0	0	0	0
NS98	9	0	9.34	2.92	0	0	0.32	0	0	0	0
NS100	9	0	9.79	2.2	0	0	0.25	0	0	0	0
NS102	9	0	9.73	2.39	0.11	0	0.3	0	0	0	0
NS103	9	0	10	2.79	0	0	0.35	0	0	0	0
NS107	9	0	0	1.5	11.5	0	0.28	0	0	0	0.4
NS109	9	0	8.34	2.39	2.13	0	0.28	0	0	0	0
NS112	9	0	6.37	2.7	6.69	0	0.37	0	0	0	0
NS115	9	0	7	2.85	0	0	0.37	0	0	0	0
NS121	9	0	9.63	2.36	1.11	0	0.25	0	0	0	0
NS142	9	0	10.7	2.64	0	0	0.35	0	0	0	0
NS149	9	0	5.91	2.13	2.66	0	0.21	0	0	0	0
NS151	9	0	6.12	3	0	0	0.39	0	0	0	0
NS152	9	0	1.51	2.49	0	0	0.32	0	0	0	0
NS154	9	0	3.36	2.43	0	0	0.37	0	0	0	0
NS157	9	0	6.95	2.39	0	0	0.23	0	0	0	0
NS161	9	0	3.74	2.92	0	0	0.35	0	0	0	0
NS193	9	0	8.9	2.05	1.15	0	0.23	0	0	0	0
NS194	9	0	5.05	2.34	5.43	0	0.23	0	0	0	0
NS123	10	0	4.38	1.9	0	0	0.19	0	0	0	0
NS124	10	0	4.09	1.88	0	0	0.19	0	0	0	0
NS126	10	0	4.64	1.37	0	0	0.21	0	0	0	0
NS127	10	0	7.12	1.37	0	0	0.19	0	0	0	0
NS128	10	0	5.09	1.33	0	0	0.16	0	0	0	0
NS129	10	0	3.77	1.29	0	0	0.14	0	0	0	0
NS130	10	0	4.6	1.35	0	0	0.16	0	0	0	0
NS132	10	0	2.68	1.39	0	0	0.14	0	0	0	0
NS134	10	0	3.07	1.42	0	0	0.14	0	0	0	0
NS135	10	0	2.93	1.44	0	0	0.14	0	0	0	0
NS136	10	0	2.86	1.44	0	0	0.16	0	0	0	0
NS138	10	0	3	1.63	0	0	0.16	0	0	0	0
NS140	10	0	3.33	1.67	0	0	0.16	0	0	0	0
NSF/2.	11	0	8.28	6.82	0	0	1.18	0	0	0	0
NSF/2.	11	0	8.61	6.7	0	0	1.16	0	0	0	0
NSF/2.	11	0	7.95	6.91	0	0	1.2	0	0	0	0
NSF/2.	11	0	7.63	6.65	0	0	1.23	0	0	0	0

Table 5 (cont.)

UNIT	NO.		Rb	Ba	Th	U	K	Nb	La	Ce	Sr	Nd	P	Zr	Ti	Y
1	NS3		15.06	166.17	6.68	0.18	5740.49	39.15	19.27	48.55	152.42	29.78	2079.54	233.30	17565.35	33.55
1	NS6		22.97	219.17	5.24	1.61	7882.27	36.12	18.00	56.30	203.07	31.75	2011.90	213.28	16588.16	29.86
1	NS7		19.13	242.43	5.19	1.60	7857.37	39.55	22.55	56.57	191.90	29.86	2092.63	229.46	17763.19	32.46
1	NS21		35.76	378.56	8.20	1.54	9144.10	48.44	33.82	79.30	49.50	41.84	2398.13	280.12	15904.73	40.56
1	NS24		36.15	425.95	6.85	0.61	12867.32	38.47	25.56	61.67	144.69	32.33	1889.70	239.69	16267.43	33.53
1	NS28		73.53	595.38	12.57	1.42	24568.29	20.35	30.36	37.83	53.44	29.04	569.53	225.11	6618.48	25.10
1	NS31		41.24	351.20	7.91	0.02	14216.32	39.11	24.41	39.60	192.16	32.98	1684.58	226.83	12943.21	32.39
1	NS195		73.09	632.01	12.13	0.55	24236.23	37.46	27.06	68.32	63.44	31.83	1400.91	266.85	12478.59	32.71
		$\bar{x}$	39.62	376.36	8.10	0.94	13314.05	37.33	25.13	56.02	131.33	32.43	1765.86	239.33	14516.14	32.52
		s	22.68	170.40	2.84	0.67	7377.50	7.80	5.33	14.05	66.02	4.05	567.18	22.65	3744.10	4.29
		e	16.03	120.42	2.01	0.47	5213.78	5.51	3.77	9.93	46.66	2.86	400.83	16.01	2646.01	3.03
		($\bar{x}$+e)/prim	87.63	71.08	118.86	67.43	74.11	60.09	42.07	37.15	8.44	26.06	22.81	22.80	13.20	7.81
		$\bar{x}$/prim	62.39	53.85	95.25	44.85	53.26	52.36	36.58	31.56	6.22	23.95	18.59	21.37	11.17	7.15
		($\bar{x}$-e)/prim	37.15	36.62	71.64	22.27	32.40	44.63	31.10	25.97	4.01	21.84	14.37	19.94	9.13	6.48
2	NS10		10.31	243.95	4.05	0.08	2764.40	35.95	28.00	81.25	342.03	54.19	8551.65	218.99	28284.41	48.50
2	NS13		9.84	266.57	4.10	1.69	2353.48	38.59	32.11	76.73	265.56	57.23	9171.37	245.06	29519.38	53.88
		$\bar{x}$	10.07	255.26	4.08	0.89	2558.94	37.27	30.06	78.99	303.80	55.71	8861.51	232.03	28901.89	51.19
		s	0.33	16.00	0.04	1.13	290.57	1.86	2.91	3.19	54.07	2.15	438.21	18.43	873.26	3.80
		e	0.47	22.69	0.06	1.61	412.15	2.64	4.13	4.53	76.70	3.05	621.57	26.14	1238.66	5.40
		($\bar{x}$+e)/prim	16.61	39.77	48.62	52.26	11.88	55.98	49.76	47.05	18.03	43.40	99.82	23.05	23.19	12.44
		$\bar{x}$/prim	15.87	36.52	47.97	42.26	10.24	52.28	43.75	44.50	14.40	41.15	93.28	20.72	22.23	11.25
		($\bar{x}$-e)/prim	15.12	33.28	47.32	32.26	8.59	48.57	37.74	41.95	10.76	38.90	86.74	18.38	21.28	10.06
3	NS36		44.04	69.94	1.56	1.57	8297.35	24.35	10.67	18.40	44.73	18.43	1187.06	141.54	13350.86	26.89
3	NS37		46.22	140.55	1.64	1.66	12506.21	20.84	4.18	7.60	147.40	9.95	1106.32	116.69	11144.70	17.64
3	NS39		55.26	161.91	1.67	1.69	14046.14	17.18	4.40	7.97	227.80	0.38	894.66	102.85	9849.78	15.80
3	NS41		45.04	301.33	0.34	1.67	10791.95	29.38	10.47	32.89	204.15	20.31	1424.91	151.99	14411.98	23.06
3	NS44		60.79	66.38	1.64	1.66	14531.78	22.19	4.04	22.37	169.63	12.98	1267.80	124.40	11969.02	18.63
3	NS46		71.47	758.07	1.60	0.32	19413.06	21.91	3.95	18.33	133.15	10.07	1224.16	121.94	11564.35	18.29
3	NS196		36.01	90.30	1.62	1.63	8546.39	26.51	3.99	25.65	122.54	13.47	1283.07	139.56	13093.08	22.59
		$\bar{x}$	51.26	226.93	1.44	1.46	12590.41	23.20	5.96	19.03	149.92	12.23	1198.28	128.43	12197.68	20.41
		s	12.00	247.80	0.48	0.50	3882.92	3.98	3.16	9.14	59.86	6.54	165.74	16.84	1533.48	3.88
		e	9.06	187.02	0.37	0.38	2930.51	3.00	2.38	6.90	45.18	4.93	125.09	12.71	1157.35	2.93
		($\bar{x}$+e)/prim	95.00	59.23	21.23	87.46	62.08	36.74	12.14	14.61	9.25	12.67	13.93	12.60	10.27	5.13
		$\bar{x}$/prim	80.73	32.47	16.93	69.39	50.36	32.53	8.67	10.72	7.11	9.03	12.61	11.47	9.38	4.49
		($\bar{x}$-e)/prim	66.47	5.71	12.64	51.31	38.64	28.33	5.21	6.84	4.96	5.39	11.30	10.33	8.49	3.84
4	NS173		30.32	71.27	4.68	1.67	6408.76	45.79	26.92	58.39	59.41	32.42	1817.69	178.93	19360.85	31.33
4	NS175		18.24	2890.61	4.06	1.68	2577.62	43.45	22.79	75.20	257.24	27.25	1872.24	166.61	19225.97	26.39
4	NS176		16.91	340.25	5.50	1.65	2436.49	47.67	33.56	65.82	324.38	31.90	1894.06	170.20	13033.13	24.74
4	NS178		13.43	230.83	5.30	1.63	1427.86	53.68	34.20	62.53	248.92	32.25	2038.08	177.54	13653.61	25.92
4	NS181		12.52	438.77	4.79	1.62	838.45	54.94	27.81	61.86	245.29	29.48	2046.81	191.07	14211.15	25.15
4	NS182		65.19	112.79	8.04	1.70	22671.40	83.75	31.14	70.69	23.73	34.04	3353.89	292.02	21617.97	18.97
4	NS183		52.59	80.05	6.63	1.73	15208.35	73.49	33.00	71.36	25.05	33.64	2869.46	254.63	18680.42	29.06
4	NS184		8.87	207.88	4.60	1.64	593.56	50.81	27.18	61.28	246.20	32.15	1889.70	171.44	12673.43	26.87
4	NS185		9.74	395.93	6.73	1.66	1066.74	60.92	29.21	57.72	195.86	30.55	2365.40	194.44	16000.65	29.06
4	NS187		14.18	186.84	6.78	0.47	3050.80	61.02	31.46	66.90	180.47	33.48	2415.58	195.98	16075.59	27.95
4	NS188		9.99	262.94	4.01	1.65	1286.73	44.47	21.88	49.88	384.76	25.86	1848.24	142.00	11900.07	22.58
4	NS190		23.63	130.76	6.97	3.79	6184.62	59.34	33.82	60.81	161.68	31.76	2448.32	201.52	16498.24	28.25
4	NS191		12.39	288.44	4.42	1.66	2220.65	43.56	20.13	53.79	369.39	25.07	1695.49	139.51	11621.31	23.35
		$\bar{x}$	22.15	433.65	5.58	1.74	5074.77	55.61	28.70	62.79	209.42	30.76	2196.54	190.46	15734.80	26.13
		s	17.55	747.28	1.31	0.70	6598.75	12.20	4.77	7.17	119.13	2.97	481.87	42.02	3219.01	3.26
		e	9.72	414.00	0.72	0.39	3655.82	6.76	2.65	3.97	66.00	1.65	266.96	23.28	1783.39	1.80
		($\bar{x}$+e)/prim	50.20	72.05	74.15	101.13	34.92	87.47	45.63	37.61	13.05	23.94	25.93	19.08	13.48	6.14
		$\bar{x}$/prim	34.89	62.05	65.64	82.64	20.30	77.99	41.78	35.37	9.92	22.72	23.12	17.01	12.10	5.74
		($\bar{x}$-e)/prim	19.58	52.05	57.13	64.14	5.68	68.51	37.93	33.14	6.80	21.50	20.31	14.93	10.73	5.35

Table 6. Incompatible element content of greenstone units of the Bridgetown Formation, an average N-type

UNIT	NO.		Rb	Ba	Th	U	K	Nb	La	Ce	Sr	Nd	P	Zr	Ti	Y
5	NS49		67.51	384.92	15.61	6.29	12086.98	11.95	17.76	52.67	29.47	35.04	2075.18	214.57	7322.89	23.96
5	NS197		75.70	617.29	19.11	7.25	17997.65	13.95	18.61	60.63	70.65	34.75	1924.61	260.80	7379.85	24.41
		$\bar{x}$	71.61	501.10	17.36	6.77	15042.32	12.95	18.19	56.65	50.06	34.90	1999.89	237.69	7351.37	24.18
		s	5.79	164.31	2.47	0.68	4179.47	1.41	0.60	5.63	29.12	0.21	106.47	32.69	40.27	0.32
		e	8.21	233.06	3.51	0.97	5928.33	2.00	0.85	7.98	41.30	0.29	151.01	46.36	57.12	0.45
		($\bar{x}$+e)/prim	125.71	105.05	245.59	368.59	83.88	20.97	27.71	36.41	4.33	25.99	22.64	25.36	5.70	5.41
		$\bar{x}$/prim	112.77	71.70	204.29	322.50	60.17	18.17	26.47	31.92	2.37	25.78	21.05	21.22	5.65	5.32
		($\bar{x}$-e)/prim	99.84	38.35	162.99	276.41	36.46	15.36	25.24	27.42	0.42	25.56	19.46	17.08	5.61	5.22
6	NS57		26.02	183.45	0.27	1.52	10874.96	19.07	3.73	21.74	37.31	12.67	831.38	105.67	10461.27	21.35
6	NS60		36.95	277.78	1.61	1.62	14830.63	24.52	1.88	19.98	54.38	11.43	1267.80	112.68	11252.61	19.64
6	NS72		5.04	36.77	3.65	1.53	2071.22	17.17	3.71	0.72	46.38	11.14	746.28	98.58	9403.16	20.68
6	NS76.2		10.91	75.76	4.08	1.57	5420.88	20.68	0.53	24.44	37.96	14.64	957.94	117.08	11354.53	25.18
		$\bar{x}$	19.73	143.44	2.40	1.56	8299.42	20.36	2.46	16.72	44.01	12.47	950.85	108.50	10617.89	21.71
		s	14.49	108.95	1.78	0.05	5667.64	3.12	1.55	10.82	8.05	1.59	228.50	8.12	902.89	2.41
		e	14.49	108.95	1.78	0.05	5667.64	3.12	1.55	10.82	8.05	1.59	228.50	8.12	902.89	2.41
		($\bar{x}$+e)/prim	53.89	36.11	49.27	76.45	55.87	32.94	5.84	15.52	2.47	10.39	12.41	10.41	8.86	5.30
		$\bar{x}$/prim	31.07	20.52	28.29	74.29	33.20	28.56	3.59	9.42	2.09	9.21	10.01	9.69	8.17	4.77
		($\bar{x}$-e)/prim	8.26	4.94	7.32	72.12	10.53	24.18	1.33	3.32	1.70	8.04	7.60	8.96	7.47	4.24
7	NS64		4.46	54.46	1.53	1.54	1257.68	10.52	3.64	6.91	72.72	1.52	576.07	76.03	7418.81	20.63
7	NS69		3.98	58.89	0.53	1.56	950.52	9.82	3.68	7.03	104.99	3.71	628.44	73.49	7265.94	22.77
7	NS198		6.26	109.29	1.59	1.61	1876.14	9.33	3.91	0.05	106.41	1.83	440.78	67.44	6660.45	19.20
		$\bar{x}$	4.90	74.21	1.22	1.57	1361.45	9.89	3.74	4.66	94.71	2.35	548.43	72.32	7115.07	20.87
		s	1.20	30.46	0.60	0.04	471.45	0.60	0.15	4.00	19.05	1.18	96.84	4.41	401.06	1.80
		e	1.39	35.21	0.69	0.04	545.03	0.69	0.17	4.62	22.03	1.37	111.95	5.10	463.66	2.08
		($\bar{x}$+e)/prim	9.91	15.66	22.41	76.75	7.63	14.85	5.69	3.63	5.53	2.75	6.95	6.91	5.83	5.04
		$\bar{x}$/prim	7.72	10.62	14.31	74.76	5.45	13.88	5.45	2.63	4.49	1.74	5.77	6.46	5.47	4.59
		($\bar{x}$-e)/prim	5.53	5.58	6.22	72.78	3.27	12.91	5.20	1.63	3.44	0.73	4.59	6.00	5.12	4.13
8	NS74		5.75	46.07	1.00	0.83	2614.97	19.47	3.63	6.82	88.38	1.96	859.75	109.44	10464.27	23.38
8	NS76.1		5.37	34.84	0.28	1.42	3063.25	19.64	3.54	24.78	30.42	13.96	899.03	114.37	10928.88	22.85
		$\bar{x}$	5.56	40.45	0.64	1.13	2839.11	19.56	3.59	15.80	59.40	7.96	879.39	111.90	10696.58	23.11
		s	0.27	7.94	0.51	0.41	316.98	0.12	0.06	12.70	40.98	8.49	27.77	3.49	328.53	0.37
		e	0.38	11.26	0.73	0.59	449.62	0.18	0.09	18.01	58.13	12.04	39.40	4.94	466.00	0.53
		($\bar{x}$+e)/prim	9.36	7.40	9.56	81.63	13.15	27.68	5.35	10.90	3.82	7.88	9.67	10.43	8.59	5.20
		$\bar{x}$/prim	8.76	5.79	7.56	53.69	11.36	27.43	5.22	8.90	2.82	5.88	9.26	9.99	8.23	5.08
		($\bar{x}$-e)/prim	8.16	4.18	5.56	25.75	9.56	27.18	5.09	6.90	1.82	3.88	8.84	9.55	7.87	4.96
9	NS147		10.83	63.74	1.62	1.64	2419.89	11.89	4.00	7.51	438.76	1.60	556.44	77.50	7640.63	19.80
9	NS80		42.43	279.44	1.61	1.63	13784.64	11.87	4.02	20.04	375.93	0.17	578.26	79.38	8015.32	20.43
9	NS82		21.72	156.82	1.60	1.62	6811.38	13.18	3.96	7.37	99.16	3.89	661.18	86.32	8683.76	20.95
9	NS86		16.80	111.29	1.61	1.63	4956.00	11.03	3.93	7.40	144.56	3.91	530.25	80.01	7745.54	21.19
9	NS90		29.35	121.65	1.61	1.63	7392.49	11.10	0.01	0.19	300.53	0.43	534.61	80.58	7985.34	21.47
9	NS92		50.82	200.83	1.60	1.62	12676.39	9.51	3.94	0.27	214.17	1.17	484.43	71.30	6930.22	17.38
9	NS93		23.14	86.45	1.63	1.65	5458.24	10.28	3.91	1.15	349.36	0.68	525.89	73.17	7349.87	18.65
9	NS96		18.22	76.10	1.57	1.59	4819.02	10.00	3.80	7.24	170.33	1.32	471.33	73.37	7032.13	19.08
9	NS97		35.77	155.61	1.57	1.58	10227.45	9.85	3.77	7.19	86.83	3.80	493.15	67.16	6726.39	17.76
9	NS98		44.71	222.05	1.59	1.60	14726.86	14.12	3.69	20.55	112.65	9.56	621.90	92.29	9220.31	21.14
9	NS100		30.13	126.22	1.59	1.61	7417.39	9.41	3.87	7.35	278.29	0.65	480.06	70.50	6975.18	18.92
9	NS102		48.25	206.88	1.57	1.58	12585.07	11.30	3.79	0.93	117.83	9.74	545.52	79.49	7562.69	19.52
9	NS103		44.79	184.03	1.62	1.64	11177.97	12.05	3.88	20.05	176.33	11.76	643.72	89.01	8839.63	22.78
9	NS107		24.54	141.62	1.58	1.56	8446.78	10.07	3.86	2.27	270.21	1.14	506.25	74.10	7131.05	19.58
9	NS109		7.63	57.48	0.41	1.62	2291.21	10.27	3.94	7.41	536.61	3.91	517.16	77.35	7556.70	20.33
9	NS112		8.19	57.57	0.06	1.67	2901.37	12.65	3.93	7.44	91.84	0.53	691.73	86.70	8500.91	25.47
9	NS115		9.51	37.72	1.60	1.62	1701.81	14.23	3.77	2.48	285.99	8.81	678.63	90.72	9007.49	21.72
9	NS121		14.55	74.71	1.61	1.63	3768.88	10.50	4.00	7.52	85.06	3.97	486.61	72.93	7424.81	19.68
9	NS142		5.60	21.74	1.63	1.65	664.12	13.72	3.81	1.90	268.64	3.79	650.27	88.40	8357.03	19.69
9	NS149		7.89	83.01	1.55	1.57	3013.44	10.62	4.06	7.48	104.21	0.46	388.41	67.45	6741.38	16.75

UNIT	NO.		Rb	Ba	Th	U	K	Nb	La	Ce	Sr	Nd	P	Zr	Ti	Y
9	NS151		29.88	168.79	1.60	1.62	9305.98	15.27	3.79	21.47	169.12	10.38	731.00	94.34	9481.09	22.41
9	NS152		2.42	7.24	1.56	1.57	83.02	12.49	3.85	19.40	55.60	14.61	628.44	81.32	7880.43	21.45
9	NS154		5.50	30.69	0.52	0.03	1490.12	12.89	3.89	1.16	150.07	1.11	707.00	81.71	7679.59	20.82
9	NS157		28.35	151.78	1.58	1.59	11119.86	9.73	3.85	7.29	153.49	3.86	429.87	71.47	7571.68	16.24
9	NS161		16.66	91.26	1.52	1.53	5221.64	13.24	3.59	6.67	74.95	7.64	665.54	98.89	9226.30	22.48
9	NS193		28.70	163.57	3.33	0.34	6823.83	9.43	3.82	7.24	277.94	3.83	425.51	65.94	6480.59	16.85
9	NS194		24.62	123.58	1.63	0.70	6039.34	10.82	4.24	7.78	336.58	0.53	453.88	73.89	7394.83	19.82
		$\bar{x}$	23.37	118.59	1.52	1.47	6567.56	11.54	3.74	7.95	212.04	4.20	558.78	79.46	7820.03	20.09
		s	14.30	67.33	0.55	0.41	4228.33	1.67	0.76	6.60	123.40	4.10	96.24	8.87	838.53	2.08
		e	5.50	25.90	0.21	0.16	1626.28	0.64	0.29	2.54	47.46	1.58	37.01	3.41	322.51	0.80
		($\bar{x}$+e)/prim	45.47	20.67	20.33	77.62	32.78	17.09	5.87	5.91	12.30	4.26	6.27	7.40	6.26	4.59
		$\bar{x}$/prim	36.81	16.97	17.85	70.07	26.27	16.19	5.45	4.48	10.05	3.10	5.88	7.09	6.02	4.42
		($\bar{x}$-e)/prim	28.14	13.26	15.38	62.52	19.77	15.28	5.02	3.05	7.80	1.93	5.49	6.79	5.77	4.24
10	NS123		3.76	145.53	1.59	1.60	83.02	7.35	3.88	7.42	185.46	3.92	333.86	57.65	5977.02	17.48
10	NS124		3.77	73.96	1.57	1.55	45.66	8.08	3.81	7.46	250.33	1.42	370.96	60.74	5947.04	16.55
10	NS126		16.20	36.26	1.58	1.60	2569.31	5.73	3.82	7.52	70.16	3.97	405.87	40.35	4307.41	11.30
10	NS127		26.95	41.36	1.58	1.60	4607.33	6.21	3.77	7.44	92.15	3.93	357.86	45.29	4328.39	12.10
10	NS128		36.23	84.60	1.50	0.42	6886.09	5.72	3.73	0.81	94.61	0.85	288.04	42.99	4199.50	10.48
10	NS129		14.95	6.96	1.57	3.42	1643.70	5.45	3.76	7.54	60.79	3.95	257.49	40.93	4064.61	10.78
10	NS130		39.97	89.48	0.24	1.58	6902.70	5.67	3.69	7.34	147.42	3.88	296.77	43.73	4256.45	11.14
10	NS132		20.85	379.71	1.59	1.61	7624.93	5.70	3.85	2.68	129.47	3.96	281.49	45.46	4370.35	13.21
10	NS134		13.33	84.75	1.56	1.58	2498.75	4.99	3.75	7.54	299.10	3.99	279.31	42.84	4475.27	11.65
10	NS135		14.03	54.64	1.57	1.59	2536.11	5.59	0.29	7.49	226.13	3.95	274.94	46.01	4577.18	12.14
10	NS136		13.41	59.40	1.58	1.60	2623.27	6.02	3.70	7.45	200.80	3.93	294.58	46.07	4565.19	13.20
10	NS138		5.72	29.89	1.59	1.61	369.42	6.26	3.83	7.59	231.85	0.06	309.86	51.39	5176.68	14.56
10	NS140		7.35	4.96	0.38	0.01	581.10	6.69	3.80	7.50	221.99	3.95	303.31	51.06	5248.62	14.96
		$\bar{x}$	16.66	83.96	1.38	1.52	2997.80	6.11	3.52	6.60	170.02	3.21	311.87	47.27	4730.29	13.05
		s	11.62	96.63	0.47	0.77	2691.77	0.84	0.97	2.19	76.25	1.41	43.21	6.25	647.93	2.24
		e	6.44	53.53	0.26	0.43	1491.29	0.46	0.54	1.21	42.25	0.78	23.94	3.46	358.96	1.24
		($\bar{x}$+e)/prim	36.37	19.67	19.29	92.79	17.96	9.23	5.90	4.40	10.06	2.95	3.53	4.53	3.91	3.14
		$\bar{x}$/prim	26.23	12.01	16.21	72.42	11.99	8.58	5.12	3.72	8.06	2.37	3.28	4.22	3.64	2.87
		($\bar{x}$-e)/prim	16.10	4.35	13.12	52.05	6.03	7.93	4.33	3.03	6.06	1.79	3.03	3.91	3.36	2.59
11	NSF/2.5		7.96	195.68	4.81	1.00	3254.19	42.92	34.92	72.32	775.25	40.29	2230.11	270.79	21522.05	34.34
11	NSF/2.6		7.46	188.10	4.22	1.00	2656.48	42.10	28.56	66.19	863.41	38.05	2193.01	267.97	21147.36	34.21
11	NSF/2.7		9.23	236.99	4.94	1.00	3876.80	43.05	30.46	77.27	786.45	46.60	2267.20	270.04	21812.81	34.93
11	NSF/2.8		14.32	219.42	3.47	1.00	4951.84	41.92	30.77	70.63	696.22	41.17	2297.75	270.77	20991.49	33.20
		$\bar{x}$	9.74	210.05	4.36	1.00	3684.83	42.50	31.18	71.60	780.33	41.53	2247.02	269.90	21368.43	34.17
		s	3.14	22.37	0.67	0.00	980.67	0.57	2.68	4.58	68.41	3.63	45.40	1.33	370.60	0.72
		e	3.14	22.37	0.67	0.00	980.67	0.57	2.68	4.58	68.41	3.63	45.40	1.33	370.60	0.72
		($\bar{x}$+e)/prim	20.30	33.26	59.18	47.62	18.66	60.41	49.29	42.92	40.22	33.35	24.13	24.22	16.72	7.67
		$\bar{x}$/prim	15.35	30.05	51.31	47.62	14.74	59.61	45.38	40.34	36.98	30.67	23.65	24.10	16.44	7.51
		($\bar{x}$-e)/prim	10.40	26.85	43.44	47.62	10.82	58.81	41.48	37.76	33.74	27.99	23.17	23.98	16.15	7.35
primitive mantle			0.635	6.989	0.085	0.021	250	0.713	0.687	1.775	21.1	1.354	95	11.2	1300	4.55
N-type MORB			0.56	6.3	0.12	0.047	600	2.33	2.5	7.5	90	7.3	510	74	7600	28
E-type MORB			5.04	57	0.6	0.18	2100	8.3	6.3	15	155	9	620	73	6000	22
OIB			31	350	4	1.02	12000	48	37	80	660	38.5	2700	280	17200	29
N-type/prim			0.88	0.90	1.41	2.24	2.40	3.27	3.64	4.23	4.27	5.39	5.37	6.61	5.85	6.15
E-type/prim			7.94	8.16	7.06	8.57	8.40	11.64	9.17	8.45	7.35	6.65	6.53	6.52	4.62	4.84
OIB/prim			48.82	50.08	47.06	48.57	48.00	67.32	53.86	45.07	31.28	28.43	28.42	25.00	13.23	6.37

[Sun and McDonough (1989)] Elements in parts per million.
$\bar{x}$ = average, s = standard deviation, e = standard error, prim = primitive mantle composition

Table 6 (cont.)

Unit	2	2	2	2	2	2	2	3	3	3	3	5
SiO_2	68.48	68.88	68.01	68.55	68.43	68.29	68.61	70.74	70.42	70.64	70.22	64.76
TiO_2	0.00	0.00	0.00	0.00	0.00	0.00	0.00	0.00	0.00	0.00	0.00	0.00
Al_2O_3	20.32	20.30	20.43	20.47	20.31	20.17	20.48	20.70	20.81	20.37	20.38	18.98
Cr_2O_3	0.00	0.00	0.00	0.00	0.00	0.00	0.00	0.00	0.00	0.00	0.00	0.00
Fe_2O_3	0.00	0.00	0.00	0.00	0.00	0.00	0.00	0.00	0.00	0.00	0.00	0.00
FeO	0.19	0.12	0.46	0.23	0.31	0.09	0.22	0.16	0.36	0.21	0.00	0.24
MnO	0.00	0.00	0.00	0.00	0.00	0.00	0.00	0.00	0.00	0.00	0.00	0.00
MgO	0.00	0.00	0.12	0.00	0.08	0.00	0.00	0.00	0.10	0.08	0.00	0.00
CaO	0.07	0.00	0.00	0.00	0.00	0.00	0.00	0.15	0.20	0.05	0.13	0.15
Na_2O	11.02	10.93	10.82	10.95	11.04	11.13	11.25	11.48	10.66	11.17	11.36	0.37
K_2O	0.18	0.12	0.44	0.21	0.16	0.10	0.10	0.08	0.37	0.24	0.05	15.25
H_2O	0.00	0.00	0.00	0.00	0.00	0.00	0.00	0.00	0.00	0.00	0.00	0.00
H_2O-	0.00	0.00	0.00	0.00	0.00	0.00	0.00	0.00	0.00	0.00	0.00	0.00
TOTAL	100.26	100.35	100.28	100.41	100.33	99.78	100.66	103.31	102.92	102.76	102.14	99.75
Si	11.92	11.95	11.86	11.91	11.90	11.93	11.89	11.94	11.93	11.98	11.97	11.94
Ti	0.00	0.00	0.00	0.00	0.00	0.00	0.00	0.00	0.00	0.00	0.00	0.00
Al	4.17	4.15	4.20	4.19	4.16	4.15	4.18	4.12	4.16	4.07	4.10	4.13
Fe^{+2}	0.03	0.02	0.07	0.03	0.05	0.01	0.03	0.02	0.05	0.03	0.00	0.04
Mg	0.00	0.00	0.03	0.00	0.02	0.00	0.00	0.00	0.03	0.02	0.00	0.00
Ca	0.01	0.00	0.00	0.00	0.00	0.00	0.00	0.03	0.04	0.01	0.02	0.03
Na	3.72	3.68	3.66	3.69	3.72	3.77	3.78	3.76	3.50	3.67	3.76	0.13
K	0.04	0.03	0.10	0.05	0.04	0.02	0.02	0.02	0.08	0.05	0.01	3.59
TOTAL	19.88	19.82	19.92	19.86	19.89	19.89	19.91	19.89	19.78	19.84	19.86	19.85
	NUMBER OF IONS ON THE BASIS OF 32 (O)											
AB	98.60	99.28	96.60	98.76	98.51	99.41	99.42	98.82	96.79	98.36	99.10	3.53
AN	0.35	0.00	0.82	0.00	0.55	0.00	0.00	0.44	2.20	1.37	0.26	0.79
OR	1.06	0.72	2.58	1.24	0.94	0.59	0.58	0.73	1.00	0.26	0.66	95.68

Mol.%

Unit	5	5	5	6	6	7	7	7	9	9	9
SiO_2	64.02	65.75	64.69	68.59	65.14	70.91	67.32	68.29	69.71	69.66	69.82
TiO_2	0.00	0.00	0.00	0.00	0.00	0.00	0.00	0.00	0.00	0.00	0.00
Al_2O_3	19.27	18.31	19.34	20.44	20.19	19.62	19.97	20.64	19.07	19.02	19.00
Cr_2O_3	0.00	0.00	0.00	0.00	0.00	0.00	0.00	0.00	0.00	0.00	0.00
Fe_2O_3	0.00	0.00	0.00	0.00	0.00	0.00	0.00	0.00	0.00	0.00	0.00
FeO	0.15	0.37	0.25	0.14	0.35	0.00	0.17	0.00	0.14	0.00	0.17
MnO	0.00	0.00	0.00	0.00	0.00	0.00	0.00	0.00	0.00	0.00	0.00
MgO	0.00	0.00	0.00	0.00	0.16	0.00	0.00	0.00	0.00	0.00	0.00
CaO	0.18	0.00	0.42	0.31	0.27	0.08	0.10	0.18	0.10	0.05	0.05
Na_2O	0.38	0.27	0.48	10.91	9.99	11.90	9.51	11.44	12.30	12.14	12.26
K_2O	15.24	14.52	15.14	0.08	0.60	0.08	2.91	0.07	0.06	0.20	0.07
H_2O	0.00	0.00	0.00	0.00	0.00	0.00	0.00	0.00	0.00	0.00	0.00
H_2O-	0.00	0.00	0.00	0.00	0.00	0.00	0.00	0.00	0.00	0.00	0.00
TOTAL	99.24	99.22	100.32	100.47	96.70	102.59	99.98	100.62	101.38	101.07	101.37
Si	11.88	12.11	11.87	11.90	11.79	12.06	11.88	11.85	12.04	12.06	12.05
Ti	0.00	0.00	0.00	0.00	0.00	0.00	0.00	0.00	0.00	0.00	0.00
Al	4.21	3.98	4.18	4.18	4.31	3.93	4.15	4.22	3.88	3.88	3.87
Fe^{+2}	0.02	0.06	0.04	0.02	0.05	0.00	0.03	0.00	0.02	0.00	0.02
Mg	0.00	0.00	0.00	0.00	0.04	0.00	0.00	0.00	0.00	0.00	0.00
Ca	0.04	0.00	0.08	0.06	0.05	0.01	0.02	0.03	0.02	0.01	0.01
Na	0.14	0.10	0.17	3.67	3.50	3.92	3.26	3.85	4.12	4.07	4.10
K	3.61	3.41	3.54	0.02	0.14	0.02	0.66	0.02	0.01	0.04	0.02
TOTAL	19.89	19.65	19.89	19.85	19.88	19.95	19.99	19.97	20.09	20.06	20.07
AB	3.62	2.75	4.50	97.99	93.75	99.17	99.20	99.25	99.23	98.72	99.40
AN	0.95	0.00	2.17	1.54	2.55	0.45	0.40	0.35	0.33	1.04	0.39
OR	95.43	97.25	93.32	0.47	3.70	0.38	0.40	0.45	0.44	0.24	0.21

Table 7. Feldspar mineral chemistry of greenstone units.

Unit	1	1	1	1	1	1	2	2	2	2	2	3
Analysis	1.00	2.00	3.00	4.00	5.00	6.00	1.00	2.00	3.00	4.00	5.00	1.00
SiO_2	26.51	27.21	27.16	27.29	26.94	27.05	25.94	25.92	25.86	25.84	26.18	29.97
TiO_2	0.08	0.00	0.00	0.00	0.00	0.00	0.00	0.00	0.00	0.00	0.11	0.00
Al_2O_3	20.26	20.71	20.75	20.76	21.03	20.98	20.23	20.20	20.53	20.60	20.10	18.50
Fe_2O_3	0.00	0.00	0.00	0.00	0.00	0.00	0.00	0.00	0.00	0.00	0.00	0.00
FeO	25.36	23.55	23.94	23.33	23.88	24.15	29.91	30.01	30.13	29.14	28.80	17.74
MnO	0.00	0.15	0.00	0.00	0.00	0.00	0.12	0.09	0.18	0.13	0.15	0.28
MgO	16.54	19.08	18.24	18.58	17.96	18.02	13.81	13.59	13.65	14.06	13.87	24.33
CaO	0.00	0.00	0.00	0.08	0.05	0.00	0.00	0.00	0.00	0.00	0.00	0.16
Na_2O	0.00	0.00	0.00	0.00	0.00	0.00	0.00	0.00	0.00	0.00	0.00	0.00
K_2O	0.00	0.00	0.00	0.00	0.00	0.00	0.00	0.00	0.00	0.00	0.00	0.00
H_2O	11.52	11.63	11.62	11.65	11.62	11.61	11.26	11.26	11.25	11.30	11.32	11.95
F	0.00	0.00	0.00	0.00	0.00	0.00	0.00	0.00	0.00	0.00	0.00	0.00
Cl	0.00	0.00	0.00	0.00	0.00	0.00	0.00	0.00	0.00	0.00	0.00	0.00
O=F	0.00	0.00	0.00	0.00	0.00	0.00	0.00	0.00	0.00	0.00	0.00	0.00
O=Cl	0.00	0.00	0.00	0.00	0.00	0.00	0.00	0.00	0.00	0.00	0.00	0.00
Total	100.27	102.33	101.71	101.69	101.48	101.81	101.27	101.07	101.60	101.07	100.53	102.93
Si^{+4}	2.75	2.73	2.75	2.76	2.74	2.74	2.72	2.73	2.71	2.71	2.76	2.91
Al^{+4}	1.25	1.27	1.25	1.24	1.26	1.26	1.28	1.27	1.29	1.29	1.24	1.09
T site	4.00	4.00	4.00	4.00	4.00	4.00	4.00	4.00	4.00	4.00	4.00	4.00
Al^{+6}	1.23	1.19	1.23	1.23	1.25	1.24	1.23	1.24	1.24	1.25	1.25	1.03
Ti	0.01	0.00	0.00	0.00	0.00	0.00	0.00	0.00	0.00	0.00	0.01	0.00
Fe^{+3}	0.00	0.00	0.00	0.00	0.00	0.00	0.00	0.00	0.00	0.00	0.00	0.00
Fe^{+2}	2.20	1.98	2.03	1.97	2.03	2.05	2.63	2.64	2.64	2.55	2.54	1.44
Mn^{+2}	0.00	0.01	0.00	0.00	0.00	0.00	0.01	0.01	0.02	0.01	0.01	0.02
Mg	2.56	2.86	2.75	2.80	2.72	2.72	2.16	2.13	2.13	2.20	2.18	3.52
Ca	0.00	0.00	0.00	0.01	0.01	0.00	0.00	0.00	0.00	0.00	0.00	0.02
Na	0.00	0.00	0.00	0.00	0.00	0.00	0.00	0.00	0.00	0.00	0.00	0.00
K	0.00	0.00	0.00	0.00	0.00	0.00	0.00	0.00	0.00	0.00	0.00	0.00
O site	6.00	6.04	6.01	6.01	6.01	6.01	6.02	6.02	6.03	6.02	5.99	6.03
O	10.00	10.00	10.00	10.00	10.00	10.00	10.00	10.00	10.00	10.00	10.00	10.00
OH	8.00	8.00	8.00	8.00	8.00	8.00	8.00	8.00	8.00	8.00	8.00	8.00
F	0.00	0.00	0.00	0.00	0.00	0.00	0.00	0.00	0.00	0.00	0.00	0.00
Cl	0.00	0.00	0.00	0.00	0.00	0.00	0.00	0.00	0.00	0.00	0.00	0.00
Charge	14	14	14	14	14	14	14	14	14	14	14	14

Table 8. Chlorite mineral chemistry of greenstone units.

Unit	4	4	4	4	4	4	6	6	6	7	7	7
Analysis	1.00	2.00	3.00	4.00	5.00	6.00	1.00	2.00	3.00	1.00	2.00	3.00
SiO_2	28.27	28.62	28.92	28.36	29.02	28.88	28.84	28.96	29.38	28.10	28.78	28.87
TiO_2	0.08	0.00	0.00	0.00	0.00	0.00	0.00	0.00	0.00	0.00	0.00	0.00
Al_2O_3	19.14	19.08	18.56	18.80	18.91	18.87	20.22	19.98	19.94	19.11	19.54	19.47
Fe_2O_3	0.00	0.00	0.00	0.00	0.00	0.00	0.00	0.00	0.00	0.00	0.00	0.00
FeO	15.69	14.96	15.10	14.94	15.30	14.77	14.57	14.58	11.83	15.09	15.55	15.98
MnO	0.35	0.35	0.32	0.35	0.34	0.25	0.13	0.15	0.33	0.43	0.37	0.39
MgO	24.78	25.01	24.28	24.90	25.65	24.87	26.13	26.12	25.82	24.87	24.74	25.38
CaO	0.11	0.09	0.07	0.05	0.08	0.09	0.06	0.05	0.00	0.00	0.00	0.00
Na_2O	0.00	0.00	0.00	0.00	0.00	0.00	0.00	0.00	0.05	0.00	0.00	0.00
K_2O	0.00	0.00	0.00	0.00	0.00	0.11	0.00	0.00	0.00	0.00	0.00	0.00
H_2O	12.02	12.07	12.07	12.06	12.05	12.08	12.11	12.11	12.28	12.05	12.05	12.02
F	0.00	0.00	0.00	0.00	0.00	0.00	0.00	0.00	0.00	0.00	0.00	0.00
Cl	0.00	0.00	0.00	0.00	0.00	0.00	0.00	0.00	0.00	0.00	0.00	0.00
O=F	0.00	0.00	0.00	0.00	0.00	0.00	0.00	0.00	0.00	0.00	0.00	0.00
O=Cl	0.00	0.00	0.00	0.00	0.00	0.00	0.00	0.00	0.00	0.00	0.00	0.00
Total	100.44	100.18	99.32	99.46	101.35	99.92	102.06	101.95	99.63	99.65	101.03	102.11
Si^{+4}	2.81	2.84	2.90	2.84	2.84	2.87	2.79	2.80	2.88	2.81	2.83	2.81
Al^{+4}	1.19	1.16	1.10	1.16	1.16	1.13	1.21	1.20	1.12	1.19	1.17	1.19
T site	4.00	4.00	4.00	4.00	4.00	4.00	4.00	4.00	4.00	4.00	4.00	4.00
Al^{+6}	1.05	1.07	1.09	1.05	1.03	1.08	1.09	1.09	1.19	1.06	1.10	1.05
Ti	0.01	0.00	0.00	0.00	0.00	0.00	0.00	0.00	0.00	0.00	0.00	0.00
Fe^{+3}	0.00	0.00	0.00	0.00	0.00	0.00	0.00	0.00	0.00	0.00	0.00	0.00
Fe^{+2}	1.30	1.24	1.26	1.25	1.25	1.23	1.18	1.18	0.97	1.26	1.28	1.30
Mn^{+2}	0.03	0.03	0.03	0.03	0.03	0.02	0.01	0.01	0.03	0.04	0.03	0.03
Mg	3.67	3.70	3.62	3.71	3.75	3.68	3.77	3.77	3.78	3.71	3.63	3.69
Ca	0.01	0.01	0.01	0.01	0.01	0.01	0.01	0.01	0.00	0.00	0.00	0.00
Na	0.00	0.00	0.00	0.00	0.00	0.00	0.00	0.00	0.01	0.00	0.00	0.00
K	0.00	0.00	0.00	0.00	0.00	0.01	0.00	0.00	0.00	0.00	0.00	0.00
O site	6.07	6.05	6.01	6.05	6.06	6.03	6.06	6.05	5.97	6.07	6.04	6.07
O	10.00	10.00	10.00	10.00	10.00	10.00	10.00	10.00	10.00	10.00	10.00	10.00
OH	8.00	8.00	8.00	8.00	8.00	8.00	8.00	8.00	8.00	8.00	8.00	8.00
F	0.00	0.00	0.00	0.00	0.00	0.00	0.00	0.00	0.00	0.00	0.00	0.00
Cl	0.00	0.00	0.00	0.00	0.00	0.00	0.00	0.00	0.00	0.00	0.00	0.00
Charge	14	14	14	14	14	14	14	14	14	14	14	14

Table 8 (cont.)

Unit	8	8	9	9	9	9	9	11	11	11
Analysis	1.00	2.00	1.00	2.00	3.00	4.00	5.00	1.00	2.00	3.00
SiO_2	28.71	28.31	28.42	27.10	28.56	28.77	28.81	27.20	26.28	26.35
TiO_2	0.00	0.00	0.00	0.00	0.00	0.00	0.00	0.00	0.00	0.00
Al_2O_3	19.81	19.67	19.79	19.21	20.08	19.65	19.50	18.17	18.50	19.56
Fe_2O_3	0.00	0.00	0.00	0.00	0.00	0.00	0.00	0.00	0.00	0.00
FeO	10.75	10.37	15.38	14.29	15.06	15.18	15.03	27.39	27.77	28.33
MnO	0.28	0.26	0.35	0.30	0.31	0.29	0.31	0.36	0.30	0.41
MgO	27.06	27.30	25.32	23.89	25.17	25.51	24.90	16.90	16.10	16.10
CaO	0.00	0.00	0.06	0.09	0.06	0.13	0.21	0.08	0.08	0.11
Na_2O	0.00	0.00	0.00	0.00	0.00	0.00	0.00	0.00	0.00	0.00
K_2O	0.00	0.00	0.00	0.00	0.00	0.00	0.00	0.04	0.00	0.00
H_2O	12.32	12.33	12.05	12.08	12.08	12.06	12.07	11.37	11.33	11.32
F	0.00	0.00	0.00	0.00	0.00	0.00	0.00	0.00	0.00	0.00
Cl	0.00	0.00	0.00	0.00	0.00	0.00	0.00	0.00	0.00	0.00
O=F	0.00	0.00	0.00	0.00	0.00	0.00	0.00	0.00	0.00	0.00
O=Cl	0.00	0.00	0.00	0.00	0.00	0.00	0.00	0.00	0.00	0.00
Total	98.93	98.24	101.37	96.96	101.32	101.59	100.83	101.51	100.36	102.18
Si^{+4}	2.83	2.81	2.79	2.79	2.79	2.81	2.84	2.82	2.77	2.72
Al^{+4}	1.17	1.19	1.21	1.21	1.21	1.19	1.16	1.18	1.23	1.28
T site	4.00	4.00	4.00	4.00	4.00	4.00	4.00	4.00	4.00	4.00
Al^{+6}	1.13	1.11	1.07	1.12	1.11	1.07	1.10	1.04	1.07	1.11
Ti	0.00	0.00	0.00	0.00	0.00	0.00	0.00	0.00	0.00	0.00
Fe^{+3}	0.00	0.00	0.00	0.00	0.00	0.00	0.00	0.00	0.00	0.00
Fe^{+2}	0.89	0.86	1.26	1.23	1.23	1.24	1.24	2.37	2.45	2.45
Mn^{+2}	0.02	0.02	0.03	0.03	0.03	0.02	0.03	0.03	0.03	0.04
Mg	3.98	4.04	3.70	3.66	3.67	3.71	3.65	2.61	2.53	2.48
Ca	0.00	0.00	0.01	0.01	0.01	0.01	0.02	0.01	0.01	0.01
Na	0.00	0.00	0.00	0.00	0.00	0.00	0.00	0.00	0.00	0.00
K	0.00	0.00	0.00	0.00	0.00	0.00	0.00	0.01	0.00	0.00
O site	6.02	6.04	6.07	6.05	6.05	6.06	6.03	6.07	6.08	6.08
O	10.00	10.00	10.00	10.00	10.00	10.00	10.00	10.00	10.00	10.00
OH	8.00	8.00	8.00	8.00	8.00	8.00	8.00	8.00	8.00	8.00
F	0.00	0.00	0.00	0.00	0.00	0.00	0.00	0.00	0.00	0.00
Cl	0.00	0.00	0.00	0.00	0.00	0.00	0.00	0.00	0.00	0.00
Charge	14	14	14	14	14	14	14	14	14	14

Table 8 (cont.)

Unit	3	6	6	6	7	7	7	7
SiO_2	55.11	57.78	57.89	57.49	56.67	56.35	56.08	54.88
TiO_2	0.00	0.00	0.00	0.00	0.00	0.00	0.07	0.00
Al_2O_3	2.15	0.51	0.51	0.87	0.74	0.89	0.97	3.89
Cr_2O_3	0.00	0.00	0.00	0.00	0.13	0.00	0.58	0.00
Fe_2O_3	0.00	0.00	0.00	0.00	0.00	0.00	0.00	0.00
FeO	8.98	5.89	5.81	5.86	7.83	8.07	8.78	6.64
MnO	0.30	0.23	0.29	0.28	0.27	0.33	0.29	0.25
MgO	19.22	20.62	21.02	20.41	19.96	20.32	19.36	17.78
CaO	11.98	13.06	13.17	13.35	12.95	12.99	12.32	11.64
Na_2O	0.85	0.34	0.43	0.31	0.33	0.35	0.82	1.12
K_2O	0.11	0.00	0.00	0.00	0.05	0.24	0.08	0.09
H_2O	2.14	2.17	2.19	2.17	2.16	2.16	2.15	2.12
F	0.00	0.00	0.00	0.00	0.00	0.00	0.00	0.00
Cl	0.00	0.00	0.00	0.00	0.00	0.00	0.00	0.00
O=F	0.00	0.00	0.00	0.00	0.00	0.00	0.00	0.00
O=Cl	0.00	0.00	0.00	0.00	0.00	0.00	0.00	0.00
Total	100.84	100.60	101.31	100.74	101.09	101.70	101.50	98.41
Si^{+4}	7.72	7.97	7.94	7.93	7.87	7.81	7.81	7.77
Al^{+4}	0.28	0.03	0.06	0.07	0.12	0.15	0.16	0.23
Fe^{+3}	0.00	0.00	0.00	0.00	0.00	0.00	0.00	0.00
Ti^{+4}	0.00	0.00	0.00	0.00	0.00	0.00	0.01	0.00
T site	8.00	8.00	8.00	8.00	7.99	7.95	7.98	8.00
Al^{+6}	0.08	0.06	0.02	0.07	0.00	0.00	0.00	0.42
Fe^{+3}	0.00	0.00	0.00	0.00	0.00	0.00	0.00	0.00
Ti	0.00	0.00	0.00	0.00	0.00	0.00	0.00	0.00
Cr	0.00	0.00	0.00	0.00	0.01	0.00	0.06	0.00
Mg	4.01	4.24	4.30	4.20	4.13	4.20	4.02	3.75
Fe^{+2}	0.91	0.68	0.67	0.68	0.85	0.80	0.92	0.79
Zn	0.00	0.00	0.00	0.00	0.00	0.00	0.00	0.00
Mn	0.00	0.02	0.01	0.03	0.00	0.00	0.00	0.03
Ca(1)	0.00	0.00	0.00	0.02	0.00	0.00	0.00	0.02
M1	5.00	5.00	5.00	5.00	5.00	5.00	5.00	5.00
M2	0.00	0.00	0.00	0.00	0.00	0.00	0.00	0.00
M3	0.14	0.00	0.00	0.00	0.06	0.13	0.11	0.00
Mg	0.00	0.00	0.00	0.00	0.00	0.00	0.00	0.00
Fe^{+2}	0.04	0.01	0.02	0.00	0.03	0.04	0.03	0.00
Zn	1.80	1.93	1.94	1.97	1.91	1.83	1.84	1.76
Mn	0.02	0.06	0.04	0.03	0.00	0.00	0.02	0.24
Ca(2)	2.00	2.00	2.00	2.00	2.00	2.00	2.00	2.00
Na(1)	0.00	0.00	0.00	-0.02	0.02	0.10	0.00	-0.02
M4 site	0.21	0.03	0.07	0.06	0.09	0.09	0.20	0.07
Ca(3)	0.02	0.00	0.00	0.00	0.01	0.04	0.01	0.02
Na(2)	0.23	0.03	0.07	0.04	0.11	0.24	0.21	0.07
K	22.00	22.00	22.00	22.00	22.00	22.00	22.00	22.00
A site	2.00	2.00	2.00	2.00	2.00	2.00	2.00	2.00

NUMBER OF IONS ON THE BASIS OF 13 (Si, Al, Fe^{+2}, Mn, Ti, Mg)

Table 9. Amphibole mineral chemistry of greenstone units.

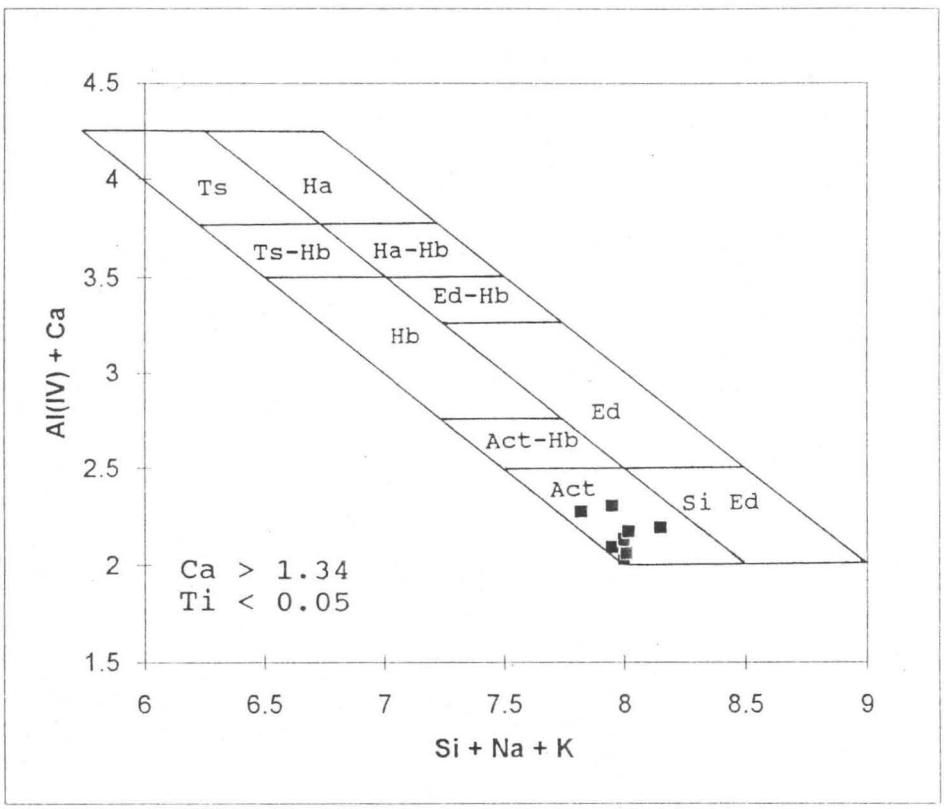

Ts: tschermakite; Ha: ferro- and magnesiohastingsite;
Ed: edenite; Hb: Fe- and Mg-hornblende; Act: actinolite

Figure 4. Amphibole classification diagram (Giret et al., 1980).

Unit	3	3	3	3	6	6	6	6	6	7	7	7	7	7
SiO_2	32.63	33.22	33.02	34.26	36.92	37.00	33.12	35.02	34.35	37.04	36.94	36.25	36.58	36.62
TiO_2	0.00	0.00	0.00	0.00	0.05	0.16	0.06	0.05	0.00	0.16	0.12	0.00	0.21	0.12
Al_2O_3	16.24	16.82	16.79	19.19	21.10	20.94	18.20	19.72	19.47	21.34	21.89	21.02	21.63	22.18
Fe_2O_3	18.76	17.97	18.57	16.05	16.82	15.70	16.53	15.37	15.69	14.32	13.50	13.94	13.45	12.99
Mn_2O_3	0.00	0.00	0.00	0.00	0.00	0.00	0.00	0.00	0.00	0.00	0.00	0.00	0.00	0.00
FeO	0.03	0.04	0.03	0.04	0.04	0.00	0.04	0.04	0.04	2.30	2.55	2.80	2.03	2.83
MnO	0.29	0.36	0.32	0.85	0.26	0.26	0.31	0.27	0.31	0.00	0.55	0.19	0.16	0.68
CaO	16.23	17.21	16.97	17.45	21.67	21.90	16.60	19.65	18.97	23.75	23.03	22.65	23.69	23.04
Na_2O	0.00	0.00	0.00	0.00	0.00	0.00	0.00	0.00	0.05	0.00	0.00	0.00	0.00	0.00
H2O	1.59	1.62	1.62	1.67	1.84	1.83	1.62	1.72	1.69	3.42	3.32	3.33	3.30	3.27
Total	85.77	87.24	87.32	89.51	98.69	97.79	86.47	91.84	90.57	102.33	101.90	100.18	101.05	101.73
Si^{+4}	3.07	3.07	3.05	3.06	3.00	3.03	3.06	3.05	3.03	3.08	3.07	3.08	3.07	3.05
Al^{+4}	0.00	0.00	0.00	0.00	0.00	0.00	0.00	0.00	0.00	0.00	0.00	0.00	0.00	0.00
Z site	3.07	3.07	3.05	3.06	3.00	3.03	3.06	3.05	3.03	3.08	3.07	3.08	3.07	3.05
Al^{+6}	1.80	1.83	1.83	2.02	2.02	2.02	1.98	2.02	2.03	2.09	2.15	2.11	2.14	2.18
Fe^{+3}	1.33	1.25	1.29	1.08	1.03	0.97	1.15	1.01	1.04	0.90	0.85	0.89	0.85	0.81
Mn^{+3}	0.00	0.00	0.00	0.00	0.00	0.00	0.00	0.00	0.00	0.00	0.00	0.00	0.00	0.00
Ti	0.00	0.00	0.00	0.00	0.00	0.01	0.00	0.00	0.00	0.01	0.01	0.00	0.01	0.01
Fe^{+2}	0.00	0.00	0.00	0.00	0.00	0.00	0.00	0.00	0.00	0.16	0.18	0.20	0.14	0.20
Mn^{+2}	0.01	0.01	0.01	0.03	0.01	0.01	0.01	0.01	0.01	0.00	0.04	0.01	0.01	0.05
Y site	3.14	3.10	3.14	3.13	3.07	3.01	3.15	3.04	3.08	3.16	3.22	3.21	3.15	3.24
Mn^{+3}	0.00	0.00	0.00	0.00	0.00	0.00	0.00	0.00	0.00	0.00	0.00	0.00	0.00	0.00
Mn^{+2}	0.01	0.01	0.01	0.03	0.01	0.01	0.01	0.01	0.01	0.00	0.00	0.00	0.00	0.00
Fe^{+2}	0.00	0.00	0.00	0.00	0.00	0.00	0.00	0.00	0.00	0.00	0.00	0.00	0.00	0.00
Ca	1.64	1.70	1.68	1.67	1.89	1.92	1.64	1.83	1.80	2.12	2.05	2.06	2.13	2.06
Na	0.00	0.00	0.00	0.00	0.00	0.00	0.00	0.00	0.01	0.00	0.00	0.00	0.00	0.00
X site	1.65	1.72	1.70	1.70	1.90	1.93	1.66	1.84	1.82	2.12	2.05	2.07	2.13	2.06
O	12.00	12.00	12.00	12.00	12.00	12.00	12.00	12.00	12.00	12.00	12.00	12.00	12.00	12.00
OH	1.00	1.00	1.00	1.00	1.00	1.00	1.00	1.00	1.00	1.90	1.85	1.89	1.85	1.81
Total	20.86	20.88	20.88	20.89	20.96	20.97	20.86	20.93	20.93	22.26	22.19	22.25	22.20	22.17

Unit	7	7	7	7	7	7	7	9	9	9	9	9	9	9
SiO_2	36.61	36.76	37.51	36.62	37.02	34.73	33.36	37.12	36.77	36.62	36.92	36.97	37.14	36.90
TiO_2	0.15	0.00	0.24	0.00	0.27	0.00	0.00	0.13	0.00	0.00	0.08	0.00	0.00	0.00
Al_2O_3	21.48	21.39	21.32	21.27	21.43	20.66	19.33	22.22	22.06	22.18	22.06	22.52	22.84	22.49
Fe_2O_3	13.91	14.33	16.56	14.22	14.11	15.00	15.08	13.53	13.41	13.24	13.49	13.06	12.76	12.99
Mn_2O_3	0.00	0.00	0.00	0.00	0.00	0.00	0.00	0.00	0.00	0.00	0.00	0.00	0.00	0.00
FeO	2.85	3.06	0.00	2.38	2.62	0.03	0.04	2.73	2.68	2.93	2.65	2.60	2.88	2.84
MnO	0.00	0.13	0.17	0.00	0.18	0.19	0.24	0.00	0.18	0.00	0.18	0.13	0.20	0.15
CaO	23.61	23.50	23.54	23.81	23.36	19.95	18.44	24.04	23.66	23.87	23.71	23.95	23.63	23.65
Na_2O	0.00	0.00	0.00	0.00	0.00	0.00	0.06	0.00	0.00	0.00	0.00	0.00	0.00	0.00
H2O	3.36	3.41	1.88	3.39	3.39	1.73	1.65	3.35	3.32	3.30	3.33	3.29	3.26	3.28
Total	101.97	102.58	101.22	101.70	102.39	92.29	88.20	103.11	102.07	102.15	102.42	102.52	102.71	102.30
Si^{+4}	3.06	3.06	2.98	3.07	3.08	3.00	3.02	3.05	3.06	3.04	3.06	3.05	3.05	3.05
Al^{+4}	0.00	0.00	0.02	0.00	0.00	0.00	0.00	0.00	0.00	0.00	0.00	0.00	0.00	0.00
Z site	3.06	3.06	3.00	3.07	3.08	3.00	3.02	3.05	3.06	3.04	3.06	3.05	3.05	3.05
Al^{+6}	2.12	2.10	1.98	2.10	2.10	2.11	2.06	2.15	2.16	2.17	2.15	2.19	2.21	2.19
Fe^{+3}	0.87	0.90	0.99	0.90	0.88	0.98	1.03	0.84	0.84	0.83	0.84	0.81	0.79	0.81
Mn^{+3}	0.00	0.00	0.00	0.00	0.00	0.00	0.00	0.00	0.00	0.00	0.00	0.00	0.00	0.00
Ti	0.01	0.00	0.01	0.00	0.02	0.00	0.00	0.01	0.00	0.00	0.00	0.00	0.00	0.00
Fe^{+2}	0.20	0.21	0.00	0.17	0.18	0.00	0.00	0.19	0.19	0.20	0.18	0.18	0.20	0.20
Mn^{+2}	0.00	0.01	0.01	0.00	0.01	0.01	0.01	0.00	0.01	0.00	0.01	0.01	0.01	0.01
Y site	3.20	3.22	3.00	3.17	3.19	3.09	3.10	3.19	3.20	3.20	3.20	3.19	3.21	3.21
Mn^{+3}	0.00	0.00	0.00	0.00	0.00	0.00	0.00	0.00	0.00	0.00	0.00	0.00	0.00	0.00
Mn^{+2}	0.00	0.00	0.00	0.00	0.00	0.01	0.01	0.00	0.00	0.00	0.00	0.00	0.00	0.00
Fe^{+2}	0.00	0.00	0.00	0.00	0.00	0.00	0.00	0.00	0.00	0.00	0.00	0.00	0.00	0.00
Ca	2.11	2.10	2.01	2.14	2.08	1.85	1.79	2.12	2.11	2.12	2.10	2.12	2.08	2.10
Na	0.00	0.00	0.00	0.00	0.00	0.00	0.01	0.00	0.00	0.00	0.00	0.00	0.00	0.00
X site	2.12	2.10	2.01	2.14	2.08	1.86	1.81	2.12	2.11	2.13	2.11	2.12	2.08	2.10
O	12.00	12.00	12.00	12.00	12.00	12.00	12.00	12.00	12.00	12.00	12.00	12.00	12.00	12.00
OH	1.87	1.90	1.00	1.90	1.88	1.00	1.00	1.84	1.84	1.83	1.84	1.81	1.79	1.81
Total	22.25	22.28	21.01	22.28	22.24	20.95	20.93	22.20	22.20	22.20	22.20	22.17	22.13	22.16

Table 10. Epidote mineral chemistry of greenstone units.

Unit	9	9	10	10	11	11	11	11	11	11	11	11	11
SiO_2	36.91	37.08	35.66	38.53	37.34	37.20	36.36	36.78	37.36	36.50	36.84	36.73	36.42
TiO_2	0.12	0.16	0.20	0.00	0.09	0.00	0.00	0.00	0.00	0.00	0.00	0.00	0.14
Al_2O_3	22.14	22.54	22.04	19.08	23.02	24.06	24.12	23.35	23.78	23.77	24.57	24.55	22.03
Fe_2O_3	13.41	13.10	14.76	14.33	15.29	11.14	10.27	11.56	11.53	10.90	10.04	9.94	12.96
Mn_2O_3	0.00	0.00	0.00	0.00	0.00	0.00	0.00	0.00	0.00	0.00	0.00	0.00	0.00
FeO	3.03	2.81	0.03	0.00	0.04	2.86	3.28	2.86	2.69	2.96	2.86	2.83	2.80
MnO	0.00	0.14	0.00	0.00	0.26	0.21	0.20	0.31	0.27	0.34	0.00	0.16	0.13
CaO	23.68	23.98	15.72	14.78	22.96	23.51	23.00	23.06	23.35	23.25	23.40	23.22	23.39
Na_2O	0.00	0.00	0.00	0.17	0.00	0.00	0.00	0.00	0.00	0.00	0.00	0.00	0.00
H2O	3.32	3.30	1.72	1.71	1.89	3.09	2.97	3.11	3.13	3.04	2.96	2.94	3.25
Total	102.61	103.12	90.13	88.60	100.89	102.07	100.19	101.03	102.11	100.75	100.66	100.37	101.12
Si^{+4}	3.05	3.04	3.09	3.37	2.96	3.04	3.02	3.05	3.05	3.02	3.03	3.03	3.05
Al^{+4}	0.00	0.00	0.00	0.00	0.04	0.00	0.00	0.00	0.00	0.00	0.00	0.00	0.00
Z site	3.05	3.04	3.09	3.37	3.00	3.04	3.02	3.05	3.05	3.02	3.03	3.03	3.05
Al^{+6}	2.16	2.18	2.25	1.97	2.11	2.32	2.36	2.28	2.29	2.32	2.38	2.38	2.17
Fe^{+3}	0.83	0.81	0.96	0.94	0.91	0.68	0.64	0.72	0.71	0.68	0.62	0.62	0.82
Mn^{+3}	0.00	0.00	0.00	0.00	0.00	0.00	0.00	0.00	0.00	0.00	0.00	0.00	0.00
Ti	0.01	0.01	0.01	0.00	0.01	0.00	0.00	0.00	0.00	0.00	0.00	0.00	0.01
Fe^{+2}	0.21	0.19	0.00	0.00	0.00	0.20	0.23	0.20	0.18	0.20	0.20	0.19	0.20
Mn^{+2}	0.00	0.01	0.00	0.00	0.01	0.01	0.01	0.02	0.02	0.02	0.00	0.01	0.01
Y site	3.21	3.20	3.23	2.91	3.04	3.21	3.24	3.22	3.20	3.23	3.20	3.20	3.20
Mn^{+3}	0.00	0.00	0.00	0.00	0.00	0.00	0.00	0.00	0.00	0.00	0.00	0.00	0.00
Mn^{+2}	0.00	0.00	0.00	0.00	0.01	0.00	0.00	0.00	0.00	0.00	0.00	0.00	0.00
Fe^{+2}	0.00	0.00	0.00	0.00	0.00	0.00	0.00	0.00	0.00	0.00	0.00	0.00	0.00
Ca	2.10	2.11	1.46	1.38	1.95	2.06	2.04	2.05	2.04	2.06	2.06	2.05	2.10
Na	0.00	0.00	0.00	0.03	0.00	0.00	0.00	0.00	0.00	0.00	0.00	0.00	0.00
X site	2.10	2.11	1.46	1.41	1.96	2.06	2.05	2.05	2.05	2.06	2.06	2.05	2.10
O	12.00	12.00	12.00	12.00	12.00	12.00	12.00	12.00	12.00	12.00	12.00	12.00	12.00
OH	1.83	1.81	1.00	1.00	1.00	1.68	1.64	1.72	1.71	1.68	1.62	1.62	1.82
Total	22.19	22.17	20.78	20.69	21.00	21.99	21.94	22.03	22.01	22.00	21.90	21.90	22.17

Table 10 (cont.)

Unit	2	2	2	6	6
SiO_2	29.90	30.00	29.85	28.50	45.27
TiO_2	39.21	38.01	39.52	25.62	24.30
Al_2O_3	0.96	1.62	0.75	5.75	4.11
Cr_2O_3	0.00	0.00	0.00	0.28	0.00
Fe_2O_3	0.00	0.00	0.00	0.00	0.00
FeO	0.72	1.19	0.73	4.61	0.72
MnO	0.00	0.00	0.00	0.12	0.00
MgO	0.00	0.00	0.00	9.30	0.85
CaO	29.07	29.21	28.90	19.69	22.75
Na_2O	0.00	0.00	0.00	0.00	0.00
K_2O	0.00	0.00	0.00	0.00	0.00
TOTAL	99.86	100.03	99.75	93.87	98.00
Si	3.93	3.94	3.93	3.93	5.64
Ti	3.87	3.75	3.91	2.66	2.28
Al	0.15	0.25	0.12	0.94	0.60
Cr	0.00	0.00	0.00	0.03	0.00
Fe^{+3}	0.00	0.00	0.00	0.00	0.00
Fe^{+2}	0.08	0.13	0.08	0.53	0.08
Mn	0.00	0.00	0.00	0.01	0.00
Mg	0.00	0.00	0.00	1.91	0.16
Ca	4.09	4.11	4.07	2.91	3.04
Na	0.00	0.00	0.00	0.00	0.00
K	0.00	0.00	0.00	0.00	0.00
Total	12.12	12.18	12.11	12.93	11.79

NUMBER OF IONS ON THE BASIS OF 20 (O)

Table 11. Titanite mineral chemistry of greenstone units.

Unit	10	10	10	10	10
SiO_2	52.16	49.76	50.12	50.05	50.62
TiO_2	0.96	2.2	1.48	1.82	1.3
Al_2O_3	1.97	3.79	4.14	3.92	4.02
Cr_2O_3	0.29	0.11	0.15	0.15	0.43
Fe_2O_3	0	0	0	0	0
FeO	8.17	9.86	7.71	9.29	7.87
MnO	0.23	0.23	0	0.19	0.22
NiO	0	0	0	0	0
MgO	15.87	14.26	15.16	14.51	14.73
CaO	20.94	20.58	21.34	20.3	21.65
Na_2O	0.26	0.47	0.35	0.57	0.45
K_2O	0	0	0	0	0
Total	100.85	101.26	100.45	100.8	101.29
Si^{+4}	1.92	1.84	1.85	1.86	1.86
Al^{+4}	0.08	0.16	0.15	0.14	0.14
T site	2	2	2	2	2
Al^{+6}	0.01	0.01	0.03	0.03	0.04
Ti	0.03	0.06	0.04	0.05	0.04
Cr	0.01	0	0	0	0.01
Fe^{+3}	0	0	0	0	0
Fe^{+2}	0.25	0.31	0.24	0.29	0.24
Mn^{+2}	0.01	0.01	0	0.01	0.01
Ni	0	0	0	0	0
Mg	0.87	0.79	0.84	0.8	0.81
Ca	0.83	0.82	0.85	0.81	0.85
Na	0.02	0.03	0.03	0.04	0.03
K	0	0	0	0	0
M1	2.02	2.03	2.03	2.03	2.03
M2	6	6	6	6	6
O	0	0	0	0	0
Mg	0.87	0.79	0.84	0.8	0.81
Fe	0.26	0.32	0.24	0.3	0.25
Ca	0.83	0.82	0.85	0.81	0.85
Tot	1.96	1.93	1.93	1.91	1.91

Table 12. Pyroxene mineral chemistry of greenstone unit 10.

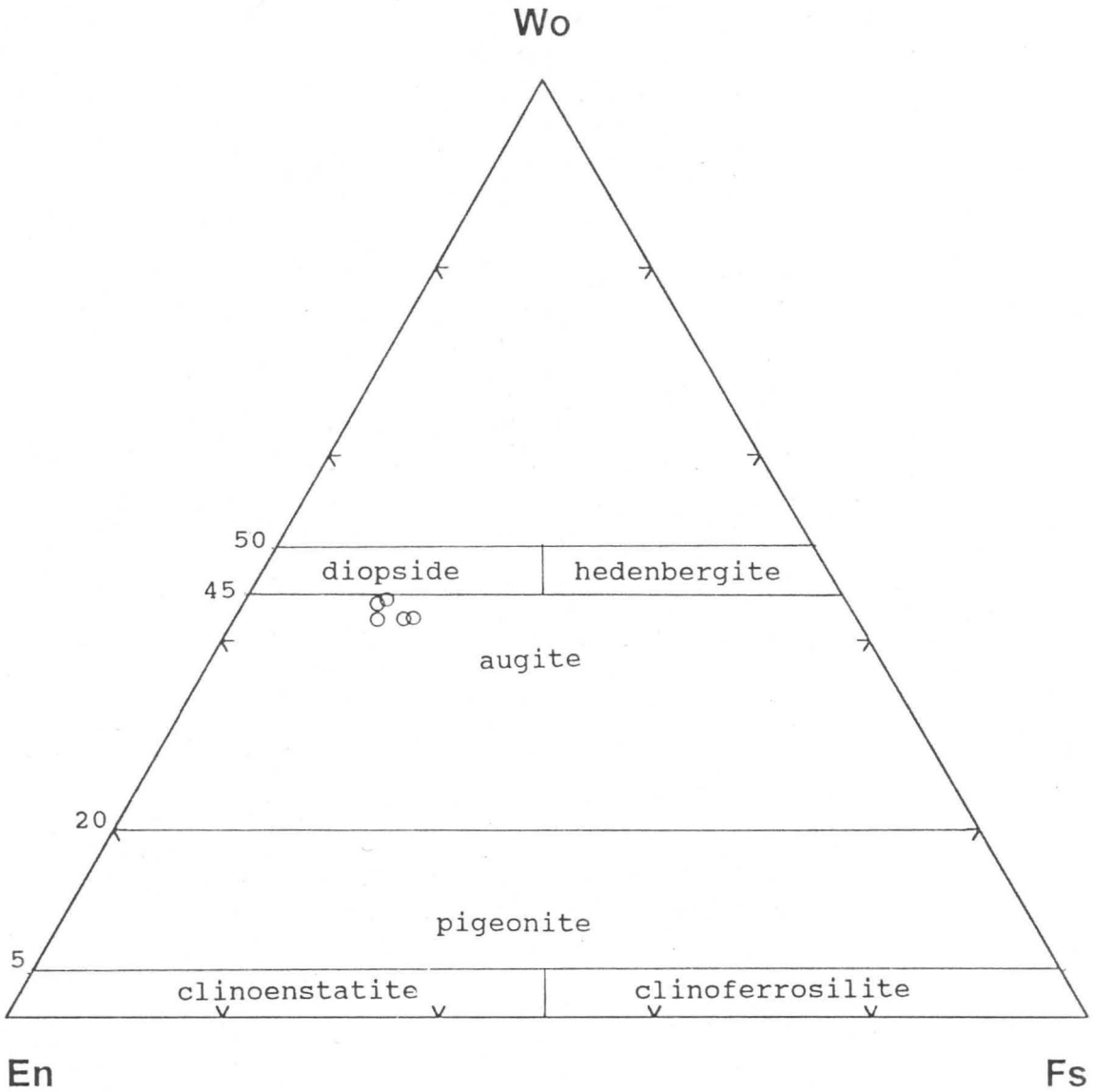

Figure 5. Ca-Mg-Fe clinopyroxene classification diagram (Morimoto, 1989).

	unit 5	unit 5	unit 5	unit 5	unit 5	unit 5	unit 5	unit 5	unit 5
Analysis	1	2	3	4	5	6	7	8	9
SiO_2	32.17	30.50	31.33	31.34	34.85	32.89	37.75	48.54	48.79
TiO_2	6.14	4.41	3.98	3.27	8.35	3.25	5.32	0.00	0.06
Al_2O_3	17.53	18.45	18.83	18.73	16.34	19.10	16.84	34.35	34.01
Cr_2O_3	0.00	0.00	0.00	0.00	0.00	0.00	0.00	0.00	0.00
Fe_2O_3	0.00	0.00	0.00	0.00	0.00	0.00	0.00	0.00	0.00
FeO	17.12	17.72	17.71	17.63	14.65	17.54	15.85	2.14	2.13
MnO	0.12	0.11	0.11	0.10	0.10	0.00	0.12	0.00	0.00
MgO	13.70	16.31	15.86	16.66	14.20	15.14	13.19	1.47	1.40
CaO	0.21	0.14	0.06	0.00	0.00	0.09	0.07	0.00	0.00
Na_2O	0.16	0.12	0.07	0.00	0.08	0.00	0.06	0.11	0.17
K_2O	4.67	2.69	3.91	3.58	6.06	4.46	4.63	10.65	10.88
H_2O	4.07	4.09	4.07	4.08	4.10	4.09	4.16	4.51	4.51
Total	95.89	94.54	95.93	95.39	98.73	96.56	97.99	101.77	101.95
Si^{+4}	4.96	4.74	4.82	4.83	5.16	5.00	5.56	6.33	6.36
Al^{+4}	3.04	3.26	3.18	3.17	2.84	3.00	2.44	1.67	1.64
Fe^{+4}	0.00	0.00	0.00	0.00	0.00	0.00	0.00	0.00	0.00
Ti^{+4}	0.00	0.00	0.00	0.00	0.00	0.00	0.00	0.00	0.00
T site	8.00	8.00	8.00	8.00	8.00	8.00	8.00	8.00	8.00
Al^{+6}	0.14	0.13	0.23	0.24	0.01	0.43	0.48	3.61	3.59
Ti^{+6}	0.71	0.52	0.46	0.38	0.93	0.37	0.59	0.00	0.01
Cr	0.00	0.00	0.00	0.00	0.00	0.00	0.00	0.00	0.00
Fe^{+3}	0.00	0.00	0.00	0.00	0.00	0.00	0.00	0.00	0.00
Fe^{+2}	2.21	2.30	2.28	2.27	1.81	2.23	1.95	0.23	0.23
Mn^{+2}	0.02	0.01	0.01	0.01	0.01	0.00	0.01	0.00	0.00
Mg	3.15	3.78	3.63	3.83	3.13	3.43	2.90	0.29	0.27
Li	0.00	0.00	0.00	0.00	0.00	0.00	0.00	0.00	0.00
O site	6.22	6.74	6.61	6.73	5.90	6.46	5.94	4.13	4.10
Ba	0.00	0.00	0.00	0.00	0.00	0.00	0.00	0.00	0.00
Ca	0.03	0.02	0.01	0.00	0.00	0.01	0.01	0.00	0.00
Na	0.05	0.04	0.02	0.00	0.02	0.00	0.02	0.03	0.04
K	0.92	0.53	0.77	0.70	1.14	0.87	0.87	1.77	1.81
A site	1.00	0.59	0.80	0.70	1.17	0.88	0.90	1.80	1.85
O	20.00	20.00	20.00	20.00	20.00	20.00	20.00	20.00	20.00
OH	4.00	4.00	4.00	4.00	4.00	4.00	4.00	4.00	4.00
F	0.00	0.00	0.00	0.00	0.00	0.00	0.00	0.00	0.00
Cl	0.00	0.00	0.00	0.00	0.00	0.00	0.00	0.00	0.00

Table 13. Mica mineral chemistry of greenstone unit 5.

	b.chert	b.chert	b.chert	b.chert	b.chert	b.chert	b.chert	b.chert	b.chert	b.chert	b.chert
Analysis	1	2	3	4	5	6	7	8	9	10	11
SiO_2	1.86	2.74	2.90	0.00	0.00	0.00	0.05	0.00	0.00	0.00	0.00
TiO_2	0.00	0.00	0.00	0.00	0.00	0.00	0.00	0.00	0.00	0.00	0.00
Al_2O_3	0.55	0.77	0.77	26.24	26.47	26.43	19.72	24.38	24.25	25.37	25.05
Cr_2O_3	0.30	0.20	0.31	45.23	45.18	43.52	45.35	39.86	39.26	38.90	39.05
Fe_2O_3	0.00	0.00	0.00	0.00	0.00	0.00	0.00	0.00	0.00	0.00	0.00
FeO	76.20	72.21	73.89	14.01	13.68	17.29	33.55	32.23	34.11	32.62	33.07
MnO	0.00	0.00	0.00	0.00	0.00	0.00	0.49	0.40	0.43	0.38	0.41
MgO	0.21	0.29	0.29	15.39	15.64	13.28	0.67	2.36	0.92	1.91	1.48
CaO	0.00	0.07	0.06	0.00	0.00	0.00	0.00	0.00	0.00	0.00	0.00
Na_2O	0.00	0.00	0.00	0.00	0.00	0.00	0.00	0.00	0.00	0.00	0.00
K_2O	0.00	0.00	0.00	0.00	0.00	0.00	0.00	0.00	0.00	0.00	0.00
TOTAL	79.12	76.28	78.22	100.87	100.97	100.52	99.83	99.23	98.97	99.18	99.06
Si	0.86	1.29	1.33	0.00	0.00	0.00	0.01	0.00	0.00	0.00	0.00
Ti	0.00	0.00	0.00	0.00	0.00	0.00	0.00	0.00	0.00	0.00	0.00
Al	0.30	0.43	0.42	7.35	7.39	7.52	6.29	7.59	7.64	7.88	7.82
Cr	0.11	0.07	0.11	8.50	8.46	8.30	9.71	8.32	8.30	8.10	8.18
Fe^{+3}	0.00	0.00	0.00	0.00	0.00	0.00	0.00	0.00	0.00	0.00	0.00
Fe^{+2}	29.52	28.43	28.32	2.78	2.71	3.49	7.60	7.12	7.63	7.19	7.33
Mn	0.00	0.00	0.00	0.00	0.00	0.00	0.11	0.09	0.10	0.09	0.09
Mg	0.15	0.20	0.20	5.45	5.52	4.78	0.27	0.93	0.37	0.75	0.58
Ca	0.00	0.04	0.03	0.00	0.00	0.00	0.00	0.00	0.00	0.00	0.00
Na	0.00	0.00	0.00	0.00	0.00	0.00	0.00	0.00	0.00	0.00	0.00
K	0.00	0.00	0.00	0.00	0.00	0.00	0.00	0.00	0.00	0.00	0.00
Total	30.93	30.46	30.41	24.08	24.08	24.09	23.99	24.05	24.03	24.01	24.00

NUMBER OF IONS ON THE BASIS OF 32 (O)

Table 14. Spinel mineral chemistry of banded chert at Spitskop.

	chert	chert	chert	chert	chert	chert	chert	chert	chert
Analysis	1	2	3	4	5	6	7	8	9
SiO_2	31.21	34.11	35.87	19.40	24.60	25.00	16.16	20.79	17.90
TiO_2	0.00	0.06	0.00	0.06	0.00	0.06	0.44	0.08	0.00
Al_2O_3	17.38	17.72	18.45	42.42	39.60	37.81	39.95	26.01	45.41
Cr_2O_3	4.66	2.79	3.36	1.65	1.43	1.63	1.79	2.46	1.53
Fe_2O_3	0.00	0.00	0.00	0.00	0.00	0.00	0.00	0.00	0.00
FeO	16.16	14.62	14.07	16.57	9.33	11.34	20.05	3.87	10.44
MnO	0.00	0.00	0.00	0.00	0.00	0.00	0.00	0.00	0.00
MgO	19.63	15.58	14.66	2.82	7.48	8.14	2.13	1.90	3.31
CaO	0.22	0.39	0.33	0.53	0.36	0.32	0.60	0.31	0.57
Na_2O	0.06	0.11	0.05	0.13	0.13	0.08	0.27	0.18	0.18
K_2O	0.22	0.42	0.43	1.26	1.57	0.95	2.18	1.64	1.91
H_2O	4.14	4.23	4.27	4.17	4.36	4.32	4.01	4.47	4.29
Total	93.68	90.03	91.49	89.01	88.86	89.65	87.58	61.71	85.54
Si^{+4}	4.84	5.39	5.53	3.15	3.83	3.89	2.78	4.66	2.95
Al^{+4}	3.16	2.61	2.47	4.85	4.17	4.11	5.22	3.34	5.05
Fe^{+4}	0.00	0.00	0.00	0.00	0.00	0.00	0.00	0.00	0.00
Ti^{+4}	0.00	0.00	0.00	0.00	0.00	0.00	0.00	0.00	0.00
T site	8.00	8.00	8.00	8.00	8.00	8.00	8.00	8.00	8.00
Al^{+6}	0.02	0.69	0.89	3.28	3.09	2.81	2.87	3.52	3.76
Ti^{+6}	0.00	0.01	0.00	0.01	0.00	0.01	0.06	0.01	0.00
Cr	0.57	0.35	0.41	0.21	0.18	0.20	0.24	0.44	0.20
Fe^{+3}	0.00	0.00	0.00	0.00	0.00	0.00	0.00	0.00	0.00
Fe^{+2}	2.10	1.93	1.81	2.25	1.21	1.47	2.88	0.72	1.44
Mn^{+2}	0.00	0.00	0.00	0.00	0.00	0.00	0.00	0.00	0.00
Mg	4.54	3.67	3.37	0.68	1.74	1.89	0.55	0.63	0.81
Li	0.00	0.00	0.00	0.00	0.00	0.00	0.00	0.00	0.00
O site	7.22	6.65	6.48	6.43	6.22	6.38	6.60	5.33	6.21
Ba	0.00	0.00	0.00	0.00	0.00	0.00	0.00	0.00	0.00
Ca	0.04	0.07	0.05	0.09	0.06	0.05	0.11	0.07	0.10
Na	0.02	0.03	0.01	0.04	0.04	0.02	0.09	0.08	0.06
K	0.04	0.08	0.08	0.26	0.31	0.19	0.48	0.47	0.40
A site	0.10	0.18	0.15	0.39	0.41	0.27	0.68	0.62	0.56
O	20.00	20.00	20.00	20.00	20.00	20.00	20.00	20.00	20.00
OH	4.00	4.00	4.00	4.00	4.00	4.00	4.00	4.00	4.00
F	0.00	0.00	0.00	0.00	0.00	0.00	0.00	0.00	0.00
Cl	0.00	0.00	0.00	0.00	0.00	0.00	0.00	0.00	0.00

Table 15. Mica mineral chemistry of banded chert at Spitskop.

Opmerking: Later sal ons sien dat die skuifspannings soos deur middel van vgl. 2.2 bereken, nie die werklike maksimum skuifspannings is nie, aangesien die skuifspanning-verdeling oor die snit nie konstant is nie. Die skuifspannings is die gemiddelde skuifspannings.

Vir praktiese ontwerpdoeleindes in gevalle van boutverbindings soos in figuur 2.10 is die gemiddelde skuifspanning 'n aanvaarde kriterium. Let verder op dat in figuur 2.10(b) daar 'n klein ongebalanseerde moment P.e optree, wat normaalweg vir praktiese doeleindes geïgnoreer word.

2.3.2 Voorbeelde

Voorbeeld 2.1

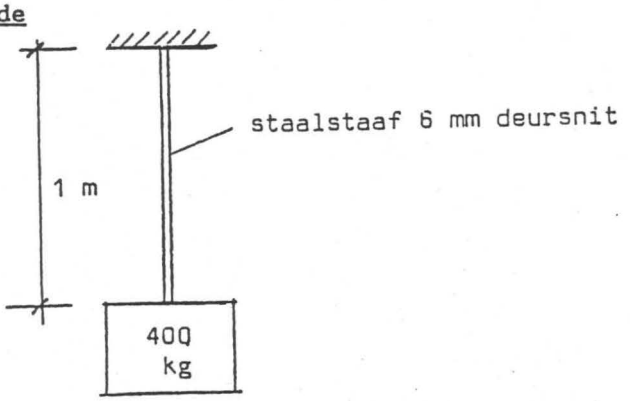

'n Staalstafie, 6 mm deursnit hang vertikaal en is konsentries belaai met 'n massa van 400 kg. Wat is die spanning in die stafie?

Oplossing:

Om hierdie probleem op te los, moet ons eers 'n idealisering maak:

Omdat die massa van die stafie baie klein is in vergelyking met die massa van die gewig wat daaraan hang, kan dit sonder verlies van akkuraatheid buite rekening gelaat word.

Omdat die spanning

$$\sigma = \frac{P}{A}$$

moet ons die krag P in die staaf en ook die deursnitoppervlakte van die staaf bereken.

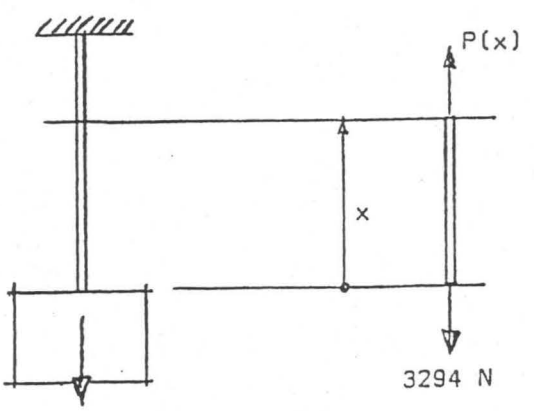

400 x 9,81 = 3294 N

Opmerking: Later sal ons sien dat die skuifspannings soos deur middel van vgl. 2.2 bereken, nie die werklike maksimum skuifspannings is nie, aangesien die skuifspanning-verdeling oor die snit nie konstant is nie. Die skuifspannings is die gemiddelde skuifspannings.

Vir praktiese ontwerpdoeleindes in gevalle van boutverbindings soos in figuur 2.10 is die gemiddelde skuifspanning 'n aanvaarde kriterium. Let verder op dat in figuur 2.10(b) daar 'n klein ongebalanseerde moment P.e optree, wat normaalweg vir praktiese doeleindes geïgnoreer word.

2.3.2 Voorbeelde

Voorbeeld 2.1

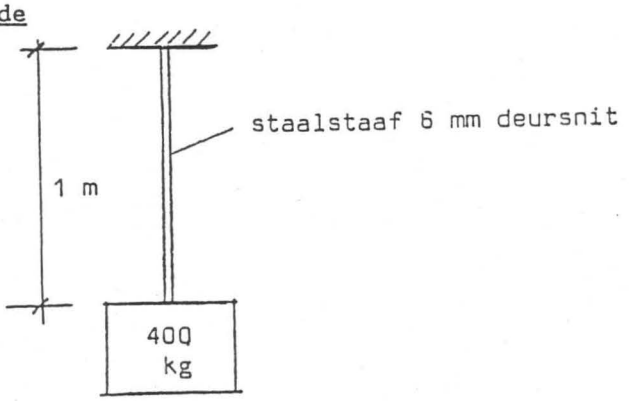

'n Staalstafie, 6 mm deursnit hang vertikaal en is konsentries belaai met 'n massa van 400 kg. Wat is die spanning in die stafie?

Oplossing:

Om hierdie probleem op te los, moet ons eers 'n idealisering maak:

Omdat die massa van die stafie baie klein is in vergelyking met die massa van die gewig wat daaraan hang, kan dit sonder verlies van akkuraatheid buite rekening gelaat word.

Omdat die spanning

$$\sigma = \frac{P}{A}$$

moet ons die krag P in die staaf en ook die deursnitoppervlakte van die staaf bereken.

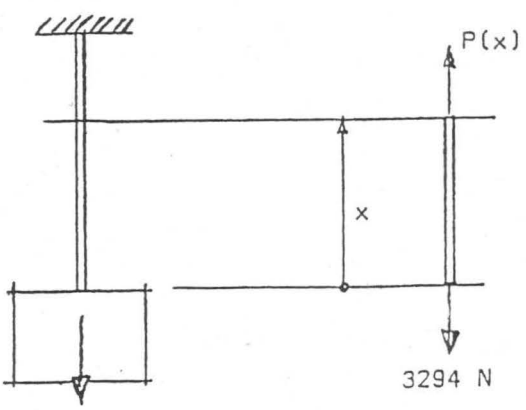

400 x 9,81 = 3294 N

Opmerking: Later sal ons sien dat die skuifspannings soos deur middel van vgl. 2.2 bereken, nie die werklike maksimum skuifspannings is nie, aangesien die skuifspanning-verdeling oor die snit nie konstant is nie. Die skuifspannings is die gemiddelde skuifspannings.

Vir praktiese ontwerpdoeleindes in gevalle van boutverbindings soos in figuur 2.10 is die gemiddelde skuifspanning 'n aanvaarde kriterium. Let verder op dat in figuur 2.10(b) daar 'n klein ongebalanseerde moment P.e optree, wat normaalweg vir praktiese doeleindes geïgnoreer word.

2.3.2 Voorbeelde

Voorbeeld 2.1

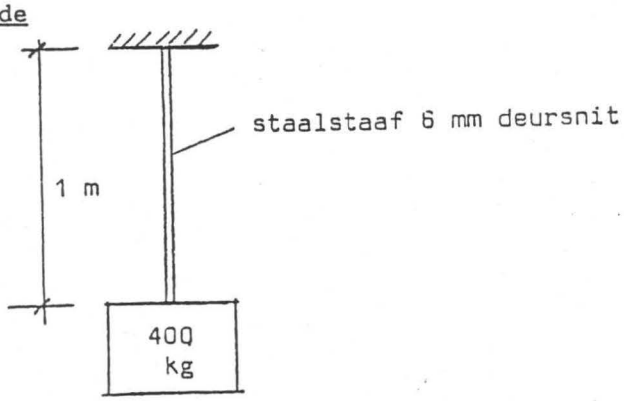

'n Staalstafie, 6 mm deursnit hang vertikaal en is konsentries belaai met 'n massa van 400 kg. Wat is die spanning in die stafie?

Oplossing:

Om hierdie probleem op te los, moet ons eers 'n idealisering maak:

Omdat die massa van die stafie baie klein is in vergelyking met die massa van die gewig wat daaraan hang, kan dit sonder verlies van akkuraatheid buite rekening gelaat word.

Omdat die spanning

$$\sigma = \frac{P}{A}$$

moet ons die krag P in die staaf en ook die deursnitoppervlakte van die staaf bereken.

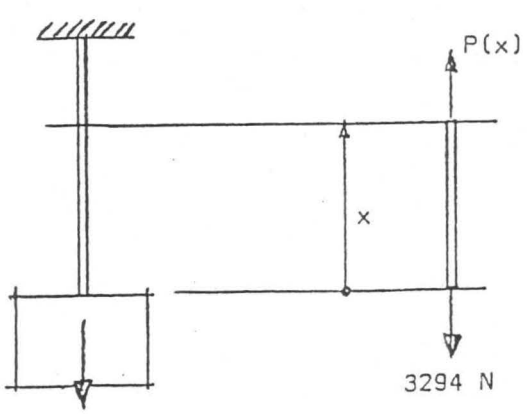

400 x 9,81 = 3294 N

Opmerking: Later sal ons sien dat die skuifspannings soos deur middel van vgl. 2.2 bereken, nie die werklike maksimum skuifspannings is nie, aangesien die skuifspanning-verdeling oor die snit nie konstant is nie. Die skuifspannings is die gemiddelde skuifspannings.

Vir praktiese ontwerpdoeleindes in gevalle van boutverbindings soos in figuur 2.10 is die gemiddelde skuifspanning 'n aanvaarde kriterium. Let verder op dat in figuur 2.10(b) daar 'n klein ongebalanseerde moment P.e optree, wat normaalweg vir praktiese doeleindes geïgnoreer word.

2.3.2 Voorbeelde

Voorbeeld 2.1

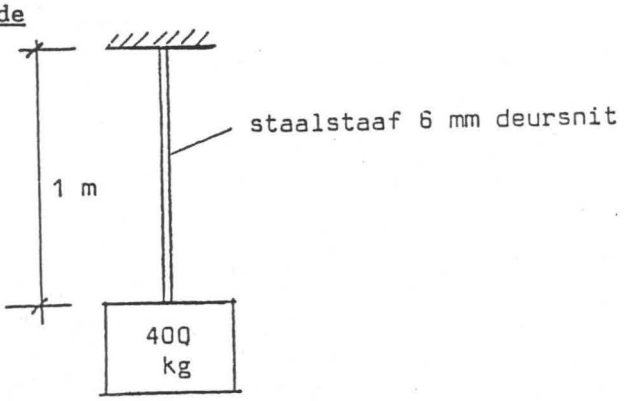

'n Staalstafie, 6 mm deursnit hang vertikaal en is konsentries belaai met 'n massa van 400 kg. Wat is die spanning in die stafie?

Oplossing:

Om hierdie probleem op te los, moet ons eers 'n idealisering maak:

Omdat die massa van die stafie baie klein is in vergelyking met die massa van die gewig wat daaraan hang, kan dit sonder verlies van akkuraatheid buite rekening gelaat word.

Omdat die spanning

$$\sigma = \frac{P}{A}$$

moet ons die krag P in die staaf en ook die deursnitoppervlakte van die staaf bereken.

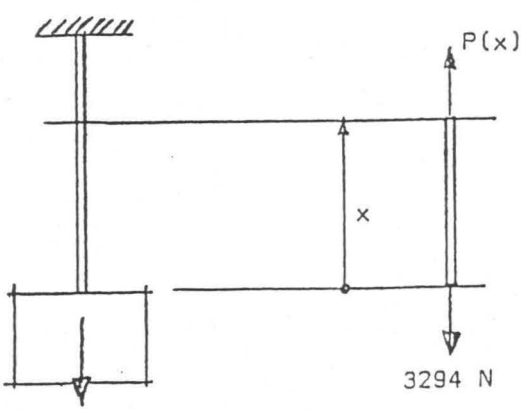

400 x 9,81 = 3294 N

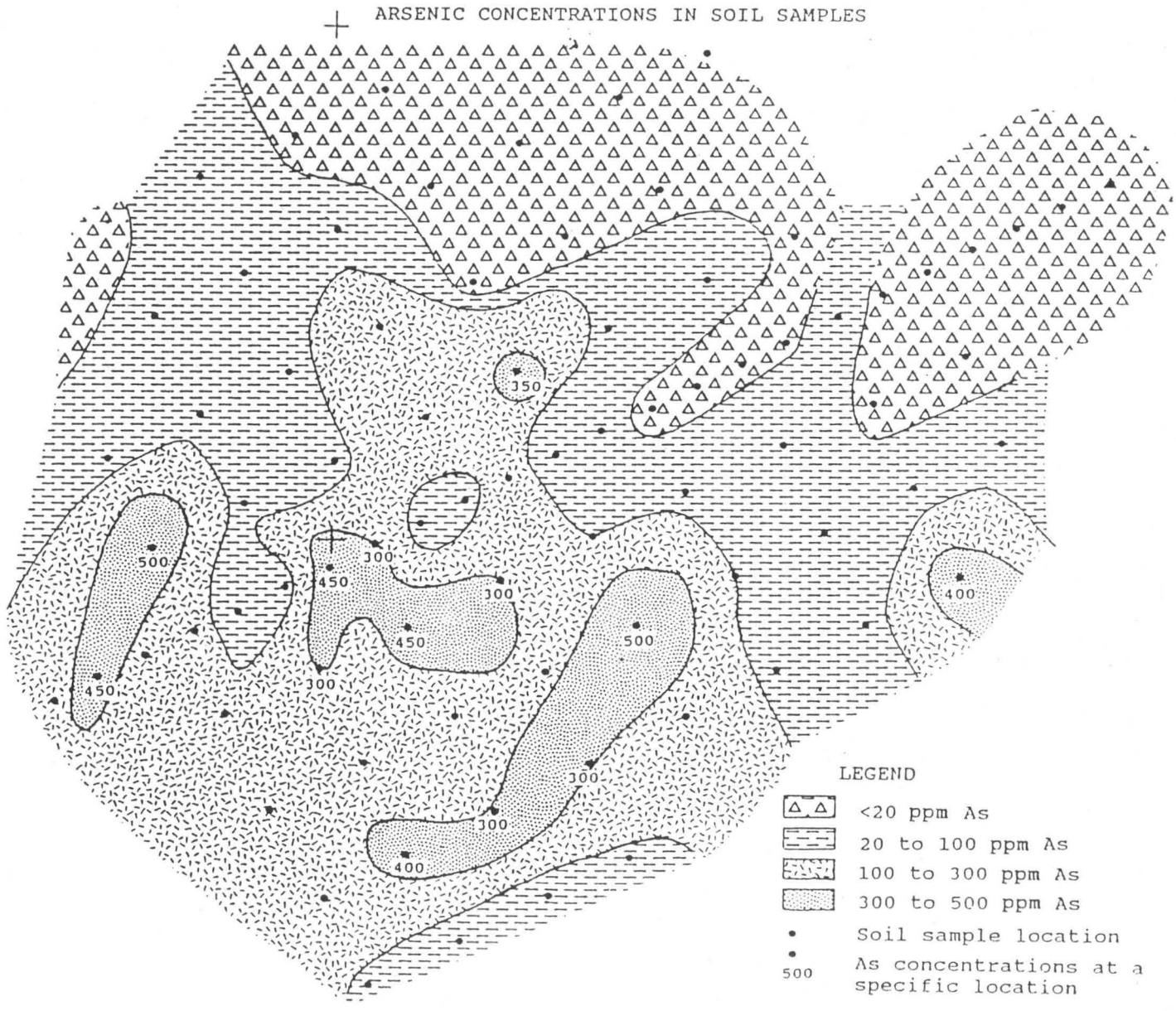

GOLD CONCENTRATIONS IN SOIL SAMPLES

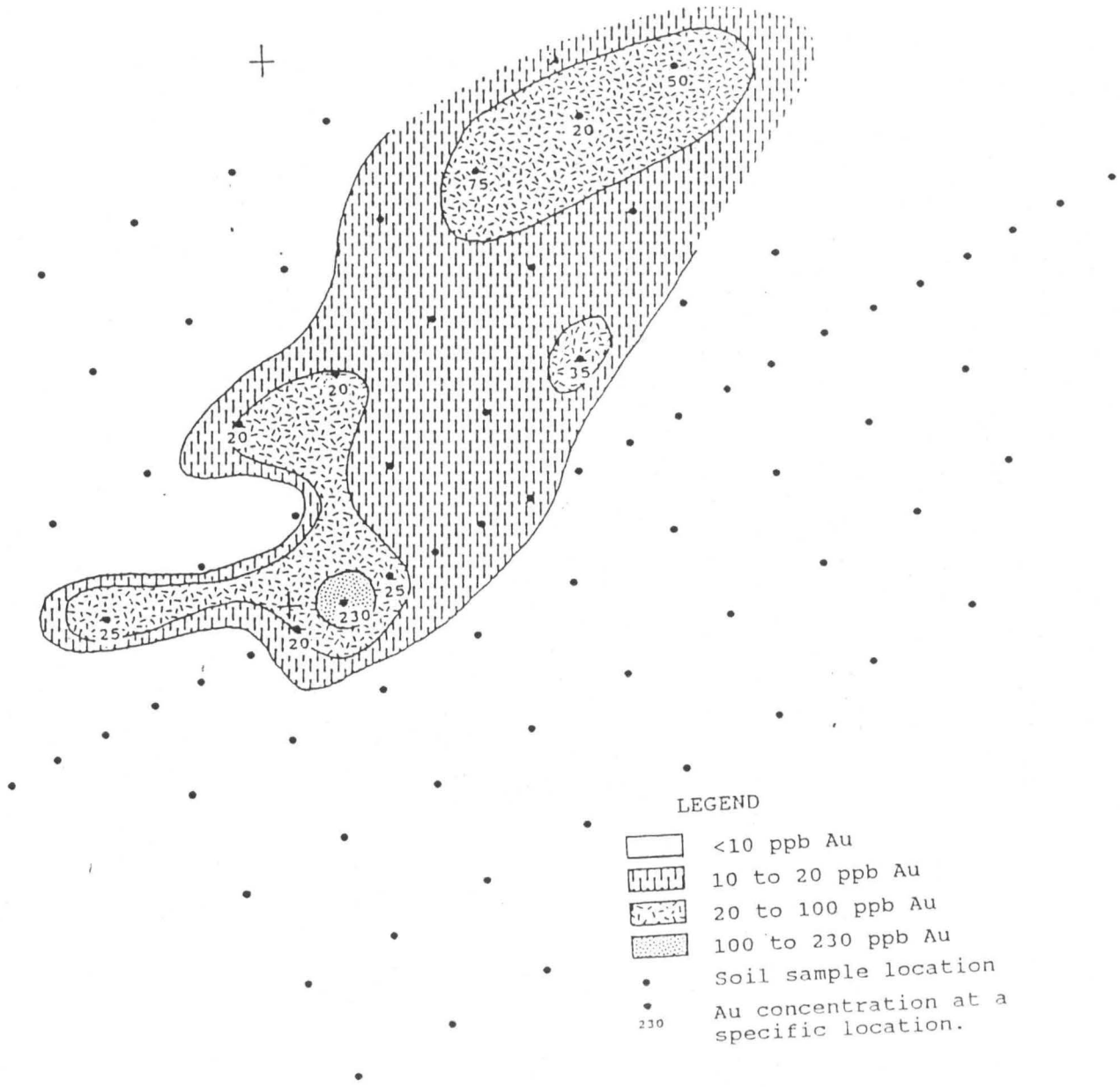

GOLD CONCENTRATIONS IN SOIL SAMPLES

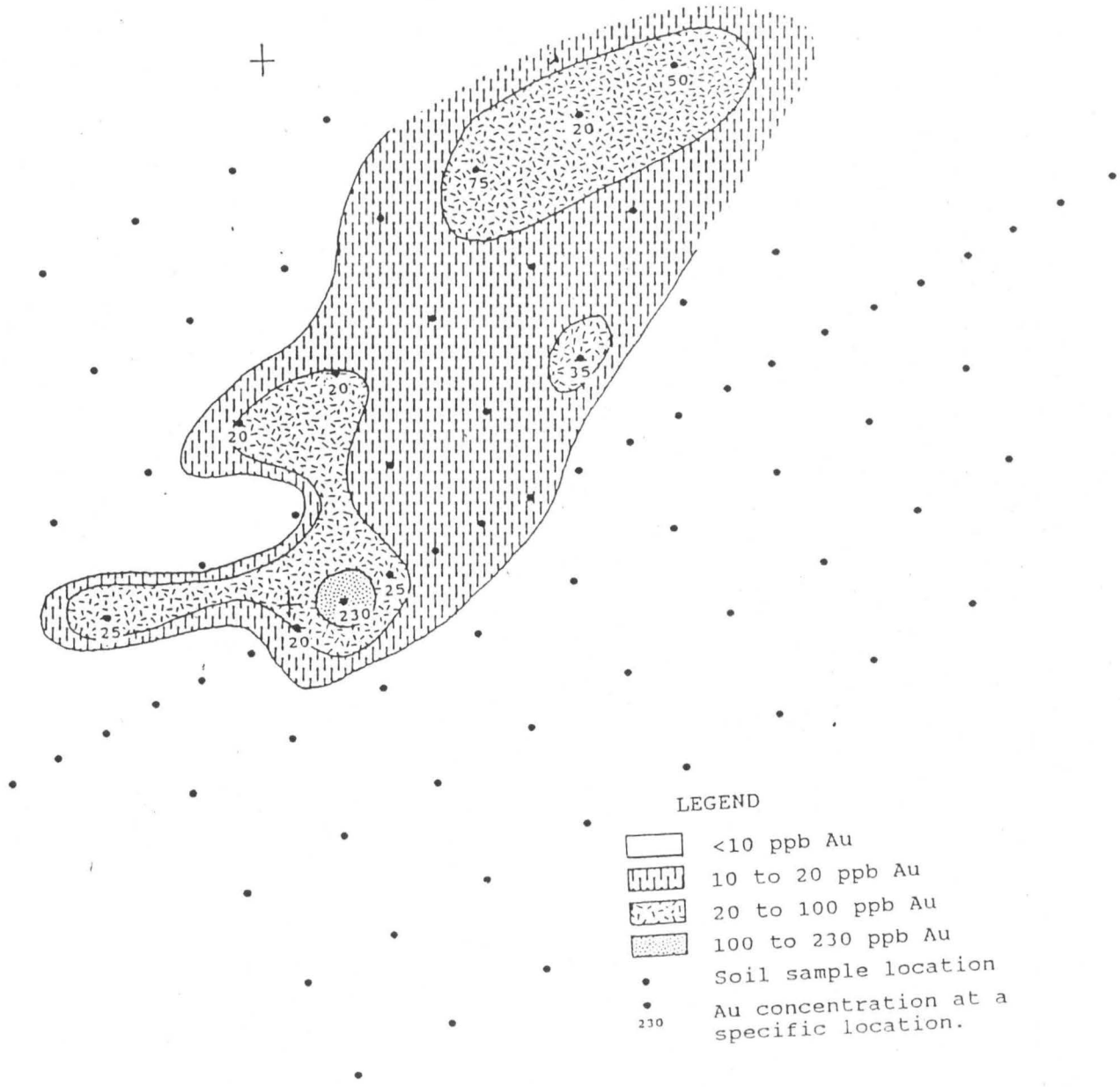

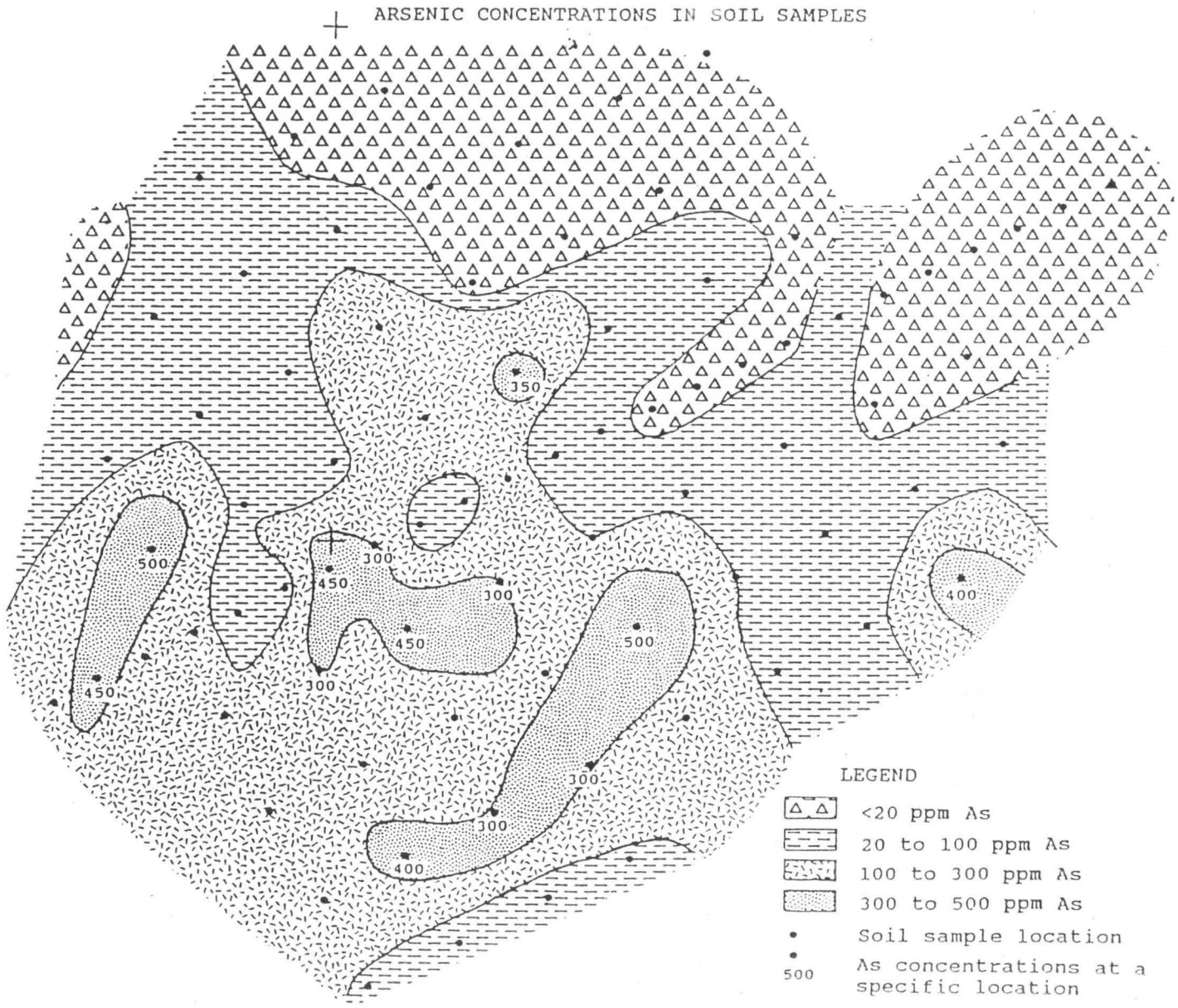

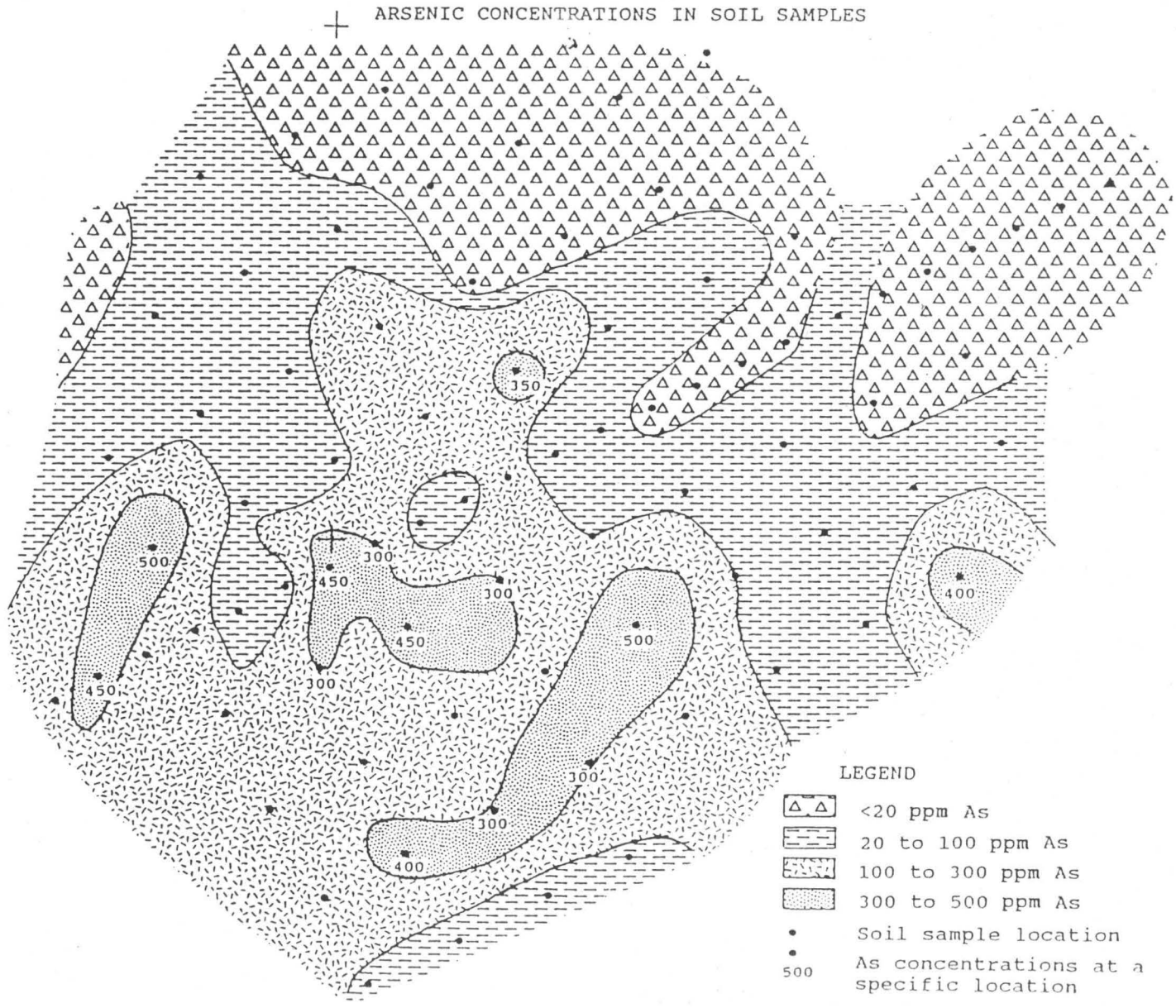

GOLD CONCENTRATIONS IN SOIL SAMPLES

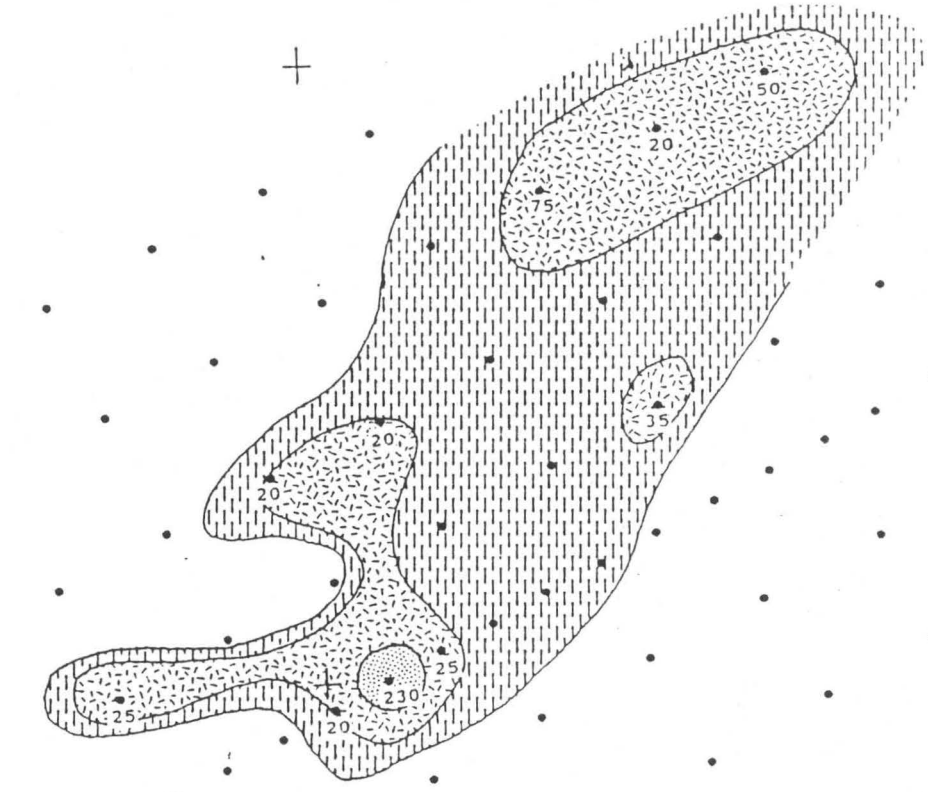

LEGEND

- <10 ppb Au
- 10 to 20 ppb Au
- 20 to 100 ppb Au
- 100 to 230 ppb Au
- Soil sample location
- 230 Au concentration at a specific location.

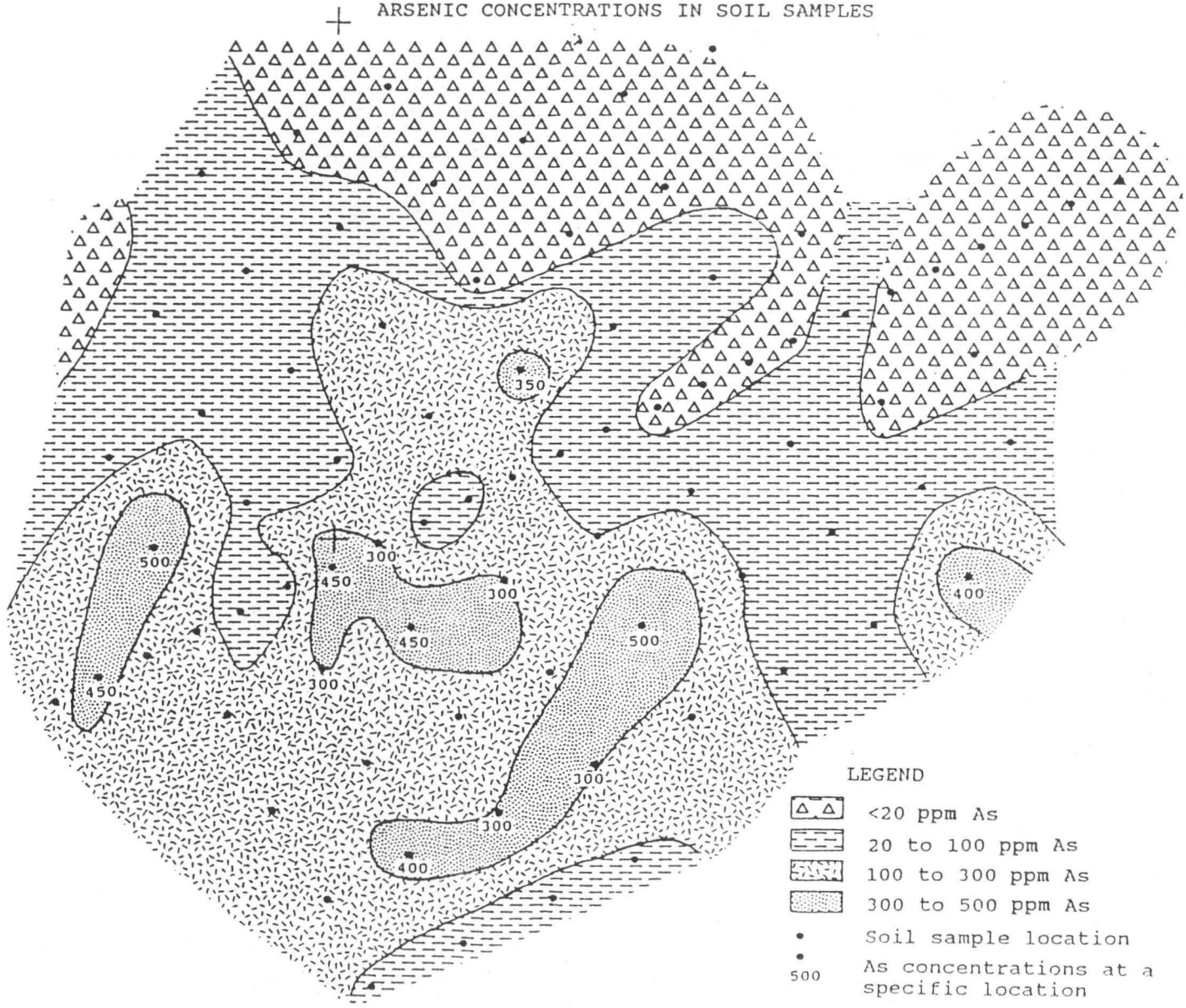

GOLD CONCENTRATIONS IN SOIL SAMPLES

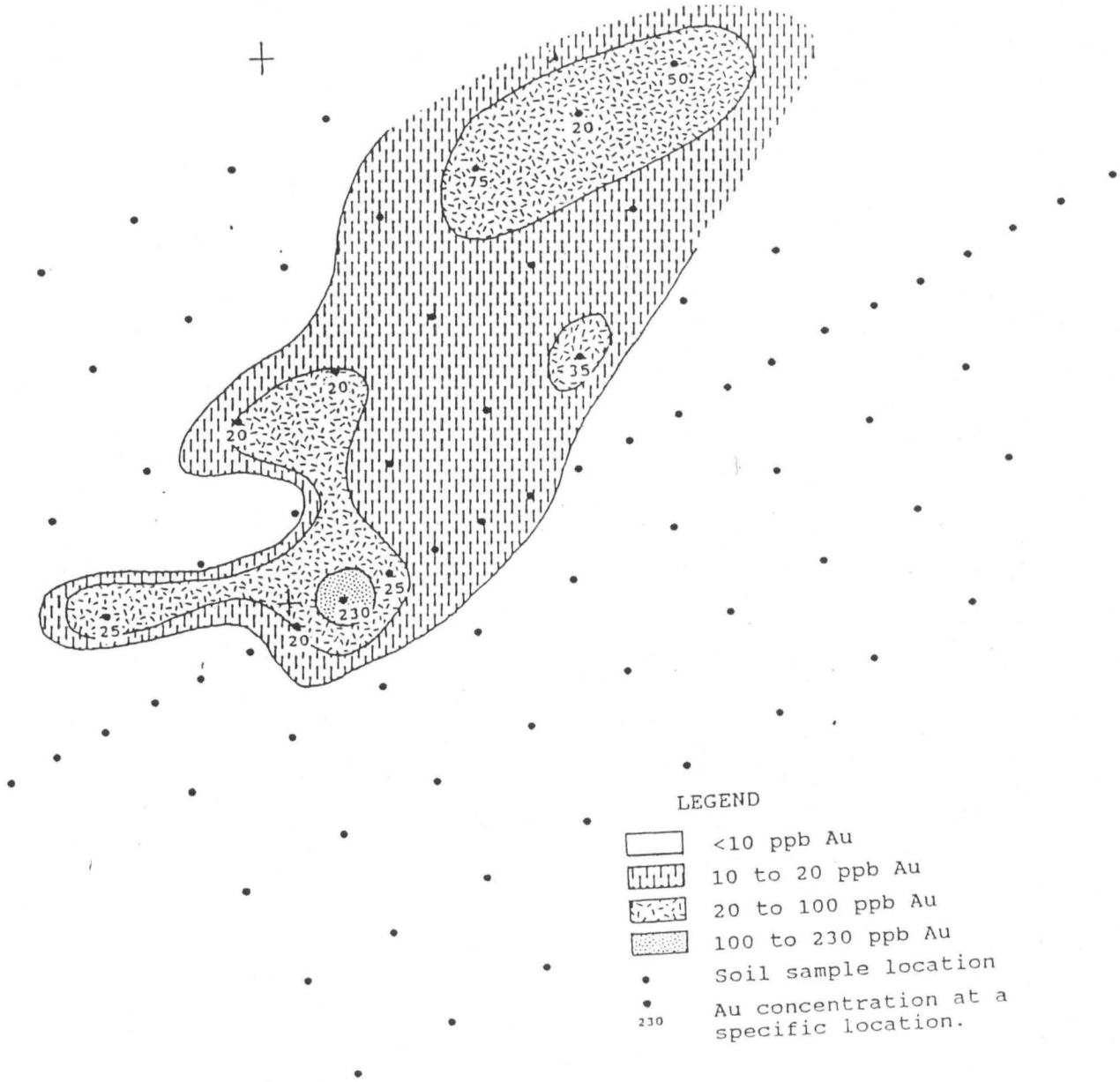

GOLD CONCENTRATIONS IN SOIL SAMPLES

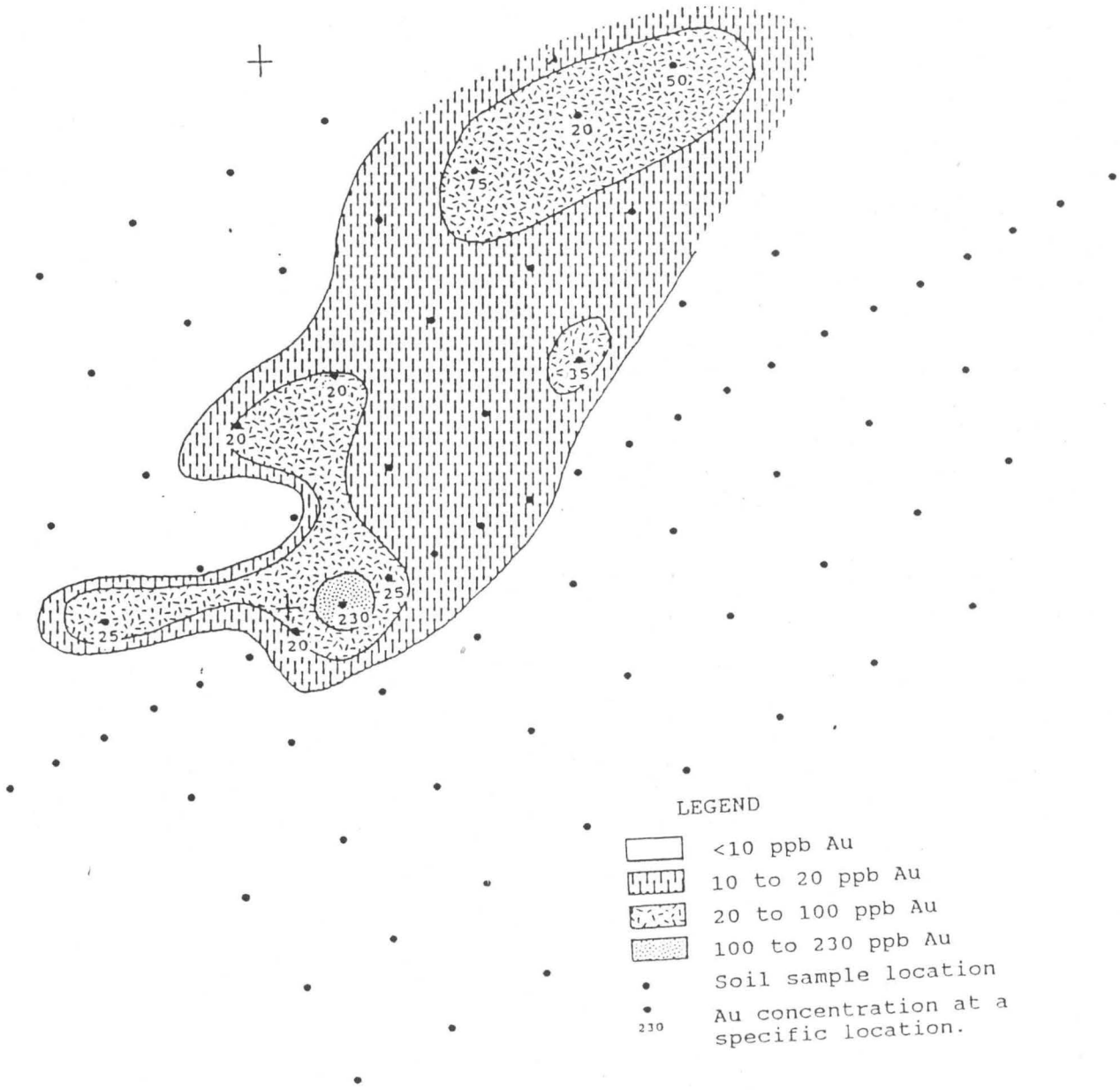

SHEET A

LEGEND

- Alluvium and recent blown sands
- Sandy soil and loam
- Eocene gravels (g), silcretes (s), ferricretes (f)

Malmesbury Group
- Graywacke with feldspathic grit and conglomerate
- Graywacke
- Grit
- Banded chert
- Quartz schist
- Quartz-feldspar-sericite schist
- Mottled carbonate
- Phyllite
- Limestone

Not in stratigraphic order
Bridgetown Formation
- Intrusive metabasite
- Chert
- Dolomite
- Muscovite-quartz schist
- Greenschist
- Banded phyllite with chert lenses and graphitic schist lenses

- Silicified fault breccias and quartz veins/bodies
- Zone characterized by numerous mineralized quartz outcrops
- Silicified schist
- Silicified breccia in chert
- Limonitic zone
- NSF/2.8 Sample location
- Possible fault
- Strike and dip of main foliation
- Vertical dip of main foliation
- Horizontal dip of main foliation

Modified after
- Strike and dip of secondary foliation; trend and plunge of secondary lineation
- Antiform
- Antiform, existence uncertain
- Synform
- Synform, existence uncertain
- Rivers and streams
- Farm buildings
- Main roads
- Quarry

N

SCALE
0 100 200 300 400 500 600 700 800 900 1000
metres

FARM BOUNDARIES

km
0 2 4